

Future Physics Programme of BESIII

IHEP-Physics-Report-BESIII-2020-4-7

Published in Chinese Physics C **44**, 040001 (2020)

M. Ablikim^{1,§}, M. N. Achasov^{10,d,§}, P. Adlarson^{58,§}, S. Ahmed^{15,§}, M. Albrecht^{4,§},
 M. Alekseev^{57A,57C,§}, A. Amoroso^{57A,57C,§}, F. F. An^{1,§}, Q. An^{54,42,§}, Y. Bai^{41,§},
 O. Bakina^{27,§}, R. Baldini Ferroli^{23A,§}, Y. Ban^{35,§}, K. Begzsuren^{25,§}, J. V. Bennett^{5,§},
 N. Berger^{26,§}, M. Bertani^{23A,§}, D. Bettoni^{24A,§}, F. Bianchi^{57A,57C,§}, J. Biernat^{58,§},
 J. Bloms^{51,§}, I. Boyko^{27,§}, R. A. Briere^{5,§}, L. Calibbi^{34,¶}, H. Cai^{59,§}, X. Cai^{1,42,§},
 A. Calcaterra^{23A,§}, G. F. Cao^{1,46,§}, N. Cao^{1,46,§}, S. A. Cetin^{45B,§}, J. Chai^{57C,§},
 J. F. Chang^{1,42,§}, W. L. Chang^{1,46,§}, J. Charles^{1,¶}, G. Chelkov^{27,b,c,§}, Chen^{6,§}, G. Chen^{1,§},
 H. S. Chen^{1,46,§}, J. C. Chen^{1,§}, M. L. Chen^{1,42,§}, S. J. Chen^{33,§}, Y. B. Chen^{1,42,§},
 H. Y. Cheng^{VI,¶}, W. Cheng^{57C,§}, G. Cibinetto^{24A,§}, F. Cossio^{57C,§}, X. F. Cui^{34,§},
 H. L. Dai^{1,42,§}, J. P. Dai^{37,h,§}, X. C. Dai^{1,46,§}, A. Dbeyssi^{15,§}, D. Dedovich^{27,§},
 Z. Y. Deng^{1,§}, A. Denig^{26,§}, I. Denysenko^{27,§}, M. Destefanis^{57A,57C,§},
 S. Descotes-Genon^{IV,¶}, F. De Mori^{57A,57C,§}, Y. Ding^{31,§}, C. Dong^{34,§}, J. Dong^{1,42,§},
 L. Y. Dong^{1,46,§}, M. Y. Dong^{1,42,46,§}, Z. L. Dou^{33,§}, S. X. Du^{62,§}, S. I. Eidelman^{II,V,VIII,¶},
 J. Z. Fan^{44,§}, J. Fang^{1,42,§}, S. S. Fang^{1,46,§}, Y. Fang^{1,§}, R. Farinelli^{24A,24B,§},
 L. Fava^{57B,57C,§}, F. Feldbauer^{4,§}, G. Felici^{23A,§}, C. Q. Feng^{54,42,§}, M. Fritsch^{4,§},
 C. D. Fu^{1,§}, Y. Fu^{1,§}, Q. Gao^{1,§}, X. L. Gao^{54,42,§}, Y. Gao^{44,§}, Y. Gao^{55,§}, Y. G. Gao^{6,§},
 Z. Gao^{54,42,§}, B. Garillon^{26,§}, I. Garzia^{24A,§}, E. M. Gersabeck^{49,§}, A. Gilman^{50,§},
 K. Goetzen^{11,§}, L. Gong^{34,§}, W. X. Gong^{1,42,§}, W. Gradl^{26,§,†}, M. Greco^{57A,57C,§},
 L. M. Gu^{33,§}, M. H. Gu^{1,42,§}, Y. T. Gu^{13,§}, A. Q. Guo^{22,§}, F. K. Guo^{VII,46,¶}, L. B. Guo^{32,§},
 R. P. Guo^{1,46,§}, Y. P. Guo^{26,§}, A. Guskov^{27,§}, S. Han^{59,§}, X. Q. Hao^{16,§}, F. A. Harris^{47,§},
 K. L. He^{1,46,§}, F. H. Heinsius^{4,§}, T. Held^{4,§}, Y. K. Heng^{1,42,46,§}, Y. R. Hou^{46,§},
 Z. L. Hou^{1,§}, H. M. Hu^{1,46,§}, J. F. Hu^{37,h,§}, T. Hu^{1,42,46,§}, Y. Hu^{1,§}, G. S. Huang^{54,42,§},
 J. S. Huang^{16,§}, X. T. Huang^{36,§}, X. Z. Huang^{33,§}, Z. L. Huang^{31,§}, N. Huesken^{51,§},
 T. Hussain^{56,§}, W. Ikegami Andersson^{58,§}, W. Imoehl^{22,§}, M. Irshad^{54,42,§}, Q. Ji^{1,§},
 Q. P. Ji^{16,§}, X. B. Ji^{1,46,§}, X. L. Ji^{1,42,§}, H. L. Jiang^{36,§}, X. S. Jiang^{1,42,46,§}, X. Y. Jiang^{34,§},
 J. B. Jiao^{36,§}, Z. Jiao^{18,§}, D. P. Jin^{1,42,46,§}, S. Jin^{33,§}, Y. Jin^{48,§}, T. Johansson^{58,§},
 N. Kalantar-Nayestanaki^{29,§}, X. S. Kang^{31,§}, R. Kappert^{29,§}, M. Kavatsyuk^{29,§},
 B. C. Ke^{1,§}, I. K. Keshk^{4,§}, T. Khan^{54,42,§}, A. Khoukaz^{51,§}, P. Kiese^{26,§}, R. Kiuchi^{1,§},
 R. Kliemt^{11,§}, L. Koch^{28,§}, O. B. Kolcu^{45B,f,§}, B. Kopf^{4,§}, M. Kuemmel^{4,§}, M. Kuessner^{4,§},
 A. Kupsc^{58,§}, M. Kurth^{1,§}, M. G. Kurth^{1,46,§}, W. Kühn^{28,§}, J. S. Lange^{28,§}, P. Larin^{15,§},
 L. Lavezzi^{57C,§}, H. Leithoff^{26,§}, T. Lenz^{26,§}, C. Li^{58,§}, Cheng Li^{54,42,§}, D. M. Li^{62,§},
 F. Li^{1,42,§}, F. Y. Li^{35,§}, G. Li^{1,§}, H. B. Li^{1,46,§,★}, H. J. Li^{9,j,§}, J. C. Li^{1,§}, J. W. Li^{40,§},
 Ke Li^{1,§}, L. K. Li^{1,§}, Lei Li^{3,§}, P. L. Li^{54,42,§}, P. R. Li^{30,§}, Q. Y. Li^{36,§}, W. D. Li^{1,46,§},
 W. G. Li^{1,§}, X. H. Li^{54,42,§}, X. L. Li^{36,§}, X. N. Li^{1,42,§}, X. Q. Li^{34,§}, Z. B. Li^{43,§},
 H. Liang^{1,46,§}, H. Liang^{54,42,§}, Y. F. Liang^{39,§}, Y. T. Liang^{28,§}, G. R. Liao^{12,§},
 L. Z. Liao^{1,46,§}, J. Libby^{21,§}, C. X. Lin^{43,§}, D. X. Lin^{15,§}, Y. J. Lin^{13,§}, B. Liu^{37,h,§},
 B. J. Liu^{1,§}, C. X. Liu^{1,§}, D. Liu^{54,42,§}, D. Y. Liu^{37,h,§}, F. H. Liu^{38,§}, Fang Liu^{1,§},
 Feng Liu^{6,§}, H. B. Liu^{13,§}, H. M. Liu^{1,46,§}, Huanhuan Liu^{1,§}, Huihui Liu^{17,§},
 J. B. Liu^{54,42,§}, J. Y. Liu^{1,46,§}, K. Y. Liu^{31,§}, Ke Liu^{6,§}, Q. Liu^{46,§}, S. B. Liu^{54,42,§},
 T. Liu^{1,46,§}, X. Liu^{30,§}, X. Y. Liu^{1,46,§}, Y. B. Liu^{34,§}, Z. A. Liu^{1,42,46,§}, Zhiqing Liu^{26,§}, Y.
 F. Long^{35,§}, X. C. Lou^{1,42,46,§}, H. J. Lu^{18,§}, J. D. Lu^{1,46,§}, J. G. Lu^{1,42,§}, Y. Lu^{1,§},
 Y. P. Lu^{1,42,§}, C. L. Luo^{32,§}, M. X. Luo^{61,§}, P. W. Luo^{43,§}, T. Luo^{9,j,§}, X. L. Luo^{1,42,§},
 S. Lusso^{57C,§}, X. R. Lyu^{46,§,★,‡}, F. C. Ma^{31,§}, H. L. Ma^{1,§}, L. L. Ma^{36,§}, M. M. Ma^{1,46,§},
 Q. M. Ma^{1,§}, X. N. Ma^{34,§}, X. X. Ma^{1,46,§}, X. Y. Ma^{1,42,§}, Y. M. Ma^{36,§}, F. E. Maas^{15,§},
 M. Maggiora^{57A,57C,§}, S. Maldaner^{26,§}, S. Malde^{52,§}, Q. A. Malik^{56,§}, A. Mangoni^{23B,§},

Y. J. Mao^{35,§}, Z. P. Mao^{1,§}, S. Marcello^{57A,57C,§}, Z. X. Meng^{48,§}, J. G. Messchendorp^{29,§},
 G. Mezzadri^{24A,§}, J. Min^{1,42,§}, T. J. Min^{33,§}, R. E. Mitchell^{22,§}, X. H. Mo^{1,42,46,§},
 Y. J. Mo^{6,§}, C. Morales Morales^{15,§}, N. Yu. Muchnoi^{10,d,§}, H. Muramatsu^{50,§},
 A. Mustafa^{4,§}, S. Nakhoul^{11,g,§}, Y. Nefedov^{27,§}, F. Nerling^{11,g,§}, I. B. Nikolaev^{10,d,§},
 Z. Ning^{1,42,§}, S. Nisar^{8,k,§}, S. L. Niu^{1,42,§}, S. L. Olsen^{46,§}, Q. Ouyang^{1,42,46,§},
 S. Pacetti^{23B,§}, Y. Pan^{54,42,§}, M. Papenbrock^{58,§}, P. Patteri^{23A,§}, M. Pelizaeus^{4,§},
 H. P. Peng^{54,42,§}, K. Peters^{11,g,§}, A. A. Petrov^{X,¶}, J. Pettersson^{58,§}, J. L. Ping^{32,§},
 R. G. Ping^{1,46,§}, A. Pitka^{4,§}, R. Poling^{50,§}, V. Prasad^{54,42,§}, M. Qi^{33,§}, T. Y. Qi^{2,§},
 S. Qian^{1,42,§}, C. F. Qiao^{46,§}, N. Qin^{59,§}, X. P. Qin^{13,§}, X. S. Qin^{4,§}, Z. H. Qin^{1,42,§},
 J. F. Qiu^{1,§}, S. Q. Qu^{34,§}, K. H. Rashid^{56,i,§}, C. F. Redmer^{26,§}, M. Richter^{4,§},
 M. Ripka^{26,§}, A. Rivetti^{57C,§}, V. Rodin^{29,§}, M. Rolo^{57C,§}, G. Rong^{1,46,§},
 J. L. Rosner^{IX,¶,★}, Ch. Rosner^{15,§}, M. Rump^{51,§}, A. Sarantsev^{27,e,§}, M. Savrie^{24B,§},
 K. Schoenning^{58,§}, W. Shan^{19,§}, X. Y. Shan^{54,42,§}, M. Shao^{54,42,§}, C. P. Shen^{2,§},
 P. X. Shen^{34,§}, X. Y. Shen^{1,46,§}, H. Y. Sheng^{1,§}, X. Shi^{1,42,§}, X. D Shi^{54,42,§}, J. J. Song^{36,§},
 Q. Q. Song^{54,42,§}, X. Y. Song^{1,§}, S. Sosio^{57A,57C,§}, C. Sowa^{4,§}, S. Spataro^{57A,57C,§}, F. F.
 Sui^{36,§}, G. X. Sun^{1,§}, J. F. Sun^{16,§}, L. Sun^{59,§}, S. S. Sun^{1,46,§}, X. H. Sun^{1,§}, Y. J. Sun^{54,42,§},
 Y. K Sun^{54,42,§}, Y. Z. Sun^{1,§}, Z. J. Sun^{1,42,§}, Z. T. Sun^{1,§}, Y. T Tan^{54,42,§}, C. J. Tang^{39,§},
 G. Y. Tang^{1,§}, X. Tang^{1,§}, V. Thoren^{58,§}, B. Tsednee^{25,§}, I. Uman^{45D,§}, B. Wang^{1,§},
 B. L. Wang^{46,§}, C. W. Wang^{33,§}, D. Y. Wang^{35,§}, H. H. Wang^{36,§}, K. Wang^{1,42,§},
 L. L. Wang^{1,§}, L. S. Wang^{1,§}, M. Wang^{36,§}, M. Z. Wang^{35,§}, Meng Wang^{1,46,§},
 P. L. Wang^{1,§}, R. M. Wang^{60,§}, W. P. Wang^{54,42,§}, X. Wang^{35,§}, X. F. Wang^{1,§},
 X. L. Wang^{9,j,§}, Y. Wang^{54,42,§}, Y. F. Wang^{1,42,46,§}, Z. Wang^{1,42,§}, Z. G. Wang^{1,42,§},
 Z. Y. Wang^{1,§}, Zongyuan Wang^{1,46,§}, T. Weber^{4,§}, D. H. Wei^{12,§}, P. Weidenkaff^{26,§},
 H. W. Wen^{32,§}, S. P. Wen^{1,§}, U. Wiedner^{4,§}, G. Wilkinson^{52,§}, M. Wolke^{58,§}, L. H. Wu^{1,§},
 L. J. Wu^{1,46,§}, Z. Wu^{1,42,§}, L. Xia^{54,42,§}, Y. Xia^{20,§}, S. Y. Xiao^{1,§}, Y. J. Xiao^{1,46,§},
 Z. J. Xiao^{32,§}, Y. G. Xie^{1,42,§}, Y. H. Xie^{6,§}, T. Y. Xing^{1,46,§}, X. A. Xiong^{1,46,§},
 Q. L. Xiu^{1,42,§}, G. F. Xu^{1,§}, L. Xu^{1,§}, Q. J. Xu^{14,§}, W. Xu^{1,46,§}, X. P. Xu^{40,§}, F. Yan^{55,§},
 L. Yan^{57A,57C,§}, W. B. Yan^{54,42,§}, W. C. Yan^{2,§}, Y. H. Yan^{20,§}, H. J. Yang^{37,h,§},
 H. X. Yang^{1,§}, L. Yang^{59,§}, R. X. Yang^{54,42,§}, S. L. Yang^{1,46,§}, Y. H. Yang^{33,§},
 Y. X. Yang^{12,§}, Yifan Yang^{1,46,§}, Z. Q. Yang^{20,§}, M. Ye^{1,42,§}, M. H. Ye^{7,§}, J. H. Yin^{1,§},
 Z. Y. You^{43,§}, B. X. Yu^{1,42,46,§}, C. X. Yu^{34,§}, J. S. Yu^{20,§}, C. Z. Yuan^{1,46,§,¶},
 X. Q. Yuan^{35,§}, Y. Yuan^{1,§}, A. Yuncu^{45B,a,§}, A. A. Zafar^{56,§}, Y. Zeng^{20,§}, B. X. Zhang^{1,§},
 B. Y. Zhang^{1,42,§}, C. C. Zhang^{1,§}, D. H. Zhang^{1,§}, H. H. Zhang^{43,§}, H. Y. Zhang^{1,42,§},
 J. Zhang^{1,46,§}, J. L. Zhang^{60,§}, J. Q. Zhang^{4,§}, J. W. Zhang^{1,42,46,§}, J. Y. Zhang^{1,§},
 J. Z. Zhang^{1,46,§}, K. Zhang^{1,46,§}, L. Zhang^{44,§}, S. F. Zhang^{33,§}, T. J. Zhang^{37,h,§},
 X. Y. Zhang^{36,§}, Y. Zhang^{54,42,§}, Y. H. Zhang^{1,42,§}, Y. T. Zhang^{54,42,§}, Yang Zhang^{1,§},
 Yao Zhang^{1,§}, Yi Zhang^{9,j,§}, Yu Zhang^{46,§}, Z. H. Zhang^{6,§}, Z. P. Zhang^{54,§},
 Z. Q. Zhang^{III,¶}, Z. Y. Zhang^{59,§}, G. Zhao^{1,§}, J. W. Zhao^{1,42,§}, J. Y. Zhao^{1,46,§},
 J. Z. Zhao^{1,42,§}, Lei Zhao^{54,42,§}, Ling Zhao^{1,§}, M. G. Zhao^{34,§}, Q. Zhao^{1,§}, S. J. Zhao^{62,§},
 T. C. Zhao^{1,§}, Y. B. Zhao^{1,42,§}, Z. G. Zhao^{54,42,§}, A. Zhemchugov^{27,b,§}, B. Zheng^{55,§},
 J. P. Zheng^{1,42,§}, Y. Zheng^{35,§}, Y. H. Zheng^{46,§}, B. Zhong^{32,§}, L. Zhou^{1,42,§},
 L. P. Zhou^{1,46,§}, Q. Zhou^{1,46,§}, X. Zhou^{59,§}, X. K. Zhou^{46,§}, X. R. Zhou^{54,42,§},
 Xingyu Zhou^{2,§}, Xiaoyu Zhou^{20,§}, Xu Zhou^{20,§}, A. N. Zhu^{1,46,§}, J. Zhu^{34,§}, J. Zhu^{43,§},
 K. Zhu^{1,§}, K. J. Zhu^{1,42,46,§}, S. H. Zhu^{53,§}, W. J. Zhu^{34,§}, X. L. Zhu^{44,§}, Y. C. Zhu^{54,42,§},
 Y. S. Zhu^{1,46,§}, Z. A. Zhu^{1,46,§}, J. Zhuang^{1,42,§}, B. S. Zou^{1,§}, J. H. Zou^{1,§}

- ¹ *Institute of High Energy Physics, Beijing 100049, People's Republic of China*
- ² *Beihang University, Beijing 100191, People's Republic of China*
- ³ *Beijing Institute of Petrochemical Technology, Beijing 102617, People's Republic of China*
- ⁴ *Bochum Ruhr-University, D-44780 Bochum, Germany*
- ⁵ *Carnegie Mellon University, Pittsburgh, Pennsylvania 15213, USA*
- ⁶ *Central China Normal University, Wuhan 430079, People's Republic of China*
- ⁷ *China Center of Advanced Science and Technology, Beijing 100190, People's Republic of China*
- ⁸ *COMSATS University Islamabad, Lahore Campus, Defence Road, Off Raiwind Road, 54000 Lahore, Pakistan*
- ⁹ *Fudan University, Shanghai 200443, People's Republic of China*
- ¹⁰ *G.I. Budker Institute of Nuclear Physics SB RAS (BINP), Novosibirsk 630090, Russia*
- ¹¹ *GSI Helmholtzcentre for Heavy Ion Research GmbH, D-64291 Darmstadt, Germany*
- ¹² *Guangxi Normal University, Guilin 541004, People's Republic of China*
- ¹³ *Guangxi University, Nanning 530004, People's Republic of China*
- ¹⁴ *Hangzhou Normal University, Hangzhou 310036, People's Republic of China*
- ¹⁵ *Helmholtz Institute Mainz, Johann-Joachim-Becher-Weg 45, D-55099 Mainz, Germany*
- ¹⁶ *Henan Normal University, Xinxiang 453007, People's Republic of China*
- ¹⁷ *Henan University of Science and Technology, Luoyang 471003, People's Republic of China*
- ¹⁸ *Huangshan College, Huangshan 245000, People's Republic of China*
- ¹⁹ *Hunan Normal University, Changsha 410081, People's Republic of China*
- ²⁰ *Hunan University, Changsha 410082, People's Republic of China*
- ²¹ *Indian Institute of Technology Madras, Chennai 600036, India*
- ²² *Indiana University, Bloomington, Indiana 47405, USA*
- ²³ *(A)INFN Laboratori Nazionali di Frascati, I-00044, Frascati, Italy; (B)INFN and University of Perugia, I-06100, Perugia, Italy*
- ²⁴ *(A)INFN Sezione di Ferrara, I-44122, Ferrara, Italy; (B)University of Ferrara, I-44122, Ferrara, Italy*
- ²⁵ *Institute of Physics and Technology, Peace Ave. 54B, Ulaanbaatar 13330, Mongolia*
- ²⁶ *Johannes Gutenberg University of Mainz, Johann-Joachim-Becher-Weg 45, D-55099 Mainz, Germany*
- ²⁷ *Joint Institute for Nuclear Research, 141980 Dubna, Moscow region, Russia*
- ²⁸ *Justus-Liebig-Universitaet Giessen, II. Physikalisches Institut, Heinrich-Buff-Ring 16, D-35392 Giessen, Germany*
- ²⁹ *KVI-CART, University of Groningen, NL-9747 AA Groningen, The Netherlands*
- ³⁰ *Lanzhou University, Lanzhou 730000, People's Republic of China*
- ³¹ *Liaoning University, Shenyang 110036, People's Republic of China*
- ³² *Nanjing Normal University, Nanjing 210023, People's Republic of China*
- ³³ *Nanjing University, Nanjing 210093, People's Republic of China*
- ³⁴ *Nankai University, Tianjin 300071, People's Republic of China*
- ³⁵ *Peking University, Beijing 100871, People's Republic of China*
- ³⁶ *Shandong University, Jinan 250100, People's Republic of China*

- ³⁷ *Shanghai Jiao Tong University, Shanghai 200240, People's Republic of China*
- ³⁸ *Shanxi University, Taiyuan 030006, People's Republic of China*
- ³⁹ *Sichuan University, Chengdu 610064, People's Republic of China*
- ⁴⁰ *Soochow University, Suzhou 215006, People's Republic of China*
- ⁴¹ *Southeast University, Nanjing 211100, People's Republic of China*
- ⁴² *State Key Laboratory of Particle Detection and Electronics, Beijing 100049, Hefei 230026, People's Republic of China*
- ⁴³ *Sun Yat-Sen University, Guangzhou 510275, People's Republic of China*
- ⁴⁴ *Tsinghua University, Beijing 100084, People's Republic of China*
- ⁴⁵ *(A)Ankara University, 06100 Tandogan, Ankara, Turkey; (B)Istanbul Bilgi University, 34060 Eyup, Istanbul, Turkey; (C)Uludag University, 16059 Bursa, Turkey; (D)Near East University, Nicosia, North Cyprus, Mersin 10, Turkey*
- ⁴⁶ *University of Chinese Academy of Sciences, Beijing 100049, People's Republic of China*
- ⁴⁷ *University of Hawaii, Honolulu, Hawaii 96822, USA*
- ⁴⁸ *University of Jinan, Jinan 250022, People's Republic of China*
- ⁴⁹ *University of Manchester, Oxford Road, Manchester, M13 9PL, United Kingdom*
- ⁵⁰ *University of Minnesota, Minneapolis, Minnesota 55455, USA*
- ⁵¹ *University of Muenster, Wilhelm-Klemm-Str. 9, 48149 Muenster, Germany*
- ⁵² *University of Oxford, Keble Rd, Oxford, UK OX13RH*
- ⁵³ *University of Science and Technology Liaoning, Anshan 114051, People's Republic of China*
- ⁵⁴ *University of Science and Technology of China, Hefei 230026, People's Republic of China*
- ⁵⁵ *University of South China, Hengyang 421001, People's Republic of China*
- ⁵⁶ *University of the Punjab, Lahore-54590, Pakistan*
- ⁵⁷ *(A)University of Turin, I-10125, Turin, Italy; (B)University of Eastern Piedmont, I-15121, Alessandria, Italy; (C)INFN, I-10125, Turin, Italy*
- ⁵⁸ *Uppsala University, Box 516, SE-75120 Uppsala, Sweden*
- ⁵⁹ *Wuhan University, Wuhan 430072, People's Republic of China*
- ⁶⁰ *Xinyang Normal University, Xinyang 464000, People's Republic of China*
- ⁶¹ *Zhejiang University, Hangzhou 310027, People's Republic of China*
- ⁶² *Zhengzhou University, Zhengzhou 450001, People's Republic of China*
- ^I *Aix-Marseille Univ, Université de Toulon, CNRS, CPT, Marseille, France*
- ^{II} *Budker Institute of Nuclear Physics, SB RAS, Novosibirsk, 630090, Russia*
- ^{III} *Laboratoire de l'Accélérateur Linéaire, IN2P3-CNRS et Université Paris-Sud 11, F-91898, Orsay Cedex, France*
- ^{IV} *Laboratoire de Physique Théorique, UMR 8627, CNRS, Univ. Paris-Sud, Université Paris-Saclay, 91405 Orsay Cedex, France*
- ^V *Lebedev Physical Institute RAS, 119991 Moscow, Russia*
- ^{VI} *Institute of Physics, Academia Sinica, Taiwan 115, Republic of China*
- ^{VII} *Institute of Theoretical Physics, Beijing 100190, People's Republic of China*
- ^{VIII} *Novosibirsk State University, Novosibirsk, 630090, Russia*
- ^{IX} *University of Chicago, 5620 S. Ellis Avenue, Chicago, IL 60637, USA*

^x *Wayne State University, Detroit, MI 48201, USA*

^a *Also at Bogazici University, 34342 Istanbul, Turkey*

^b *Also at the Moscow Institute of Physics and Technology, Moscow 141700, Russia*

^c *Also at the Functional Electronics Laboratory, Tomsk State University, Tomsk, 634050, Russia*

^d *Also at the Novosibirsk State University, Novosibirsk, 630090, Russia*

^e *Also at the NRC "Kurchatov Institute", PNPI, 188300, Gatchina, Russia*

^f *Also at Istanbul Arel University, 34295 Istanbul, Turkey*

^g *Also at Goethe University Frankfurt, 60323 Frankfurt am Main, Germany*

^h *Also at Key Laboratory for Particle Physics, Astrophysics and Cosmology, Ministry of Education; Shanghai Key Laboratory for Particle Physics and Cosmology; Institute of Nuclear and Particle Physics, Shanghai 200240, People's Republic of China*

ⁱ *Also at Government College Women University, Sialkot - 51310. Punjab, Pakistan.*

^j *Also at Key Laboratory of Nuclear Physics and Ion-beam Application (MOE) and Institute of Modern Physics, Fudan University, Shanghai 200443, People's Republic of China*

^k *Also at Harvard University, Department of Physics, Cambridge, MA, 02138, USA*

★ Editor

§ BESIII collaborator

¶ External contributing author

† Correspondence: gradl@uni-mainz.de

‡ Correspondence: xiaorui@ucas.ac.cn

Correspondence: yuancz@ihep.ac.cn

Abstract

There has recently been a dramatic renewal of interest in the subjects of hadron spectroscopy and charm physics. This renaissance has been driven in part by the discovery of a plethora of charmonium-like XYZ states at BESIII and B factories, and the observation of an intriguing proton-antiproton threshold enhancement and the possibly related $X(1835)$ meson state at BESIII, as well as the threshold measurements of charm mesons and charm baryons.

We present a detailed survey of the important topics in tau-charm physics and hadron physics that can be further explored at BESIII over the remaining lifetime of BEPCII operation. This survey will help in the optimization of the data-taking plan over the coming years, and provides physics motivation for the possible upgrade of BEPCII to higher luminosity.

Working Group and Conveners

Part One: Introduction

Conveners: Mingyi Dong, Hai-Bo Li,
Shengsen Sun, Ulrich Wiedner

Part Two: Light Hadron Physics

Conveners: Shuangshi Fang, Beijiang Liu, Marc Pelizaeus,

Part Three: Charmonium Physics

Conveners: Wolfgang Kuehn, Ryan Mitchell,
Changzheng Yuan, Kai Zhu

Part Four: R values, QCD and τ Physics

Conveners: Achim Denig, Rinaldo Baldini Ferroli, Xiaohu Mo,
Christoph Florian Redmer, Karin Schoenning,
Wenbiao Yan, Jianyong Zhang

Part Five: Charm Physics

Conveners: Hai-Bo Li, Jim Libby, Xiao-Rui Lyu, Hailong Ma,
Hajime Muramatsu, Karin Schoenning

Part Six: Exotic Decays and New Physics

Conveners: Shenjian Chen, Alexey Petrov, Dayong Wang,

Part Seven: Summary

Conveners: Hai-Bo Li, Xiao-Rui Lyu, Xinchou Lou

Contents

Abstract	vii
1 Introduction	1
1.1 Motivation	1
1.2 The BESIII detector and its upgrades	2
1.2.1 Upgrade of ETOF	3
1.2.2 Upgrade of Inner MDC with a CGEM inner tracker	4
1.2.3 Upgrade of Inner Chamber with an improved inner MDC	9
1.3 BEPCII upgrades	12
Bibliography	15
2 Light Hadron Physics	17
2.1 Introduction	17
2.2 Meson spectroscopy and the search for QCD exotics	17
2.2.1 Glueballs	18
2.2.2 Hybrids	22
2.2.3 Multiquarks	23
2.3 Baryon spectroscopy	26
2.4 BESIII amplitude analysis	27
2.5 Other physics opportunities	28
2.5.1 Light meson decays	28
2.5.2 Two photon physics	29
2.6 Prospects	30
Bibliography	33
3 Charmonium Physics	37
3.1 Introduction	37
3.2 Charmonium States Below Open Charm Threshold	41
3.2.1 The Theoretical Framework	41
3.2.2 Results with the Current $\psi(3686)$ Data Set	42
3.2.3 Prospects for the Charmonium Program	43
3.3 XYZ Physics	49
3.3.1 Overview of BESIII Accomplishments	50
3.3.2 Broad Problems in XYZ Physics	54

3.3.3	Possibilities for XYZ Data Taking	56
3.3.4	Comparisons with Other Experiments	59
3.4	Summary of Data Requirements	61
Bibliography		63
4	R values, QCD and τ Physics	67
4.1	Introduction	67
4.2	BESIII measurements related to precision variables $(g - 2)_\mu$ and $\alpha_{\text{em}}(s)$	68
4.2.1	The anomalous magnetic moment of the muon, $(g - 2)_\mu$	68
4.2.2	The running of the electromagnetic fine structure constant, $\alpha_{\text{em}}(s)$	72
4.2.3	Measurement of exclusive hadronic channels via ISR	73
4.2.4	Inclusive R scan data	76
4.2.5	Measurements of meson transition form factors	78
4.3	Baryon form factors	84
4.3.1	Formalism	85
4.3.2	State of the art	86
4.3.3	Prospects with BESIII	91
4.4	Fragmentation function	93
4.5	τ physics at BESIII	94
4.5.1	Measurement of the τ mass	96
4.5.2	Some τ -physics topics at BESIII	100
4.5.3	Measurement of branching fraction of $\psi(3686) \rightarrow \tau^+ \tau^-$	102
4.5.4	Mass measurement for some hadrons	102
4.5.5	Discussion	102
4.6	Relative phase in vector charmonium decays	103
4.7	Study of $\phi(\mathbf{2170})$ with the energy scan method	103
4.8	Prospects	106
Bibliography		109
5	Charm physics	119
5.1	Introduction	119
5.2	$D^{0(+)}$ and D_s^+ physics	121
5.2.1	Leptonic decays	121
5.2.2	Semileptonic decays	126
5.2.3	Quantum-correlated measurements of D^0 hadronic decays	130
5.2.4	Impact on CKM measurements	135
5.2.5	CP violation and D mixing	137
5.2.6	CPT violation in charm mixing	137
5.2.7	Absolute measurement of hadronic decays	139
5.3	Charmed baryons	141
5.3.1	Λ_c^+ physics	141
5.3.2	Prospects in Λ_c^+ physics	142
5.3.3	Σ_c and Ξ_c physics	144
5.3.4	The EM structure of charmed baryons	145

5.4	Summary	147
Bibliography		149
6	Exotic Decays and New Physics	155
6.1	Introduction	155
6.2	Rare decays of charmonia and charmed hadrons	156
6.2.1	Weak decays of charmonia states	156
6.2.2	Rare radiative and rare leptonic $D_{(s)}$ decays	158
6.3	Symmetry test in hyperon decays	161
6.3.1	Probing CP asymmetry in hyperon decays	162
6.3.2	Constraint on BNV from $\Lambda - \bar{\Lambda}$ oscillation	166
6.3.3	More symmetry violation in hyperon decays	167
6.4	Charged Lepton Flavor (Number) Violation decays	168
6.4.1	Decays of $J/\psi, \psi(3686) \rightarrow l_1 l_2, l_1 l_2 \gamma$	170
6.4.2	$\chi_c(\eta_c) \rightarrow l_1 l_2$ via photon tagging in $\psi(3686) \rightarrow \gamma \chi_c(\eta_c)$	173
6.4.3	(radiative) Leptonic decays of $D^0 \rightarrow l_1 l_2, \gamma l_1 l_2$	174
6.4.4	CLFV and LNV $D_{(s)}$ decays with light mesons	175
6.5	Searches for light (invisible) NP particles	175
6.5.1	Physics of the Dark Sector	175
6.5.2	(radiative) Invisible decays of charmonia	178
6.5.3	Invisible decays of D mesons	178
6.5.4	Invisible decays of light mesons	179
6.6	Off-resonance searches	179
6.6.1	Rare charm production: $e^+ e^- \rightarrow D^*(2007)$	180
6.6.2	Dark photon and dark Higgs searches	181
6.6.3	Axion-Like particles	182
6.6.4	Searches for fractionally charged particles	182
Bibliography		185
7	Summary	193
Bibliography		197
	Acknowledgements	198

Chapter 1

Introduction

1.1 Motivation

The purpose of this White Paper is to examine the BESIII program [1], to consider further physics opportunities, and to plan for possible upgrades to the BEPCII accelerator and the BESIII detector [2], in order to fulfill the physics potentials with the BESIII experiment. The BESIII Yellow Book [1] documented the original plan for the BESIII physics program before its commission. The discovery of the $Z_c(3900)$ [3], followed by many experimental results on the XYZ hadrons [4–6] by BESIII, were pleasant surprises, which were not foreseen in the Yellow Book. Another surprise came from the first systematical absolute measurements of the Λ_c^+ decay properties based on threshold $\Lambda_c^+\bar{\Lambda}_c^-$ pair production [7, 8]. The physics related to the XYZ hadrons and (heavier) charmed baryons have also become focal points for the Belle II and LHCb experiments, and present exciting area for the BESIII experiment going forward. In addition to these, a full spectrum of other important experimental opportunities, as will be discussed in this White Paper, will be continually pursued by BESIII, such as light hadron spectroscopy and charmed meson physics.

The integration of quantum theory and Maxwell’s electrodynamics leads to a new, powerful theoretical scenario, *i.e.*, of quantum electrodynamics (QED), which was the first building block of what is called today the Standard Model (SM) of particle physics. Experimental progress led to the discoveries of new particles, and characterizations of their properties, which helped to develop the theoretical framework further to a common understanding of the weak and electromagnetic interactions, called electroweak theory. The modern theory of the strong interaction, called quantum chromodynamics (QCD), was modeled in a similar way on the basis of exact color SU(3) symmetry for the quarks and gluons.

Despite being so successful, several issues remain un-answered in the SM. The strong interaction only allows the existence of composite objects; free quarks and gluons have never been observed. This is called confinement, but it is far from being theoretically understood due to its non-perturbative nature. A detailed study of composite objects and their properties will shed light on this part of QCD. Furthermore, one might suspect that additional features or underlying symmetries beyond the SM might have not been discovered yet, which is usually summarized by the phrase ‘new physics’.

The hadron physics experiments in the 1970's and 1980's concentrated on studying the spectroscopy of the newly discovered hadrons containing relatively heavy charm and bottom quarks, or tried to understand specific questions in the light-hadron sector with dedicated experiments. For the heavy-quark mesons, no clearly superfluous or ambiguous hadron states have been reported. Recent discoveries of 'exotic' charmonium-like states have made the picture more complicated [9]. Furthermore, the situation has always been less straightforward for light mesons and baryons containing solely light quarks [10]. Here, the high density of states and their broad widths often make the identification and interpretation of observed signals rather ambiguous. So far the unambiguous identification and understanding of gluonic hadrons is clearly missing. However, the self-interaction of gluons is central to QCD and leads to a flux tube of gluons binding the quarks inside a hadron together. Due to the self-interaction, bound states of pure gluons (named glueballs) or their mixing with conventional mesonic state, should exist as well as so-called hybrids, where quarks and gluonic excitations contribute explicitly to the quantum numbers.

The energy regime that BESIII is operating in and the detector design allow for a detailed study of the charmonium and light-quark region. Charmonium physics received a major renewal of interest when in the 2000's many new, unexpected resonances, called X , Y and Z states [9], were discovered, that could not be accommodated by the quark model. Many of those were found by the Belle, BaBar, CDF, D0 and later the LHC experiments, but only BESIII is dedicated to the energy region where most of these states appear. It is therefore no surprise that detailed studies with much higher statistics can only be performed at BESIII. Nowadays, BESIII is one of the main contributors to the understanding of these XYZ states. At the same time, the high production cross section of charmonia at BEPCII together with a modern, almost hermetic detector for charged and neutral particles, allows also for high-precision studies of light-quark hadrons in the decay of charmonia. Since this decay into light quarks proceeds via gluons, it is likely that the desired studies of gluonic excitations may be performed at BESIII, as will be shown in this White Paper.

Despite the discovery of charm quark more than 40 years ago, many questions about charmed particles still remain unsolved [9]. An upgraded BEPCII and BESIII can make key contributions to lepton flavor universality, the unitarity of the Cabibbo-Kobayashi-Maskawa (CKM) matrix, validity of lattice QCD (LQCD), as well as theories of decay constants and form factors by studying leptonic and semileptonic decays of charmed particles. It can give insights into the applicability of QCD in low-energy nonperturbative contexts and can greatly expand our knowledge of charmed baryon properties. Open questions here include missing Λ_c decay modes (*e.g.*, those with as yet undetected neutral or excited final-state baryons) and baryon electromagnetic structure.

1.2 The BESIII detector and its upgrades

The BESIII detector and BEPCII accelerator represent major upgrades over the previous version of BES [11, 12] and BEPC [13]; the facility is used for studies of hadron physics and τ -charm physics. The BEPCII collider, installed in the same tunnel as BEPC, is a

double-ring multi-bunch collider with a design luminosity of $1 \times 10^{33} \text{ cm}^{-2}\text{s}^{-1}$ optimized at a center-of-mass (cms) energy of $2 \times 1.89 \text{ GeV}$, an increase of a factor of 100 over its predecessor. The design luminosity was reached in 2016, setting a new world record for the accelerator in this energy regime [14].

The BESIII detector is designed to fulfill the physics requirements, and the technical requirements for a high luminosity, multi-bunch collider. Detailed descriptions of the BESIII detector can be found in Ref. [2]. Figure 1.1 shows a schematic view of the BESIII detector, which covers 93% of 4π solid angle. It consists of the following components:

- A Helium-gas based drift chamber (MDC) with a single wire resolution that is better than $120 \mu\text{m}$ and a dE/dx resolution that is better than 6%. The momentum resolution in the 1.0 T magnetic field is better than 0.5% for charged tracks with a momentum of $1 \text{ GeV}/c$.
- A CsI(Tl) crystal calorimeter with an energy resolution that is better than 2.5% and position resolution better than 6 mm for 1 GeV electrons and gammas.
- A Time-of-Flight (TOF) system with an intrinsic timing resolution of 68 ps in barrel part and resolution of 110 ps in end-cap part.
- A super-conducting solenoid magnet with a central field of 1.0 Tesla.
- A 9-layer RPC-based muon chamber system with a spatial resolution that is better than 2 cm.

Details of each sub-detector and their performance, together with the trigger system, are discussed in Ref. [2].

The BESIII detector has been operating since 2009, and BEPCII has delivered around 30 fb^{-1} of integrated luminosity at different cms energies. The experiment has received several upgrades, and new upgrades for both the detector and accelerator are being considered.

1.2.1 Upgrade of ETOF

In order to improve the capability of particle identification of the BESIII experiment, the end-cap time-of-flight (ETOF) detector was upgraded with multi-gap resistive plate chamber (MRPC) technology in 2015 [15]. The MRPC is a new type of gaseous detector that has been successfully used as TOF detectors in several experiments. The new ETOF system of BESIII consists of two end-caps; each end-cap station has 36 trapezoidal shaped MRPC modules arranged in circular double layers as shown in Figs. 1.2 and 1.3. Each MRPC is divided into 12 readout strips which are read out from both ends in order to improve the timing resolution. The readout electronics system of MRPC detectors consists of FEE boards, time-to-digital conversion modules, calibration-threshold-test-power board, fast control module and a clock module in NIM crates that communicates with and is controlled by the data acquisition system. A multi-peak phenomenon in the time-over-threshold distribution is observed, and the reflection of the inductive signal at the ends of the strip is the main contribution. An empirical calibration function based on

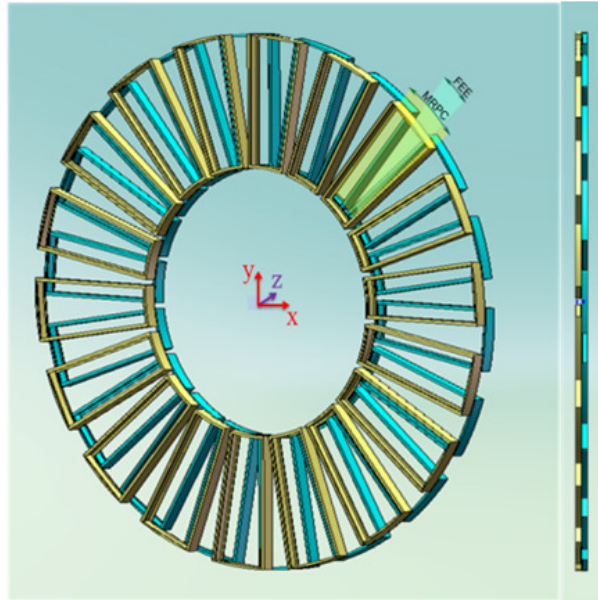


Figure 1.2: Schematic drawing of MRPC ETOF at BESIII.

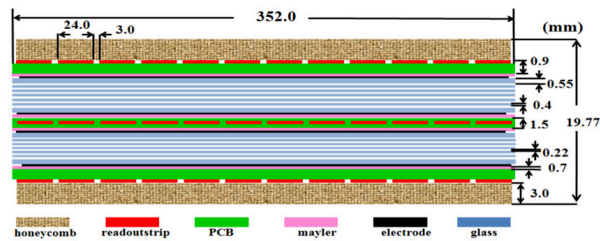


Figure 1.3: The cross-sectional view of a MRPC module along its length for the ETOF at BESIII.

Table 1.1: List of the requirements for the new inner tracker.

Value	Requirements
σ_{xy}	$\leq 130 \mu\text{m}$
σ_z	$\leq 1 \text{ mm}$
dp/p for 1 GeV/c	0.5%
Material budget	$\leq 1.5\% X_0$
Angular Coverage	$93\% \times 4\pi$
Hit Rate	10^4 Hz/cm^2
Minimum Radius	65.5 mm
Maximum Radius	180.7 mm

requirements of BESIII, as listed in Table 1.1.

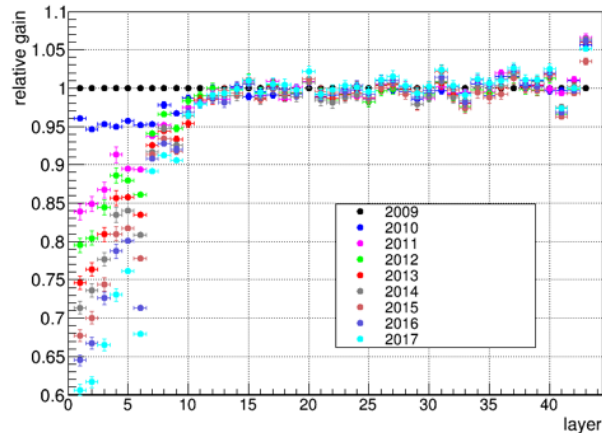


Figure 1.4: Relative gain decrease of the cells in each year as a function of the MDC layer.

The CGEM-IT consists of three layers of triple cylindrical GEM [17], shown in Fig. 1.5. Each layer is assembled with five cylindrical structures: one cathode, three GEMs and the anode readout (see Fig. 1.5) [18]. The GEMs and electrode foils are produced in planes and then shaped as cylinders. The assembly is performed inside a vertical inserting machine. To minimize the material budget, no support frames are used inside the active area and the GEM foils are mechanically stretched, being glued to Permaglass rings at their ends. The Permaglass rings are used only outside the active area to operate as gas sealing structure and gap spacers. A sandwich of a PMI foam, called Rohacell, and kapton is used in order to provide mechanical rigidity to the anode and the cathode electrodes. Rohacell is a very light material that limits the material budget to 0.3% of radiation length (X_0) per layer.

The readout anode circuit is manufactured with the $5 \mu\text{m}$ copper clad, $50 \mu\text{m}$ thick polyimide substrate. Two foils with copper segmented in strips are used to provide two-dimensional readout. The strip pitch is $650 \mu\text{m}$, with $570 \mu\text{m}$ wide X-strips parallel to CGEM axis, providing the $r - \phi$ coordinates, while the V-strips, having a stereo angle with respect to the X-strips, are $130 \mu\text{m}$ wide and, together with the other view, gives the z coordinate. The stereo angle depends on the layer geometry. A jagged-strip layout

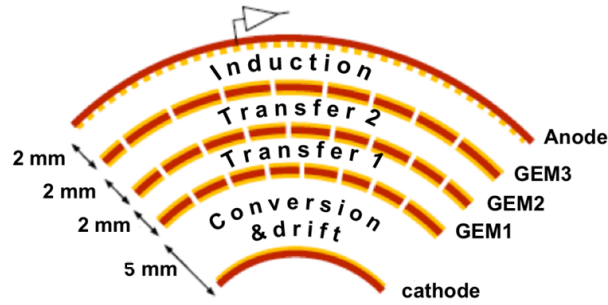


Figure 1.5: Cross-section of the triple GEM detector used for the BESIII CGEM-IT.

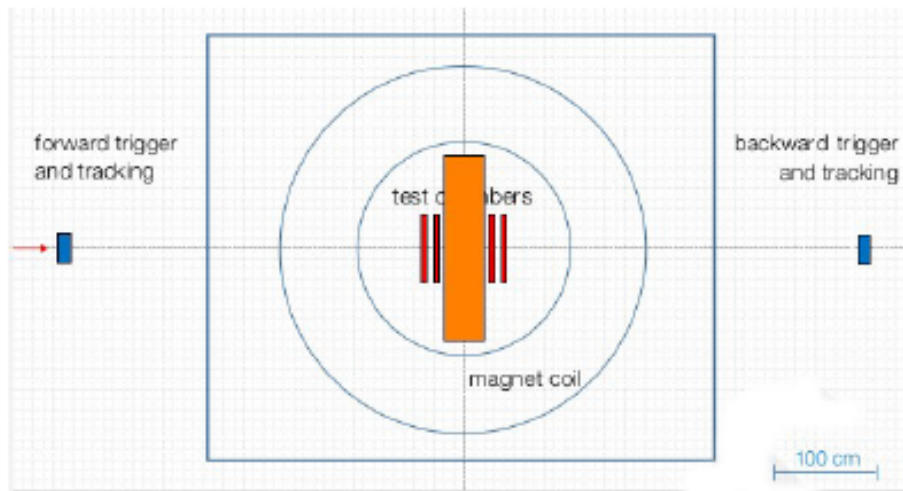


Figure 1.6: Sketch of the setup for the CGEM test beam.

is used to reduce the inter-strip capacitance up to 30%. An innovative readout based on analogue information and data-pushing architecture has been developed. A dedicated ASIC has been developed to provide time and charge information for each strip.

In order to verify that the CGEM-IT can reach the required performance, an extensive series of beam tests have been conducted in the last few years within the test beam activities of the RD51 Collaboration of CERN. The tests were performed both on $10 \times 10 \text{ cm}^2$ planar GEM chambers and on a cylindrical prototype with the dimension of the second layer of the final CGEM-IT [19]. All the tests were performed in the H4 line of the SPS, in CERN North Area. Since the CGEM-IT will operate in a magnetic field, all the test chambers were placed inside Goliath, a dipole magnet that can reach up to 1.5 T in both polarities. Pion and muon beams with momentum of 150 GeV/c were used. Two scintillators were placed upstream and downstream the magnet to operate as a trigger. A typical setup using the cylindrical prototype is shown in Fig. 1.6.

The performance of the planar GEM chambers in magnetic field was studied with the charge centroid method. The presence of an external magnetic field induces a deformation of the avalanche shape at the anode due to the Lorentz force: the charge centroid method performance degrades almost linearly with the magnetic field strength as shown in Fig. 1.7.

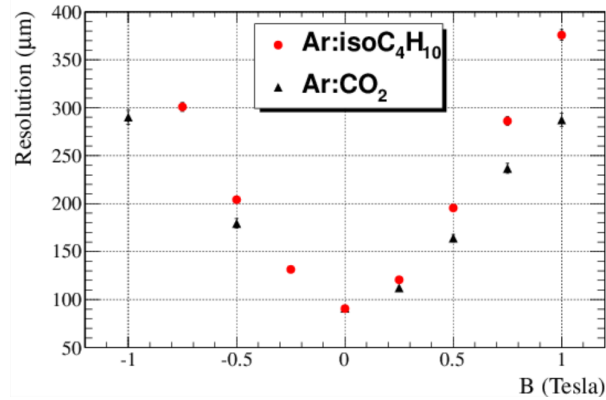


Figure 1.7: Resolution with respect to the magnetic field strength for Ar/iC₄H₁₀(90/10) and Ar/CO₂(70/30).

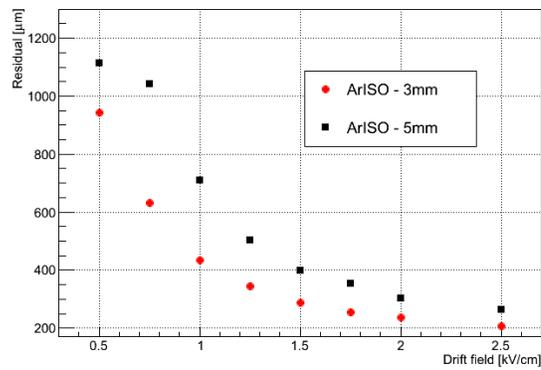


Figure 1.8: Resolution with respect to drift field in 1 T magnetic field for two different drift gaps: 3 mm drift gap and 5 mm drift gap.

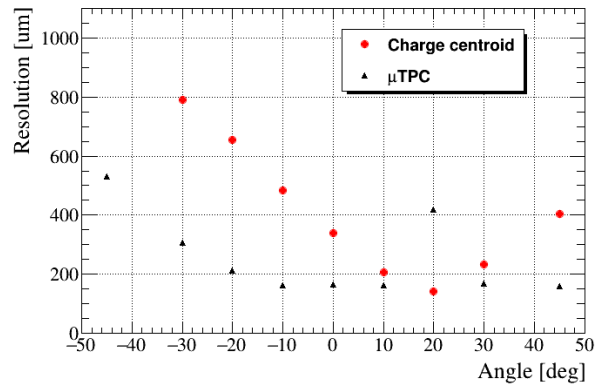


Figure 1.9: Resolution comparison between charge centroid and μ -TPC with respect to the incident angle of the track in 1 T magnetic field.

It is still possible to improve the performance by a proper optimization of the drift field as shown in Fig. 1.8. With the proper choice of gas mixture ($\text{Ar}/i\text{C}_4\text{H}_{10}(90/10)$) and drift field (2.5 kV/cm) it is possible to achieve a resolution of 190 μm in a 1 T magnetic field.

The μ -TPC is another available method for track reconstruction. It is an innovative approach that exploits the few millimeters drift gap as a Time Projection Chamber. Indeed, the time of arrival of the induced charge on the strip can be used to reconstruct the first ionization position in the drift gap and thus improve the spatial resolution. The μ -TPC method can improve and overcome the charge centroid limits granting a spatial resolution lower than 200 μm for a large angle interval, as shown in Fig. 1.9. Further studies are ongoing. By merging these two methods it will be possible for the spatial resolution of the CGEM-IT to satisfy the requirements of BESIII.

The construction of the CGEM-IT will be completed, and then a long term cosmic-ray test will be performed to evaluate the performance of the whole CGEM-IT before the replacement of the inner chamber of the MDC.

1.2.3 Upgrade of Inner Chamber with an improved inner MDC

In addition to the construction of the CGEM-IT, an improved new inner MDC has been built that can replace the aged inner part of the MDC if needed [20].

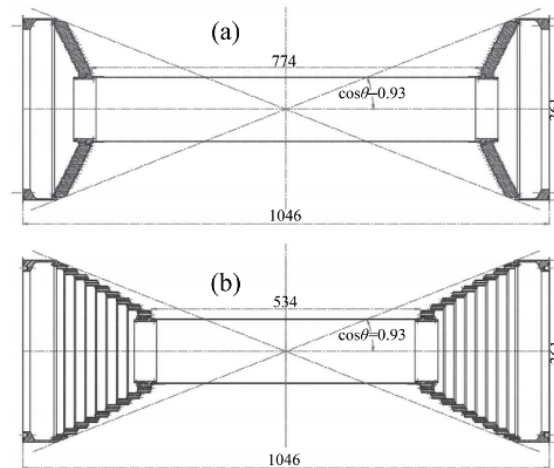


Figure 1.10: Overview of the mechanical structure of the inner MDC. (a) The old inner chamber. (b) The new inner chamber.

The new inner MDC is designed with multi-stepped end-plates. Each step contains one sense-wire layer and one field-wire layer, which can shorten the wire length exceeding the effective detection solid angle, and minimize the ineffective area in the very forward and backward region and hence reduce the background event rate of all cells, as shown in Fig. 1.10. The maximum reduction of the rate of background events is more than 30% for the first layer cells. With this design, the new inner MDC is expected to have a longer lifetime and improved performance due to the lower occupancy.

The new inner MDC is mainly composed of two multi-stepped endplates and an inner carbon fiber cylinder. The length of the new inner chamber is 1092 mm, and the radial

extent is from 59 mm to 183.5 mm, including 8 stereo sense wire layers, comprising 484 cells in total. Similar to the old chamber, the drift cells of the new chamber have a nearly square shape, as shown in Fig. 1.11. The size of each cell is about $12\text{ mm} \times 12\text{ mm}$ with a sense wire located in the center, surrounded by eight field wires. The sense wires are $25\text{ }\mu\text{m}$ gold-plated tungsten wires, while the field wires are $110\text{ }\mu\text{m}$ gold-plated aluminum wires.

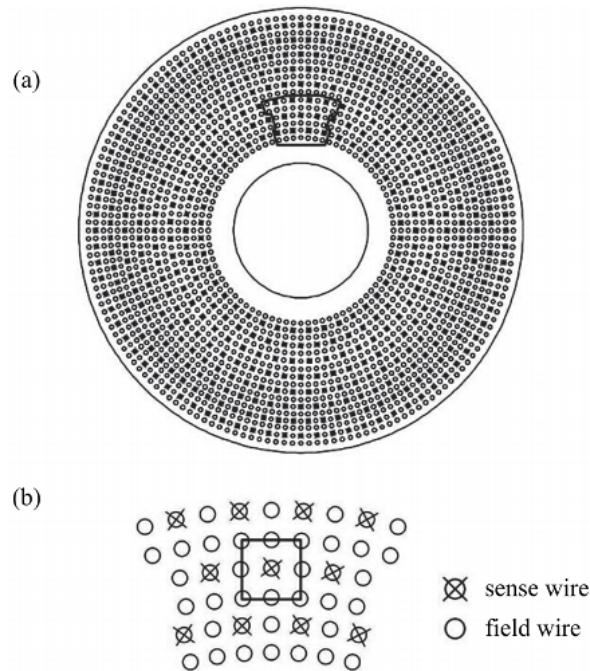


Figure 1.11: End view of the new inner chamber and the layout of the cells. (a) End view of the new inner chamber. (b) The drift cells of the chamber.

In the construction of the new inner chamber, two aluminum endplates were manufactured with an eight-step structure for each one. A total of 2096 wire holes with a diameter of 3.2 mm were drilled in each endplate with the mean value of the tolerances of $14\text{ }\mu\text{m}$. A carbon fiber inner cylinder with a thickness of 1.0 mm , was covered with two layers of $100\text{ }\mu\text{m}$ thick aluminum foils on its inner surface and outer surface respectively for electromagnetic shielding. The endplates and the cylinder were assembled with a precision better than $30\text{ }\mu\text{m}$. Wire stringing was performed after the mechanical structure was assembled. Good quality of wire stringing was achieved by monitoring the wire tension and leakage current during the stringing. The non-uniformity of wire tension was less than 10% , and the leakage current was lower than 2 nA for each wire.

After the completion of the construction of the new chamber, a cosmic-ray test without magnetic field was carried out to evaluate its performance, shown in Fig. 1.12. The results of the cosmic-ray test show that the new inner chamber achieves a spatial resolution of $127\text{ }\mu\text{m}$ and a dE/dx resolution of 6.4% , shown in Fig. 1.13 and Fig. 1.14, which satisfy the design specifications. These performances verify the successful construction of the new chamber, and now the new inner chamber is ready to be used if needed.



Figure 1.12: The cosmic-ray test of the new inner MDC.

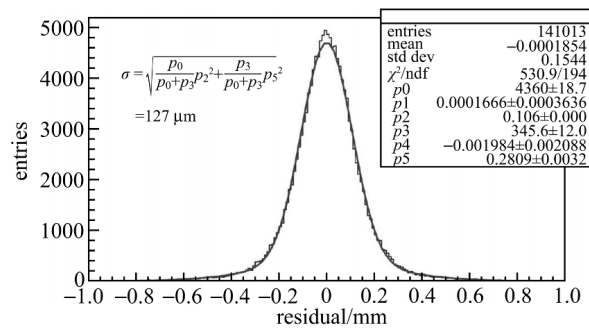
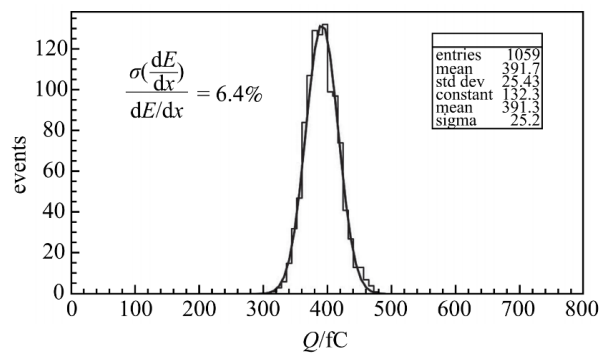


Figure 1.13: Residual distribution of the new inner MDC, showing the results of a fit with a double-Gaussian function.

Figure 1.14: The dE/dx resolution with the new inner MDC, showing the results of a fit with a single Gaussian function.

A decision on whether to install the CGEM or new inner MDC will be made, according to the results of their beam and cosmic-ray tests.

1.3 BEPCII upgrades

BEPCII delivered its first physics data in 2009 on the $\psi(3686)$ resonance. Since then, BESIII has collected about 30 fb^{-1} integrated luminosity at different energy points from 2.0 to 4.6 GeV. By using these data samples, the BESIII collaboration has published more than 270 papers, which have been making significant contributions to hadron spectroscopy, tests of various aspects of QCD, charmed hadron decays, precision test of the SM, probes of new physics beyond the SM, as well as τ mass measurement. Nowadays, the BESIII experiment plays a leading role in the study of the τ -charm energy region.

During the past 10 years of successful running, better understanding of the machine is achieved. With the increasing physics interest, two upgrade plans of BEPCII were proposed and approved. The first one is to increase the maximum beam energy up to 2.45 GeV, to expand the energy territory. The second is the top-up injection to increase the data taking efficiency. The activities of these two upgrades begin in 2017.

Before 2019, the beam energy of BEPCII ranges from 1.0 to 2.3 GeV. In order to extend the physics potential of BESIII, an upgrade project to increase the beam energy up to 2.45 GeV was initiated. In order to achieve this goal, some hardware modification are necessary, including the power supplies of dipole magnet, power supplies of special magnets in the interaction region, septum magnet and its water cooling system. These hardware modifications were completed during the summer shutdown in 2019, while the commissioning will be finished in the end of 2019. However, as expected, running at high energy region above 1.89 GeV, the beam current will decrease due to the limitation of Radio Frequency (RF) power and the difficulty in controlling the bunch length and emittance. Hence, the peak luminosity will go down with the increasing beam energy, which is shown in Fig. 1.15. In the future, it would be interesting to investigate the possibilities of slight increasing of the beam energy up to 2.5 GeV and slight decreasing down to 0.9 GeV, for the interests of studying Ξ_c and nucleon productions, respectively.

The top-up injection is a highly efficient operation scheme for the accelerator [21], which provides a nearly constant beam current. As there is no stop for beam refilling, the integrated luminosity can be increased by 20% to 30% for long data taking runs. The BEPCII upgrade of the top-up injection for the collision mode has started in September 2017. In order to obtain stable online luminosity, the beam current fluctuation is controlled within 1.5% with one e^+ injection and two e^- injections every 90 seconds, so that the variation of the instantaneous luminosity is less than 3% of its nominal value. The injection rates of the e^+ and e^- bunches must be higher than 60 mA/min and 180 mA/min, respectively. The commissioning of the top-up injection began after the summer shutdown in 2019 and finished by the end of year.

There are also discussions on further machine upgrades on luminosity. The recently proposed crab-waist collision scheme [22] is believed to be essential for the luminosity challenge in the next-generation high luminosity e^+e^- collider. The possibility of crab-waist scheme at BEPCII has been considered since 2007. However, it was found impossible

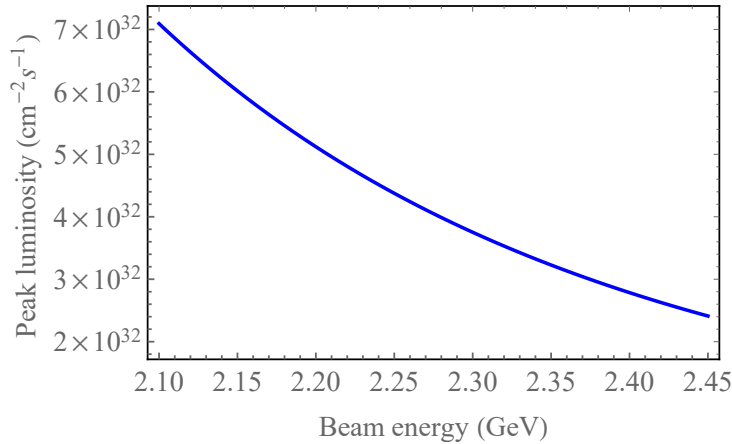


Figure 1.15: The estimation of peak luminosity of BEPCII in the energy region above 2.1 GeV.

if only minor changes on the current design are allowed. A recent upgrade proposal of BEPCII based on crab-waist scheme was discussed in detail in Ref. [23], which presents an upgrade project with the peak luminosity of $6.0 \times 10^{33} \text{ cm}^{-2}\text{s}^{-1}$. This is 10 times higher than the achieved luminosity of BEPCII at the beam energy of 2.2 GeV. The crab-waist collision with large Piwinski angle is suggested to be adopted with the parameter modifications of the BEPCII. The β functions at the interaction point would be modified from 1.0 m/1.5 cm to 0.14 m/0.8 cm in the horizontal and vertical plane, respectively. The emittance is reduced from 140 nm to 50 nm with the damping wigglers. Regarding to this proposal, a detailed design with crab-waist scheme has been studied. From the study, many physical and technical issues are investigated, such as injection, dynamic aperture, emittance coupling, high power RF, super-conducting quadrupoles/wigglers, and strong crab sextupoles etc. Finally, it is found that the crab-waist scheme is a complicated and time-consuming project and not practical with the present BESIII detector.

Another economic way to increase luminosity is by raising up beam current, which would potentially gain a factor of 2 improvement of peak luminosity. For this purpose, one needs to suppress bunch lengthening, which require higher RF voltage. The scenario of expected luminosity, beam current and SR power is shown in Fig. 1.16. The RF, cryogenic and feedback systems need to be upgraded accordingly according to the higher beam current. Nearly all the photon absorbers along the ring and some vacuum chambers also need to be replaced in order to protect the machine from heat of SR. The budget is estimated to be about 100-200 million CNY and it will take about 3 years to prepare the upgraded components and 1 year of installation and commissioning. This upgrade scheme with higher beam current is more realistic at present than the crab-waist scheme.

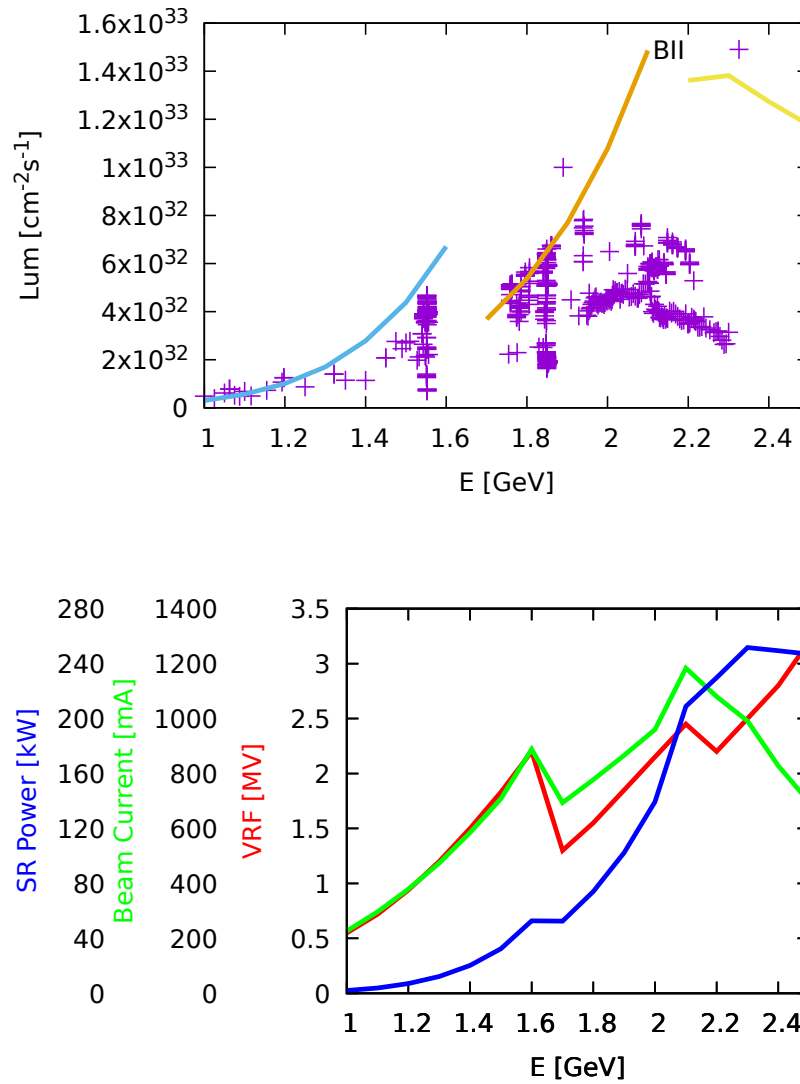


Figure 1.16: Scenario of BEPCII upgrade by increasing beam current. The lines show the expected performances after upgrade. The points in the upper plot show the achieved values of the current BEPCII.

Bibliography

- [1] D. M. Asner *et al.*, Int. J. Mod. Phys. A **24**, S1 (2009).
- [2] M. Ablikim *et al.* (BESIII Collaboration), Nucl. Instrum. Methods Phys. Res., Sect. A **614**, 345 (2010).
- [3] M. Ablikim *et al.* (BESIII Collaboration), Phys. Rev. Lett. **110**, 252001 (2013).
- [4] M. Ablikim *et al.* (BESIII Collaboration), Phys. Rev. Lett. **111**, 242001 (2013).
- [5] M. Ablikim *et al.* (BESIII Collaboration), Phys. Rev. Lett. **112**, 132001 (2014).
- [6] M. Ablikim *et al.* (BESIII Collaboration), Phys. Rev. Lett. **112**, 022001 (2014).
- [7] M. Ablikim *et al.* (BESIII Collaboration), Phys. Rev. Lett. **116**, 052001 (2016).
- [8] M. Ablikim *et al.* (BESIII Collaboration), Phys. Rev. Lett. **115**, 221805 (2015).
- [9] For recent reviews, see N. Brambilla, S. Eidelman, C. Hanhart, A. Nefediev, C. P. Shen, C. E. Thomas, A. Vairo and C. Z. Yuan, arXiv:1907.07583 [hep-ex]; F. K. Guo, C. Hanhart, U. G. Meißner, Q. Wang, Q. Zhao and B. S. Zou, Rev. Mod. Phys. **90**, 015004 (2018); H. X. Chen, W. Chen, X. Liu and S. L. Zhu, Phys. Rept. **639**, 1 (2016); N. Brambilla *et al.*, Eur. Phys. J. C **71**, 1534 (2011).
- [10] For a review, see E. Klempt and A. Zaitsev, Phys. Rept. **454**, 1 (2007).
- [11] J. Z. Bai *et al.* (BES Collaboration), Nucl. Instrum. Methods Phys. Res., Sect. A **344**, 319 (1994).
- [12] J. Z. Bai *et al.* (BES Collaboration), Nucl. Instrum. Methods Phys. Res., Sect. A **458**, 627 (2001).
- [13] M. H. Ye and Z. P. Zheng, Int. J. Mod. Phys. A **2**, 1707 (1987); S. X. Fang and S. Y. Chen, Part. Accel. **26**, 51 (1990).
- [14] <https://phys.org/news/2016-04-becpii-luminosity-world-11033cm2s.html>
- [15] P. Cao *et al.*, Nucl. Instrum. Methods Phys. Res., Sect. A (in press), doi:10.1016/j.nima.2019.163053.
- [16] M. Y. Dong *et al.*, Chin. Phys. C **40**, 016001 (2016).

- [17] F. Sauli, Nucl. Instrum. Methods Phys. Res., Sect. A **386**, 531 (1997).
- [18] A. Amoroso *et al.*, Nucl. Instrum. Methods Phys. Res., Sect. A **824**, 515 (2016).
- [19] G. Mezzadri *et al.*, PoS MPGD **2017**, 048 (2019).
- [20] Y. J. Xie *et al.*, Chin. Phys. C **40**, 096003 (2016).
- [21] M. Aiba *et al.*, Nucl. Instrum. Methods Phys. Res., Sect. A **880**, 98 (2018).
- [22] P. Raimondi, talk presented at the 2nd Workshop on Super B factory, LNF-INFN, Frascati, 2006.
- [23] A. Bogomyagkov, talk presented at the 14th International Workshop on Tau Lepton Physics, IHEP, Beijing, 2016.

Chapter 2

Light Hadron Physics

2.1 Introduction

The generally accepted theory for the strong interaction, quantum chromodynamics (QCD), remains a challenging part of the standard model in the low- and medium-energy regime. In the high energy regime, asymptotic freedom of the partons constituting hadrons allows systematic calculations in QCD using perturbation theory. In the low-energy regime where the energies are (much) smaller than a typical strong interaction scale, there are well-established theoretical methods, chiral perturbation theory (ChPT). In the intermediate-energy regime, the non-Abelian character of QCD requires a non-perturbative approach which must rely either on lattice QCD (LQCD) or on QCD-inspired models. Therefore, the study of light hadrons is central to the understanding of confinement physics.

Significant progress in the light-quark sector appeared in the last few years due to unprecedented high-statistics data sets from experiments at both electron and hadron machines. Due to the non-Abelian structure of QCD bound states beyond the constituent quark degrees of freedom, *e.g.*, multi-quark states or states with gluonic degrees of freedom (hybrids, glueballs) are expected. Their unambiguous identification and systematic study would provide a validation of and valuable input to the quantitative understanding of QCD. Over the last decade, there have been several relevant reviews [1–6] on this subject, which cover in great detail both meson spectroscopy and baryon spectroscopy.

Data with unprecedented statistical accuracy and clearly defined initial and final state properties offer BESIII great opportunities to investigate hadron spectroscopy and led to significant advances in recent years. The road map for the light hadron physics program at BESIII has already been defined, following the trajectory of endeavors over last decades [7, 8]. In this document we reiterate the physics case on the basis of achieved results.

2.2 Meson spectroscopy and the search for QCD exotics

Confinement is a unique property of QCD. The quark model describes mesons as bound states of quarks and antiquarks. LQCD and QCD-motivated models for hadrons, however,

Table 2.1: Glueball masses (in units of MeV/c^2) from the quenched [10, 11] and unquenched [12, 13] lattice QCD studies.

	m_π	$m_{0^{++}}$	$m_{2^{++}}$	$m_{0^{-+}}$
quenched Ref. [10]	—	1710(50)(80)	2390(30)(120)	2560(35)(120)
quenched Ref. [11]	—	1730(50)(80)	2400(25)(120)	2590(40)(130)
unquenched $N_f = 2$ [12]	938	1417(30)	2363(39)	2573(55)
	650	1498(58)	2384(67)	2585(65)
unquenched $N_f = 2 + 1$ [13]	360	1795(60)	2620(50)	—

predict a richer spectrum of mesons that takes into account not only the quark degrees of freedom but also the gluonic degrees of freedom. A primary goal of the BESIII experiment is to search for and study those QCD exotics or states with a composition that is different from normal mesons and baryons. Understanding these will provide critical information on the quantitative understanding of confinement.

2.2.1 Glueballs

The spectrum of glueballs is predicted by quenched LQCD [9–11] with the lightest one having scalar quantum numbers 0^{++} and a mass between $1.5 \text{ GeV}/c^2$ and $1.7 \text{ GeV}/c^2$. Also the next-higher glueball states have nonexotic quantum numbers, 2^{++} (mass 2.3 – $2.4 \text{ GeV}/c^2$) and 0^{-+} (mass 2.3 – $2.6 \text{ GeV}/c^2$), and hence will be mixed into the conventional meson spectrum and difficult to be identified experimentally. It requires systematic studies to identify a glueball by searching for outnumbering of conventional quark model states and comparing a candidates properties to the expected properties of glueballs and conventional mesons.

In a simple constituent-gluon picture, these three states correspond to two-gluon systems in a relative S wave, with different combinations of helicities. Table 2.1 summarizes the quenched and unquenched lattice results for the masses of the lightest glueballs. The masses of scalar and tensor glueballs from quenched LQCD are consistent with those obtained by $N_f = 2$ [12] and $N_f = 2 + 1$ [13] unquenched LQCD.

Glueballs are expected to appear in so-called gluon-rich environments. The radiative decays of the J/ψ meson provide such a gluon-rich environment and are therefore regarded as one of the most promising hunting grounds for glueballs. Recent LQCD calculations predict that the partial width of J/ψ radiatively decaying into the pure gauge scalar glueball is $0.35(8) \text{ keV}$, which corresponds to a branching ratio of $3.8(9) \times 10^{-3}$ [14]; the partial decay width for a tensor glueball is estimated to be $1.01(22)(10) \text{ keV}$ which corresponds to a large branching ratio $1.1(2)(1) \times 10^{-2}$ [15]; the partial decay width for a pseudoscalar glueball is estimated to be $0.0215(74) \text{ keV}$ which corresponds to a branching ratio $2.31(80) \times 10^{-4}$ [16]. With the unique advantage of high-statistics J/ψ sample, a systematics research program of glueballs has been performed at BESIII. The pseudoscalar sector draws special attention due to the small number of expected resonances of the quark

model. However, experimental input is very limited for now and the hope is in BESIII for significant improvements. In the scalar sector and tensor sector already a large number of resonances is observed. However, the nature of all of these states is still controversial, but the program at BESIII can provide crucial information to map out the scalar and tensor excitations.

The scalar mesons

A related review on the topic can be found in the section “Note on Scalar Mesons below 2 GeV” in PDG [5]. The most striking observation is that the $f_0(1370)$, $f_0(1500)$ and $f_0(1710)$ appear to be supernumerary. Many papers interpret the existence of these three scalars as a manifestation of the underlying light quarkonium nonet and the lowest-mass scalar glueball.

Challenges in the interpretation of the scalar sector involve both experimental and theoretical efforts. The following key questions account for the major differences in the models on scalar mesons and need to be addressed in the future:

- Is the $f_0(1370)$ a true $q\bar{q}$ resonance or generated by $\rho\rho$ molecular dynamics?
- Even though the fact of a supernumerary state is suggestive, the decay rates and production mechanisms are also needed to unravel the quark content of $f_0(1500)$ and $f_0(1710)$. In the partial wave analysis (PWA) of $J/\psi \rightarrow \gamma\eta\eta$ [18] and $J/\psi \rightarrow \gamma K_S K_S$ [19] at BESIII, the branching fractions of the $f_0(1710)$ are one order of magnitude larger than those of the $f_0(1500)$. With the new measurements from BESIII, the known branching fraction of $J/\psi \rightarrow \gamma f_0(1710)$ [5] is up to 1.7×10^{-3} , which is already comparable to the LQCD calculation of scalar glueball ($3.8(9) \times 10^{-3}$ [14]). The production property suggests $f_0(1710)$ has large gluonic component than $f_0(1500)$. More precise measurements of the partial decay widths in the future will improve the understanding of the internal structure of these states. A significant property of glueball decays is their expected flavor symmetric coupling to final-state hadrons, even though some modifications from phase space, the glueball wave function, and the decay mechanism are expected.
- How many distinct resonances exist around 1.7 GeV/ c^2 ? The $f_0(1710)$ and $f_0(1790)$ were observed at BES and the $X(1810)$ was observed in $J/\psi \rightarrow \gamma\omega\phi$ [20].
- What is the nature of the $f_0(2100)$? Besides $f_0(1710)$, large production of scalars around 2.1 GeV/ c^2 is also observed in $J/\psi \rightarrow \gamma\eta\eta$ [18], $J/\psi \rightarrow \gamma\pi^0\pi^0$ [21] and $J/\psi \rightarrow \gamma K_S K_S$ [19]. The pattern of production in the gluon-rich radiative J/ψ decays agrees well with that of the ground state glueball and its first excitation as predicted by LQCD. It is notable that the $f_0(2100)$ is also largely produced in $p\bar{p}$ annihilation. An additional way to unveil its nature is to measure the ratio of its decay modes into $\eta\eta'$ and $\eta'\eta'$. Furthermore, the number of existing scalars in the $f_0(2100)$ region needs clarification.

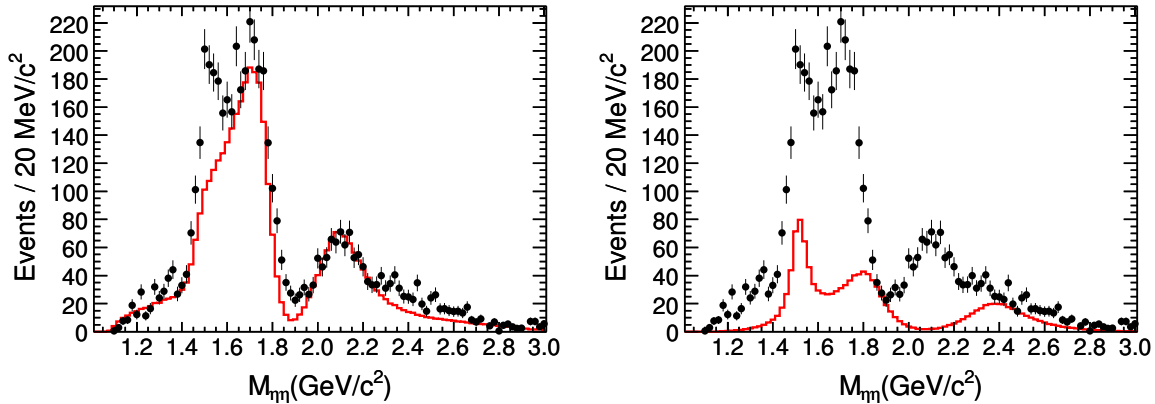


Figure 2.1: Invariant mass distribution of $\eta\eta$ from $J/\psi \rightarrow \gamma\eta\eta$, and the projection of the PWA fit from BESIII: (a) the 0^+ component, (b) the 2^+ component [18]. Dots with error bars are data. Solid histograms are the projections of the PWA fit.

The tensor mesons

Within the quark model, there are two quark configurations, the ${}^3P_2(L = 1, S = 1, J = 2)$ and the ${}^3F_2(L = 3, S = 1, J = 2)$ nonets. Hence, the tensor sector is extremely busy and there are a large number of tensor states appear in the PDG [5]. The three tensors $f_2(2010)$, $f_2(2300)$ and $f_2(2340)$ observed in $\pi^-p \rightarrow \phi\phi n$ [22] are also observed in $J/\psi \rightarrow \gamma\phi\phi$ [23]. Figure 2.1 and 2.2 show the resulting PWA fit result of the $\eta\eta$ and $\phi\phi$ invariant mass spectra. The large production rate of the $f_2(2340)$ in $J/\psi \rightarrow \gamma\phi\phi$ and $J/\psi \rightarrow \gamma\eta\eta$ [18] indicates $f_2(2340)$ is a good candidate of tensor glueball. Significant tensor contribution around $2.4 \text{ GeV}/c^2$ also presents in $J/\psi \rightarrow \gamma\pi^0\pi^0$ [21] and $J/\psi \rightarrow \gamma K_S K_S$ [19]. However, the measured production rate of $f_2(2370)$ appears to be substantially lower than the LQCD calculated value [15]. It is desirable to search for more decay modes to establish and characterize the lowest tensor glueball.

The pseudoscalar mesons

The $I = 0$ $J^{PC} = 0^{-+}$ ground states are the η and the η' . Only radial excitations are expected in the quark model for 0^{-+} states. The small number of expected pseudoscalars in the quark model provide a clean and promising environment for the search of glueballs.

A striking observation is that there are two pseudoscalar states near $1.4 \text{ GeV}/c^2$, the $\eta(1405)$ and the $\eta(1475)$, listed in the PDG [5]. The $\eta(1405)$ as a supernumerary state was proposed to be the ground state pseudoscalar glueball candidate. However, the extra state appears to be relatively far from the expected mass of the pseudoscalar glueball of $2 \text{ GeV}/c^2$. This is known as the long standing “E- ν puzzle” [24]. BESIII reported the first observation of the isospin-violating decay $\eta(1405) \rightarrow \pi^0 f_0(980)$ in $J/\psi \rightarrow \gamma 3\pi$ [25], together with an anomalous lineshape of the $f_0(980)$, as shown in Fig. 2.3. The f_0 mass, deduced from a Breit-Wigner fit to the mass spectra, is slightly shifted compared to its nominal value, with a width of $< 11.8 \text{ MeV}$ (90% C.L.), much smaller than its nominal value. The observed isospin violation is $(17.9 \pm 4.2)\%$, too large to be explained

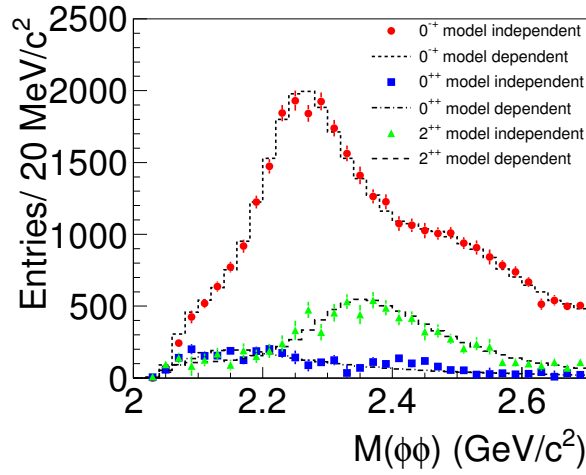


Figure 2.2: Intensities of individual J^{PC} components from the model-independent fit in the mass distribution of $\phi\phi$ from $J/\psi \rightarrow \gamma\phi\phi$, comparing with the projection of the model-dependent PWA fit from BESIII [23].

by $f_0(980)$ - $a_0(980)$ mixing, also observed by BESIII [26, 27]. Based on this observation, Wu et al. [28] suggest that a triangular singularity mixing $\eta\pi\pi$ and $K^*\bar{K}$ could be large enough to account for the data. The splitting of $\eta(1405)$ and $\eta(1475)$ could also be due to this triangle anomaly.

It is also crucial to examine carefully the existence of the $\eta(1295)$, in order to nail down the first excitation of η . Alternatively, the $\eta(1295)$ could be explained as a misidentified $f_1(1285)$.

The $X(1835)$ observed in $J/\psi \rightarrow \gamma\eta'\pi^+\pi^-$, which will be discussed in Sec. 2.2.3, is determined to have 0^{-+} quantum numbers. In the same reaction, two additional structures, the $X(2120)$ and the $X(2370)$, are observed. However, the spin-parity of these two new structures are not yet determined. $X(2370)$ is also observed in $J/\psi \rightarrow \gamma\eta'K\bar{K}$. It is crucial to explore other decay modes of $X(2370)$ and establish its spin-parity.

Aside from the $\eta(2225)$, very little is known in the pseudoscalar sector above $2 \text{ GeV}/c^2$ where the lightest pseudoscalar glueball is expected to be by LQCD calculations. A PWA of the decay $J/\psi \rightarrow \gamma\phi\phi$ [23] is performed in order to study the intermediate states. The most remarkable feature of the PWA results is that 0^{-+} states are dominant. The existence of the $\eta(2225)$ is confirmed and two additional pseudoscalar states, $\eta(2100)$ and $X(2500)$, are found.

Besides the radiative J/ψ decays, flavor filter reactions could also play an important role in unraveling the quark content of the pseudoscalars (*e.g.*, $J/\psi \rightarrow \gamma X$, $X \rightarrow \gamma V$ and $J/\psi \rightarrow VX$, where V stands for ρ , ω , ϕ and X stands for the pseudoscalars). $\eta(1475) \rightarrow \gamma\phi$ and $X(1835) \rightarrow \gamma\phi$ are observed in the decay of $J/\psi \rightarrow \gamma\gamma\phi$ at BESIII [29], which indicates that both $\eta(1475)$ and $X(1835)$ contain a sizeable $s\bar{s}$ component.

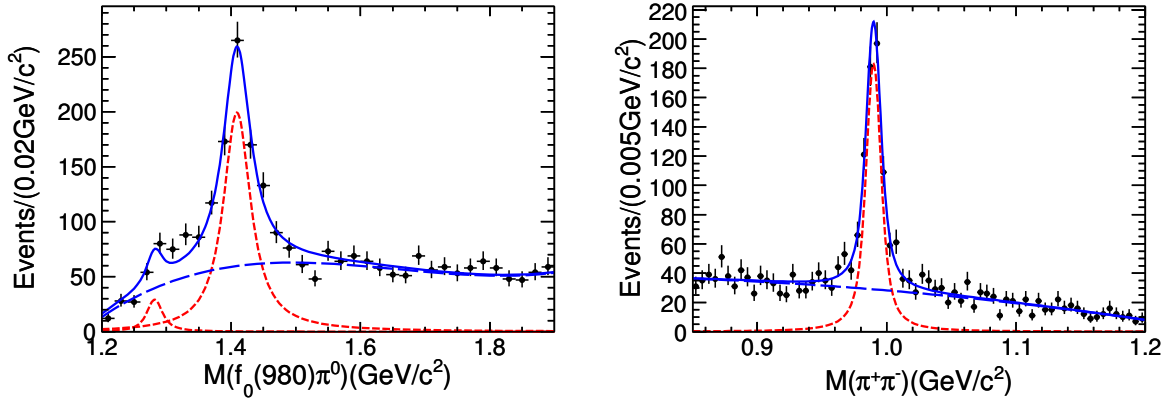


Figure 2.3: (a) Invariant mass of $f_0(980)\pi^0$; (b) Invariant mass of $\pi^+\pi^-$ with the $\pi^+\pi^-\pi^0$ ($3\pi^0$) mass in the $\eta(1405)$ mass region, measured at BESIII [25].

2.2.2 Hybrids

Since the expected quantum numbers of low-lying glueballs are not exotic, they should manifest themselves as additional states that cannot be accommodated within the $q\bar{q}$ nonets. Their unambiguous identification is complicated by the fact that they can mix when overlapping with $q\bar{q}$ states of the same quantum numbers. An easy way to avoid mixing with regular mesons are additional degrees of freedom leading to exotic quantum numbers. Such degrees of freedom could arise from explicit gluonic contributions. Those particles carry a special name and are called hybrids. In many models, some of the hybrid mesons can have a unique signature, the already mentioned exotic (not allowed in a simple $q\bar{q}$ system) J^{PC} quantum numbers. This signature simplifies the spectroscopy of such exotic hybrid mesons because they do not mix with conventional $q\bar{q}$ states. LQCD calculations support the existence of exotic-quantum-number states within the meson spectrum, independent of specific models. As shown in Fig. 2.4 [30], LQCD calculations consistently show that the $J^{PC} = 1^{-+}$ nonet is the lightest hybrid.

Currently, there are three experimental candidates for a light 1^{-+} hybrid: the $\pi_1(1400)$ and the $\pi_1(1600)$, observed in diffractive reactions and $\bar{p}N$ annihilation, and the $\pi_1(2015)$, seen only in diffraction. The $\pi_1(1400)$ has only been observed in its decay into the $\pi\eta$ final state, and is generally considered too light to be a hybrid meson. Reviews like [2, 4] provide a summary of the experimental studies.

An amplitude analysis of $\chi_{c1} \rightarrow \eta\pi^+\pi^-$ or $\chi_{c1} \rightarrow \eta'\pi^+\pi^-$ was performed at CLEO-c [31] and BESIII [32]. For these final states, the only allowed S -wave decay of the χ_{c1} goes through the spin-exotic 1^{-+} wave, which then decays to $\eta(^{\prime})\pi$. It turns out that a significant contribution of an exotic 1^{-+} wave is needed to describe the data in the $\eta'\pi^+\pi^-$ channel, but not in the $\eta\pi^+\pi^-$ channel.

While there is evidence for the isovector member of the $J^{PC} = 1^{-+}$ nonet, we also expect two isoscalar states (η_1 and η'_1), which are crucial to establish the nonet nature of the π_1 states. However, there is still no experimental evidence for these two isoscalar states. The gluon-rich radiative J/ψ decays may provide an ideal laboratory for the search for such isoscalar 1^{-+} states. Model predictions for their decay modes are $f_1\eta$, $a_1\pi$ and

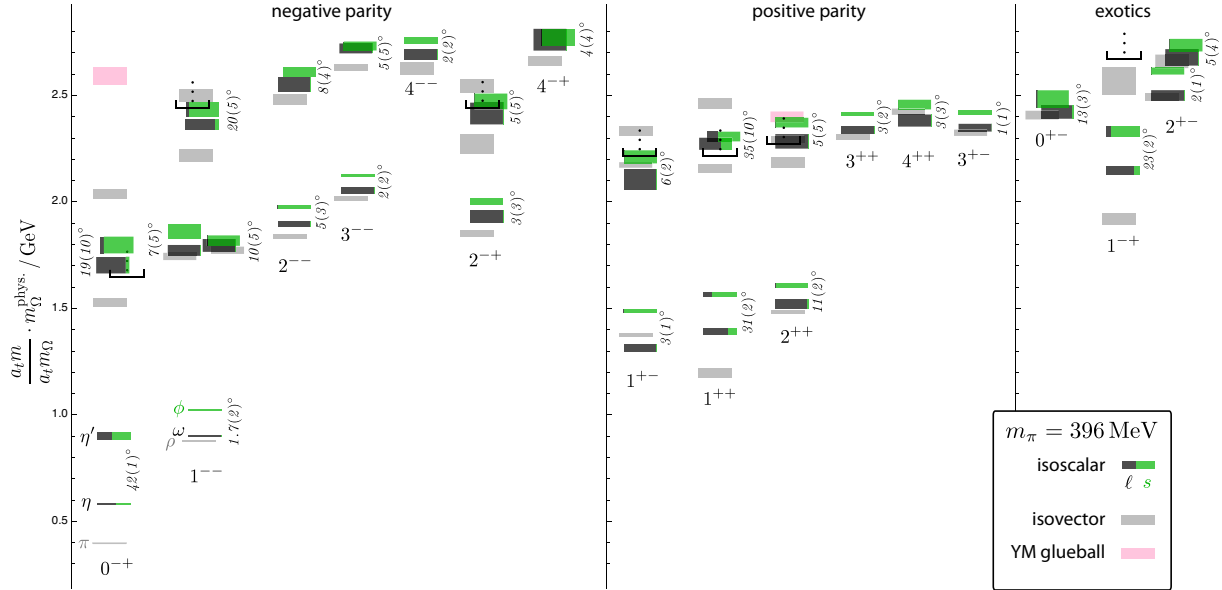


Figure 2.4: Light-quark nonstrange meson spectrum resulting from LQCD [30], sorted by the quantum numbers J^{PC} . Note that these results have been obtained with an unphysical pion mass, $m_\pi = 396$ MeV/ c^2 .

$\eta\eta'$, etc [33–36].

2.2.3 Multiquarks

An early quark model prediction was the existence of multiquark states, specifically bound meson-antimeson molecular states. In the light quark sector the $f_0(980)$ and $a_0(980)$ are considered to be strong candidates for $K\bar{K}$ molecules. However, in general, it is challenging to definitively identify a light multiquark state in an environment of many broad and often overlapping conventional states.

Two generic types of multiquark states have been often discussed. Molecular states are a loosely bound state of a pair of mesons near threshold. Tetraquarks are tightly bound diquark-antidiquark states. A prediction of tetraquark models is that they come in flavour multiplets. In addition, an enhancement near threshold may also arise from threshold effects due to rescattering of the two outgoing mesons close to the threshold. This could result in mass shifts due to the thresholds. Couple-channel effects result in the mixing of two-meson states with $q\bar{q}$ resonances.

In general, a multiquark state is expected to be broad since it can easily decay into mesons and/or baryons when its mass is above the mass threshold for producing these hadrons. Multiquark states may only be experimentally observable when their masses are near these mass thresholds either below or just above them; otherwise the multiquark states might be too wide to be experimentally distinguishable from non-resonant background.

After the discoveries of $a_0(980)$ and $f_0(980)$ several decades ago, explanations about

the nature of these two light scalar mesons have still been controversial. These two states, with similar masses but different decay modes and isospins, are difficult to accommodate in the traditional quark-antiquark model, and many alternative formulations have been proposed to explain their internal structure, including tetra-quarks [37–41], $K\bar{K}$ molecule [42], or quark-antiquark gluon hybrid [43]. Further insights into $a_0(980)$ and $f_0(980)$ are expected from their mixing [44]. The mixing mechanism in the system of $a_0(980) - f_0(980)$ is considered to be a sensitive probe to clarify the nature of these two mesons. In particular, the leading contribution to the isospin-violating mixing transition amplitudes for $f_0(980) \rightarrow a_0^0(980)$ and $a_0^0(980) \rightarrow f_0(980)$, is shown to be dominated by the difference of the unitarity cut which arises from the mass difference between the charged and neutral $K\bar{K}$ pairs. As a consequence, a narrow peak of about 8 MeV/ c^2 is predicted between the charged and neutral $K\bar{K}$ thresholds. The corresponding signal is predicted in the isospin-violating processes of $J/\psi \rightarrow \phi a_0^0(980)$ [45, 46] and $\chi_{c1} \rightarrow \pi^0 f_0(980)$ [47]. The signals of $f_0(980) \rightarrow a_0^0(980)$ and $a_0^0(980) \rightarrow f_0(980)$ mixing are first observed in $J/\psi \rightarrow \phi f_0(980) \rightarrow \phi a_0^0(980) \rightarrow \phi \eta \pi^0$ and $\chi_{c1} \rightarrow \pi^0 a_0^0(980) \rightarrow \pi^0 f_0(980) \rightarrow \pi^0 \pi^+ \pi^-$ at BESIII [26, 27]. The statistical significance of the signal versus the values of $g_{a_0 K^+ K^-}$ and $g_{f_0 K^+ K^-}$ is shown in Fig. 2.5. The regions with higher statistical significance indicate larger probability for the emergence of the two coupling constants. This direct measurement of $a_0(980) - f_0(980)$ mixing is a sensitive probe to the internal structure of those ground state scalars and sheds important light on their nature. The new results from BESIII provide critical constraints to the development of theoretical models for $a_0(980)$ and $f_0(980)$.

The state $X(1835)$ was first observed by the BES experiment as a peak in $J/\psi \rightarrow \gamma \eta' \pi^+ \pi^-$ decays [48]. This observation was later confirmed by BESIII [49]. The $X(1835)$ was also observed in the $\eta K_S^0 K_S^0$ channel, where its spin-parity was determined to be $J^P = 0^-$ by a PWA [50]. An anomalously strong enhancement at the proton-antiproton ($p\bar{p}$) mass threshold, dubbed $X(p\bar{p})$, was first observed by BES in $J/\psi \rightarrow \gamma p\bar{p}$ decays [51]; this observation was confirmed by BESIII [52] and CLEO [53]. This enhancement was subsequently determined to have spin-parity $J^P = 0^-$ by BESIII [54]. Using a high-statistics sample of J/ψ events, BESIII studied the $J/\psi \rightarrow \gamma \eta' \pi^+ \pi^-$ process and observed a significant abrupt change in the slope of the $\eta' \pi^+ \pi^-$ invariant mass distribution at the proton-antiproton ($p\bar{p}$) mass threshold [55]. Two models are used to characterize the $\eta' \pi^+ \pi^-$ line shape around 1.85 GeV/ c^2 : one which explicitly incorporates the opening of a decay threshold in the mass spectrum (Flatté formula) (Fig. 2.6(a)), and another which is the coherent sum of two resonant amplitudes (Fig. 2.6 (b)). Both fits show almost equally good agreement with data, and suggest the existence of either a broad state with strong couplings to the final state $p\bar{p}$ or a narrow state just below the $p\bar{p}$ mass threshold. The goodness-of-fit are equivalent for both fits. One supports the existence of a $p\bar{p}$ molecule-like state and the other a bound state with greater than 7σ significance. Further study of the fine lineshape of $X(1835)$ in other decay modes will provide conclusive information on the nature of the state.

An analysis of $J/\psi \rightarrow p K^- \bar{\Lambda}$ was performed at BES [56]. Enhancements both at the $p\bar{\Lambda}$ and the $K^- \bar{\Lambda}$ mass thresholds are observed. Further investigations in other decay modes and production mechanisms are needed to clarify the nature of those structures.

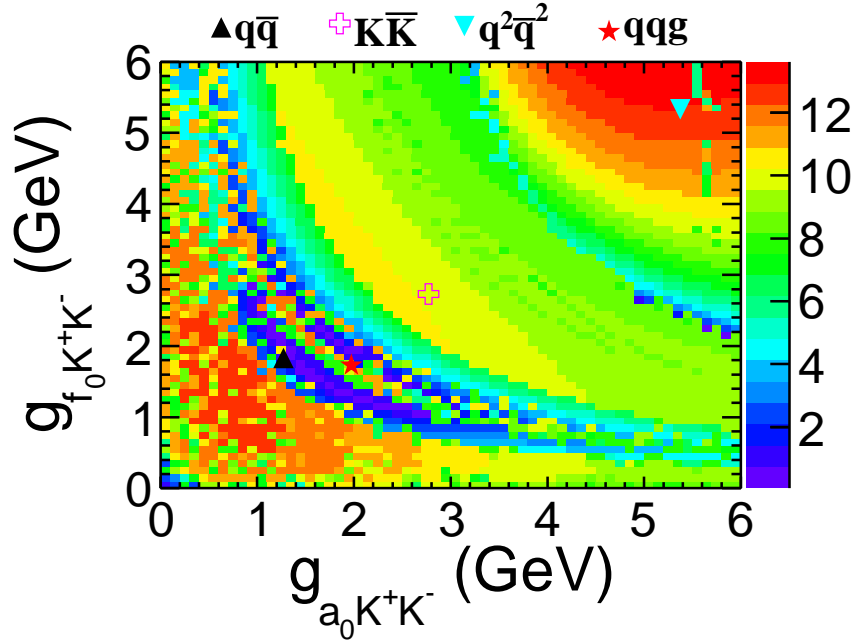


Figure 2.5: The statistical significance of the signal scanned in the two-dimensional space of $g_{a_0 K^+ K^-}$ and $g_{f_0 K^+ K^-}$. The regions with higher statistical significance indicate larger probability for the emergence of the two coupling constants. The markers indicate predictions from various illustrative theoretical models.

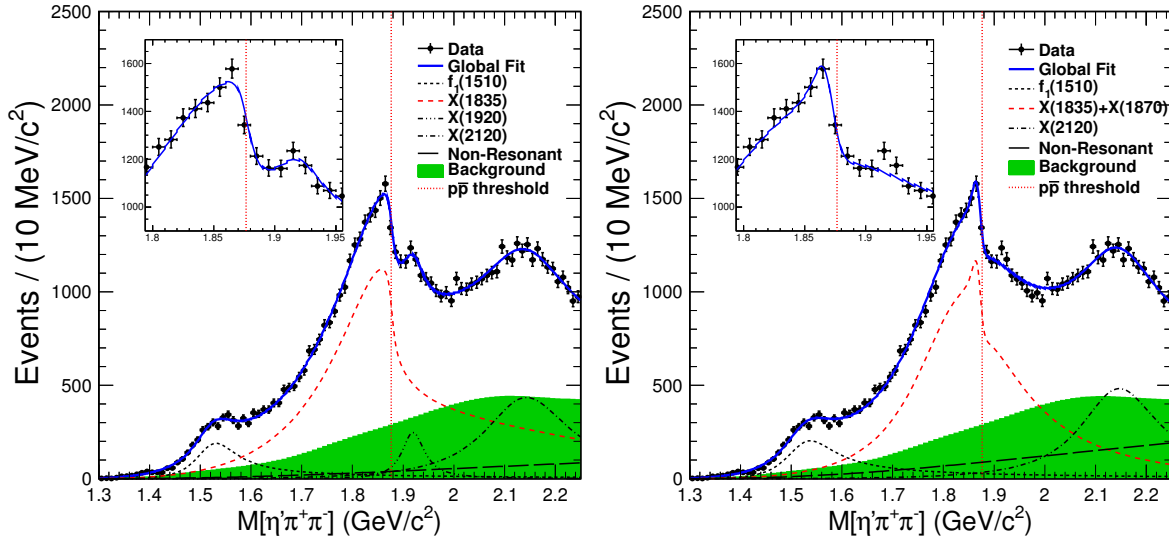


Figure 2.6: An anomalous line shape of the $\eta' \pi^+ \pi^-$ mass spectrum near the $p\bar{p}$ mass threshold in $J/\psi \rightarrow \gamma \eta' \pi^+ \pi^-$. (a) shows the fit results with a Flatté formula and (b) shows the fit results with the coherent sum of two Breit-Wigner amplitudes

2.3 Baryon spectroscopy

Baryons are the basic building blocks of our world. Since baryons represent the simplest system in which all the three colors of QCD neutralize into colorless objects, understanding the baryon structure is absolutely necessary before we claim that we really understand QCD. Given many recent experimental results, our present understanding of baryon spectroscopy is clearly incomplete. Many fundamental issues in baryon spectroscopy are still not well understood [57, 58]. Most important among them is the problem of missing resonances: in quark models based on approximate flavor SU(3) symmetry it is expected that resonances form multiplets; many excited states are predicted which have not been observed (for a review see Ref. [59]). More recently, LQCD calculations [60] have also predicted a similar pattern as quark models. The possibility of new, as yet unappreciated, effective symmetries could be addressed with the accumulation of more data. The new symmetries may not have obvious relation with QCD, just like nuclear shell model and collective motion model.

In addition to baryons made of u and d quarks, the search for hyperon resonances remains an important challenge. Some of the lowest excitation resonances have not yet been experimentally established, which are necessary to establish the spectral pattern of hyperon resonances.

Charmonium decays provide an excellent place to study excited nucleons and hyperons – N^* , Λ^* , Σ^* and Ξ^* resonances [61]. The corresponding Feynman graph for the production of these excited nucleons and hyperons is shown in Fig. 2.7 where ψ represents charmonium.

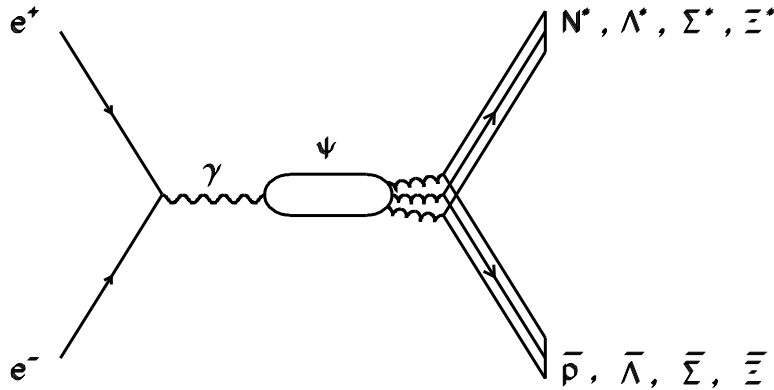


Figure 2.7: $\bar{p}N^*$, $\bar{\Lambda}\Lambda^*$, $\bar{\Sigma}\Sigma^*$ and $\bar{\Xi}\Xi^*$ production from e^+e^- collision through ψ meson.

Complementary to other facilities, the baryon program at BESIII has several advantages [62]. For instance, πN and $\pi\pi N$ systems from $\psi \rightarrow \bar{N}N\pi$ and $\bar{N}N\pi\pi$ processes have an isospin of 1/2 due to isospin conservation; ψ mesons decay to baryon-antibaryon pairs through three or more gluons providing a favorable place for producing hybrid (qqqg) baryons, and for searching for some “missing” N^* resonances which have weak coupling

to both πN and γN , but stronger coupling to $g^3 N$. The phase space of $\psi(3686)$ decays is larger than that of J/ψ decays, thus having more potential to investigate higher excitations of baryons and hyperons. In a PWA of $\psi(3686) \rightarrow p\bar{p}\pi^0$ [63], two new N^* resonances $N(2300)$ and $N(2570)$ have been observed with J^P assignments of $1/2^+$ and $5/2^-$, respectively.

Besides the high-statistics data samples of charmonium events, the large number of Λ_c hadronic decays collected at BESIII provide a novel laboratory for studying light baryon excitations.

2.4 BESIII amplitude analysis

The basic task of experimental study of hadron spectroscopy is to systematically map out all the resonances with the determination of their properties like mass, width, spin-parity as well as partial decay widths with high sensitivity and accuracy. Extracting resonance properties from experimental data is however far from straightforward; resonances tend to be broad and plentiful, leading to intricate interference patterns, or they are buried under a background in the same and in other waves. The key to success lies in high statistical precision complemented with sophisticated analysis methods. PWA or amplitude analysis techniques are the state-of-the-art way to disentangle contributions from individual, and even small, resonances and to determine their quantum numbers. Multiparticle decays are usually modeled using the phenomenological approach of the isobar model, which describes multiparticle final states by sequential two-body decays into intermediate resonances (isobars), that eventually decay into the final state observed in the experiment. Event-based fits allow one to take into account the full correlation between final-state particles.

Facing the extremely high statistics at BESIII, the PWA fits will be computationally very expensive. The pioneer approach of harnessing GPU parallel acceleration in PWA was performed in the framework of BESIII [64]. The GPUPWA framework [65] provides facilities for amplitude calculation, minimization and plotting and is widely used for analyses at BESIII. A high performance computing cluster has been established in the computing center at IHEP, which is equipped with hundreds of GPUs. In addition, for baryon spectroscopy analyses, the amplitudes can be extremely complicated. FDC-PWA, a package for automatic Feynman diagram calculation [66], has been extensively used to generate a complete set of Fortran source code for PWA amplitudes.

One notoriously difficult problem is the parameterization of the dynamical properties of resonances, especially for those resonances related to thresholds. Coupled-channel analyses are mandatory to extract the partial width and other pole properties. The correct analytical properties of the amplitude are essential for an extrapolation from the experimental data into the complex plane in order to determine the pole positions. The proper implementation of dynamical function in PWA requires cooperation between theorists and experimentalists. In the PWA of $J/\psi \rightarrow \gamma\pi^0\pi^0$ [21], $J/\psi \rightarrow \gamma K_S K_S$ [19] and $J/\psi \rightarrow \gamma\phi\phi$ [23], the results of mass-independent amplitude analysis are provided, which extract a piecewise function that describes the dynamics of the two-body meson system while making minimal assumptions about the properties and number of poles in the am-

plitude. Such a model-independent description allows the experiment-theory cooperation to develop phenomenological models, which can then be used to fit experimental data in the future. Global studies in different reactions and kinematics across experiments are also needed to clarify the underlying production mechanisms.

2.5 Other physics opportunities

2.5.1 Light meson decays

Light meson decays are an important tool for studies of the strong interaction in the non-perturbative region and for determination of some SM parameters. As the neutral members of the ground state pseudoscalar nonet, both η and η' play an important role in understanding low energy quantum chromodynamics (QCD). Decays of the η/η' probe a wide variety of physics issues, *e.g.*, $\pi^0 - \eta$ mixing, light quark masses and pion-pion scattering. In particular the η' meson, much heavier than the Goldstone bosons of broken chiral symmetry, plays a special role as the predominant singlet state arising from the strong axial $U(1)$ anomaly. In addition, the decays of both η and η' mesons are used to search for processes beyond the Standard Model (SM) and to test fundamental discrete symmetries.

The main decays of the η/η' mesons are hadronic and radiative. Alternatively, one can divide the decays into the two following classes. The first class consists of hadronic decays into three pseudoscalar mesons, such as $\eta' \rightarrow \eta\pi\pi$. Those processes are already included in the lowest order, $\mathcal{O}(p^2)$, of chiral perturbation theory (ChPT) [67]. The second class includes anomalous processes involving an odd number of pseudoscalar mesons, such as $\eta' \rightarrow \rho^0\gamma$ and $\eta' \rightarrow \pi^+\pi^-\pi^+\pi^-$. They are driven by the ‘‘Wess-Zumino-Witten’’ (WZW) term [68, 69] which enters at order $\mathcal{O}(p^4)$ order [70]. The dynamics of η' decays remains a subject of extensive studies aiming at precision tests of ChPT in the $SU_L(3) \times SU_R(3)$ sector (*i.e.*, involving an s quark). Model-dependent approaches for describing low-energy meson interactions, such as vector meson dominance (VMD) [71, 72], and the large number of colors, N_C , extensions of ChPT [73], together with dispersive methods, could be extensively tested in η' decays.

Due to the high production rate of light mesons in charmonium (*e.g.*, J/ψ) decays, the BESIII experiment also offers a unique possibility to investigate the light meson decays. The decays of $J/\psi \rightarrow \gamma\eta(\eta')$ and $J/\psi \rightarrow \phi\eta(\eta')$ provide clean and efficient sources of η/η' mesons for the decay studies. During several run periods from 2009 to 2019, a total data sample of 10^{10} J/ψ events was collected with the BESIII detector [74, 75]. In recent years much important progress on η/η' decays was achieved at the BESIII experiment. In addition to the improved accuracy of the branching fractions of η' , observations of new η' decay modes, including $\eta' \rightarrow \rho^\mp\pi^\pm$ [76] and $\eta' \rightarrow \gamma e^+e^-$ [77], $\eta' \rightarrow \pi^+\pi^-\pi^+\pi^-$, and $\eta' \rightarrow \pi^+\pi^-\pi^0\pi^0$ [78], have been reported for the first time. The precision of the $\eta' \rightarrow \pi^+\pi^-\gamma$ $M(\pi^+\pi^-)$ distribution from BESIII [79] with clear $\rho^0 - \omega$ interference is comparable to the $e^+e^- \rightarrow \pi^+\pi^-$ data and allows comparison of these two reactions in both model-dependent and model-independent ways [80, 81]. A further investigation on the extra contribution, *i.e.*, the box anomaly or $\rho(1405)$, is necessary besides the

Table 2.2: The available η/η' decays calculated with the expected 1×10^{10} J/ψ events at BESIII.

Decay Mode	$\mathcal{B} (\times 10^{-4})$ [5]	η/η' events
$J/\psi \rightarrow \gamma\eta'$	51.5 ± 1.6	5.2×10^7
$J/\psi \rightarrow \gamma\eta$	11.04 ± 0.34	1.1×10^7
$J/\psi \rightarrow \phi\eta'$	7.5 ± 0.8	7.5×10^6
$J/\psi \rightarrow \phi\eta$	4.5 ± 0.5	4.5×10^6
$J/\psi \rightarrow \omega\eta$	17.4 ± 2.0	1.7×10^7
$J/\psi \rightarrow \omega\eta'$	1.82 ± 0.21	1.8×10^6

contributions from $\rho^0(770)$ and ω . In particular a competitive extraction of the $\omega \rightarrow \pi^+\pi^-$ branching fraction is possible [82].

Despite the impressive progress, many η/η' decays are still to be observed and explored. With a sample of 10^{10} J/ψ events collected, the available η and η' events from radiative decays of $J/\psi \rightarrow \gamma\eta, \gamma\eta'$, and hadronic decays of $J/\psi \rightarrow \phi(\omega)\eta, \phi(\omega)\eta'$, are summarized in Table 2.2, making further more detailed η/η' studies possible. A list of the specific decay channels where the new data are expected to have an important impact is shown in Table 2.3.

Table 2.3: A few topics for the η and η' programs.

η decay mode	physics highlight	η' mode	physics highlight
$\eta \rightarrow \pi^0 2\gamma$	ChPT	$\eta' \rightarrow \pi\pi$	CPV
$\eta \rightarrow \gamma B$	leptophobic dark boson	$\eta' \rightarrow 2\gamma$	chiral anomaly
$\eta \rightarrow 3\pi^0$	$m_u - m_d$	$\eta' \rightarrow \gamma\pi\pi$	box anomaly, form factor
$\eta \rightarrow \pi^+\pi^-\pi^0$	$m_u - m_d, \text{ CV}$	$\eta' \rightarrow \pi^+\pi^-\pi^0$	$m_u - m_d, \text{ CV}$
$\eta \rightarrow 3\gamma$	CPV	$\eta' \rightarrow \pi^0\pi^0\eta$	cusplike effect [83]

In addition, the high production rate of ω in J/ψ hadronic decays, *e.g.*, $\mathcal{B}(J/\psi \rightarrow \omega\eta) = (1.74 \pm 0.20) \times 10^{-3}$ [5], allows one to select a clean sample of 1.7×10^7 events, which offers a unique opportunity to test the theoretical calculations [84–86] by investigating the Dalitz plot of $\omega \rightarrow \pi^+\pi^-\pi^0$.

2.5.2 Two photon physics

Production of resonances by two-photon fusion, as well as decays of resonances into two photons, provide important information on hadron structure. The anomalous magnetic moment of the muon $\alpha_\mu \equiv (g-2)_\mu/2$ is a precision observable of the Standard Model. The accuracy of the SM prediction of $(g-2)_\mu$ is currently limited by the knowledge of the hadronic light-by-light contribution. Not only contributing to the $(g-2)_\mu$ studies, the two-photon width can be used to identify non- $q\bar{q}$ states, because $\gamma\gamma$ decay of non- $q\bar{q}$ mesons like glueballs, hybrids, multiquark objects, or mesonic molecules is expected to be suppressed in various models. BESIII offers some good opportunities for precision

measurements of the production of low-mass hadronic systems in two-photon collisions with the two-photon invariant mass region accessible up to $3 \text{ GeV}/c^2$.

2.6 Prospects

Although years of continuous experimental efforts have been made to search for QCD exotic hadrons beyond quark model, no compelling evidence has been unambiguously established yet. The experimental search for QCD exotics (glueballs, hybrids, multiquarks) continues to be an exciting problem, which is limited by the current data. Recent progress in LQCD reaffirms the existence of glueballs and hybrids. Other LQCD calculations indicate that radiative J/ψ decays are a promising hunting ground for glueballs. BESIII will continue playing a leading role in this search.

High precision data and systematic studies with various production mechanisms and decay modes are needed to determine resonance properties. The primary requirement for the data taking of light hadron program at BESIII is to have sufficient high-statistics J/ψ events for the systematic study of glueballs. The pseudoscalar glueball is clearly the main focus of research with its production rate in radiative J/ψ decays predicted to be $\mathcal{O}(10^{-4})$ by LQCD. A major difficulty for the identification of glueballs is the lack of first-principle theoretical predictions of glueball couplings and decay rates. Due to the "flavour-blindness" of gluons, there will be no dominant decay mode of a glueball. The decay rate of a glueball into a certain final state may be estimated to be at the level of $\mathcal{O}(10^{-3}) \sim \mathcal{O}(10^{-2})$ in analogy to η_c or $\chi_{c0,2}$ decays. But mixing with ordinary mesons complicates the situation in the light-quark mass range. The detection efficiency of a typical decay mode of a pseudoscalar glueball is estimated to be a few percent from simulation studies. Recently, a new decay mode of $X(2370)$ has been observed in the spectrum of $\eta'K\bar{K}$ of $J/\psi \rightarrow \gamma\eta'K\bar{K}$. We performed a feasibility study for determination of the spin-parity of $X(2370)$. The neutral channel $J/\psi \rightarrow \gamma\eta'K_S^0\bar{K}_S^0$ provides a clean environment to perform the amplitude analysis as it does not suffer from significant backgrounds such as $J/\psi \rightarrow \pi^0\eta'K_S^0\bar{K}_S^0$, which are present in the charged channel $J/\psi \rightarrow \pi^0\eta'K^+K^-$. MC samples with statistics equivalent to current data and 10 billions of J/ψ are generated with a certain set of amplitude parameters. Amplitude analyses have been performed to the MC samples with various hypothesis. Table 2.4 shows that the spin-parity of $X(2370)$ can be unambiguously determined with higher statistics of data. BESIII accumulated 10 billion J/ψ events, which are mandatory for mapping out the spectrum of light hadrons in J/ψ decays. In addition, $\psi(3686)$ decays have larger phase space for studying mesons and baryons with higher mass, even though the production rates of light hadrons are typically suppressed with respect to J/ψ . η_c and χ_c events from $\psi(3686)$ decays can also provide an opportunity for investigating QCD exotics. Currently, BESIII collected 450 million of $\psi(3686)$ events. The light hadron physics program can be benefit from the high statistics $\psi(3686)$ data set for the charmonium program in the future.

In exploratory physics program for a future high luminosity τ -charm experiment, electromagnetic couplings to glueball candidates and their form factors can be further extracted with higher accuracy, which are critical in understanding the nature of glueballs. High-statistics charmonium decays also provide an opportunity for investigating low-lying

Table 2.4: A feasibility study for determination of the spin-parity of $X(2370)$ in amplitude analysis of $J/\psi \rightarrow \gamma\eta'K_S^0K_S^0$. The significance is obtained by comparing the likelihoods of amplitude analyses with different spin-parity hypothesis of $X(2370)$.

	current statistics (1.3 billions of J/ψ)	expected statistics (10 billions of J/ψ)
significance for 0^{-+} assignment of $X(2370)$	3.2σ	13.2σ

exotic hybrid nonets. In future, the available high-statistics light-meson events from decays can be used not only for some precision measurements of QCD at low energy, but also for probing physics beyond the SM.

In the next few years, many experiments (COMPASS, BESIII, etc.) will continue to be active, while a number of new experiments (GlueX, Belle II, PANDA, etc.) appear on the horizon. Definitive conclusions on the nature of confinement will need complementary studies with these experiments. Key features of these experiments are high statistics and high sensitivity to explore hadron spectroscopy. COMPASS [87] has comprehensively studied a_J and π_J -like mesons up to masses of $2 \text{ GeV}/c^2$ in diffractive scattering of hadron beams. GlueX [88] is designed to search for and measure the spectrum of light-mass hybrid mesons. It began its physics run in 2017 and will start a high luminosity run with an updated detector in 2019. An important advantage of this experiment is the use of polarized photons, which simplifies the initial states and production process. PANDA [89] is designed for high-precision studies of the hadron spectrum at cms energies between 2.3 and 5.5 GeV. It is scheduled to start data taking with full setup in 2026. In $\bar{p}p$ annihilations, spin-exotic states (*e.g.*, oddballs) can be produced. Belle II [72] will start collecting data in 2019, and will accumulate 50 ab^{-1} data at the $\Upsilon(4S)$ peak by 2027. Although not its primary goal as a next generation flavour factory, Belle II can also explore the light quark sector using the two-photon process, because a glueball should have suppressed couplings to $\gamma\gamma$. Hadronic decays of heavy hadrons may also serve as a well-defined source for light mesons. BESIII remains unique for studying and searching for QCD exotics and new excited baryons, as its high-statistics data sets of charmonia provide a gluon rich environment with clearly defined initial and final state properties.

Bibliography

- [1] N. Brambilla *et al.*, Eur. Phys. J. C **74**, 2981 (2014).
- [2] C. A. Meyer and Y. Van Haarlem, Phys. Rev. C **82**, 025208 (2010).
- [3] V. Crede and C. A. Meyer, Prog. Part. Nucl. Phys. **63**, 74 (2009).
- [4] E. Klempt and A. Zaitsev, Phys. Rept. **454**, 1 (2007).
- [5] C. Amsler and N. A. Tornqvist, Phys. Rept. **389**, 61 (2004).
- [6] S. Godfrey and J. Napolitano, Rev. Mod. Phys. **71**, 1411 (1999).
- [7] L. Kopke and N. Wermes, Phys. Rept. **174**, 67 (1989).
- [8] K. T. Chao and Y. F. Wang, Int. J. Mod. Phys. A **24**, suppl. 1 (2009).
- [9] G. S. Bali *et al.* (UKQCD Collaboration), Phys. Lett. B **309**, 378 (1993).
- [10] C. J. Morningstar and M. J. Peardon, Phys. Rev. D **60**, 034509 (1999).
- [11] Y. Chen *et al.*, Phys. Rev. D **73**, 014516 (2006).
- [12] W. Sun *et al.*, Chin. Phys. C **42**, 093103 (2018) .
- [13] E. Gregory *et al.*, JHEP **1210**, 170 (2012).
- [14] L. C. Gui *et al.* (CLQCD Collaboration), Phys. Rev. Lett. **110**, 021601 (2013).
- [15] Y. B. Yang *et al.* (CLQCD Collaboration), Phys. Rev. Lett. **111**, 091601 (2013).
- [16] L. C. Gui, J. M. Dong, Y. Chen and Y. B. Yang, arXiv:1906.03666 [hep-lat].
- [17] M. Tanabashi *et al.* (Particle Data Group), Phys. Rev. D **98**, 030001 (2018).
- [18] M. Ablikim *et al.* (BESIII Collaboration), Phys. Rev. D **87**, 092009 (2013); Erratum: [Phys. Rev. D **87**, 119901 (2013)].
- [19] M. Ablikim *et al.* (BESIII Collaboration), Phys. Rev. D **98**, 072003 (2018).
- [20] M. Ablikim *et al.* (BESIII Collaboration), Phys. Rev. D **87**, 032008 (2013).
- [21] M. Ablikim *et al.* (BESIII Collaboration), Phys. Rev. D **92** 052003 (2015); Erratum: [Phys. Rev. D **93**, 039906 (2016)].

- [22] A. Etkin *et al.*, Phys. Rev. Lett. **41**, 784 (1978); Phys. Lett. B **165**, 217 (1985); Phys. Lett. B **201**, 568 (1988).
- [23] M. Ablikim *et al.* (BESIII Collaboration), Phys. Rev. D **93**, 112011 (2016).
- [24] A. Masoni, C. Cicalo and G. L. Usai,
- [25] M. Ablikim *et al.* (BESIII Collaboration), Phys. Rev. Lett. **108**, 182001 (2012).
- [26] M. Ablikim *et al.* (BESIII Collaboration), Phys. Rev. D **83**, 032003 (2011).
- [27] M. Ablikim *et al.* (BESIII Collaboration), Phys. Rev. Lett. **121**, 022001 (2018).
- [28] J. J. Wu, X. H. Liu, Q. Zhao and B. S. Zou, Phys. Rev. Lett. **108**, 081803 (2012).
- [29] M. Ablikim *et al.* (BESIII Collaboration), Phys. Rev. D **97**, 051101 (2018).
- [30] J. J. Dudek *et al.*, Phys. Rev. D **83**, 111502 (2011).
- [31] G. S. Adams *et al.* (CLEO Collaboration), Phys. Rev. D **84**, 112009 (2011).
- [32] M. Ablikim *et al.* (BESIII Collaboration), Phys. Rev. D **95**, 032002 (2017).
- [33] N. Isgur, R. Kokoski and J. Paton, Phys. Rev. Lett. **54**, 869 (1985)
- [34] P. R. Page, E. S. Swanson and A. P. Szczepaniak, Phys. Rev. D **59**, 034016 (1999)
- [35] P. Z. Huang, H. X. Chen and S. L. Zhu, Phys. Rev. D **83**, 014021 (2011)
- [36] H. X. Chen, Z. X. Cai, P. Z. Huang and S. L. Zhu, Phys. Rev. D **83**, 014006 (2011)
- [37] R. L. Jaffe, Phys. Rev. D **15**, 267 (1977).
- [38] M. G. Alford and R. L. Jaffe, Nucl. Phys. B **578**, 367 (2000).
- [39] L. Maiani, F. Piccinini, A. D. Polosa and V. Riquer, Phys. Rev. Lett. **93**, 212002 (2004).
- [40] L. Maiani, A. D. Polosa and V. Riquer, Phys. Lett. B **651**, 129 (2007).
- [41] G. 't Hooft, G. Isidori, L. Maiani, A. D. Polosa and V. Riquer, Phys. Lett. B **662**, 424 (2008).
- [42] J. D. Weinstein and N. Isgur, Phys. Rev. D **41**, 2236 (1990).
- [43] S. Ishida *et al.*, in Proceedings of the 6th International Conference on Hadron Spectroscopy, Manchester, United Kingdom, 1995 (World Scientific, Singapore, 1995), p.454.
- [44] N. N. Achasov, S. A. Devyanin and G. N. Shestakov, Phys. Lett. **88B**, 367 (1979).
- [45] J. J. Wu, Q. Zhao and B. S. Zou, Phys. Rev. D **75**, 114012 (2007).

- [46] C. Hanhart, B. Kubis and J. R. Pelaez, Phys. Rev. D **76**, 074028 (2007).
- [47] J. J. Wu and B. S. Zou, Phys. Rev. D **78**, 074017 (2008).
- [48] M. Ablikim *et al.* (BES Collaboration), Phys. Rev. Lett. **95**, 262001 (2005).
- [49] M. Ablikim *et al.* (BESIII Collaboration), Phys. Rev. Lett. **106**, 072002 (2011).
- [50] M. Ablikim *et al.* (BESIII Collaboration), Phys. Rev. Lett. **115**, 091803 (2015).
- [51] J. Z. Bai *et al.* (BES Collaboration), Phys. Rev. Lett. **91**, 022001 (2003).
- [52] M. Ablikim *et al.* (BESIII Collaboration), Chin. Phys. C **34**, 421 (2010).
- [53] J. P. Alexander *et al.* (CLEO Collaboration), Phys. Rev. D **82**, 092002 (2010).
- [54] M. Ablikim *et al.* (BESIII Collaboration), Phys. Rev. Lett. **108**, 112003 (2012).
- [55] M. Ablikim *et al.* (BESIII Collaboration), Phys. Rev. Lett. **117**, 042002 (2016).
- [56] M. Ablikim *et al.* (BES Collaboration), Phys. Rev. Lett. **93**, 112002 (2004).
- [57] S. Capstick *et al.*, arXiv:hep-ph/0012238.
- [58] E. Klempt and J. M. Richard, Rev. Mod. Phys. **82**, 1095 (2010).
- [59] S. Capstick and W. Roberts, Prog. Part. Nucl. Phys. **45**, S241 (2000).
- [60] R. G. Edwards, J. J. Dudek, D. G. Richards and S. J. Wallace, Phys. Rev. D **84**, 074508 (2011).
- [61] B. -S. Zou, Nucl. Phys. A **684**, 330 (2001).
- [62] B. S. Zou *et al.* (BES Collaboration), PiN Newslett. **16**, 174 (2002).
- [63] M. Ablikim *et al.* (BESIII Collaboration), Phys. Rev. Lett. **110**, 022001 (2013).
- [64] M. Battaglieri *et al.*, Acta Phys. Polon. B **46**, 257 (2015).
- [65] N. Berger, L. Bei Jiang and W. Jike, J. Phys. Conf. Ser. **219**, 042031 (2010).
- [66] J. X. Wang, Nucl. Instrum. Methods Phys. Res., Sect. A **534**, 241 (2004).
- [67] J. Gasser and H. Leutwyler, Annals Phys. **158**, 142 (1984).
- [68] J. Wess and B. Zumino, Phys. Lett. B **37**, 95 (1971).
- [69] E. Witten, Nucl. Phys. B **223**, 422 (1983).
- [70] J. Bijnens, A. Bramon and F. Cornet, Z. Phys. C **46**, 599 (1990).
- [71] J. J. Sakurai, Annals Phys. **11**, 1 (1960).

- [72] L. G. Landsberg, Phys. Rept. **128**, 301 (1985).
- [73] R. Kaiser and H. Leutwyler, Eur. Phys. J. C **17**, 623 (2000).
- [74] M. Ablikim *et al.* (BESIII Collaboration), Chin. Phys. C **36**, 915 (2012).
- [75] M. Ablikim *et al.* (BESIII Collaboration), Chin. Phys. C **41**, 013001 (2017).
- [76] M. Ablikim *et al.* (BESIII Collaboration), Phys. Rev. Lett. **118**, 012001 (2017).
- [77] M. Ablikim *et al.* (BESIII Collaboration), Phys. Rev. D **92**, 012001 (2015).
- [78] M. Ablikim *et al.* (BESIII Collaboration), Phys. Rev. Lett. **112**, 251801 (2014);
Addendum: [Phys. Rev. Lett. **113**, 039903 (2014)].
- [79] M. Ablikim *et al.* (BESIII Collaboration), Phys. Rev. Lett. **120**, 242003 (2018).
- [80] B. Kubis and J. Plenter, Eur. Phys. J. C **75**, 283 (2015).
- [81] F. Stollenwerk, C. Hanhart, A. Kupsc, U. G. Meissner and A. Wirzba, Phys. Lett. B **707**, 184 (2012).
- [82] C. Hanhart, S. Holz, B. Kubis and A. Kup, A. Wirzba and C. W. Xiao, Eur. Phys. J. C **77**, 98 (2017); Erratum: Eur. Phys. J. C **78**, 450 (2018).
- [83] B. Kubis and S. P. Schneider, Eur. Phys. J. C **62**, 511 (2009).
- [84] F. Niecknig, B. Kubis, and S. P. Schneider, Eur. Phys. J. C **72**, 2014 (2012).
- [85] I. V. Danilkin *et al.*, Phys. Rev. D **91**, 094029 (2015).
- [86] C. Terschlusen, B. Strandberg, S. Leupold, and F. Eichstadt, Eur. Phys. J. A **49**, 116 (2013).
- [87] F. Gautheron *et al.* (COMPASS Collaboration), SPSC-P-340, CERN-SPSC-2010-014.
- [88] P. Eugenio, PoS ConfinementX, 349 (2012).
- [89] M. F. M. Lutz *et al.* (PANDA Collaboration), arXiv:0903.3905 [hep-ex].
- [90] T. Abe *et al.* (Belle II Collaboration), arXiv:1011.0352 [physics.ins-det]; E. Kou *et al.*, arXiv:1808.10567 [hep-ex].

Chapter 3

Charmonium Physics

3.1 Introduction

Heavy quarkonia are frequently referred to as the “positronium of QCD” [1] due to consistent, one-to-one correspondence of the level schemes that reflect Coulomb-like interactions at small distances. Within the BESIII energy range, charmonium states both below and above the open charm threshold are accessible (Figs. 3.1 and 3.2). The spectrum of charmonium states with masses below the open charm threshold has been well-established for several decades. These states can therefore be used to precisely test predictions based on various theoretical techniques, ranging from models (like the quark model) to approximations of QCD (like non-relativistic QCD, described below) to numerical calculations of the full QCD Lagrangian (*i.e.*, LQCD). The fact that the energy scales range from the charmonium mass to Λ_{QCD} in charmonium processes make them a rich laboratory to probe both perturbative and non-perturbative QCD [2].

The relative simplicity of the lowest-lying (least massive) charmonium states allows for precision tests of QCD and QCD-inspired models in a region where both non-perturbative and perturbative aspects of QCD play a role. The higher-mass states, on the other hand, pose serious challenges even to our qualitative understanding of mesons. Several of these states provide potential evidence for a wealth of exotic configurations of quarks and gluons, including: tetraquark states (two quarks and two antiquarks), hadronic molecules (two hadrons), hybrid mesons (a quark and antiquark with an excited gluonic field), and so on.

The charmonium group studies both of these regions of the charmonium spectrum, providing a unique and important look at the dynamics of strong force physics. These studies include: searching for new charmonium states, determining the internal structure of previously established charmonium states, measuring masses and widths, precisely measuring transitions (both radiative and hadronic) between charmonium states, and finding new decay channels. The capabilities of the BESIII experiment are uniquely suited to the study of both light and heavy charmonium states. The lighter charmonium states are primarily studied using large and clean samples of $\psi(3686)$ (*i.e.*, $\psi(2S)$ or ψ') decays; the heavy charmonium states are produced using higher-energy collisions, where exotic charmonium states are either produced directly or through the decays of other states.

As noted above, the spectrum of states above open charm threshold (Figs. 3.1 and 3.2) are clearly quite convoluted. The past decade has seen the discovery of a large number of new states that are yet to be satisfactorily understood. These states have been named “X”, “Y”, and “Z” since their internal structure is still unclear[§]. One thing is clear: these new states cannot all be conventional bound states of a charm quark and antiquark. They are likely evidence for more exotic configurations of quarks and gluons (such as tetraquarks, meson molecules, or hybrid mesons, etc.). Their existence therefore provides a crucial opportunity to study the dynamics of quarks and gluons in a new environment. At BESIII, the accessible e^+e^- cms energies allow us to directly produce a large number of these states, which in turn allows us to measure their masses, widths, and decay modes. The effort to understand these new states (which we refer to as “XYZ physics”) is described further in Sec. 3.3.

Future studies of the charmonium system, both above and below open-charm threshold, will require additional data sets. These requirements will be detailed throughout this chapter and summarized in Sec. 3.4. For further studies of charmonium below open-charm threshold, around 3 billion $\psi(3686)$ decays are required, representing about an order-of-magnitude increase in statistics over the current sample of about 450 million $\psi(3686)$ decays. Above open-charm threshold, we require three types of additional data samples: (1) a large number of additional data samples, each with an integrated luminosity of approximately 500 pb^{-1} and spread over a variety of cms energies, in order to study the spectrum of the Y states and to study the evolution of the Z states; (2) a small number of larger data samples, each composed of approximately 5 fb^{-1} , to do detailed studies of the Z states; and (3) samples of higher-energy data to explore the poorly established mass region above $4.6 \text{ GeV}/c^2$, where mysterious peaks in the $\Lambda_c^+\bar{\Lambda}_c^-$ [4] and $\pi^+\pi^-\psi(2S)$ cross sections [5] have been observed.

[§] The “Y” states usually have $J^{PC} = 1^{--}$; the “Z” states are electrically charged; and the “X” states are the remainder. Note that the naming scheme is revised in the latest edition of the Review of Particle Physics by PDG [3], but we use the older scheme in this White Paper for consistency.

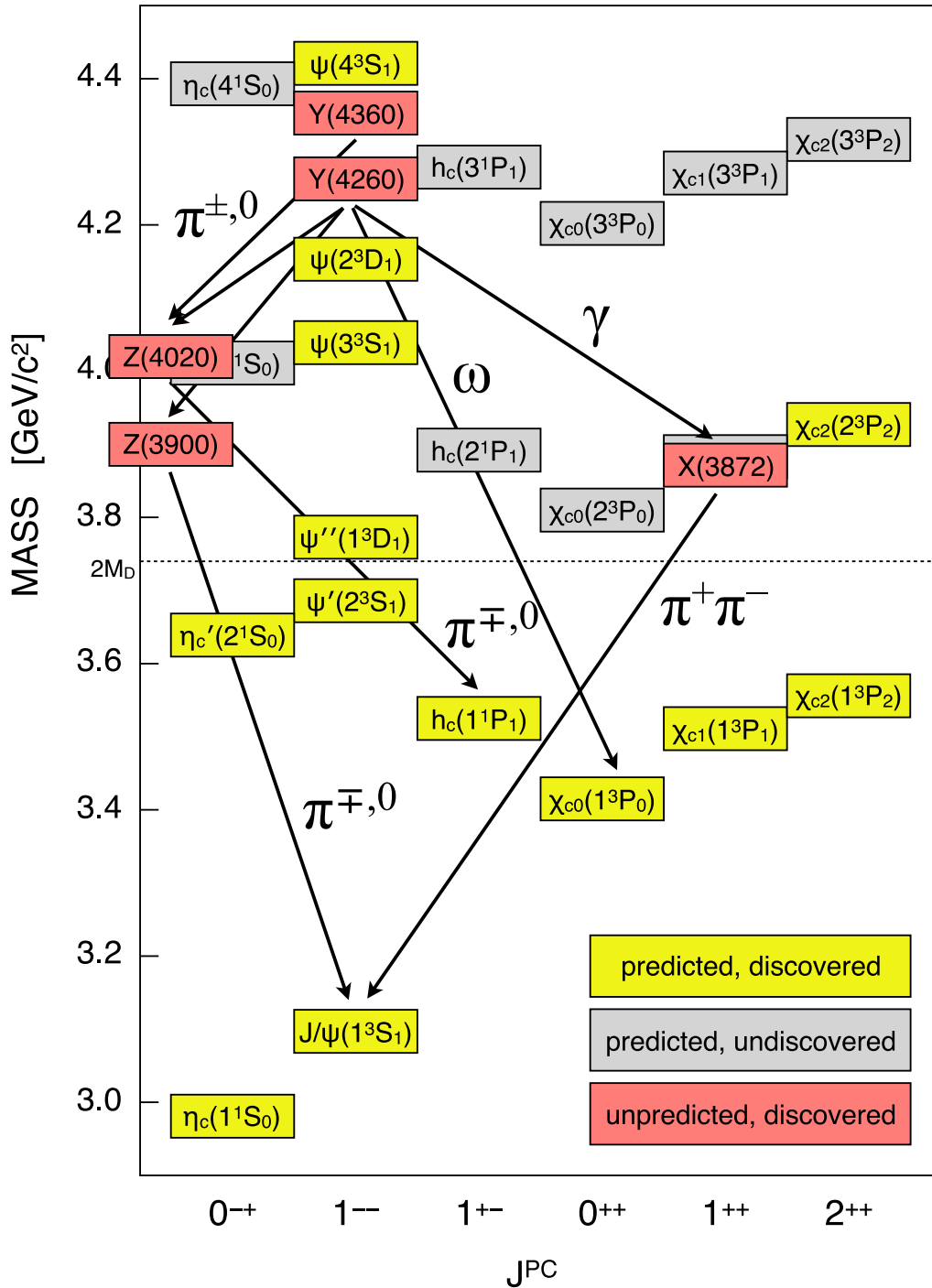


Figure 3.1: The charmonium spectrum. Yellow boxes denote states predicted by the quark model [6] that have already been discovered; gray boxes are for predicted states that have not yet been discovered; and the red boxes are for states that were unexpectedly discovered – likely pointing towards the existence of exotic hadrons. All of these states have been studied at BESIII. A few of the key transitions studied at BESIII are indicated by black arrows.

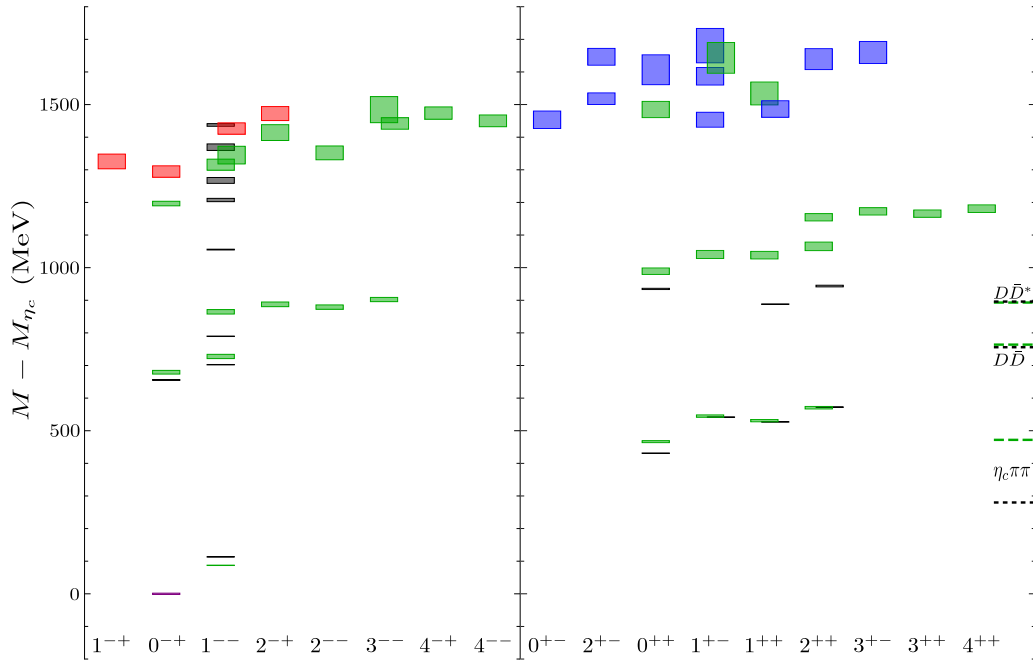


Figure 3.2: The charmonium and hybrid spectrum. Green boxes represent masses of charmonium states calculated by lattice QCD with $M_\pi \sim 240$ MeV [7]; red and blue boxes represent the lightest and first-excited hybrid states; black boxes are world averaged experimental results in 2015 [8]; dashed lines show the location of some lower thresholds for strong decay from computing (coarse green) or experiments (fine grey). The states are labeled with their quantum numbers J^{PC} and their masses are shown with η_c mass subtracted. The vertical size of the boxes denote the standard uncertainty.

3.2 Charmonium States Below Open Charm Threshold

The goal of BESIII studies of charmonium states below the open charm threshold is to investigate the spectroscopy, transitions, and decays of charmonium states by mainly analyzing (but not limited to) the $\psi(3686)$ data. The $\psi(3686)$ data is especially well suited for the study of charmonium states due to many transitions between the $\psi(3686)$ and lower-lying states. Thus, starting with a sample of $\psi(3686)$ data, one gains access to most of the charmonium states below open-charm threshold. Figure 3.3 shows the low-lying charmonium ($c\bar{c}$) spectrum and some of the commonly observed transitions.

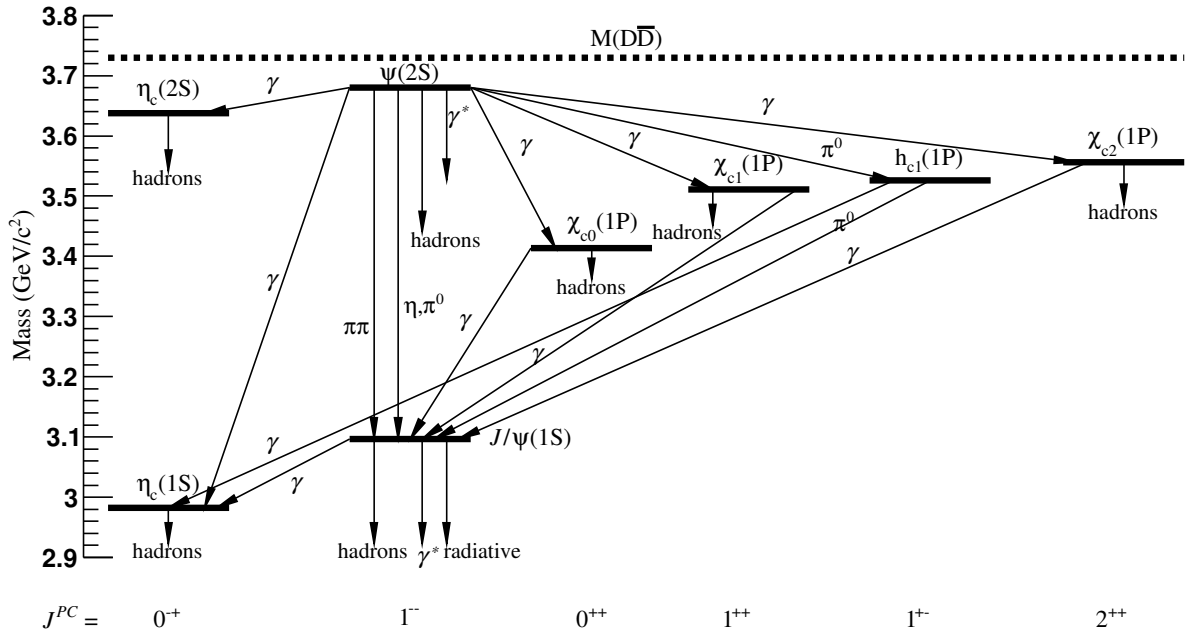


Figure 3.3: The low-lying charmonium ($c\bar{c}$) spectrum and some observed transitions.

3.2.1 The Theoretical Framework

The charmonium meson system is an ideal, and to some extent unique, laboratory to investigate the boundary between perturbative and non-perturbative QCD in a controlled environment. Since reliable calculations of non-perturbative QCD are still difficult, several phenomenological models and effective theories have been proposed. These models and calculational techniques can be tested and further developed using the phenomenology of charmonium states. For example, non-relativistic QCD (NRQCD) [9–11], expressed as a Pauli two-component field theory, can be constructed in correspondence with the hierarchy of energy scales in charmonium. NRQCD can be regarded as an effective theory that expands full QCD in powers of v , where v is the relative velocity between the c and \bar{c} quarks.

According to potential model calculations and lattice simulations, $v^2 \sim 0.3$ in the charmonium system [12]. For small v , multitude energy scales are observed as the hard m_c , soft $m_c v$, and ultra-soft $m_c v^2$, respectively. The effects at energy scale m_c can be integrated out explicitly. The resultant theory, NRQCD, reduced in the number of dynamical degrees of freedom, is simpler than full QCD, and it turns out to be very useful in calculating charmonium-relevant processes such as inclusive production, and annihilation decays and spectroscopy. Starting from NRQCD one can obtain the effective theory potential NRQCD (pNRQCD) [13–15] by integrating out the scale $m_c v$. Here the role of potentials and the quantum mechanical nature of the problem can be reduced to the zeroth order Schrödinger equation for the two heavy quarks. These effective field theories, as well as potential models and LQCD, make it possible to calculate a wide range of charmonium observables in a controlled and systematic way, therefore allowing an investigation of one of the most elusive sectors of the SM: low-energy QCD.

These charmonium observables can be taken from spectroscopy (*e.g.*, masses and widths), transitions (*e.g.*, transition rates), leptonic and electromagnetic decays, radiative decays, hadronic decays, rare and forbidden decays, and some miscellaneous topics such as Bell inequalities in high energy physics and special topics in $B\bar{B}$ final states, where B refers to baryon. BESIII is well suited to address the remaining experimental questions that are related to the low-mass, *i.e.* below open-charm threshold, charmonium spectrum, such as precise determinations of the mass and width of the η_c , h_c , and η'_c . The QCD multipole expansion (QCDME) [16, 17] is a feasible approach to charmonium hadronic transitions. Its results can be examined via observations at BESIII such as $\pi\pi$ transitions of S -Wave (P -Wave or D -Wave) charmonium states, the η transition $\psi(3686) \rightarrow \eta J/\psi$, and iso-spin violating π^0 transition $\psi(3686) \rightarrow \pi^0 h_c$. Many radiative transition channels, including $E1$ (electric dipole) and $M1$ (magnetic dipole) transitions, can be investigated with the BESIII $\psi(3686)$ data sample using the cascade transition chain. Other EM related processes, such as charmonium leptonic and EM decays, can also be studied at BESIII. In addition, studies of the hadronic decays will shed light on the $\rho - \pi$ puzzle [18] and reveal the inertial structure and decay dynamics of charmonium states. The baryonic decays are a special topic since the structure of baryons is comparatively more complicated than that of mesons. BESIII can investigate the baryonic decays via two-body, three-body, multi-body, and semi-inclusive modes. With a large $\psi(3686)$ data sample, BESIII can also search for rare and forbidden charmonium decays to explore some interesting topics such as CP violation or lepton flavor violation.

With the theory tools and the impressive number of collected charmonium states, BESIII will make a difference in this field allowing to carry on important investigation within the SM and beyond it.

3.2.2 Results with the Current $\psi(3686)$ Data Set

BESIII has so far collected a total of 448 million $\psi(3686)$ decays (including 107 million in 2009 and 341 million in 2012). These data samples have led to the publication of more than 30 papers. Some of the most important of these are as follows:

1. Measurements of the h_c in $\psi(3686)$ decays [19]. Clear signals are observed for $\psi(3686) \rightarrow \pi^0 h_c$ with and without the subsequent radiative decay $h_c \rightarrow \gamma \eta_c$. In

addition, first measurements of the absolute branching ratios $\mathcal{B}(\psi(3686) \rightarrow \pi^0 h_c) = (8.4 \pm 1.3 \pm 1.0) \times 10^{-4}$ and $\mathcal{B}(h_c \rightarrow \gamma \eta_c) = (54.3 \pm 6.7 \pm 5.2)\%$ are presented. Figure 3.4 shows the recoil mass of the π^0 with or without the subsequent radiative decay $h_c \rightarrow \gamma \eta_c$.

2. Observation of χ_{c1} decays into vector meson pairs [20]. The first measurements of decays of χ_{c1} to vector meson pairs (VV) $\phi\phi$, $\omega\omega$, and $\omega\phi$ are presented. The branching fractions are measured to be $(4.4 \pm 0.3 \pm 0.5) \times 10^{-4}$, $(6.0 \pm 0.3 \pm 0.7) \times 10^{-4}$, and $(2.2 \pm 0.6 \pm 0.2) \times 10^{-5}$, for $\chi_{c1} \rightarrow \phi\phi$, $\omega\omega$, and $\omega\phi$, respectively, which indicates that the hadron helicity selection rule is significantly violated in χ_{cJ} decays. Figure 3.5 shows the invariant mass spectra of VV in different final states.
3. Measurement of the mass and width of the η_c using $\psi(3686) \rightarrow \gamma \eta_c$ [21]. A novel model that incorporates full interference between the signal reaction, $\psi(3686) \rightarrow \gamma \eta_c$, and a nonresonant radiative background is used to successfully describe the line shape of the η_c . The η_c mass is measured to be $2984.3 \pm 0.6 \pm 0.6$ MeV/ c^2 and the total width to be $32.0 \pm 1.2 \pm 1.0$ MeV. Figure 3.6 shows the invariant mass distributions for the decays $K_S K^+ \pi^-$, $K^+ K^- \pi^0$, $\eta \pi^+ \pi^-$, $K_S K^+ \pi^+ \pi^- \pi^-$, $K^+ K^- \pi^+ \pi^- \pi^0$, and $3(\pi^+ \pi^-)$, respectively, with the fit results (for the constructive solution) superimposed.
4. First observation of the $M1$ transition between the radially excited charmonium S -wave spin-triplet and the radially excited S -wave spin-singlet states: $\psi(3686) \rightarrow \gamma \eta_c(2S)$ [22]. Analyses of the processes $\psi(3686) \rightarrow \gamma \eta_c(2S)$ with $\eta_c(2S) \rightarrow K_S^0 K^\pm \pi^\mp$ and $K^+ K^- \pi^0$ give an $\eta_c(2S)$ signal with a statistical significance of greater than 10 standard deviations under a wide range of assumptions about the signal and background properties. The product branching fraction $\mathcal{B}(\psi(3686) \rightarrow \gamma \eta_c(2S)) \times \mathcal{B}(\eta_c(2S) \rightarrow K \bar{K} \pi)$ is measured to be $(1.30 \pm 0.20 \pm 0.30) \times 10^{-5}$. Figure 3.7 shows the invariant mass spectrum for $K_S^0 K^\pm \pi^\mp$, and the simultaneous likelihood fit to the three resonances and combined background sources.
5. Observation of the h_c radiative decay $h_c \rightarrow \gamma \eta'$ [23]. Events from the reaction channels $h_c \rightarrow \gamma \eta'$ and $\gamma \eta$ are observed with a statistical significance of 8.4σ and 4.0σ , respectively, for the first time. The branching fractions for $h_c \rightarrow \gamma \eta'$ and $h_c \rightarrow \gamma \eta$ are measured to be $\mathcal{B}(h_c \rightarrow \gamma \eta') = (1.52 \pm 0.27 \pm 0.29) \times 10^{-3}$ and $\mathcal{B}(h_c \rightarrow \gamma \eta) = (4.7 \pm 1.5 \pm 1.4) \times 10^{-4}$, respectively. Figure 3.8 shows the results of the simultaneous fits to the invariant mass distributions of $M(\gamma \eta')$ and $M(\gamma \eta)$ for data.

The above list represents only part of the important results from the BESIII $\psi(3686)$ data set; more results can be found in the BESIII publication page [24].

3.2.3 Prospects for the Charmonium Program

We continue to explore important physics topics via charmonium decays. A few of these include: searches for new decay modes of the h_c , measurements of $M1$ transition processes and properties of the associated charmonium states (an $M1$ transition working

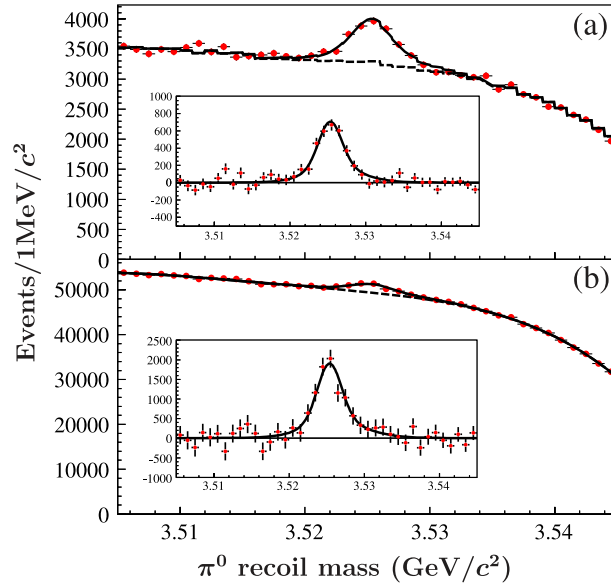


Figure 3.4: Measurements of the h_c in $\psi(3686)$ decays. (a) The π^0 recoil-mass spectrum and fit for the $E1$ -tagged analysis of $\psi(3686) \rightarrow \pi^0 h_c$, $h_c \rightarrow \gamma \eta_c$. (b) The π^0 recoil-mass spectrum and fit for the inclusive analysis of $\psi(3686) \rightarrow \pi^0 h_c$. Fits are shown as solid lines, background as dashed lines. The insets show the background-subtracted spectra.

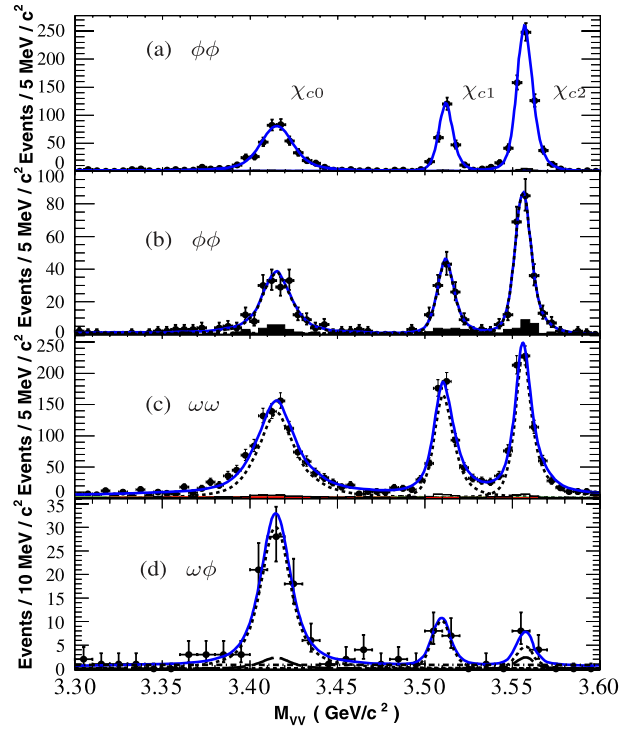


Figure 3.5: Observation of χ_{c1} decays into vector meson pairs. Invariant mass spectra of VV for (a) $\phi\phi$ mode in the $\gamma^2(K^+K^-)$ final state, (b) $\phi\phi$ mode in the $\gamma\pi^+\pi^-\pi^0 K^+K^-$ final state, (c) $\omega\omega$ mode in the $\gamma^2(\pi^+\pi^-\pi^0)$ final state, and (d) $\omega\phi$ mode in the $\gamma\pi^+\pi^-\pi^0 K^+K^-$ final state.

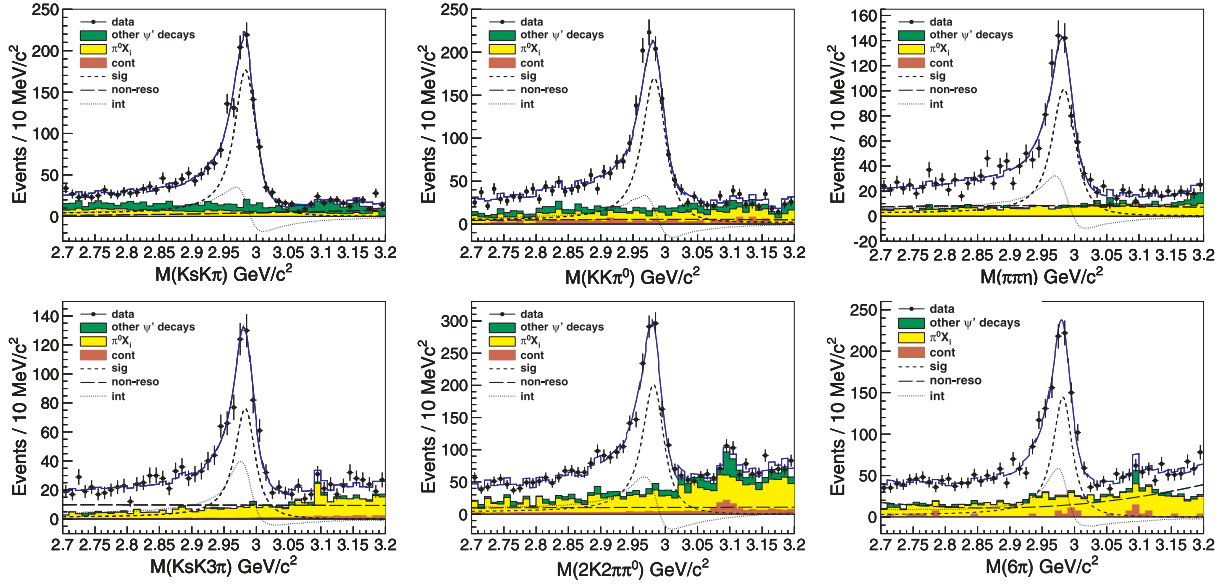


Figure 3.6: Measurement of mass and width of the η_c using $\psi(3686) \rightarrow \gamma\eta_c$. The invariant mass distributions for the decays $K_S K^+ \pi^-$, $K^+ K^- \pi^0$, $\eta \pi^+ \pi^-$, $K_S K^+ \pi^+ \pi^- \pi^-$, $K^+ K^- \pi^+ \pi^- \pi^0$, and $3(\pi^+ \pi^-)$, respectively, with the fit results (for the constructive solution) superimposed.

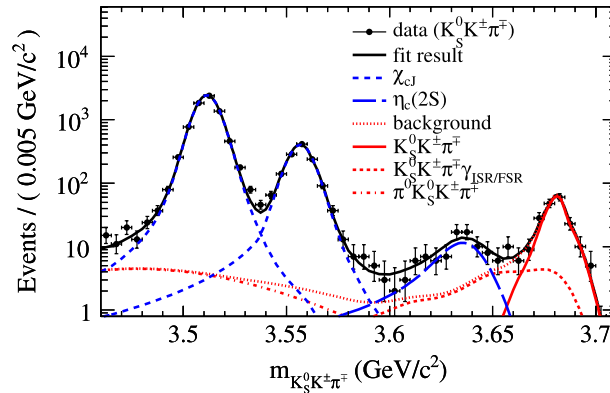


Figure 3.7: First observation of the $M1$ transition $\psi(3686) \rightarrow \gamma\eta_c(2S)$. The invariant-mass spectrum for $K_S^0 K^\pm \pi^\mp$, and the simultaneous likelihood fit to the three resonances and combined background sources.

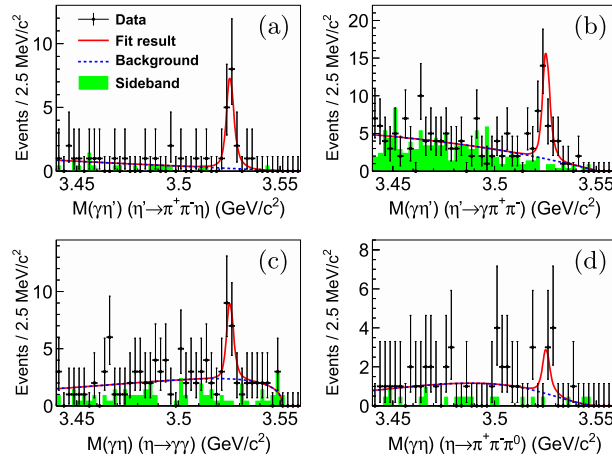


Figure 3.8: Observation of h_c radiative decay $h_c \rightarrow \gamma\eta'$. Results of the simultaneous fits to the two invariant mass distributions of (top) $M(\gamma\eta')$ and (below) $M(\gamma\eta)$ for data. (a) $M(\gamma\eta')$ distribution for $h_c \rightarrow \gamma\eta'(\eta' \rightarrow \pi^+\pi^-\eta)$. (b) $M(\gamma\eta')$ distribution for $h_c \rightarrow \gamma\eta'(\eta' \rightarrow \gamma\pi^+\pi^-)$. (c) $M(\gamma\eta)$ distribution for $h_c \rightarrow \gamma\eta(\eta \rightarrow \gamma\gamma)$. (d) $M(\gamma\eta)$ distribution for $h_c \rightarrow \gamma\eta(\eta \rightarrow \pi^+\pi^-\pi^0)$.

group has been formed), and systematic analyses of baryon final states. For many channels with larger statistics, amplitude analyses are being applied to extract more physics information. With more $\psi(3686)$ data, we can search for more decay modes of the η_c , $\eta_c(2S)$ and h_c , give more precise measurements of the masses and widths of the η_c , $\eta_c(2S)$ and h_c (and better understand the line-shapes associated with their productions), perform partial-wave analysis (PWA) on more channels, and so on. Among these topics, some important measurements may require more $\psi(3686)$ data in order to achieve the desired precision.

For $h_c \rightarrow \text{hadrons}$, at present only three channels are observed and the sum of their branching fractions is only about 1.5% [25]. Many more hadronic decay modes are expected and will be searched for at BESIII. If we expect a 5σ significant observation of a h_c decay channel with the branching fraction of 5×10^{-4} , a 2×10^9 $\psi(3686)$ sample is needed with the assumption that this channel is produced via the $\psi(3686) \rightarrow \pi^0 h_c$ transition, with 10% efficiency for the detection of the final states, and a similar background level to the $\pi^+\pi^-\pi^0$ channel. With this data sample, h_c hadronic transitions such as the spin-flip transition $h_c \rightarrow \pi^+\pi^- J/\psi$ and its radiative decays can also be searched for.

Compared with $E1$ transitions, the rates for $M1$ transitions between charmonium states are much lower. With the previously collected $\psi(3686)$ data sample, the first observation of the $M1$ transition $\psi(3686) \rightarrow \gamma\eta_c(2S)$ has been reported by BESIII [22]. However, in order to understand more about the $\eta_c(2S)$ and measure its mass, width, and decays more precisely, more $\psi(3686)$ data is necessary. For example, for the observation of the $\eta_c(2S)$ decaying into some channel with the production branching fraction $\mathcal{B}(\psi(3686) \rightarrow \gamma\eta_c(2S)) \times \mathcal{B}(\eta_c(2S) \rightarrow K_S K 3\pi)$ of about 5×10^{-6} , a 10^9 $\psi(3686)$ sample is needed with the assumption that the detection efficiency is about 5%, where the low efficiency and high background levels are due to the softness of the transition photon. With this large sample, we could also study the η_c charmonium state via $M1$ transition

to improve the precision of $\mathcal{B}(\psi(3686) \rightarrow \gamma\eta_c)$ and its comparison with theoretical predictions. A measurement of $\mathcal{B}(\psi(3686) \rightarrow \gamma\eta_c(2S))$ could be used to extract the absolute branching fractions for some specific $\eta_c(2S)$ decays. There are other radiative transitions such as $\eta_c(2S) \rightarrow \gamma J/\psi$, $\eta_c(2S) \rightarrow \gamma h_c$, $\chi_{c2} \rightarrow \gamma h_c$, and $h_c \rightarrow \gamma\chi_{c0,1}$ that are challenges for BESIII even with 10^9 $\psi(3686)$ data sample because of low decay rates or difficulty in detecting the soft photon, but these rates can be calculated in the potential model [1] and experimental searches are therefore important.

In addition to the radiative transitions, hadronic transitions are also very important and can be calculated better than the hadronic decays of charmonia. It is interesting to observe or find evidence for some hadronic transitions such as the spin-flip $\chi_{c1} \rightarrow \pi\pi\eta_c$ and $h_c \rightarrow \pi\pi J/\psi$, for which only upper limits have been set at present. We have estimated the needed statistics to see evidence for the transition $\chi_{c1} \rightarrow \pi^+\pi^-\eta_c$ and found that at least 10^9 $\psi(3686)$ events are needed according to the previous BESIII results [26]. Note that in Ref. [26] only two η_c hadronic decay channels were used. If more decay modes were included, a smaller data set could satisfy the requirement. To uncover evidence for $h_c \rightarrow \pi\pi J/\psi$, at least a sample of 2×10^9 $\psi(3686)$ decays will be needed with the assumption that there is no background. There are other hadronic transitions such as $\psi(3686) \rightarrow \eta J/\psi$ and $\psi(3686) \rightarrow \pi^0 J/\psi$, that have been observed with the present BESIII $\psi(3686)$ data sample but will be improved with a larger one.

Besides transitions between charmonium states, there are also decays of charmonia that should be measured. Both radiative decays and hadronic decays of the charmonium states should be studied for a better understanding of charmonium decay dynamics. From Ref. [27], the typical branching fractions of $\chi_{cJ} \rightarrow \gamma V$, where V represents a vector resonance, is about 10^{-6} . This means a 10^9 $\psi(3686)$ data sample would be needed to observe the signal if we assume the intermediate product branching fractions are 80% and the selection efficiency is 30%. Since the branching fractions for $\eta_c \rightarrow \gamma V$ are expected to be similar to $\eta_c \rightarrow \gamma\gamma$, they should be at the 10^{-4} level. And the improved measurement of $\eta_c \rightarrow \gamma\gamma$ will shed light on the effects of higher order QCD corrections as well as provide validation of the decoupling of the hard and soft contributions in the NRQCD framework due to its simplicity [28, 29]. With the present $\psi(3686)$ data sample at BESIII, the processes $\psi(3686) \rightarrow \gamma\pi^0$ and $\gamma\eta$ have been observed for the first time [30]. There are also many studies of J/ψ and $\psi(3686)$ decays into $\gamma p\bar{p}$, γK^+K^- , $\gamma\pi^+\pi^-$, etc. With a larger $\psi(3686)$ data sample, all of these measurements will be improved.

More and better measurements of $\psi(3686)$ hadronic decays are crucial to help solve the long standing ρ - π puzzle [18]. The ratio of the branching fractions of J/ψ and $\psi(3686)$ is expected to hold in a reasonably good degree to 12%, based on pQCD, for both inclusive and exclusive decays. But this relation is observed severely violated for the $\rho\pi$ and several other decay channels. From already obtained BESIII results, it has become more clear that kinematic effects, which have been previously ignored, might contribute significantly and the amplitude analysis method might also be necessary to clarify the different dynamic processes between the J/ψ and $\psi(3686)$. For charmonium states beyond the open-charm threshold, the studies of their decays to open-charm states will not only provide information of the decay mechanism, but also serve for the spectroscopy study. Furthermore, it is interesting to study the non- $D\bar{D}$ decays of $\psi(3770)$, such as $\psi(3770) \rightarrow p\bar{p}$, $p\bar{p}\pi^0$, $\gamma\eta_c$, $\gamma\chi_{cJ}$, $\gamma\eta_c(2S)$, and $\pi^+\pi^-J/\psi$. These can be studied using data

Table 3.1: Some tentative measurements and correspondingly required statistic of $\psi(3686)$ sample to achieve the desired precision on branching fraction. The observation and evidence are corresponding to 5σ and 3σ significance of the signal.

Measurement	Expected sensitivity	Needed $\psi(3686)$ sample ($\times 10^9$)
$h_c \rightarrow hadrons$	Observation of 5×10^{-4}	2
$\eta_c(2S) \rightarrow X$	Observation of 1×10^{-6}	5
$\chi_{c1} \rightarrow \pi^+\pi^-\eta_c$	Evidence of 3×10^{-3}	> 1
$h_c \rightarrow \pi^+\pi^-J/\psi$	Evidence of 2×10^{-3}	> 2
$\chi_{cJ} \rightarrow \gamma V$	Observation of 1×10^{-6}	1
$h_c \rightarrow p\bar{p}$	Evidence of 2×10^{-4}	> 2

collected on and around the $\psi(3770)$ peak.

The two-body baryonic decays of the χ_{cJ} can provide information on color-singlet and color-octet contributions. In addition, systematical studies of two-body baryonic decays of the J/ψ and $\psi(3686)$ will shed light on the relative angle and magnitude of the electro-magnetic and strong interaction amplitudes [31]. The $\eta_c(2S)$ and h_c decaying into $p\bar{p}$ have been searched for based on 1×10^8 $\psi(3686)$ decay sample at BESII and no obvious signal has been observed [32]. To find evidences for both of them, a data sample of 2×10^9 $\psi(3686)$ decays will be required under the assumption that the efficiency is about 40% and there is no background. Also, the similar data size is needed to study the Bell inequality [33], SU(3) flavor symmetry [34], CP violation [35, 36]. Measurement of three-body baryonic decays of higher excited charmonia will provide more information for excited baryonic states, where amplitude analysis will be required.

Some rare decays can be searched for with larger $\psi(3686)$ data samples such as the C -violating process $J/\psi \rightarrow \gamma\gamma$ via $\psi(3686) \rightarrow \pi\pi J/\psi$. This has been discussed in the new physics part.

For the excited conventional charmonium states beyond the open-charm threshold there are still many unsolved puzzles. There are only four 1^{--} states between 4.0 and 4.6 GeV predicted by potential models, but the number of observed vector resonances is larger than that. The masses and partial widths of these states decaying into e^+e^- (Γ_{ee}) can be calculated via potential models assuming they are conventional charmonia. However, strong coupling to open-charm meson pairs and relativistic corrections significantly change both the spectrum and Γ_{ee} . Better measurements would be very helpful to clarify the situation. BESIII has observed the $\psi(1^3D_2)$ state $X(3823)$ via its decay into $\gamma\chi_{c1}$ [37], but many predicted states, such as $1F$, $3S$, $2D$, $1G$, $3P$, $2F$, $4S$, $3D$ and $2G$ have not been observed yet. The characteristics of the excited conventional charmonia will be studied with the data sets collected for XYZ states.

BESIII has already collected scan samples around the J/ψ , $\psi(3686)$, and $\psi(3770)$ peaks, as well as those above 4.0 GeV. These samples are dedicated to some specific problems that we can do the best in the world, such as determinations of the resonance parameters, line shapes, interference between strong and EM amplitudes in resonance decay, etc.

Some tentative measurements and their correspondingly needed $\psi(3686)$ sample are

listed in Table 3.1. From this table a 3×10^9 $\psi(3686)$ sample may be proper to guarantee the expected precision and lead us to some exciting discoveries. But at present we consider the *XYZ* physics with higher priority, so we prefer to take the $\psi(3686)$ data only after finishing the *XYZ* proposal.

3.3 *XYZ* Physics

The discovery of the *XYZ* states has opened a new era in the study of the charmonium spectrum [38–43]. Before the discovery of the $X(3872)$ in 2003 [44], every meson in the mass region between 2.9 and 4.5 GeV/c^2 could be successfully described as a $c\bar{c}$ bound state. Simple potential models, using QCD-inspired potentials binding quarks and antiquarks, could reproduce the spectrum of charmonium states all the way from the $\eta_c(1S)$ (the ground state) up to the $\psi(4415)$ (usually considered to be the third radial excitation of the J/ψ) [6]. This simple model of the charmonium spectrum has since broken down in a dramatic fashion. Following the discovery of the *XYZ* states (Fig. 3.1), we now observe exotic hadronic configurations containing charm and anticharm quarks. These new configurations, such as tetraquarks, hadronic molecules, and hybrid mesons, allow us to probe the mysterious nonperturbative QCD which underlies the way quarks and gluons combining into larger hadronic composites.

The $X(3872)$, the first of the *XYZ* states to be discovered, was discovered in 2003 by the Belle Collaboration in the process $B \rightarrow KX(3872)$ with $X(3872) \rightarrow \pi^+\pi^-J/\psi$ [44]. Its unexpected appearance, combined with its narrow width and the fact that its mass is very close to the $D^0\bar{D}^{*0}$ mass threshold, immediately signaled that the $X(3872)$ is an unusual meson. Since its discovery, many more of its properties have been determined [3]. For example, its total width is less than 1.2 MeV/c^2 , its mass is within 0.18 MeV/c^2 of the $D^0\bar{D}^{*0}$ threshold, it has $J^{PC} = 1^{++}$, and in addition to $\pi^+\pi^-J/\psi$, it decays to $D^0\bar{D}^{*0}$ with a large branching fraction, $\gamma J/\psi$, $\gamma\psi(3686)$ and $\omega J/\psi$. It is currently believed to be a mixture of $\chi_{c1}(2P)$ and a tetraquark or meson molecule [38]. However, many important open questions remain and further investigation is needed.

In 2013, BESIII discovered that it has experimental access to the $X(3872)$ through the process $e^+e^- \rightarrow \gamma X(3872)$ using cms energies in the vicinity of 4.26 GeV [45], which, in itself, provides an important hint at the relation between the $Y(4260)$ and $X(3872)$ [46]. This discovery has initiated a new and vigorous program at BESIII to search for new decay modes of the $X(3872)$, which will in turn offer new insight into its nature.

The discovery of the $X(3872)$ quickly led to the discovery of many more states with exotic configurations of quarks and gluons. For example, the search for the decay $X(3872) \rightarrow \omega J/\psi$ led to the discovery of the $X(3915)$ in the process $B \rightarrow KX(3915)$ with $X(3915) \rightarrow \omega J/\psi$ [47]. This state was originally a candidate to be the quark model $\chi_{c0}(2P)$ state, but its mass and decay patterns were inconsistent with that interpretation. Moreover, since that time a better candidate for the $\chi_{c0}(2P)$ state, the $X(3860)$, has been discovered [48] (see also in Ref. [49]). This leaves the nature of the $X(3915)$ an unsettled question. Searching for the $X(3915)$ in the process $e^+e^- \rightarrow \gamma X(3915)$ is currently an important topic at BESIII. In addition, it is also important to search for resonant signals for the broad $X(3860)$ and the conjectured narrow 2^{++} X_2 with a mass around 4 GeV/c^2 [50],

the predicted spin partner of the $X(3872)$, in the process $e^+e^- \rightarrow \gamma D\bar{D}$.

Also following the discovery of the $X(3872)$ was the discovery of the $Y(4260)$ by BaBar using the Initial State Radiation (ISR) process $e^+e^-(\gamma_{\text{ISR}}) \rightarrow Y(4260) \rightarrow \pi^+\pi^-J/\psi$ [51]. Because of its production mechanism, we can immediately infer that it has $J^{PC} = 1^{--}$. However, its mass is inconsistent with any of the known or expected charmonium vector excitations. For example, its mass lies between the masses of the $\psi(4160)$ and $\psi(4415)$. It is therefore supernumerary. LQCD calculations [52], as well as other models [53], suggest the $Y(4260)$ could be a hybrid meson. Another intriguing model that considers the $Y(4260)$ to be strongly coupled to $D_1(2420)\bar{D}$ predicts a nontrivial behavior for its line shape [54]. At BESIII, the $Y(4260)$ can be produced directly by simply tuning the cms energy of the e^+e^- collisions to the mass of the $Y(4260)$. In the same way, BESIII can also directly produce the $Y(4360)$ (seen in $e^+e^- \rightarrow \pi^+\pi^-\psi(3686)$), and can search for new Y states. The BESIII discovery of a multitude of new Y states (or the discovery of a complicated coupled-channel system) will be further described in the next section (Sec. 3.3.1).

The final, and perhaps most interesting, class of exotic structures are the isovector Z_c states. Since they are known to contain an isosinglet $c\bar{c}$ pair, they must also contain light quarks to account for the non-zero isospin. One of the first of these states to be observed, the $Z_c(3900)$, was discovered by BESIII in the process $e^+e^- \rightarrow \pi^\mp Z_c(3900)^\pm$ with $Z_c(3900)^\pm \rightarrow \pi^\pm J/\psi$ [55]. Its two distinctive features are that it carries an electric charge and it has a mass near the $D\bar{D}^*$ threshold. This suggests that it is a candidate for a meson molecule or tetraquark with rescattering effects due to the presence of the $D\bar{D}^*$ threshold and more complicated kinematical singularities that are also expected to be important. The lineshape of the $Z_c(3900)$ and how that shape evolves with cms energy will be one of the keys to its interpretation. As described in more detail later, disentangling the nature of the $Z_c(3900)$ is one of the primary goals of the BESIII XYZ program.

Since the discovery of the $Z_c(3900)$, other Z_c states have also been discovered. For example, BESIII discovered the $Z_c(4020)$ in the process $e^+e^- \rightarrow \pi^\mp Z_c(4020)^\pm$ with $Z_c(4020)^\pm \rightarrow \pi^\pm h_c(1P)$ [56]. Its mass is close to the $D^*\bar{D}^*$ threshold, suggesting it is closely related to the $Z_c(3900)$.

So far, the $Z_c(3900)$ and $Z_c(4020)$ have only been produced in e^+e^- collisions with cms energies around 4.2–4.4 GeV with possible connection to the reported Y states. Other potential production mechanisms, such as $B \rightarrow KZ_c$ decays, appear to be insensitive to the $Z_c(3900)$ and $Z_c(4020)$ states. A different class of Z_c states has been discovered in B decays, among which the most prominent one is the $Z_c(4430)$ seen in $B \rightarrow KZ_c(4430)$ with $Z_c(4430)^\pm \rightarrow \pi^\pm\psi(3686)$ [57]. The reason that one class of Z_c states is produced in e^+e^- collisions and a different class is produced in B decays remains a fascinating open question.

3.3.1 Overview of BESIII Accomplishments

The goal of the XYZ physics program at BESIII is to understand the novel phenomena apparent in the spectrum of charmonium states with masses above open charm threshold, as outlined in the previous section. The presence of these XYZ states provides an ideal

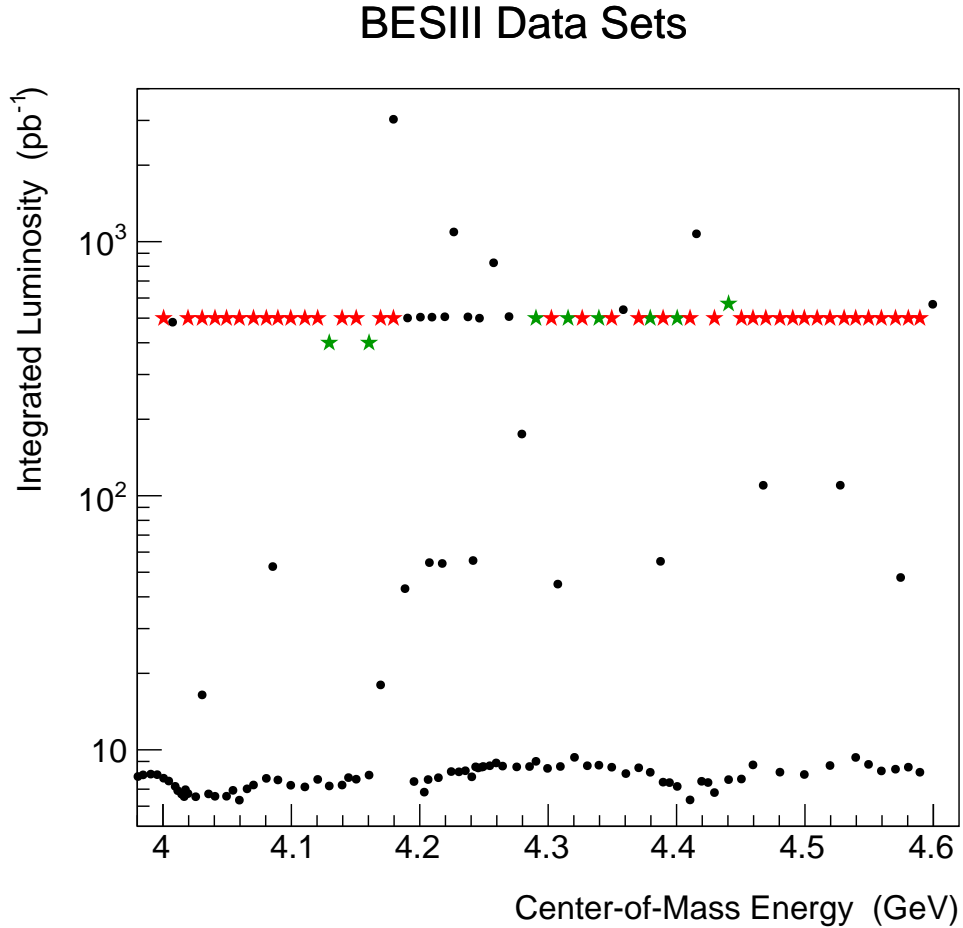


Figure 3.9: BESIII data sets that are relevant for XYZ physics. The data sets collected prior to 2019 are shown in black; those collected in 2019 are in green; and those considered for potential future measurements are shown in red.

opportunity for BESIII to study exotic and unexplored features of the strong force. BESIII is currently in a unique position to both directly access a large number of these states and to search for new states in their decays. Note that a given Y state, because it has $J^{PC} = 1^{--}$, can be produced directly at BESIII by the appropriate choice of the cms energy of the e^+e^- collisions.

BESIII has already made significant progress in studies of the XYZ states. Existing data sets are shown in Fig. 3.9. We originally had “large” data sets (with integrated luminosity at or above 500 pb^{-1}) at only a few e^+e^- cms energies: 4.01, 4.18 (primarily used for D_s physics), 4.23, 4.26, 4.36, 4.42 and 4.6 GeV. In 2017, we collected large samples at seven additional points between 4.19 and 4.27 GeV, and in 2019 eight additional energies between 4.28 and 4.44 GeV.

Using the limited amount of data collected prior to 2017, we have already made a number of important discoveries and measurements. Here we highlight eight of the most important measurements:

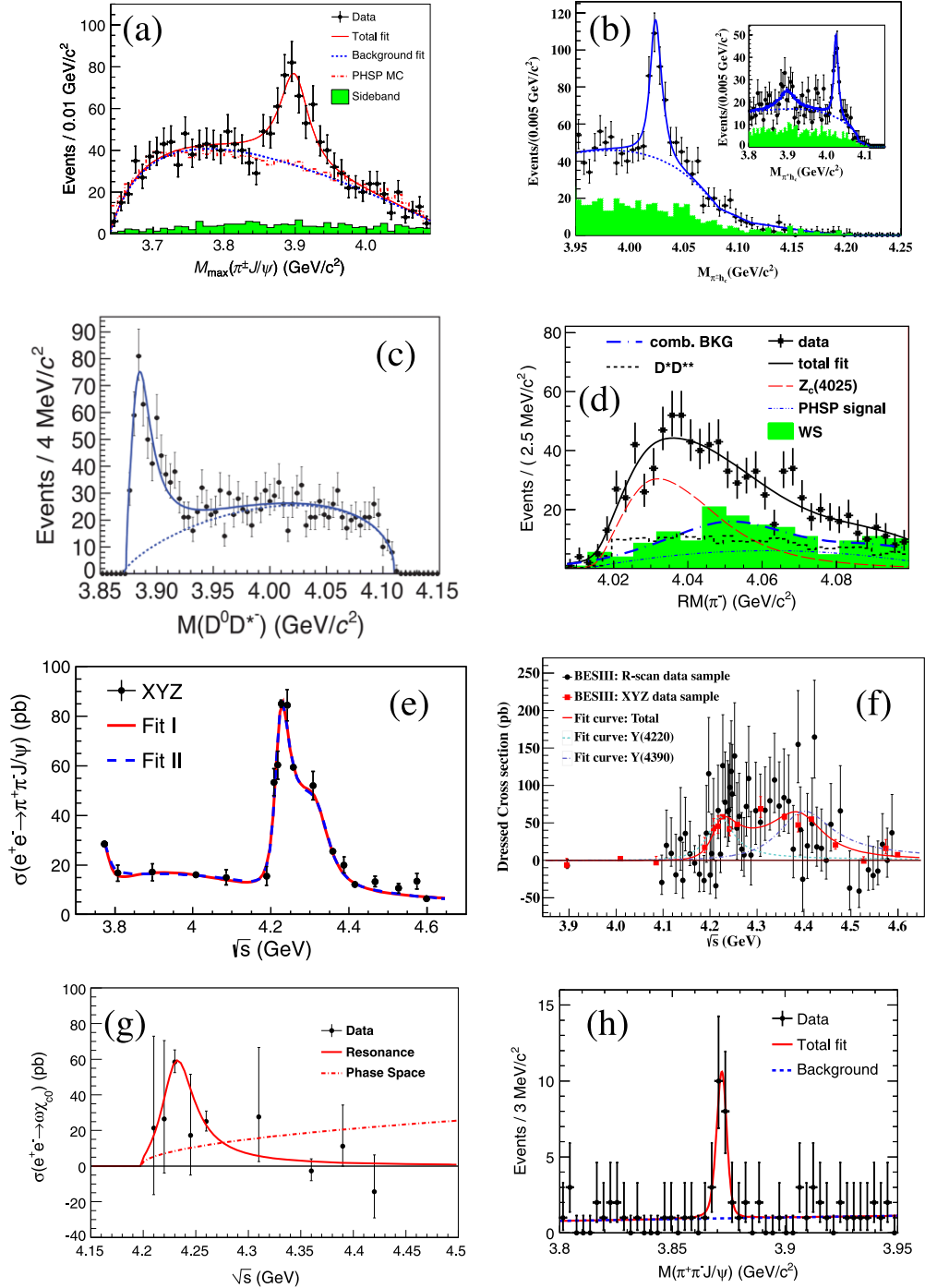


Figure 3.10: A selection of XYZ results from BESIII: (a) discovery of the $Z_c(3900)$ [55]; (b) discovery of the $Z_c(4020)$ [56]; (c) discovery of open-charm decays of the $Z_c(3900)$ [58]; (d) discovery of open-charm decays of the $Z_c(4020)$ [59]; (e) observation of $Y(4260) \rightarrow \pi^+\pi^- J/\psi$ [60]; (f) discovery of two peaks in $e^+e^- \rightarrow \pi^+\pi^- h_c$ [62]; (g) discovery of a peak in $e^+e^- \rightarrow \omega\chi_{c0}$ [63]; (h) discovery of $e^+e^- \rightarrow \gamma X(3872)$ [45].

1. We discovered the $Z_c(3900)$ in the process $e^+e^- \rightarrow \pi^\mp Z_c^\pm$ with $Z_c^\pm \rightarrow \pi^\pm J/\psi$ [55] in Fig. 3.10(a). Since the $Z_c(3900)$ has a mass in the charmonium mass region and it decays to J/ψ , we know it includes $c\bar{c}$ quarks. But since it has an electric charge, we know it must include additional quarks. The $Z_c(3900)$ is therefore a good candidate to be a tetraquark or meson molecule.

With 680 citations (as of Oct. 9, 2019), this publication is the most-cited of all of BES papers (including BES and BESIII). Additional work is ongoing to better determine the internal structure of the $Z_c(3900)$.

2. We discovered the $Z_c(4020)$ in the process $e^+e^- \rightarrow \pi^\mp Z_c^\pm$ with $Z_c^\pm \rightarrow \pi^\pm h_c$ [56] in Fig. 3.10(b). Like the $Z_c(3900)$, the $Z_c(4020)$ contains $c\bar{c}$ quarks and is electrically charged. While the $Z_c(3900)$ is near the $D\bar{D}^*$ threshold, the $Z_c(4020)$ is near the $D^*\bar{D}^*$ threshold. With 337 citations (as of Oct. 9, 2019), this publication is the second-most-cited BESIII papers.
3. We observed the $Z_c(3900)$ decaying to the open-charm channel $(D\bar{D}^* + c.c.)^\pm$ [58] in Fig. 3.10(c). With 258 citations (as of Oct. 9, 2019), this publication is the fourth-most-cited BESIII papers.
4. Similarly, we observed the $Z_c(4020)$ decaying to the open-charm channel $(D^*\bar{D}^*)^\pm$ [59] in Fig. 3.10(d). Observation of the $Z_c(3900)$ and $Z_c(4020)$ decays to these open charm channels (and the lack of evidence for $Z_c(4020)$ decays to $(D\bar{D}^* + c.c.)^\pm$), combined with their masses being close to threshold, suggest that the nature of the $Z_c(3900)$ and $Z_c(4020)$ is somehow intimately tied to these channels. With 291 citations (as of Oct. 9, 2019), this publication is the third-most-cited BESIII papers.
5. We precisely measured the cross section for $e^+e^- \rightarrow \pi^+\pi^- J/\psi$ [60]. Since this is the reaction that led to the discovery of the $Y(4260)$ (although here Initial State Radiation is not used), the aim of our measurement was to precisely determine the parameters of the $Y(4260)$. Instead, what we observed was a cross section that was inconsistent with that arising from a single ordinary resonance, as shown in Fig. 3.10(e). The cross section could be successfully fit using two resonances: one with a narrow total width and mass around 4.22 GeV/ c^2 and one with a wider total width and mass around 4.32 GeV/ c^2 . Thus, the $Y(4260)$, one of the first of the *XYZ* to be discovered, is either composed of two resonances or has a highly nontrivial line-shape due to other dynamics such as a strong coupling to the $D_1(2420)\bar{D}$. In addition, we observed the decay $Y(4260) \rightarrow \pi^0\pi^0 J/\psi$ and the neutral $Z_c(3900)$ in $e^+e^- \rightarrow \pi^0 Z_c^0 \rightarrow \pi^0\pi^0 J/\psi$ [61]. This further cements the case that the $Z_c(3900)$ is an isospin-1 multiquark state of charmonium.
6. We discovered two peaks in the cross section for $e^+e^- \rightarrow \pi^+\pi^- h_c$ [62] in Fig. 3.10(f). This, along with the above-described measurement of $e^+e^- \rightarrow \pi^+\pi^- J/\psi$, indicates that the family of Y states is more complicated than was originally thought. In particular, these two final states have different total spins for the charm and anticharm quark pair. The masses and widths of the peaks in $\pi^+\pi^- h_c$ and $\pi^+\pi^- J/\psi$ are inconsistent.

7. We discovered a peak in $e^+e^- \rightarrow \omega\chi_{c0}$ [63] in Fig. 3.10(g) that is inconsistent with the reported parameters for the $Y(4260)$. This suggests that either there is yet another Y state in this mass region or that the mass of the $Y(4260)$ should be shifted downwards.
8. We discovered the process $e^+e^- \rightarrow \gamma X(3872)$ [45] in Fig. 3.10(h), which hints at the existence of the radiative decay $Y(4260) \rightarrow \gamma X(3872)$. This is a unique transition in the sense that it is a transition between two states both of whose natures are unclear. This suggests there is an intimate connection between the $Y(4260)$ and the $X(3872)$.

There is currently a great amount of community interest in XYZ physics, as is clear from the high profile of the BESIII papers mentioned above. Since the natures of most of these phenomena are yet to be understood, the theory community has been especially active developing new techniques to aid in the interpretation of the XYZ [38]. This has led to many innovations. What is currently needed, however, is more high precision data. Therefore, new data that BESIII will provide is much anticipated and will be put to immediate use.

3.3.2 Broad Problems in XYZ Physics

The XYZ results from BESIII have helped uncover several broad problems in the field, and these are the subjects of intense studies at BESIII. Below, these are labeled the “ Y problem,” the “ Z problem,” and the “ X problem.” With more data, BESIII is in the unique position to definitively address all three. This section includes descriptions of these problems and indicates a variety of the ways they can be addressed at BESIII.

The Y Problem

Exclusive e^+e^- cross sections have shown surprisingly complex behavior as a function of cms energy. The $Y(4260)$ is more complex than a single ordinary resonance, as shown by the complicated lineshape in the $e^+e^- \rightarrow \pi^+\pi^-J/\psi$ cross section in Fig. 3.10(e); the $Y(4360)$ and $Y(4660)$ are seen in $e^+e^- \rightarrow \pi^+\pi^-\psi(3686)$; two other peaks are seen in $e^+e^- \rightarrow \pi^+\pi^-h_c$ in Fig. 3.10(f); the $Y(4220)$ is seen in $e^+e^- \rightarrow \omega\chi_{c0}$ in Fig. 3.10(g) and so on. A summary of the masses and widths of resonances extracted from recent BESIII results is shown in Fig. 3.11. There is currently very little consistency between different reactions. Furthermore, none of these complicated features are apparently present in the inclusive e^+e^- cross section, which only shows evidence for the $\psi(3770)$, $\psi(4040)$, $\psi(4160)$, and $\psi(4415)$ [64]. This is the “ Y ” problem. Are the many peaks seen in e^+e^- cross sections really new states? Or are they the results of more subtle effects? With new data, will new patterns emerge? What are their exact line shapes? Will they match theoretical predictions, such as a very asymmetric line shape for the $Y(4260)$ obtained within a molecular frame [69]? With our limited number of data points (cms energies), there is little hope in resolving the issue. We require (1) more data spread over a variety of cms energies, and (2) a global and simultaneous analysis of many final states. This latter

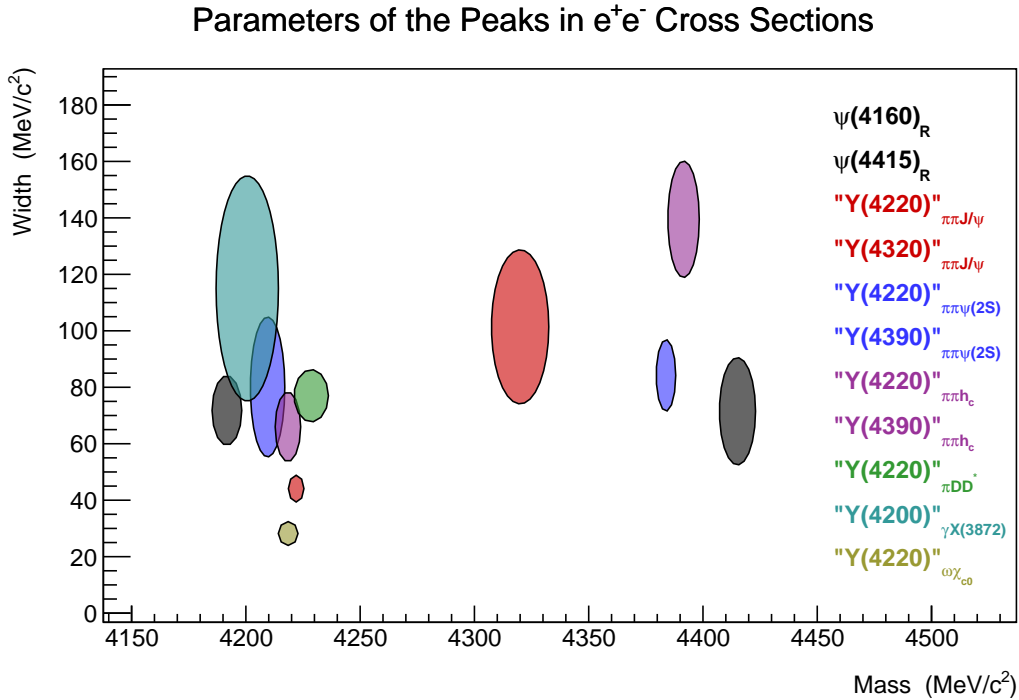


Figure 3.11: A collection of resonance parameters as determined from fits to e^+e^- cross sections. Each ellipse encloses 1σ around the measurements of resonance parameters, where the size of the ellipses are determined by adding together the statistical and systematic uncertainties in quadrature. The parameters are from inclusive hadronic cross sections [64]; $\pi^+\pi^-J/\psi$ [60]; $\pi^+\pi^-\psi(3686)$ [65]; $\pi^+\pi^-h_c$ [62]; $\pi D\bar{D}^* + c.c.$ [66]; $\gamma X(3872)$ [67]; and $\omega\chi_{c0}$ [68].

effort will likely require close collaboration with the theory community, in particular with the view on amplitude analysis.

The Z Problem

BESIII discovered the $Z_c(3900)$ in $e^+e^- \rightarrow \pi^+\pi^-J/\psi$ events at a single cms energy of 4.26 GeV in Fig. 3.10(a). Higher-energy data, however, has revealed more complex structures. There is a similar situation in $e^+e^- \rightarrow \pi^+\pi^-\psi(3686)$, where the lower-energy data appears relatively simple, but the Dalitz plots at higher energies are more complex [65]. This is the “ Z ” problem. How do the Z_c structures produced in e^+e^- annihilation change as a function of e^+e^- cms energy? Will their properties remain constant, as would be expected for a true resonance, or will their properties change, which would indicate the discovery of other effects (which are also important to study)? Again, BESIII is in a unique position to address this problem. Again, we require large data sets at a variety of energies, and we require closer cooperation with the theory community.

Using existing data samples, BESIII has successfully determined the quantum numbers of the $Z_c(3900)$ to be $J^P = 1^+$ [70]. However, the data samples have so far been insufficient

to measure the phase of the $Z_c(3900)$ with respect to the other amplitudes present in $e^+e^- \rightarrow \pi^+\pi^-J/\psi$. Such an effort to measure the Argand diagram for the $Z_c(3900)$ is currently being explored. Determining the lineshape of the $Z_c(3900)$ and studying its phase motion would allow us to distinguish between different models for the nature of the $Z_c(3900)$ [71]. There are at least two challenges. First, a larger data sample at a single cms energy is required. Second, and perhaps more importantly, we must understand all of the other resonances that are present in the $\pi^+\pi^-J/\psi$ Dalitz plots. The measurement of the phase of the $Z_c(3900)$ (and even the magnitude of its amplitude) is only as good as our understanding of the parameterization of the rest of the Dalitz plot. This is a challenging issue.

Another route for understanding the nature of the $Z_c(3900)$ would be to look for patterns of other Z_c states. BESIII has already discovered the $Z_c(4020)$, which seems to indicate that the $D\bar{D}^*$ and $D^*\bar{D}^*$ thresholds play important roles in the characteristics of the Z_c . Another important subject to study might be the putative strange hidden-charm states, like the Z_{cs} which replaces up or down quark in Z_c with strange quark. If a Z_{cs} state exists, perhaps decaying to KJ/ψ , this would provide another crucial handle on the nature of the Z_c states. To search for the heavier Z_{cs} states, larger samples of higher-energy data samples will be required.

The X Problem

The interpretation of the $X(3872)$ is intimately related to the problem of determining the parameters of the conventional $2P$ $c\bar{c}$ states – the spin-triplet $\chi_{cJ}(2P)$ and the spin-singlet $h_c(2P)$. This is because the $X(3872)$, with $J^{PC} = 1^{++}$, certainly contains some admixture from the $\chi_{c1}(2P)$ state. Sorting out the spectrum of states in this region, and determining which are exotic and which are conventional and how they mix, is the “ X ” problem.

One important piece of information in this program to sort out the $2P$ states is the mass of the $h_c(2P)$. Once this state is found, it will indicate where the $\chi_{cJ}(2P)$ states are located. Then states deviating from this pattern can be identified as exotic. Since there is already clear evidence for $e^+e^- \rightarrow \pi^+\pi^-\psi(1S, 2S)$ and $\pi^+\pi^-h_c(1P)$ at BESIII, one also expects to produce the process $\pi^+\pi^-h_c(2P)$. Search is underway, but larger data sets at higher cms energies are needed.

At least in principle, BESIII also has access to a variety of other X states through radiative transitions, $e^+e^- \rightarrow \gamma X$, in the similar way the $X(3872)$ is produced. For example, this is being used to search for the $X(3915)$ in the process $e^+e^- \rightarrow \gamma\omega J/\psi$ and to search for the $X(4140)$ in the process $e^+e^- \rightarrow \gamma\phi J/\psi$.

3.3.3 Possibilities for XYZ Data Taking

The X , Y and Z problems are all Tier A physics priorities within the charmonium group. All could benefit from additional data sets. Three qualitatively different types of data-taking plans are discussed below, each targeting different topics.

Table 3.2: Requirements for *XYZ* data-taking for a few select channels.

channel	data plan	luminosity	cross section precision	# of events
$\pi^+\pi^-J/\psi$	(1)	500 pb ⁻¹ at 4.30 GeV	3%	1270
$\pi^+\pi^-h_c(1P)$	(1)	500 pb ⁻¹ at 4.30 GeV	9%	220
$\eta J/\psi$	(1)	500 pb ⁻¹ at 4.30 GeV	30%	28
$\pi^+\pi^-\psi(3686)$	(1)	500 pb ⁻¹ at 4.30 GeV	3%	230
$\pi^+\pi^-J/\psi$	(2)	5 fb ⁻¹ at 4.23 GeV	<1%	18k
$\pi^+\pi^-J/\psi$	(2)	5 fb ⁻¹ at 4.42 GeV	3%	3k
$\pi^+\pi^-\psi(3686)$	(2)	5 fb ⁻¹ at 4.42 GeV	2%	4k

(1) High-Statistics Scan from 4.0 to 4.6 GeV

To study the *Y* problem, we need to do a detailed scan of cross sections between 4.0 and 4.6 GeV. The range is chosen in order to study a wide range of channels, important to achieve a more global picture in this region. We propose 500 pb⁻¹ per point, for points spaced at 10 MeV intervals. The intervals were chosen to cover the possibility for narrow features – the narrowest of the *XYZ* states discovered by BESIII is currently the $Z_c(4020)$ with a width of 7 MeV, and the $\pi\pi J/\psi$ cross section shows rapid changes between 4.20 and 4.23 GeV. Other cross sections are likely to include other rapidly changing features. A series of simulations are shown in Fig. 3.12. Background rates and efficiencies are based on existing data. The cross section shapes are only guesses; they need to be measured. Statistical fluctuations are not included. The error bars, however, are reliable estimates. The top part of Table 3.2 shows the precision with which cross sections could be measured for a few select channels at 4.30 GeV.

This high-statistics scan would also allow us to study the way the Z_c states evolve with cms energy. Changes in the shapes of the peaks and/or their production cross sections would provide clues about the nature of the Z_c . By combining data sets at different cms energies, we could also better explore the *X* problem.

(2) A Series of Higher-Statistics Points

For the *Z* problem, especially detailed studies of Argand diagrams, we require very high statistics samples at a few points. We currently have 1 fb⁻¹ of data for e^+e^- cms energy at 4.42 GeV. For the $\pi\pi J/\psi$ channel, this is not adequate to definitely resolve the substructure. We require on the order of 5 fb⁻¹ or more per point to have adequate statistics for unambiguous Dalitz plot analyses. Three or four of these high-statistics points would likely reveal the nature of the energy dependence of the Dalitz plot. A working group is studying the substructure within various channels using the 4.42 GeV data. As the working group progresses, the requirements on future data-taking will become more clear. The lower part of Table 3.2 lists the expected numbers of events for a few channels given future 5 fb⁻¹ data samples.

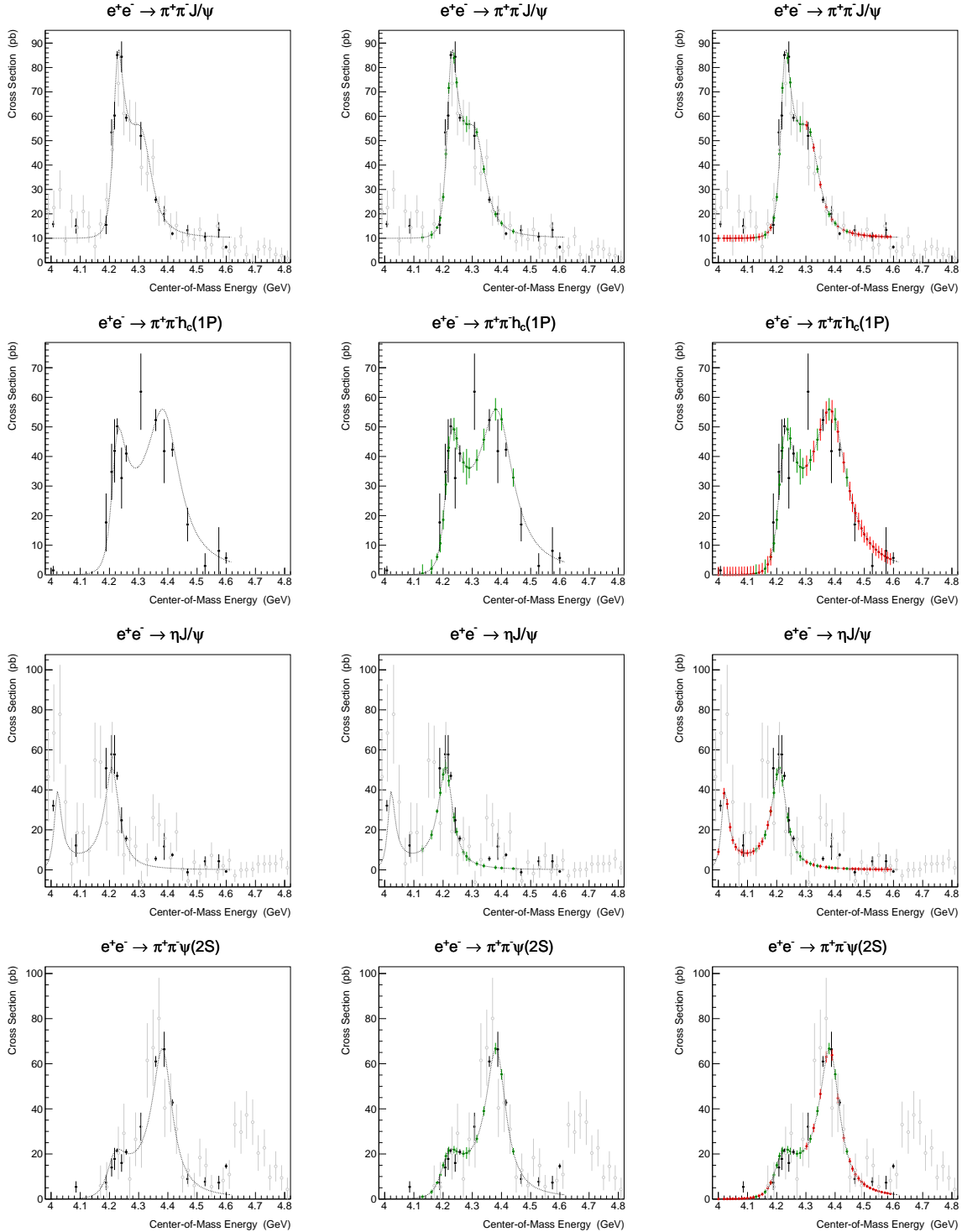


Figure 3.12: Simulations for different exclusive e^+e^- cross sections. The black points are already measured (before 2019); the green points are projections for 2019; the red points are projections for the proposal from 4.0 to 4.6 GeV, and the gray points are from Belle. The top row shows $e^+e^- \rightarrow \pi^+\pi^-J/\psi$; the second row shows $e^+e^- \rightarrow \pi^+\pi^-h_c$; the third row shows $e^+e^- \rightarrow \eta J/\psi$; the bottom row shows $e^+e^- \rightarrow \pi^+\pi^-\psi(3686)$.

(3) Possibilities for Data Above 4.6 GeV

If BESIII will take data above 4.6 GeV, a number of new exciting possibilities would become accessible. Here we list five cases. (1) We know there is an unexplained peak at 4.66 GeV in the $e^+e^- \rightarrow \pi^+\pi^-\psi(3686)$ cross section. BESIII would be able to produce and study it directly. (2) We could also study the peak at 4.63 GeV in the $\Lambda_c^+\bar{\Lambda}_c^-$ cross section. (3) We could search for new peaks; it seems likely that more than those two exist. These three goals would extend our study of the Y problem. (4) Production of a Z_{cs} tetraquark candidate in the process $e^+e^- \rightarrow KZ_{cs}$ with $Z_{cs} \rightarrow KJ/\psi$ would require cms energies above 4.6 GeV if the Z_{cs} is near the $D_s\bar{D}^*$ or $D_s^*\bar{D}$ threshold. (5) Data significantly above 4.6 GeV provide access to additional charmed baryon thresholds. BESIII would thus be able to study charmed baryons in a uniquely clean environment. (6) Data above 4.6 GeV would provide a unique opportunity to search for the excited $1^{+-} h_c$ state, expected to be around 3.9 GeV and show up in $e^+e^- \rightarrow \eta D\bar{D}^*$. The identification of this state would likely help clarify many of the J^{++} states between 3.8 and 4.0 GeV.

3.3.4 Comparisons with Other Experiments

Belle II [72] started collecting data in 2019, and will accumulate 50 ab^{-1} data at the $\Upsilon(4S)$ peak by 2027. These data samples can be used to study the XYZ and charmonium states in many different ways [73], among which ISR can produce events in the same energy range covered by BESIII. Figure 3.13 shows the effective luminosity at BEPCII energy in the Belle II data samples. We can see that 50 ab^{-1} of Belle II data corresponds to 2,000–2,800 pb^{-1} data for each 10 MeV interval between 4–5 GeV, similar statistics will be accumulated for modes like $e^+e^- \rightarrow \pi^+\pi^-J/\psi$ at Belle II and BESIII, taking into account the fact that Belle II has lower efficiency.

Table 3.3 also lists the expected ratios of numbers of events for BESIII and Belle II given BESIII data sets with 500 pb^{-1} per point and a Belle II sample of 50 ab^{-1} . Belle II has the advantage that data at different energies will be accumulated at the same time, making the analysis simpler than BESIII scans over many data points. On the other hand, Belle II needs to integrate over large energy bins, while the BESIII data is collected at individual energy points with an energy resolution spread of around 2 MeV.

The LHCb experiment has also made large contributions to our understanding of the XYZ mesons. The strength of LHCb for studies of B decays to final states with all charged particles cannot be matched by e^+e^- facilities. For example, LHCb has made precision measurements of the $X(3872)$ in the process $B \rightarrow KX$ with $X \rightarrow \pi^+\pi^-J/\psi$ and $J/\psi \rightarrow \mu^+\mu^-$ [74]. The discovery of the process $B \rightarrow KY(4260)$ with $Y(4260) \rightarrow \pi Z_c(3900)$ at D0 [75, 76] may give LHCb an opportunity to study the $Y(4260)$ and $Z_c(3900)$ in detail. However, since most of the XYZ particles decay to final states with neutral particles, the LHCb experiment is mostly complementary to the BESIII experiment. In contrast to BESIII, LHCb does not feature a high quality electromagnetic calorimeter. Thus, the identification of soft neutral pions and photons is difficult.

Finally, it should be noted that all three experiments have rather different systematics, which emphasises their complementarity.

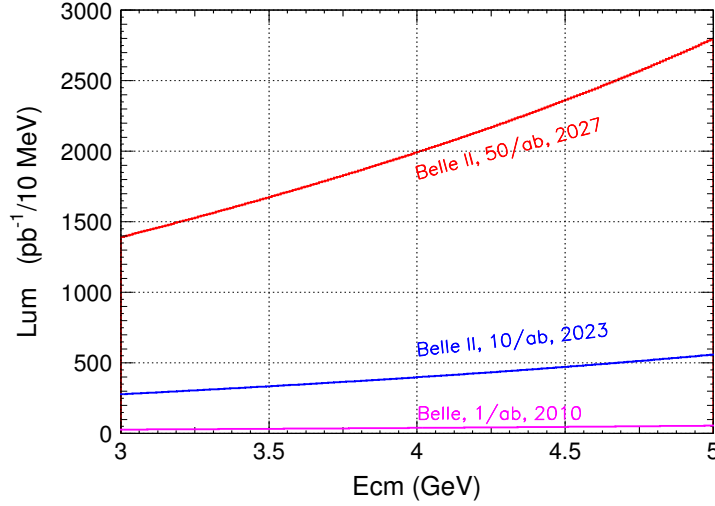


Figure 3.13: Effective luminosity at low energy in the Belle and Belle II $\Upsilon(4S)$ data samples.

Table 3.3: A comparison of BESIII and Belle II for various channels at a few different e^+e^- cms energies assuming 50 ab^{-1} of Belle II data in 10 MeV energy bins. L and N denote the expected luminosity and number of observed signals, respectively.

ISR mode	$L_{\text{BESIII}}/L_{\text{Belle II}}$	$\varepsilon_{\text{BESIII}}/\varepsilon_{\text{Belle II}}$	$N_{\text{BESIII}}/N_{\text{Belle II}}$
$\pi^+\pi^-J/\psi$ at 4.26 GeV	$0.5 \text{ fb}^{-1} / 2.2 \text{ fb}^{-1}$	46% / 10%	1.07
$\pi^+\pi^-\psi(3686)$ at 4.36 GeV	$0.5 \text{ fb}^{-1} / 2.3 \text{ fb}^{-1}$	41% / 5%	1.82
$\pi^+\pi^-\psi(3686)$ at 4.66 GeV	$0.5 \text{ fb}^{-1} / 2.5 \text{ fb}^{-1}$	35% / 6%	1.19
$\pi^+\pi^-h_c$ at 4.26 GeV	$0.5 \text{ fb}^{-1} / 2.2 \text{ fb}^{-1}$	2.7% / -%	> 5
K^+K^-J/ψ at 4.6 GeV	$0.5 \text{ fb}^{-1} / 2.4 \text{ fb}^{-1}$	29% / 7.5%	0.81
K^+K^-J/ψ at 4.9 GeV	$0.5 \text{ fb}^{-1} / 2.7 \text{ fb}^{-1}$	$\approx 29\%$ / 10%	0.54
$\Lambda_c^+\bar{\Lambda}_c^-$ at 4.6 GeV	$0.5 \text{ fb}^{-1} / 2.4 \text{ fb}^{-1}$	51% / 7.5%	1.42
$\Lambda_c^+\bar{\Lambda}_c^-$ at 4.9 GeV	$0.5 \text{ fb}^{-1} / 2.7 \text{ fb}^{-1}$	$\approx 37\%$ / 7.5%	0.91

Table 3.4: Data-taking requirements for XYZ physics (top) and charmonium physics (bottom).

Plan	Data Sets
XYZ plan (1)	500 pb ⁻¹ at a large number of points between 4.0 and 4.6 GeV
XYZ plan (2)	5 fb ⁻¹ at 4.23, 4.42 GeV for large Z_c samples
XYZ plan (3)	5 fb ⁻¹ above 4.6 GeV
charmonium plan	3×10^9 $\psi(3686)$ decays

3.4 Summary of Data Requirements

Our data-taking requirements are summarized in Table 3.4. Sensitivities to various channels in XYZ physics are given in Table 3.2; sensitivities to charmonium studies are listed in Table 3.1.

Bibliography

- [1] T. Appelquist and H.D. Politzer, Phys. Rev. Lett. **34**, 43 (1975).
- [2] D. M. Asner *et al.*, Int. J. Mod. Phys. A **24**, S1 (2009).
- [3] M. Tanabashi *et al.* (Particle Data Group), Phys. Rev. D **98**, 030001 (2018).
- [4] G. Pakhlova *et al.* (Belle Collaboration), Phys. Rev. Lett. **101**, 172001 (2008).
- [5] X. L. Wang *et al.* (Belle Collaboration), Phys. Rev. Lett. **99**, 142002 (2007).
- [6] T. Barnes, S. Godfrey and E. S. Swanson, Phys. Rev. D **72**, 054026 (2005).
- [7] G. K. C. Cheung *et al.* (Hadron Spectrum Collaboration), JHEP **1612**, 089 (2016)
- [8] K. A. Olive *et al.* (Particle Data Group), Chin. Phys. C **38**, 090001 (2014) and 2015 update.
- [9] W. E. Caswell and G. P. Lepage, Phys. Lett. B **167**, 437 (1986).
- [10] G. P. Lepage, L. Magnea, C. Nakhleh, U. Magnea and K. Hornbostel, Phys. Rev. D **46**, 4052 (1992).
- [11] G. T. Bodwin, E. Braaten and G. P. Lepage, Phys. Rev. D **51**, 1125 (1995); Erratum: [Phys. Rev. D **55**, 5853 (1997)].
- [12] Alexey A. Petrov, Andrew E. Blechman, “Effective Field Theories”, World Scientific Publishing Company Pte Limited, 2015, ISBN 9789814434935
- [13] A. Pineda and J. Soto, Nucl. Phys. Proc. Suppl. **64**, 428 (1998).
- [14] N. Brambilla, A. Pineda, J. Soto and A. Vairo, Nucl. Phys. B **566**, 275 (2000).
- [15] N. Brambilla, A. Pineda, J. Soto and A. Vairo, Rev. Mod. Phys. **77**, 1423 (2005).
- [16] Y. P. Kuang, Front. Phys. China **1**, 19 (2006).
- [17] N. Brambilla *et al.* (Quarkonium Working Group), arXiv:hep-ph/0412158.
- [18] M. E. B. Franklin *et al.*, Phys. Rev. Lett. **51**, 963 (1983).
- [19] M. Ablikim *et al.* (BESIII Collaboration), Phys. Rev. Lett. **104**, 132002 (2010).

- [20] M. Ablikim *et al.* (BESIII Collaboration), Phys. Rev. Lett. **107**, 092001 (2011).
- [21] M. Ablikim *et al.* (BESIII Collaboration), Phys. Rev. Lett. **108**, 222002 (2012).
- [22] M. Ablikim *et al.* (BESIII Collaboration), Phys. Rev. Lett. **109**, 042003 (2012).
- [23] M. Ablikim *et al.* (BESIII Collaboration), Phys. Rev. Lett. **116**, 251802 (2016).
- [24] <http://english.ihep.cas.cn/chnl/245/index.html>
- [25] M. Ablikim *et al.* (BESIII Collaboration), Phys. Rev. D **99**, 072008 (2019).
- [26] M. Ablikim *et al.* (BESIII Collaboration), Phys. Rev. D **87**, 012002 (2013).
- [27] Y. J. Gao, Y. J. Zhang and K. T. Chao, Chin. Phys. Lett. **23**, 2376 (2006).
- [28] F. Feng, Y. Jia and W. L. Sang, Phys. Rev. Lett. **115**, 222001 (2015).
- [29] F. Feng, Y. Jia and W. L. Sang, Phys. Rev. Lett. **119**, 252001 (2017).
- [30] M. Ablikim *et al.* (BESIII Collaboration), Phys. Rev. Lett. **105**, 261801 (2010).
- [31] K. Zhu, X. H. Mo and C. Z. Yuan, Int. J. Mod. Phys. A **30**, 1550148 (2015).
- [32] M. Ablikim *et al.* (BESIII Collaboration), Phys. Rev. D **88**, 112001 (2013).
- [33] N. A. Tornqvist, Phys. Lett. A **117**, 1 (1986).
- [34] L. Kopke, talk presented at XXIIrd Intern Conf. on High Energy Physics, Berkeley, USA, 1986.
- [35] X. G. He, J. P. Ma and B. McKellar, Phys. Rev. D **47**, 1744(R) (1993).
- [36] X. G. He, J. P. Ma and B. McKellar, Phys. Rev. D **49**, 4548 (1994)
- [37] M. Ablikim *et al.* (BESIII Collaboration), Phys. Rev. Lett. **115**, 011803 (2015).
- [38] R. F. Lebed, R. E. Mitchell and E. S. Swanson, Prog. Part. Nucl. Phys. **93**, 143 (2017).
- [39] H. X. Chen, W. Chen, X. Liu and S. L. Zhu, Phys. Rept. **639**, 1 (2016).
- [40] A. Esposito, A. Pilloni and A. D. Polosa, Phys. Rept. **668**, 1 (2016).
- [41] F.-K. Guo, C. Hanhart, U.-G. Meißner, Q. Wang, Q. Zhao and B.-S. Zou, Rev. Mod. Phys. **90**, 015004 (2018).
- [42] A. Ali, J. S. Lange and S. Stone, Prog. Part. Nucl. Phys. **97**, 123 (2017).
- [43] S. L. Olsen, T. Skwarnicki and D. Zieminska, Rev. Mod. Phys. **90**, 015003 (2018).
- [44] S. K. Choi *et al.* (Belle Collaboration), Phys. Rev. Lett. **91**, 262001 (2003).

- [45] M. Ablikim *et al.* (BESIII Collaboration), Phys. Rev. Lett. **112**, 092001 (2014).
- [46] F.-K. Guo, C. Hanhart, U.-G. Meißner, Q. Wang and Q. Zhao, Phys. Lett. B **725**, 127 (2013).
- [47] K. Abe *et al.* (Belle Collaboration), Phys. Rev. Lett. **94**, 182002 (2005).
- [48] K. Chilikin *et al.* (Belle Collaboration), Phys. Rev. D **95**, 112003 (2017).
- [49] F.-K. Guo and U.-G. Meißner, Phys. Rev. D **86**, 091501 (2012).
- [50] F. K. Guo, U. G. Meiner and Z. Yang, Phys. Lett. B **740**, 42 (2015)
- [51] B. Aubert *et al.* (BaBar Collaboration), Phys. Rev. Lett. **95**, 142001 (2005).
- [52] L. Liu *et al.* (Hadron Spectrum Collaboration), JHEP **1207**, 126 (2012).
- [53] F. E. Close and P. R. Page, Phys. Lett. B **628**, 215 (2005).
- [54] Q. Wang, C. Hanhart and Q. Zhao, Phys. Rev. Lett. **111**, 132003 (2013);
- [55] M. Ablikim *et al.* (BESIII Collaboration), Phys. Rev. Lett. **110**, 252001 (2013).
- [56] M. Ablikim *et al.* (BESIII Collaboration), Phys. Rev. Lett. **111**, 242001 (2013).
- [57] S. K. Choi *et al.* (Belle Collaboration), Phys. Rev. Lett. **100**, 142001 (2008).
- [58] M. Ablikim *et al.* (BESIII Collaboration), Phys. Rev. Lett. **112**, 022001 (2014).
- [59] M. Ablikim *et al.* (BESIII Collaboration), Phys. Rev. Lett. **112**, 132001 (2014).
- [60] M. Ablikim *et al.* (BESIII Collaboration), Phys. Rev. Lett. **118**, 092001 (2017).
- [61] M. Ablikim *et al.* (BESIII Collaboration), Phys. Rev. Lett. **115**, 112003 (2015).
- [62] M. Ablikim *et al.* (BESIII Collaboration), Phys. Rev. Lett. **118**, 092002 (2017).
- [63] M. Ablikim *et al.* (BESIII Collaboration), Phys. Rev. Lett. **114**, 092003 (2015).
- [64] M. Ablikim *et al.* (BES Collaboration), eConf C **070805**, 02 (2007) [Phys. Lett. B **660**, 315 (2008)].
- [65] M. Ablikim *et al.* (BESIII Collaboration), Phys. Rev. D **96**, 032004 (2017).
- [66] M. Ablikim *et al.* (BESIII Collaboration), Phys. Rev. Lett. **122**, 102002 (2019)
- [67] M. Ablikim *et al.* (BESIII Collaboration), Phys. Rev. Lett. **122**, 232002 (2019).
- [68] M. Ablikim *et al.* [BESIII Collaboration], Phys. Rev. D **99**, 091103 (2019).
- [69] M. Cleven, Q. Wang, F. K. Guo, C. Hanhart, U. G. Meißner and Q. Zhao, Phys. Rev. D **90**, 074039 (2014).

- [70] M. Ablikim *et al.* (BESIII Collaboration), Phys. Rev. Lett. **119**, 072001 (2017).
- [71] E. S. Swanson, Int. J. Mod. Phys. E **25**, 1642010 (2016).
- [72] T. Abe *et al.* (Belle II Collaboration), arXiv:1011.0352 [physics.ins-det]; E. Kou *et al.* (Belle II Collaboration), PTEP **2019**, 123C01 (2019).
- [73] A. J. Bevan *et al.* (BaBar and Belle Collaborations), Eur. Phys. J. C **74**, 3026 (2014).
- [74] R. Aaij *et al.* (LHCb Collaboration), Phys. Rev. D **92**, 011102 (2015).
- [75] V. M. Abazov *et al.* (D0 Collaboration), Phys. Rev. D **98**, 052010 (2018).
- [76] V. M. Abazov *et al.* (D0 Collaboration), Phys. Rev. D **100**, 012005 (2019).

Chapter 4

R values, QCD and τ Physics

4.1 Introduction

The R -QCD- τ working group deals with various aspects of QCD, the accepted theory of strong interactions within the Standard Model of particle physics. The cms energy of BEPCII is ideally suited to study the transition region between non-perturbative and perturbative aspects of QCD [1]. It offers a unique laboratory to test not only the validity of QCD in the few-GeV energy range, but also the validity of effective theories and hadronic models towards high energies.

BESIII has already demonstrated that the high statistics and accuracy of the data, illustrated in Fig. 4.1, allow to measure form factors of mesons and baryons with unprecedented accuracy and with paramount impact on hadron structure investigations. These form factors are not only accessible in the timelike domain via electron-positron annihilations, but can also be determined in the spacelike domain in two-photon scattering.

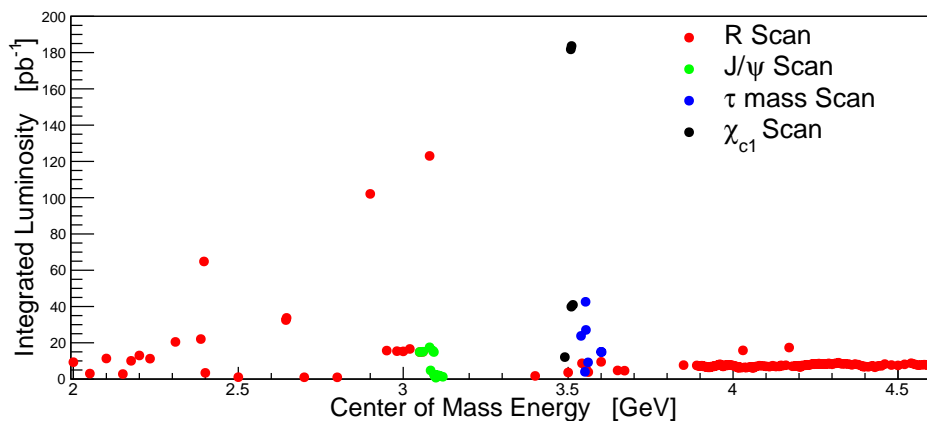


Figure 4.1: Overview of data sets and their integrated luminosities acquired for the R -QCD- τ working group. R scan data (red) were collected from 2012-2015, the J/ψ line shape scan (green) was performed in 2012, a search for the production of χ_{c1} (black) was carried out in 2017, and the latest τ mass scan data (blue) were acquired in 2018.

As is well known, the measurement of electron-positron annihilation into hadrons is

of utmost importance for precision tests of the SM. While the measurement of exclusive hadronic channels is needed for the hadronic vacuum polarization contribution of the anomalous magnetic moment of the muon, $(g - 2)_\mu$, the inclusive measurement of the hadronic cross section above 2 GeV can be used to improve the knowledge of the fine structure constant at the Z -pole. The latter is currently limiting precision tests in the electroweak sector of the SM. Thus, its improvement is of central importance for the physics programs at future high-energy electron-positron colliders, such as Higgs factories [2, 3]. The exclusive channels can be measured at BESIII via the initial state radiation (ISR) technique, while the accuracy of the inclusive R -measurement will be further improved with respect to measurements at BES and KEDR. Regarding $(g - 2)_\mu$, BESIII can also measure the transition form factors of pseudoscalar mesons, as motivated by the hadronic light-by-light scattering contributions to $(g - 2)_\mu$.

The analysis of the high-statistics energy scan between 2.0 and 4.6 GeV allows for a first precision measurement of neutron and hyperon form factors. In the case of hyperons, their self-analyzing decay does not only provide access to the absolute values of the electric and magnetic form factors, but it allows even to extract the relative phase between them. A complementary view on hadron structure is possible through the measurement of Collins asymmetries. The recent result obtained at BESIII extends previously available knowledge, which was restricted to measurements at B factories, towards lower energies. The picture of the non-perturbative features of QCD can be further extended by the investigation of fragmentation functions.

Naturally, the research program of the τ -QCD working group comprises measurements of such fundamental parameters of the SM as the mass of the τ lepton. It can be determined via an energy scan in its threshold region. The first result of BESIII is already the world's most precise measurement. Further improvement is expected with new data. Moreover, the mass of the charm quark is accessible by determining the cross section of $e^+e^- \rightarrow c\bar{c}$, which relates the physics of hadronic cross section measurements to yet another precision observable of the SM.

Finally, the precise scan measurements for the R value and τ mass measurements allow for detailed investigations of the production of charmonium resonances. The line shape of vector charmonium resonances might reveal through a relative phase of strong and electromagnetic decay amplitudes a more detailed picture of their internal structure. Even the production of non-vector resonances like the χ_{c1} in e^+e^- annihilations might be observed through interference patterns with the continuous background. Another exciting spin-off of the BESIII R -program are investigations of the light hadron spectrum, enabling studies of potentially exotic resonances, such as the $\phi(2170)$.

4.2 BESIII measurements related to precision variables $(g - 2)_\mu$ and $\alpha_{\text{em}}(s)$

4.2.1 The anomalous magnetic moment of the muon, $(g - 2)_\mu$

At present, both the SM prediction, as well as the experimental value of the anomalous magnetic moment of the muon, $a_\mu = (g - 2)_\mu/2$ [4] are determined with a relative

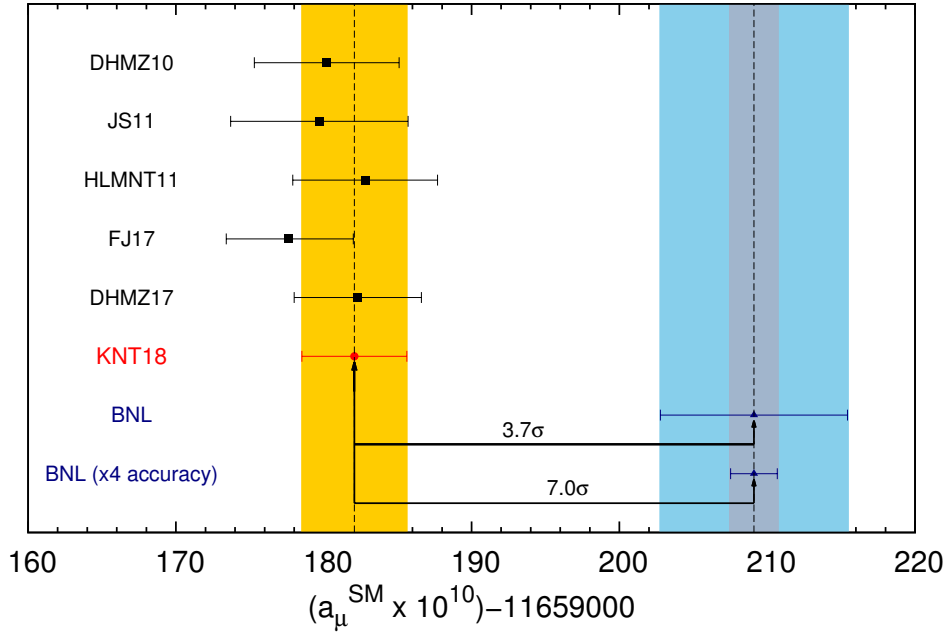


Figure 4.2: Compilation of recent results for a_μ^{SM} (figure taken from Ref. [5]). The “DHMZ17” and “KNT18” points correspond to Refs. [7] and [5], respectively. Also shown is the accuracy of the upcoming new FNAL measurement of a_μ^{exp} under the hypothetical assumption that the central mean value of a_μ^{exp} will remain unchanged.

uncertainty of about one half part per million:

$$a_\mu^{\text{SM}} = (11\,659\,182.04 \pm 3.56) \times 10^{-10} \quad [\text{Keshavarzi } et al.] [5], \quad (4.1)$$

$$a_\mu^{\text{exp}} = (11\,659\,208.9 \pm 6.3) \times 10^{-10} \quad [\text{BNL-E821}] [6]. \quad (4.2)$$

A second evaluation of a_μ^{SM} by Davier *et al.* finds $a_\mu^{\text{SM}} = (11\,659\,182.3 \pm 4.3) \times 10^{-10}$ [7]. Depending on the value used for a_μ^{SM} , a tension of 3.5 – 3.7 standard deviations between the SM prediction and the direct measurement of a_μ is observed, as illustrated in Fig. 4.2.

Currently, the SM prediction of a_μ is slightly more precise than the experimental value, but the situation will change soon [8]. New direct measurements have been started at FNAL [9] and a complementary project is under construction at J-PARC [10]. Both aim to reduce the experimental uncertainty by a factor of four. The light grey band in Fig. 4.2 represents the hypothetical situation of the new FNAL measurement yielding the same mean value for a_μ^{exp} with fourfold improved accuracy.

The main uncertainties in a_μ^{SM} originate from hadronic effects, in particular the contributions from hadronic vacuum polarization (HVP), a_μ^{HVP} , and hadronic light-by-light scattering (HLbL), a_μ^{HLbL} , as shown in Fig. 4.3. It is of vital importance to investigate whether physics models beyond the SM [11] or poorly understood hadronic effects are responsible for the observed tension. This is one of the main goals of the *R*-QCD research program.

The current estimate of a_μ^{HVP} , which enters the SM prediction, is based on dispersion

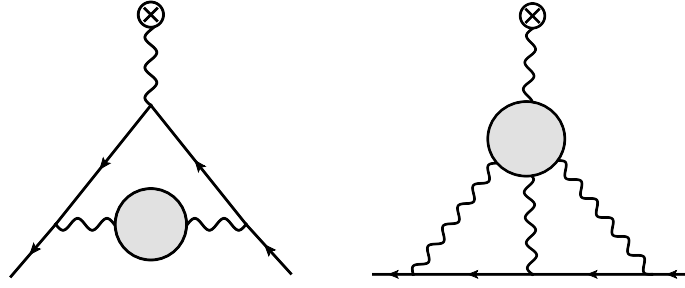


Figure 4.3: The HVP (left panel) and the HLbL (right panel) contributions to the anomalous magnetic moment of the muon.

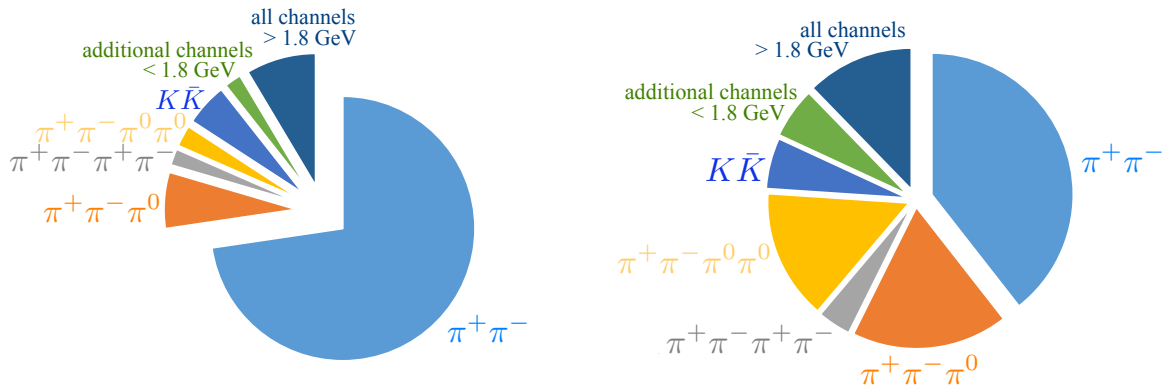


Figure 4.4: Contributions of different channels and energy ranges to the absolute value (left) and the uncertainty (right) of a_μ^{HVP} , demonstrating the importance of the processes $e^+e^- \rightarrow \pi^+\pi^-$, $e^+e^- \rightarrow \pi^+\pi^-\pi^0$, $e^+e^- \rightarrow \pi^+\pi^-2\pi^0$, and $e^+e^- \rightarrow K\bar{K}$ (numbers taken from Ref. [5]).

theory, in which experimental measurements of the annihilation cross section $e^+e^- \rightarrow$ hadrons are used as input for the evaluation of a dispersion integral:

$$a_\mu^{\text{HVP}} = \left(\frac{\alpha m_\mu}{3\pi}\right)^2 \int_{4m_\pi^2}^{\infty} ds \frac{R_{\text{had}}(s)K(s)}{s^2}, \quad (4.3)$$

where $K(s)$ is a kernel varying from 0.63 at $s = 4m_\pi^2$ to 1.0 at $s = \infty$, and $m_\mu(m_\pi)$ is the nominal mass of the pion(muon).

Within Ref. [5], the leading-order hadronic contribution is calculated to be $a_\mu^{\text{HVP}} = (684.68 \pm 2.42) \times 10^{-10}$. At BESIII, we are aiming at a further reduction of the uncertainty of a_μ^{HVP} by measuring exclusive channels of R_{had} in the most relevant energy range. Figure 4.4 shows the contributions of various exclusive hadronic channels to the absolute value (left) and the uncertainty (right) of a_μ^{HVP} . As can be seen, the channels with $\pi^+\pi^-$, $\pi^+\pi^-\pi^0$, $\pi^+\pi^-\pi^0\pi^0$, and $K\bar{K}$ are most relevant, which the current efforts at BESIII are focusing on exactly. A major program of hadronic cross section measurements, which is presented in detail in Sec. 4.2.3, has been launched.

Beyond HVP, the next important contribution to the uncertainty of $(g-2)_\mu$ is given by the HLbL contribution shown in the right panel of Fig. 4.3. The leading contribution

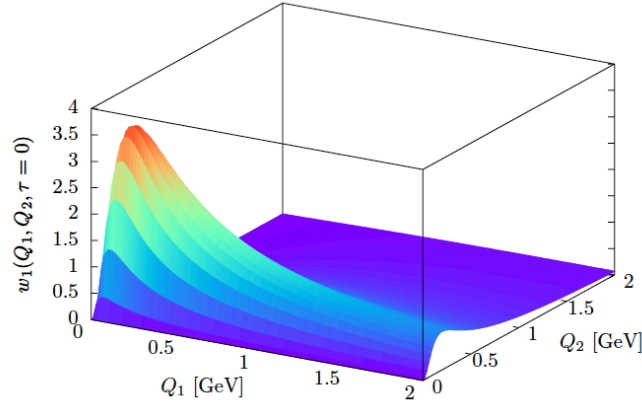


Figure 4.5: Weight of the transition form factors of the lightest pseudoscalar mesons in the calculation of a_μ^{HLbL} as a function of the virtualities of the two photons. Figure taken from Ref. [20].

to the HLbL diagram is given by the coupling of photons to the pseudoscalar mesons π^0 , η , η' as well as channels like $\pi\pi$ and $\pi\eta$, as shown in Fig. 4.9. So far, hadronic models have been used for the calculation of the HLbL diagram. Although most groups report similar values for the absolute size of the HLbL contribution, the assumed uncertainties differ largely. The calculation with the lowest uncertainties stems from Prades, de Rafael, and Vainshtein [12]. They find the following value: $a_\mu^{\text{HLbL}} = (10.5 \pm 2.6) \times 10^{-10}$.

Very recently, new theoretical approaches have been proposed by groups from Bern and Mainz [13–19] in order to attack the HLbL calculation, namely by exploiting dispersion relations. Form factor measurements of the two-photon coupling $\gamma\gamma \rightarrow P$, where P is a one-hadron or two-hadron system, are of special interest. The Belle and BaBar collaborations have determined these couplings referred to as meson TFF for the lightest pseudoscalar mesons. However, the results of the B -factories have only been obtained at very large momentum transfers above 2 GeV, while for the HLbL contribution measurements at low momentum transfers are required. This is illustrated by Fig. 4.5, which shows the weight of the light pseudoscalar TFFs in the HLbL calculation [20] as a function of the two virtualities Q_1 and Q_2 of the photons. It can clearly be seen that the region of small momentum transfers is most relevant. This is exactly where BESIII can provide precision result.

To summarize, an improvement of the SM prediction of $(g-2)_\mu$ is urgently needed in view of two upcoming direct measurements of a_μ at Fermilab and J-PARC with a fourfold improved precision. In the white paper of Ref. [21] in 2013, it was argued that new experiments, like the ones carried out at BESIII, should lead to a final reduction of the SM uncertainty of a_μ down to 3.5×10^{-10} . The recent evaluations in Refs. [5, 7, 22] show that such an accuracy has almost been achieved already. BESIII have contributed to this achievement. The future program of BESIII together with new analyses at BaBar, Belle II, and elsewhere will lead to an additional significant reduction. The midterm goal is to reduce both the HVP and HLbL uncertainties to a level similar to the future experimental uncertainty, *i.e.*, 1.6×10^{-10} . It should also be mentioned that since 2017

the theoretical and experimental work in view of a_μ^{SM} is coordinated by the $g - 2$ *Theory Initiative* [23], which is a consortium of theoretical and experimental physicists working towards an improved SM prediction. Members of the BESIII collaboration are part of this consortium.

4.2.2 The running of the electromagnetic fine structure constant, $\alpha_{\text{em}}(s)$

Due to vacuum polarization effects, the electromagnetic fine structure constant α_{em} is a “running” quantity. Its value increases with increasing momentum transfer s of the scattering process. The effective running of the fine structure constant as a function of s is usually parametrized in SM in the following way:

$$\alpha_{\text{em}}(s) = \frac{\alpha(0)}{(1 - \Delta\alpha_{\text{em}}(s))}, \quad (4.4)$$

$$\Delta\alpha_{\text{em}}(s) = \Delta\alpha_{\text{em}}^{\text{lept}}(s) + \Delta\alpha_{\text{em}}^{\text{had}(5)}(s) + \Delta\alpha_{\text{em}}^{\text{top}}(s). \quad (4.5)$$

In the above formula, $\Delta\alpha_{\text{em}}^{\text{lept}}$ denotes the vacuum polarization effects due to lepton loops, $\Delta\alpha_{\text{em}}^{\text{had}(5)}$ accounts for the effects due to loop contributions of the five lightest quarks, and the loop contributions due to the top quark are given by $\Delta\alpha_{\text{em}}^{\text{top}}$. The leptonic contribution can be computed in QED with very high precision, while the top-quark loop contribution is very small. Therefore, the total uncertainty of $\Delta\alpha_{\text{em}}$ is entirely limited by $\Delta\alpha_{\text{em}}^{\text{had}(5)}$. As in the case of $(g - 2)_\mu$, a dispersion relation can be used to relate experimental hadronic cross section data with $\Delta\alpha_{\text{em}}^{\text{had}(5)}$.

Of special interest is the knowledge of $\Delta\alpha_{\text{em}}$ for $s = M_Z^2$ since most of the electroweak precision tests have been performed at the Z^0 peak at LEP. The total correction to the fine structure constant amounts to [5]

$$\Delta\alpha_{\text{em}}(M_Z^2) = (276.11 \pm 1.11) \times 10^{-4}, \quad (4.6)$$

and the value of α_{em} at the Z pole mass is therefore known to be

$$\alpha_{\text{em}}^{-1}(M_Z^2) = 128.947 \pm 0.012. \quad (4.7)$$

A similar result of $\alpha_{\text{em}}^{-1}(M_Z^2) = 128.946 \pm 0.015$ is found in Ref. [7]. The current uncertainty of $\Delta\alpha_{\text{em}}$ represents a severe limitation for electroweak precision fits to the SM (see a review on *Electroweak model and constraints on new physics* in Ref. [24]). Typically these fits are performed using three independent input variables, such as $\alpha_{\text{em}}(M_Z^2)$, the Fermi constant G_μ , and M_Z . Among these three quantities, $\alpha_{\text{em}}(M_Z^2)$ is known with the least precision. Its relative uncertainty is 1×10^{-4} , while G_μ and M_Z are known with uncertainties of 5×10^{-7} and 2×10^{-5} , respectively. In the past, the insufficient knowledge of $\Delta\alpha_{\text{em}}$ led to imprecise predictions of the Higgs mass. Now that the Higgs mass is known with high accuracy, any new precision measurement of an electroweak observable (as for instance the electroweak mixing angle $\sin^2(\Theta_W)$) establishes a significant test of the electroweak SM. The smaller the uncertainty of $\Delta\alpha_{\text{em}}(M_Z^2)$ is, the more powerful this test will be. As will be discussed in Sec. 4.2.4, the goal of the new BESIII measurement is to reduce the uncertainty of the R measurement to 3%, which allows to improve the accuracy of the prediction of $\Delta\alpha_{\text{em}}^{\text{had}(5)}$.

4.2.3 Measurement of exclusive hadronic channels via ISR

A major campaign of ISR [25–27] measurements was launched at BESIII, mainly in order to improve the HVP contribution to $(g-2)_\mu$ and of $\Delta\alpha_{\text{em}}^{\text{had}(5)}$. The ISR technique allows for precision measurements of the hadronic cross section at high-luminosity electron-positron colliders by using events in which either the incoming electron or positron has emitted a high-energetic photon. In such a way, the available cms energy for the hadronic system is varied depending on the energy of the ISR photon, which is the reason that the technique is also called Radiative Return.

From the measurement of the hadronic cross section $\sigma(e^+e^- \rightarrow \text{hadrons} + \gamma_{\text{ISR}})$, the non-radiative cross section $\sigma(e^+e^- \rightarrow \text{hadrons})$ can be extracted using a radiator function from QED theory. This radiator function is known with a precision of 0.5% within the Monte Carlo (MC) generator PHOKHARA [28–30], which also simulates the most relevant exclusive final states in view of the HVP contribution to $(g-2)_\mu$.

At BESIII, the data set taken at a cms energy of 3.773 GeV is currently used for most of the ISR analyses. The total integrated luminosity available at this cms energy amounts to 2.9 fb^{-1} . Using this data set, the statistics of ISR hadronic events is superior to the ISR statistics of BaBar above hadronic masses of approximately 1.5 GeV. With upcoming new data and by including the already available data sets, the available ISR statistics will be similar to the BaBar statistics also at masses below 1.5 GeV.

Both the tagged and untagged ISR approaches are currently carried out at BESIII. The tagged approach requires the explicit detection of the ISR photon in the calorimeter, and allows for studies of the full hadronic mass range starting from the dipion mass threshold. An untagged measurement corresponds to the usage of ISR events, in which the ISR photon is emitted at very small polar angles, essentially collinear with the initial electron beams. Although tagging of those photons is not feasible, the momentum information can be extracted from the missing momentum of the fully reconstructed hadronic system. For kinematic reasons, the untagged approach is limited to the energy with hadron productions above approximately 1 GeV. Above 1.5 GeV, it provides significantly improved statistics compared to the tagged measurement, and furthermore, guarantees low background conditions.

The main results of the ISR program at BESIII can be summarized as follows:

- **Timelike pion form factor:** $e^+e^- \rightarrow \pi^+\pi^-$

A new measurement of the hadronic cross section of the channel $e^+e^- \rightarrow \pi^+\pi^-$ was performed in the energy range between 600 MeV and 900 MeV, which corresponds to the peak region of the $\rho(770)$ resonance [31]. In this energy range the two-pion channel indeed contributes more than 50% to a_μ^{HVP} , and the uncertainty of this exclusive channel is therefore decisive for the SM error of $(g-2)_\mu$. Thus, this is *the* flagship analysis of the BESIII ISR program. A total systematic uncertainty of 0.9% for the cross-section measurement has already been achieved. The two limiting contributions to the total systematic uncertainty are from the luminosity measurement and the theoretical radiator function, with 0.5% for each. As will be discussed below, with improved calculations of the radiator function, by including larger data sets, and by an overall improved understanding of the detector performance, the errors

of both these contributions can be reduced from 0.5% to 0.2% for each, yielding a reduced total systematic uncertainty. The mass range studied in this analysis is accessible via the tagged ISR approach only. The same holds for the mass range from the dipion mass threshold to 600 MeV, which will be studied in future, along with the mass range above 900 MeV, where the investigations can be performed in the untagged ISR approach as well.

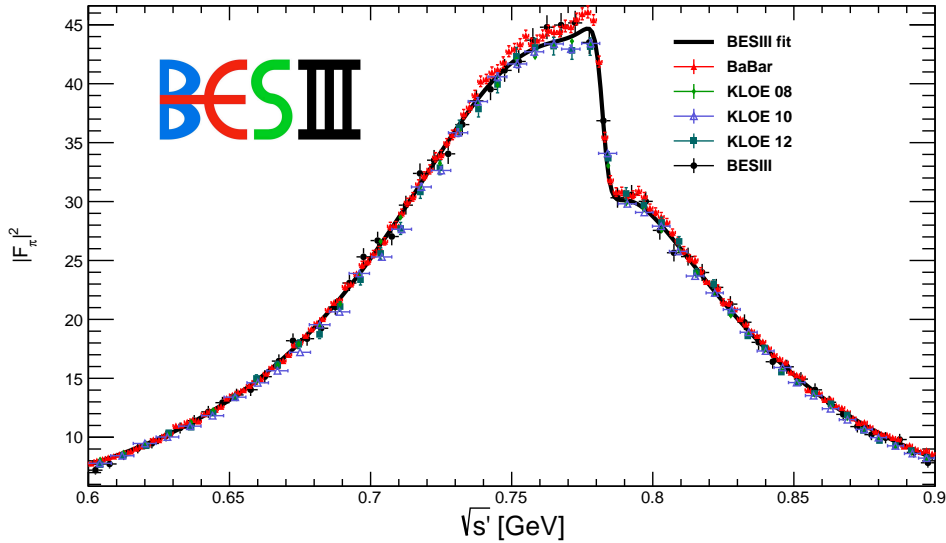


Figure 4.6: Pion form factor measurements at BESIII [31], KLOE [34–36], and BaBar [37]. The black line is a fit to the BESIII spectrum according to the Gounaris-Sakurai parametrization.

In this analysis all the experimental detection efficiencies, the luminosity, as well as the knowledge of background channels need to be determined at the per mil level. A separation of pion tracks from muon tracks turns out to be the major challenge of the analysis. As a consequence, a multivariate analysis technique is applied [32] by training an artificial neural network (ANN) for particle identification. When selecting muon events rather than pion events, the efficiency of the technique can be tested by comparing the absolute yield of $e^+e^- \rightarrow \mu^+\mu^-\gamma$ events with the PHOKHARA [33] MC prediction. An agreement between data and MC simulations at the level of $(0.5 \pm 0.3)\%$ is observed, demonstrating the excellent performance of the ANN.

From the cross section measurement, the timelike pion form factor $|F_\pi|$ is extracted, as shown in Fig. 4.6. An agreement between the BESIII data and the three KLOE [34–36] analyses is found up to the peak of the ρ resonance. At the same time, the BESIII data are systematically lower with respect to BaBar’s results [37] in this mass range. Above the ρ peak the situation is reversed. In this case, the BESIII spectrum comes out to be in good agreement with that of BaBar, while the KLOE results are systematically lower. In Fig. 4.7, we show the impact of the new

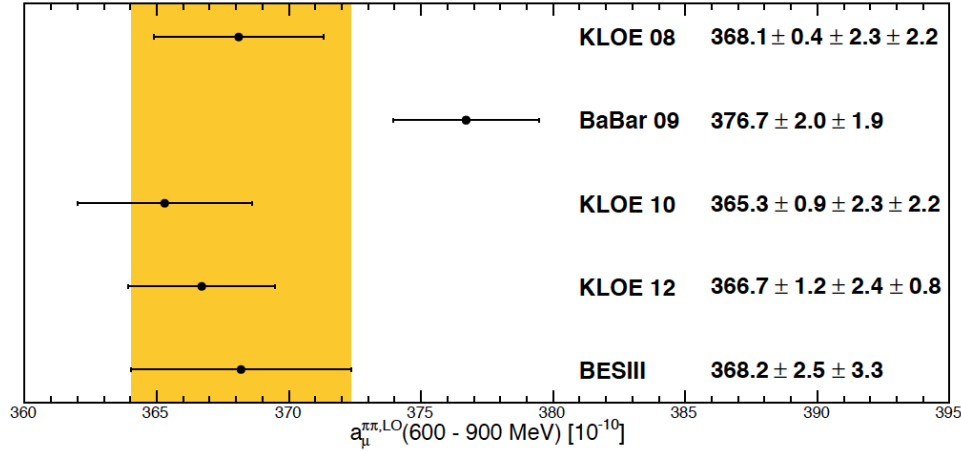


Figure 4.7: Two-pion contributions to the hadronic vacuum polarization contribution to a_μ in the energy range between 600 MeV and 900 MeV.

BESIII measurement on a_μ^{HVP} . It agrees with all three KLOE analyses in the mass range 600 – 900 MeV, while deviations from BaBar’s results are observed.

The good understanding of the radiative muon sample, which was achieved in this analysis, also led to two additional publications, which made use of the high statistics and quality of the muon data. In a first paper, the electronic width of the J/ψ resonance was determined with world-leading accuracy [38]. In a second paper a competitive dark photon limit was achieved by looking for an enhancement of events in the dimuon invariant mass [39] between 1.5 and 3.4 GeV/ c^2 .

- **Cross section of $e^+e^- \rightarrow \pi^+\pi^-\pi^0$**

The hadronic channel $e^+e^- \rightarrow \pi^+\pi^-\pi^0$, which is dominated at low energies by the $\omega(782)$ and $\phi(1020)$ resonances, has been measured by the Novosibirsk experiments CMD-2 [40] and SND [41] below 1.4 GeV. Their results show obvious scatter, although within claimed accuracy, and would benefit from improved measurements. Above the $\phi(1020)$ resonance, BaBar has also performed a measurement of this channel [42] and has observed structures which are interpreted as two excited ω states. This BaBar result is in conflict with an old DM2 measurement [43].

In contrast to the two-pion analysis discussed above, both the tagged (in the full mass range) and the untagged ISR methods (above 1 GeV) were analyzed by BESIII. Preliminary results for this ISR measurements are already available. For the final spectrum, the tagged and untagged spectra were averaged and a systematic uncertainty of better than 3% was achieved in a wide mass range from threshold up to the J/ψ resonance. In a fit to the mass spectrum assuming vector meson dominance the mass and width of the resonances, $\omega(1420)$ and $\omega(1650)$, could be obtained with unprecedented accuracy. Furthermore, the branching fraction of the J/ψ decays to three pions was measured precisely.

- **Cross section of $e^+e^- \rightarrow \pi^+\pi^-\pi^0\pi^0$**

In the channel $e^+e^- \rightarrow \pi^+\pi^-\pi^0\pi^0$ some deviations between the two Novosibirsk experiments CMD-2 [44] and SND [45] were observed below 1.4 GeV. Even larger deviations are seen in comparison with τ spectral functions which can be related to the cross section via an isospin relation. It has been speculated whether large isospin violating effects might be the reason for this observation. Above approximately 1 GeV, the BaBar collaboration has published an analysis, in which the world data set in terms of statistical and systematic precisions are exceeded by a large amount [46]. It is therefore the goal of the BESIII analysis to provide an independent high-accuracy data set besides BaBar. Furthermore, the channel is extremely interesting from the spectroscopy point of view. It has a rich internal structure, where the $\omega\pi^0$, $a_1\pi$, $\rho^+\rho^-$, and many other intermediate states play significant roles (including the $f_0(500)$ and $f_0(980)$).

Also for this channel preliminary results exist at BESIII using the tagged and untagged ISR approach. The mass range from threshold up to 3.4 GeV is covered and the cross section is determined with a systematic uncertainty of approximately 3%. Besides the cross section of $e^+e^- \rightarrow \pi^+\pi^-\pi^0\pi^0$, the cross section of the intermediate state $e^+e^- \rightarrow \omega(782)\pi^0$ is measured, and the branching fraction of the decay $J/\psi \rightarrow \pi^+\pi^-\pi^0\pi^0$ is extracted.

The existing results on $e^+e^- \rightarrow \pi^+\pi^-\pi^0$ and $e^+e^- \rightarrow \pi^+\pi^-\pi^0\pi^0$ are obtained using the 2.9 fb^{-1} data at $\sqrt{s} = 3.773\text{ GeV}$. As discussed in the case of the $e^+e^- \rightarrow \pi^+\pi^-$ analysis, including the already existing and upcoming new data sets, the systematic uncertainties, which are already at this point at world-class level, can be further reduced.

4.2.4 Inclusive R scan data

Up to an energy of 2.0 GeV, the R value is determined by the sum of measured exclusive hadronic cross sections, either via the energy scan or the ISR technique. In case of unmeasured exclusive channels, isospin invariance is assumed in that energy range. At larger values of \sqrt{s} , more exclusive channels open up, so inclusive R measurements are necessary. The energy region between 2.0 and 4.6 GeV is rich of resonances and has transitions between the smooth continuum regions and the resonances. Figure 4.8 shows a comparison of BES [47] and KEDR data [48], as well as the perturbative QCD (pQCD) prediction between 2.0 and 3.7 GeV. Agreement within uncertainties is found. It should be noted that the most recent KEDR analysis [49] in the energy interval between 3.08 and 3.72 GeV is not yet included.

Regarding the hadronic vacuum polarization contribution to $(g-2)_\mu$, theorists deal with the R values in the energy region above 1.8 GeV in different ways. Ref. [5] uses in the dispersive evaluation inclusive R values measured above 1.937 GeV. In the energy interval from 1.8 to 3.7 GeV, the contribution to the uncertainty of the muon anomaly a_μ is found to be 0.56×10^{-10} , which is roughly a factor of 3 smaller than the expected accuracy $\delta a_\mu(\text{exp}) = 16 \times 10^{-11}$ of the new direct measurements of a_μ . In Ref. [7] four-loop pQCD is used in the energy region between 1.8 and 3.7 GeV, resulting in a theory uncertainty of 0.65×10^{-10} . The open charm region between 3.7 and 5 GeV is governed by broad resonances. Its contribution to a_μ is computed with experimental data. However,

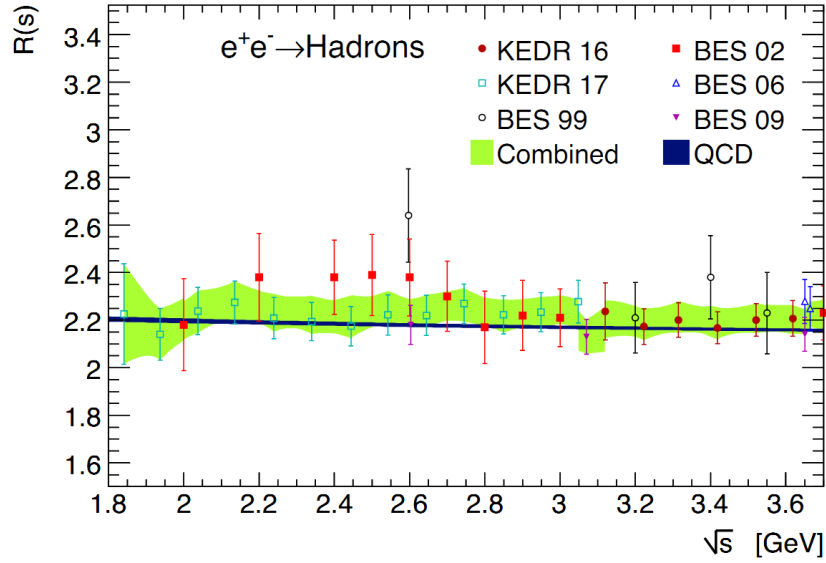


Figure 4.8: The hadronic $R(s)$ ratio in the continuum region below the $D\bar{D}$ threshold. Shown are the results from BES and KEDR as well as their average (shaded band). The solid line shows the pQCD prediction. Plot taken from Ref. [7].

Table 4.1: The $a_\mu^{\text{HVP,LO}}$ for \sqrt{s} in $[1.841, 2.0]$ GeV by different inputs in this region. Numbers are taken from Ref. [5].

input	$a_\mu^{\text{HVP,LO}} (\times 10^{10})$
Exclusive sum	6.06 ± 0.17
Inclusive data	6.67 ± 0.26
pQCD	6.38 ± 0.11
Exclusive(< 1.937 GeV) + inclusive(> 1.937 GeV)	6.23 ± 0.13

the contribution is found to be very small (0.11×10^{-10} in Ref. [5] and 0.03×10^{-10} in Ref. [7]). At even higher energies, either experimental data (for instance in the bottomonium region) or pQCD are used for the evaluation of the hadronic vacuum polarization. The uncertainties of these contributions are below the level of 0.10×10^{-10} .

The transition region between sum of exclusive channels and inclusive R data, is of interest and deserves re-examination. Table 4.1 summaries the $a_\mu^{\text{HVP,LO}}$ at $[1.841, 2.0]$ GeV by different inputs in this region [5]. The results from inclusive data and pQCD calculations agree within uncertainty, and disagree with that from exclusive sum. Hence, precise measurements of R data with exclusive sum and inclusive method are important to choose transition point between sum of exclusive channels and inclusive R data, and test pQCD prediction on R value in transition region. A new scan measurement between 1.8 and 2.0 GeV is useful to answer these questions.

Compared to $(g-2)_\mu$, the impact of inclusive R data on the running of the electromagnetic fine structure constant is much more pronounced as higher energy scales are very relevant in the dispersion integral for $\Delta\alpha_{\text{em}}$. In fact, in the case of $\Delta\alpha_{\text{em}}$, the total

uncertainty of 1.11×10^{-4} cited in Ref. [5] stems almost entirely from the energy range between 1.19 and 11.20 GeV, which amounts to $(82.82 \pm 1.05) \times 10^{-4}$. While Ref. [5] follows a more data-driven approach to calculate $\Delta\alpha_{\text{em}}$, the evaluation by Davier *et al.* in Ref. [7] relies on pQCD calculations for the R value in the energy range between 1.8 and 3.7 GeV. Above 3.7 GeV, up to 5.0 GeV, experimental information on R is used. In this energy range an experimental uncertainty of 0.67×10^{-4} out of a total uncertainty for $\Delta\alpha_{\text{em}}$ of 0.9×10^{-4} is found. This strongly motivates new data on the inclusive R ratio in the energy range covered by BESIII. The role of BESIII is twofold: on the one hand the data can prove the validity of pQCD in the description of R as required by a theory-based evaluation of $\Delta\alpha_{\text{em}}$; On the other hand the data can be directly used as input in the dispersion integral in a data-driven approach.

In order to improve the knowledge of R , the BESIII collaboration has recently carried out a series of energy scans in the range between 2.0 and 4.6 GeV with in total 130 energy points with total integrated luminosity about 1300 pb^{-1} . The total hadronic event yield exceeds 10^5 events at each energy, such that the accuracy of the data will be entirely dominated by systematic uncertainties. The goal of the BESIII experiment is to arrive at a total accuracy of the hadronic R ratio of at least 3%. A similar systematic accuracy has already been achieved in Ref. [48] at KEDR. The analysis of the data is currently ongoing, and preliminary result shows dominant uncertainty is by hadronic event generator, which is also a major challenge to describe 10^5 hadronic events at each energy. MC simulation programs based on theoretical descriptions of string fragmentation functions exist, like the LUARLW generator [50]. The KEDR collaboration used LUARLW generator, which was employed by the BES collaboration. With 10^5 hadronic events at each energy, the LUARLW generator is optimized and tuned. At the same time, a precise description of the total hadronic events in one event generator has been proposed. Making use of the existing measurements of many exclusive hadronic final states, event generator CONEXC [51], which can deal with imprecise exclusive part of the LUARLW generator, have been considered as an alternative. Hence, a more data-driven approach to the description of the total hadronic events is identified.

The energy range between 3.85 and 4.6 GeV have rich charmonium and charmonium-like states. Because the collected scan data have small energy step, we could extract resonances parameters by precisely measured R values. BES collaboration did similar work [47], but results have large uncertainty and model dependence. With more studies on these charmonium and charmonium-like states, R results could be further improved.

4.2.5 Measurements of meson transition form factors

The main motivation for the proposed program of precision measurements of meson TFFs at BESIII is to constrain the HLbL contribution to the level set by the forthcoming $(g-2)_\mu$ experiments at FNAL and J-PARC of $\delta a_\mu = 1.6 \times 10^{-10}$, in order to allow for a meaningful interpretation of these new measurements. Depending on the analysis of the hadronic contributions [7, 52] the present SM uncertainty amounts to $\delta a_\mu(\text{SM}) = \pm(49 - 58) \times 10^{-11}$, which significantly exceeds the future experimental accuracy. This motivates an intense activity to reliably estimate contributions of hadrons to a_μ .

The leading diagram of the HLbL contribution is given by pseudoscalar meson ex-

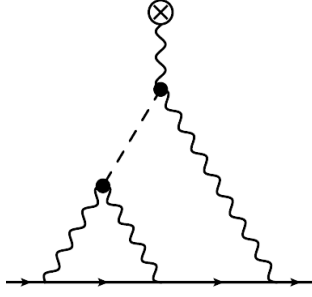


Figure 4.9: The leading terms in the hadronic light-by-light scattering (HLbL) contribution to the anomalous magnetic moment of the muon are given by the exchange of light pseudoscalar mesons as depicted by the dashed line.

change as shown in Fig. 4.9. Unlike the HVP contribution, in most of the existing estimates of the HLbL contribution, the description of the non-perturbative light-by-light matrix element is based on hadronic models rather than determined from data. These approximations are based on a requirement of consistency with the asymptotic constraints of QCD, and predict that the hadronic corrections are dominated by long-distance physics, namely due to exchange of the lightest pseudoscalar states. Unfortunately, a reliable estimate based on such models is possible only within certain kinematic regimes. This results in a large, mostly uncontrolled uncertainty of a_μ .

In order to reduce the model dependence, data-driven approaches for the HLbL contribution to a_μ have been proposed. Sum rules and a dispersive formalism can furthermore provide powerful constraints on the hadronic light-by-light scattering and its contribution to a_μ . Measurements of meson TFFs are used as input in such data-driven approaches. As will be discussed below, essentially all the relevant channels in the spacelike and timelike regions can be studied at BESIII.

TFFs describe the effect of the strong interaction on the $\gamma^*\gamma^*M$ vertex, where $M = \pi^0, \eta, \eta', \eta_c, \dots$. They are represented by functions $F_{M\gamma^*\gamma^*}(q_1^2, q_2^2)$ of the photon virtualities q_1^2 and q_2^2 . For the case of pseudoscalar mesons, there is one such function [53, 54]. For scalar, axial-vector, or tensor mesons, the $\gamma^*\gamma^*M$ vertex contains in general several such TFFs.

The spacelike region of the TFFs is accessed at e^+e^- colliders by means of the two-photon-fusion reaction $e^+e^- \rightarrow e^+e^-M$ (left panel in Fig. 4.10), where at present the measurement of both virtualities is still an experimental challenge. The common practice is to extract the TFFs when one of the outgoing leptons is tagged and the other is assumed to escape detection along the beam axis (single-tag method). The tagged lepton emits a highly off-shell photon with a transferred momentum $q_1^2 \equiv -Q^2$ and is detected, while the other, untagged, is scattered at a small angle with $q_2^2 \simeq 0$. The TFF extracted from the single-tag experiment is then $F_{M\gamma^*\gamma^*}(Q^2, 0) \equiv F_{M\gamma^*\gamma}(Q^2)$. The timelike region of the TFFs can be accessed at meson facilities through the single Dalitz decay processes $M \rightarrow l^+l^-\gamma$, which contain a single virtual photon with a transferred momentum in the range $4m_l^2 < q_1^2 < m_M^2$ (with m_l the lepton mass and m_M the meson mass) whereas $q_2^2 = 0$ (middle panel in Fig. 4.10). To complete the timelike region, e^+e^- colliders provide access to the values $q^2 > m_M^2$ through the $e^+e^- \rightarrow M\gamma$ annihilation processes (right panel in

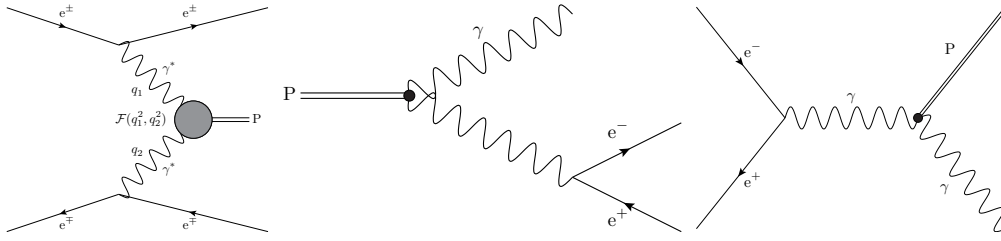


Figure 4.10: The meson TFFs in the spacelike region (left panel) as accessed through the $\gamma^*\gamma^*$ annihilation process, and in the timelike region as accessed through the γe^+e^- Dalitz decay (middle panel) and through e^+e^- annihilation into $P\gamma$ (right panel), where P stands for a pseudoscalar meson.

Fig. 4.10).

Besides their relation to the anomalous magnetic moment of the muon, the pseudoscalar meson TFFs provide a unique window on several symmetry-breaking mechanisms in QCD. In the limit of massless light quarks (u, d, s), *i.e.*, the chiral limit, the QCD Lagrangian exhibits an $SU(3)_L \times SU(3)_R$ chiral symmetry which is spontaneously broken to $SU(3)_V$, giving rise to 8 pseudoscalar Goldstone bosons (π, K, η). The QCD Lagrangian has in addition two other global symmetries: the $U(1)_V$ symmetry leading to the conservation of baryon number, and the $U(1)_A$ symmetry which is anomalous. Since the flavor-singlet axial-vector current is not conserved in the presence of this $U(1)_A$ anomaly, the η' mass does not vanish in the chiral limit. In the massless u, d, s quark world (with the other three quarks infinitely heavy), the massive η' would be a pure flavor-singlet state $\eta^0 \equiv (u\bar{u} + d\bar{d} + s\bar{s})/\sqrt{3}$. In the real world, however, the $SU(3)_V$ flavor symmetry is explicitly broken by the quark masses, which causes a mixing among π^0, η , and η' [55]. In the isospin limit ($m_u = m_d$), the π^0 can be identified as a pure isotriplet state $(u\bar{u} - d\bar{d})/\sqrt{2}$. In the absence of the $U(1)_A$ anomaly (large- N_c limit of QCD), the two isosinglet pseudoscalar mass eigenstates would consist of $(u\bar{u} + d\bar{d})/\sqrt{2}$ and $s\bar{s}$ (so-called *ideally mixed* states). The $U(1)_A$ anomaly mixes these quark flavor states towards the physical η and η' mesons, which are closer to the flavor octet $\eta^8 \equiv (u\bar{u} + d\bar{d} - 2s\bar{s})/\sqrt{6}$ and flavor singlet η^0 states, respectively. This mixing in the $\eta - \eta'$ system is probing the strange quark content of the light pseudoscalars as well as the non-perturbative gluon dynamics of QCD, responsible for the $U(1)_A$ anomaly. The mixing can also be related to physical observables [55–57], in particular through the $M \rightarrow \gamma\gamma$ decay widths and the $\gamma^*\gamma^*M$ TFFs.

Based on the experience obtained so far at BESIII, world-leading results in the field of meson TFFs have already been obtained with the existing data, as will be elaborated in the following. The overall goal of the BESIII program is to provide the first precision measurements of the TFFs of pseudoscalar mesons, of the $\pi\pi, \pi\eta$ and $\eta\eta$ systems, as well as axial and tensor mesons at small momentum transfers. A future data set of additional 20 fb^{-1} taken at $\sqrt{s} = 3.773 \text{ GeV}$ will make a first measurement of the double-virtual TFF of the lightest pseudoscalar mesons with high accuracy possible.

- **Single-tag pseudoscalar TFFs, spacelike**

The first BESIII publication of the spacelike TFF of the π^0 meson will be based on the 2.9fb^{-1} data sample obtained at a cms energy of 3.773 GeV . Preliminary results for the analysis are presented in Fig. 4.11. As described above, for single-tag events, one of the beam particles (electron or positron) is tagged in the detector. By detecting two photons from the π^0 decay, the missing momentum can be derived for the missing positron (electron), which is further required to be scattered at very small angles. By fitting the $\gamma\gamma$ invariant mass distribution in bins of Q^2 , one obtains the differential cross section $d\sigma/dQ^2$ for the signal process, which is proportional to $|F(Q^2)|^2$.

Figure 4.11 shows the product $Q^2|F(Q^2)|$ as measured by BESIII together with existing data from CELLO [58] and CLEO [59]. Note that recent BaBar [60] and Belle [61] data could only access the Q^2 range above 4 GeV^2 , and hence, are not displayed. The BESIII analysis covers the entire Q^2 range between 0.3 GeV^2 and 3.1 GeV^2 , which significantly improves the accuracy upon existing data sets. The accessible range of momentum transfer is limited by the detector acceptance for the decay photons of π^0 at lowest values of Q^2 and by statistics at largest values of Q^2 . Existing data taken in the scope of the R measurement, discussed in Sec. 4.2.4, will be used to extend the covered regions of momentum transfers down to approximately 0.1 GeV^2 . A future data set of additional 20fb^{-1} at 3.773 GeV will help to extend the covered range of momentum transfer up to approximately 10 GeV^2 , which will allow to test the discrepancy in the results of the B -factories, *i.e.*, the so-called BaBar-Belle puzzle.

The current preliminary results are in very good agreement with recent theoretical calculations using dispersion relations [62] or LQCD [63]. The data have also been considered in a recent review of the HLbL contribution to a_μ [64], where it was demonstrated that they contribute to a significant reduction of the uncertainties.

First feasibility studies of the η and η' TFF measurements have been performed at BESIII. So far only individual decay modes have been considered to reconstruct the mesons from the same data that is used for the pion TFF measurement. The covered range of momentum transfer at BESIII is found similar to the π^0 TFF result with an accuracy similar to what has been reported from previous measurements [58, 59]. A final result will make use of all major decay modes of both mesons and combine the existing and future data sets to obtain results of highest accuracy and impact.

- **Single-tag $\pi\pi$, $\pi\eta$, $\eta\eta$ TFFs, spacelike**

Besides the lowest-lying pseudoscalar mesons, $\gamma\gamma^*$ processes also allow to access the structure of scalar, axial-vector and tensor mesons through the production of multi-meson final states. A first measurement at BESIII focuses on the investigation of the $\gamma^*\gamma \rightarrow \pi^+\pi^-$ channel, with one virtual photon. Data at cms energies between 3.773 and 4.6 GeV are combined to perform the studies on an integrated luminosity of 7.5fb^{-1} . Figure 4.12 shows the full simulation of 1fb^{-1} at $\sqrt{s} = 4.23\text{ GeV}$ of the single-tagged analysis of the $\gamma\gamma^* \rightarrow \pi^+\pi^-$ after event selection in the three relevant kinematic variables to study the two-pion system. The dominating background of

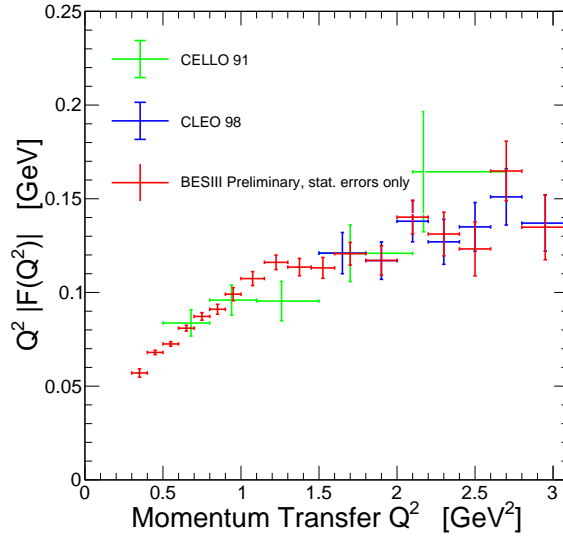


Figure 4.11: Preliminary BESIII measurement of the spacelike π^0 TFF in comparison with data from CELLO [58] and CLEO [59].

muon production in the reaction $e^+e^- \rightarrow e^+e^-\mu^+\mu^-$ is rejected by adapting the machine learning techniques, successfully used in the pion form factor measurement discussed in Sec. 4.2.3. The irreducible background contribution due to the timelike amplitude of $e^+e^- \rightarrow e^+e^-\pi^+\pi^-$ is subtracted using MC-derived distributions. The investigation at BESIII has triggered an improvement of the EKHARA 3.0 event generator [65], which allows to properly take into account interference effects between signal and background processes. Thus, a first high-statistics result, at masses starting from the two-pion mass threshold, at small momentum transfers, and with a full coverage of the helicity angle of the pion system is obtained at BESIII. While the results are awaited by the $(g-2)_\mu$ theory community [66, 67], in the threshold region, such data will also provide new empirical information on the pion polarizabilities.

The analysis of the two-pion system is currently extended to the neutral pion system, where a complementary result to the recent Belle measurement at large momentum transfers [68] is expected. Additional, future data will allow to extend the investigations also to $\pi\eta$ and $\eta\eta$ systems with high statistics. Furthermore, even higher multiplicity final states $\gamma\gamma^* \rightarrow 3\pi$, $\gamma\gamma^* \rightarrow 4\pi$ or $\gamma\gamma^* \rightarrow \eta\pi\pi$ can be performed to provide relevant information on axial and tensor mesons, like the $f_1(1285)$ and $a_2(1320)$ with high accuracy, needed as input for the calculations of the HLbL contribution to $(g-2)_\mu$.

- **Double-tag π^0 TFF, spacelike**

In the case that both scattered leptons are identified in the detector, the doubly-virtual TFF can be accessed. First event sample of this kind has been identified in the 2.9fb^{-1} data set at a cms energy of 3.773GeV . With improved statistics, the measurement of the doubly-virtual TFF can be used to compute the pion-pole contribution to HLbL in a completely model-independent way. Based on a MC

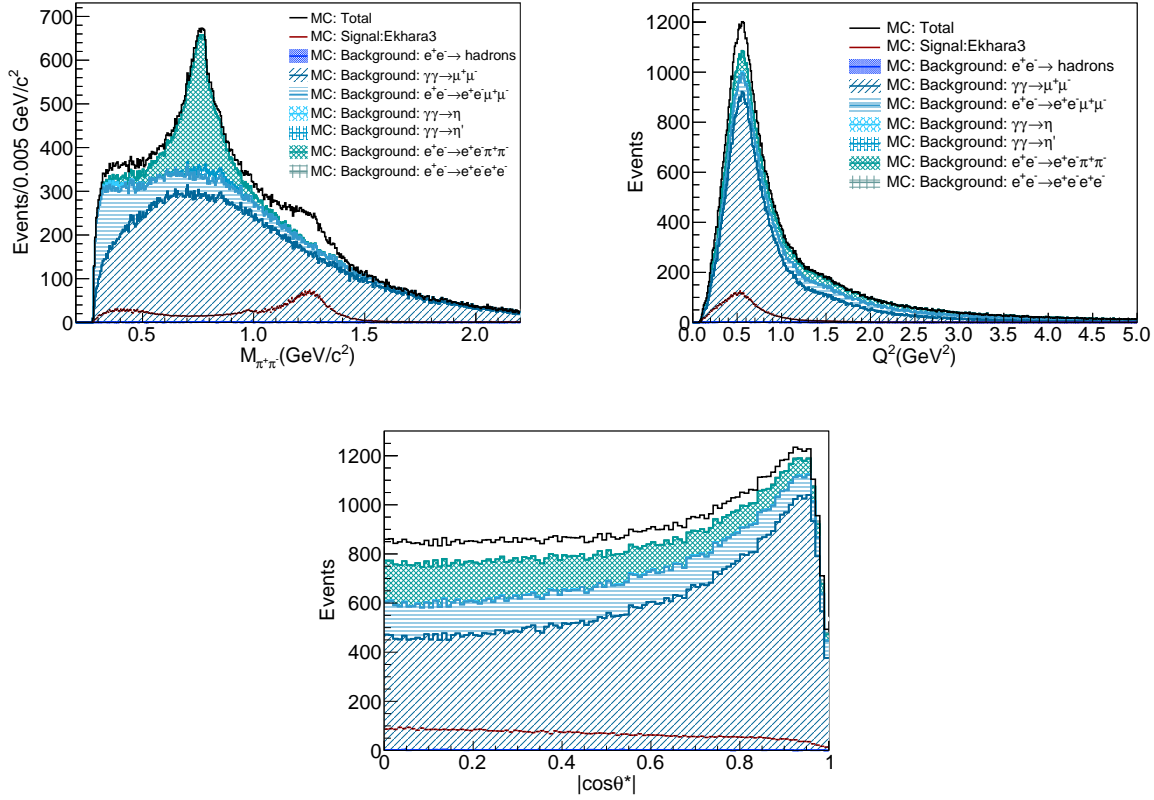


Figure 4.12: Full simulation of the single-tagged analysis of $\gamma\gamma^* \rightarrow \pi^+\pi^-$ at $\sqrt{s} = 4.23 \text{ GeV}$. The three relevant distributions of the two-pion system are shown: invariant mass of the pions (top left), momentum transfer Q^2 of the tagged lepton (top right), and helicity angle of the pions $\cos\theta^*$ (bottom).

simulation restricted by the geometric acceptance of the BESIII detector only, the result is expected to cover momentum transfers in the range of $0.3 \leq (Q_1^2, Q_2^2) \leq 2.2 \text{ GeV}^2$. The provided information is crucial to constrain the precision of data driven calculations of the HLbL contribution to $(g-2)_\mu$ [20]. In addition to the doubly-virtual TFF of π^0 , the same information of η and η' mesons will be measured. The BESIII result will be complementary to the recent measurement of the doubly-virtual η' TFF by the BaBar collaboration [54], which has been obtained at large momentum transfers only.

- **Pseudoscalar TFFs at high Q^2 , timelike**

Up to now, at high momentum transfer the timelike π^0 TFF has not yet been extracted from the annihilation reaction $e^+e^- \rightarrow \pi^0\gamma$. At BESIII it is possible to access the timelike π^0 TFF in the Q^2 range of approximately 20 GeV^2 , which allows for a comparison with the spacelike data by BaBar [60] and Belle [61]. In the case of η and η' , in addition to the comparison to spacelike measurements, the data can be compared to a timelike BaBar measurement at $Q^2 = 112 \text{ GeV}^2$ [53]. Comparisons of this kind allow to test predictions of pQCD, in which it is assumed that the spacelike

and timelike TFFs become identical and in both cases feature a Q^{-2} -dependence behavior [53].

We stress once more that the BESIII program on meson TFF measurements is of highest relevance to constrain the HLbL contribution to $(g - 2)_\mu$. In a recent review paper [64], the π^0 pole exchange contribution is evaluated in a simplistic model, which fulfills the basic theory constraints, considering already the new preliminary data from BESIII. The data allow to reduce the uncertainty of this most relevant contribution to $\pm 0.2 \times 10^{-10}$, while previous model dependent estimates have uncertainties in the range of $\pm(0.9 - 1.2) \times 10^{-10}$ (see Tab. 2 in Ref. [64]). More elaborate and model independent evaluations of the π^0 contribution, as the dispersive calculations of [62] or the lattice calculations of [63], which do not consider the BESIII data, already achieve uncertainties on the level of $\pm(0.3 - 0.4) \times 10^{-10}$. These results can be cross checked, when being confronted with present and future BESIII data. As mentioned before, the goal is to achieve a total uncertainty of all hadronic contributions to a_μ on the level of 1.6×10^{-10} .

4.3 Baryon form factors

Baryons provide a unique window to the strong interaction, since they constitute the simplest system for which the non-Abelian nature of QCD is manifest [69]. The most well-known baryon species is the nucleon. However, despite being known for more than a century, and despite its importance as the main contributor to the mass of our visible Universe, fundamental properties like its mass, spin [70, 71] and structure [72] are difficult to describe from first principles. This difficulty is a consequence of the non-perturbative interactions between the quarks inside the nucleon. At this scale, the break-down of pQCD calls for quantitative predictions from *e.g.*, Chiral Perturbation Theory [73, 74], Lattice QCD [75] or phenomenological models, *e.g.*, Skyrme models [76, 77].

The inner structure of baryons can be described and studied experimentally on a common footing through electromagnetic form factors (EMFFs), probed by processes involving hadrons interacting with virtual photons. The EMFFs are fundamental observables of non-perturbative QCD and quantify the deviation from the pointlike case. If one-photon exchange is assumed, the momentum transfer squared q^2 of the virtual photon is given by $q^2 = (p_i - p_f)^2 < 0$. Elastic, or spacelike, form factors ($q^2 < 0$) have been studied since the 1960's in electron-nucleon scattering [78]. Spin $\frac{1}{2}$ baryons have two form factors, often referred to as the electric G_E and the magnetic G_M form factor. In the so-called Breit frame, these are Fourier transforms of the charge- and magnetization density, respectively. The measured charge density of the neutron is particularly intriguing: though being negative near the center whilst positive further out can be explained in the simple quark model by d -quarks clustering in the center surrounded by the u -quark, the drop to negative values at even larger distances from the center requires more elaborate models involving *e.g.*, pion clouds [72]. One way to gain further insights into this puzzle is to replace one or several of the light quarks in the nucleon by heavier ones, *i.e.*, forming hyperons, and study how the structure changes [79]. However, since hyperons are unstable, they are unfeasible as beams or targets, and therefore, do not easily lend themselves to

electron scattering experiments. Instead, their structure can be studied in the timelike region ($q^2 > 0$) through the electron-positron annihilations, with the subsequent production of a baryon-antibaryon pair.

The somewhat abstract timelike form factors can be related to the more intuitive spacelike form factors by dispersion relations [80]. In particular, spacelike and timelike form factors should converge to the same value as $|q^2|$ reaches a certain scale [81]. For nucleons, the onset of this scale can be tested by measuring the spacelike and timelike form factors with great precision and compare them. For hyperons, this is unfeasible due to the poor experimental access to the spacelike region. However, one can utilize the fact that timelike form factors can be complex, with a relative phase that polarizes the final state [81]. For a ground-state hyperon Y , this phase is accessible, thanks to the weak, self-analyzing decays. The daughter baryon B will be emitted according to the spin of the mother hyperon Y , giving a decay angular distribution that depends on the polarization of Y :

$$W(\cos \theta_B) = \frac{1}{4\pi}(1 + \alpha_Y P_Y \cos \theta_B). \quad (4.8)$$

Since spacelike form factors are real, the same must hold for timelike form factors at large $|q^2|$. Hence, the onset of the scale, at which spacelike and timelike form factors converge to the same value, can be obtained by finding the scale at which the phase goes to zero.

Also at threshold, the relative phase must be zero. This is because the phase is a result of interfering amplitudes, *e.g.*, s -waves and d -waves. At threshold, only s -waves can contribute which means that the phase is zero. Furthermore, the absence of other waves also imply that the ratio between the electric and the magnetic form factor, *i.e.*, $|G_E/G_M|$ is equal to 1 at threshold.

4.3.1 Formalism

For spin $\frac{1}{2}$ baryons produced *via* one-photon exchange in $e^+e^- \rightarrow \gamma^* \rightarrow B\bar{B}$, the Born cross section can be parameterized in terms of G_E and G_M :

$$\sigma_{B\bar{B}}(s) = \frac{4C\pi\alpha^2\beta}{3s} \left[|G_M(s)|^2 + \frac{1}{2\tau} |G_E(s)|^2 \right]. \quad (4.9)$$

Here, $\alpha=1/137.036$ is the fine-structure constant, $\beta = \sqrt{1 - 4m_B^2 c^4/s}$ the velocity of the produced baryon, c the speed of light, s the square of the cms energy, m_B the mass of the baryon and $\tau = s/(4m_B^2)$. The Coulomb factor C is a correction to the one-photon exchange and describes the electromagnetic interaction between the outgoing B and \bar{B} . For neutral baryons, C is 1 which in combination with the vanishing phase space β factor, the cross section should be zero at threshold. For charged baryons, C is typically assumed to have the value for pointlike charged fermions $C = \varepsilon R_S$ [82], where $\varepsilon = \pi\alpha_{\text{em}}/\beta$ is an enhancement factor. In this case, the two β factors cancel and as a result, the cross section becomes non-zero at threshold. The so-called Sommerfeld resummation factor

$$R_S = \sqrt{1 - \beta^2}/(1 - e^{-\pi\alpha_{\text{em}}\sqrt{1-\beta^2}/\beta}) \quad (4.10)$$

causes the cross section to rise rapidly with the fermion velocity [83].

In many experiments, the data samples are too small to separate between G_E and G_M since that requires analysis of angular distributions. In order to compare production cross sections of different baryon-antibaryon pairs for equivalent kinematic conditions, the *effective form factor* is defined:

$$\begin{aligned} |G(s)| &\equiv \sqrt{\frac{\sigma_{B\bar{B}}(s)}{(1 + \frac{1}{2\tau})(\frac{4\pi\alpha^2\beta}{3s})}} \\ &\equiv \sqrt{\frac{2\tau|G_M(s)|^2 + |G_E(s)|^2}{2\tau + 1}}. \end{aligned} \quad (4.11)$$

In order to extract the relative phase, a full spin decomposition of the reaction is needed. The formalism has been outlined in Refs. [84, 85]. In particular, the Λ transverse polarization P_Y is given by:

$$P_Y = \frac{\sqrt{1 - \eta^2} \sin \theta \cos \theta}{1 + \eta \cos^2 \theta} \sin(\Delta\Phi), \quad (4.12)$$

where η is an angular distribution parameter related to the form factor ratio \mathcal{R} by $\eta = (\tau - \mathcal{R}^2)/(\tau + \mathcal{R}^2)$. The polarization P_Y can be extracted from Eq. (4.8).

The formalism presented outlined so far is based on the assumption that one-photon exchange dominates the production mechanism. It has been discussed whether two-photon exchange contributes to the production mechanism, leading to interference effects that results in an additional term $\kappa \cos \theta \sin^2 \theta$ in the angular distribution [86]. As a consequence, the scattering angle distribution of the produced baryon will be slightly asymmetric. This is quantified by the asymmetry

$$\mathcal{A} = \frac{N(\cos \theta > 0) - N(\cos \theta < 0)}{N(\cos \theta > 0) + N(\cos \theta < 0)}. \quad (4.13)$$

It is related to the κ parameter in the following way:

$$\mathcal{A} = \frac{3}{4} \frac{\kappa}{3 + \eta}, \quad (4.14)$$

where η is the same as in Eq. (4.12) [87]. The asymmetry \mathcal{A} is straight-forward to measure and offers a convenient way to study the importance of two-photon exchange in the timelike region.

4.3.2 State of the art

Proton EMFFs have been studied extensively in the spacelike region [78]. In particular, the development of the polarization transfer technique [88] in the late 1990's led to a veritable leap forward of the field, enabling a model independent separation of electric and magnetic form factors. The best precision of the ratio $|G_E/G_M|$ obtained with the new technique is $\sigma_p|G_E/G_M| = 1.7\%$, achieved at JLab [89]. The previously employed Rosenbluth separation technique [90] relies on one-photon exchange and comparing data

obtained with the two methods shows a large and energy-dependent disagreement. The leading explanation is the effect from two-photon exchange [91, 92].

The timelike region became accessible with the advent of high-precision, high-intensity electron-positron colliders at intermediate energies. The world data on $e^+e^- \rightarrow p\bar{p}$ are shown in Fig. 4.13. An advantage of electron-positron annihilations is the charge symmetry, which makes the measurements less sensitive to higher order processes such as two-photon exchange. However, the precision acquired so far has until recently not been compatible with that of the spacelike region [93]. The most precise measurements from BaBar (in $e^+e^- \rightarrow p\bar{p}$ [94]) and PS170 (in $\bar{p}p \rightarrow e^+e^-$ [95]) achieved $\sigma_p|G_E/G_M| \approx 10\%$ and differ by more than 3σ (bottom left panel of Fig. 4.13). Recent data from BESIII obtained with a beam energy scan [96] and the radiative return or ISR method [97] agree with the BaBar measurements. New data from BESIII, collected in a high-precision energy scan in 2015, will offer improved precision over a large q^2 range.

The cross section and effective form factor show interesting features, as can be seen in the top and bottom left panels of Fig. 4.13. The BaBar collaboration reported an oscillating behavior [94, 104] that was recently confirmed by BESIII [97]. This becomes particularly striking when being studied as a function of the relative momentum between outgoing proton and antiproton. More high-precision data are needed to establish this elusive feature at the level of many standard deviations.

The large amount of high-quality data on proton EMFFs has inspired the theory community to develop various approaches to nucleon structure, based on Chiral Perturbation Theory [105], Lattice QCD [106], Vector Meson Dominance [107], relativistic Constituent Quark Models [108] and pQCD [109].

While experiencing an era of great progress on proton timelike EMFFs, corresponding data for its isospin partner, the neutron, remain a challenge. This is primarily due to the difficulty in identifying and reconstructing the neutron and antineutron from the $e^+e^- \rightarrow n\bar{n}$ process. The cross section has been measured by the SND [110] experiment up to 2 GeV and by the FENICE experiment [?] between 2 and 3 GeV. FENICE collected only a small amount of data and identified the \bar{n} by the time-of-flight method and the annihilation pattern in the detector. The ratio $R_{np} = \sigma(e^+e^- \rightarrow n\bar{n}) / \sigma(e^+e^- \rightarrow p\bar{p})$ is expected to be close to 1 if the process is dominated by the isoscalar or isovector amplitude. In a picture where the production cross section is proportional to the square of the leading quark charge (u quark in the case of the proton and d quark in the case of the neutron), the ratio should instead be close to 0.25. More elaborate predictions are presented in Refs. [111, 112]. More precise data could shed further light on this issue.

Also hyperon EMFFs has been a fairly unexplored territory until recently. The cross section of the $e^+e^- \rightarrow Y\bar{Y}$ process (Y referring to various ground-state hyperons) has been studied by DM2 [113], BaBar [114], BESIII [115] and CLEO [116]. The latter measurement compared the production of several different ground-state hyperons, including the Ω^- , and interpreted the results in terms of di-quark correlations. The idea that certain configurations of flavor, spin and isospin of two quarks inside a hadron have important impacts on the structure of hadrons, which has been discussed since long [117]. In particular, the effects on Λ and Σ structures are outlined in Ref. [118]. However, it is difficult to draw definite conclusions from CLEO, since all data points coincided with charmonium resonances ($\psi(3686)$, $\psi(3770)$ and $\psi(4170)$). Hence, interference effects may

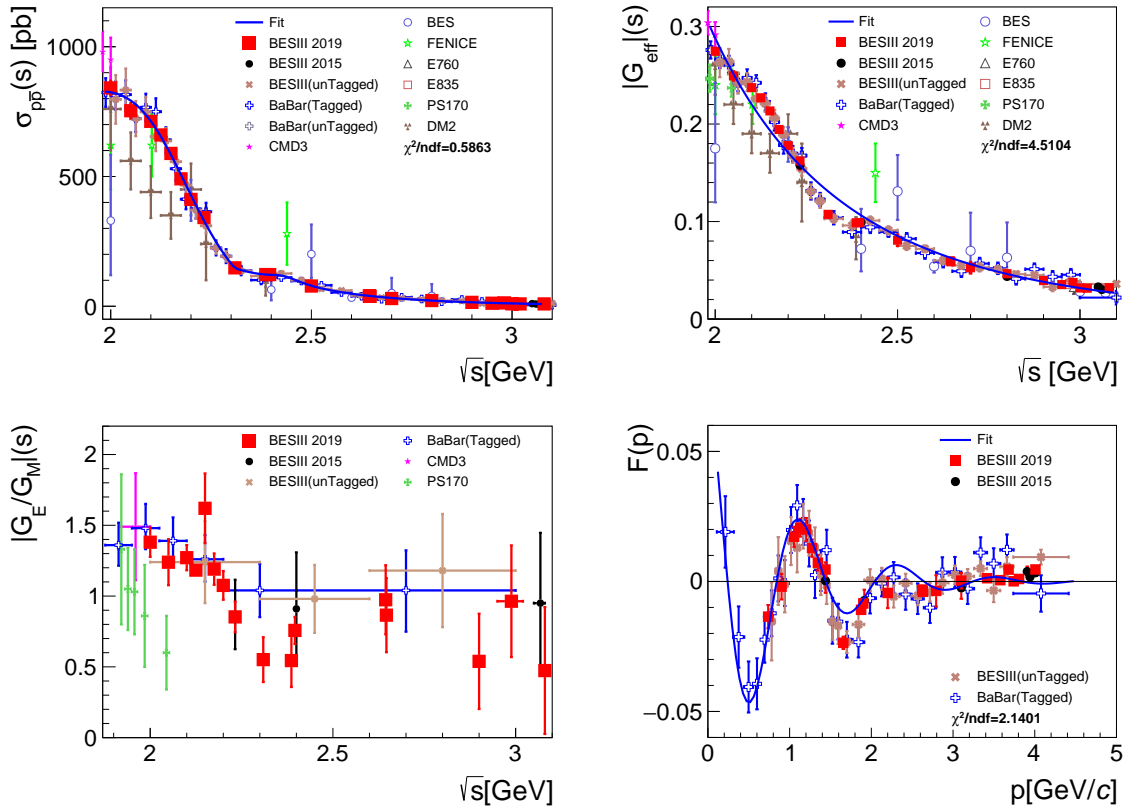


Figure 4.13: Top left: world data on $e^+e^- \rightarrow p\bar{p}$ cross section. Top right: the effective proton timelike form factor. Bottom left: world data on $R = |G_E/G_M|$. Bottom right: effective form factor after subtracting the fitted line in the top right panel. The data are from BESIII [96, 97], BaBar [94], CMD3 [98], BES [99], FENICE [100], E760 [101], E835 [102], PS170 [95] and DM2 [103].

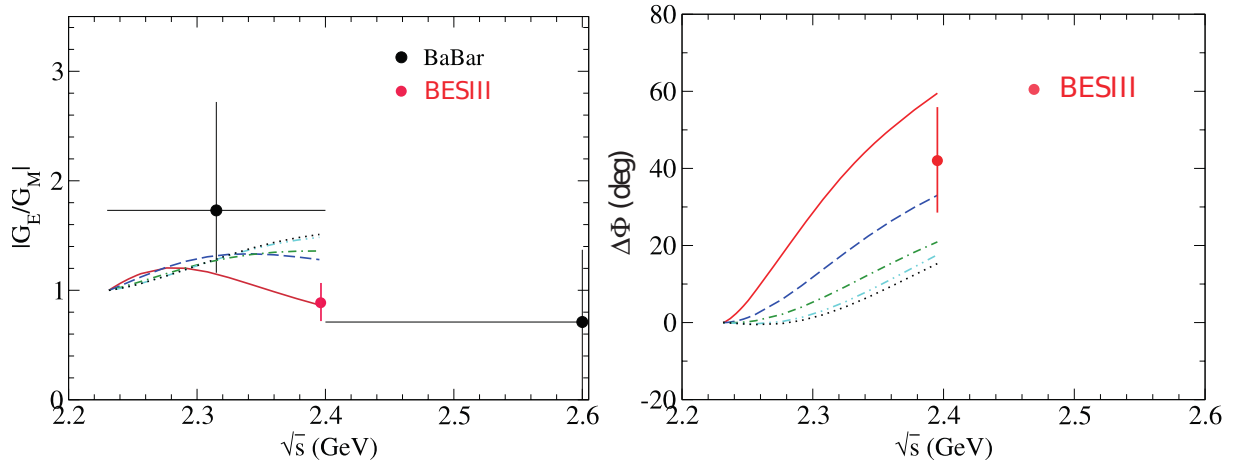


Figure 4.14: BESIII results of $|G_E/G_M|$ and $\Delta\Phi$ compared with theoretical predictions. Here, the values obtained using the PDG value for α_Λ has been used since that was used for the theory predictions. The five lines are different $\Lambda\bar{\Lambda}$ potentials, seen in [120]. Black dots are results of BaBar [114], and red dots are measurements by BESIII.

be important, which makes an unambiguous interpretation difficult.

Due to limited sample sizes, the electric and the magnetic form factors could not be separated with any conclusive precision in neither of the aforementioned experiments. However, in a more recent measurement from BESIII, dedicated data at $q = 2.396$ GeV/ c enabled a complete spin decomposition of the $e^+e^- \rightarrow \Lambda\bar{\Lambda}$ reaction, including measurement of the polarization and spin correlations. From this, it was possible to not only separate between the Λ electric and magnetic form factors, but also to determine the relative phase between $|G_E|$ and the $|G_M|$ for the first time. It was found to be significantly different from zero [119]. The prospect of measuring the relative phase $\Delta\Phi$ of the Λ hyperon by BESIII have triggered the first theory predictions based on various $\Lambda\bar{\Lambda}$ potential models [120]. It was found that the phase is more sensitive to the potential than the $|G_E/G_M|$ ratio, that in turn is more sensitive than the cross section. The theory predictions, as well as the measured values, are shown in Fig. 4.14. Note that the theory predictions were made assuming the old PDG value (from before 2019) of the Λ decay asymmetry parameter, $\alpha_\Lambda = 0.642$. The data are therefore rescaled to the old value. In Ref. [119], the phase is obtained with the 2019 update of the α_Λ from PDG, $\alpha_\Lambda = 0.750$.

The effective form factor of the Λ_c^+ EMFFs have been obtained from measurements at Belle [121] and BESIII [122]. Furthermore, BESIII also measured the ratio \mathcal{R} between the Λ_c^+ electric and magnetic form factors. In this measurement, as well as in measurements of the proton and Λ hyperon EMFFs near threshold, interesting features can be discerned: the cross section undergoes a sharp rise close to threshold, followed by a plateau in the case of the positively charged proton [94, 98, 123] and Λ_c^+ [122], as shown in Fig. 4.15. Various FSI models have been employed to explain this behavior [105]. In the case of the Λ_c^+ , where there is some discrepancy between data from Belle and BESIII, the cross section has been studied with a theory model taking into account the $Y(4630)$ resonance [125]. The threshold of the neutral Λ is particularly interesting. The cross section of $e^+e^- \rightarrow$

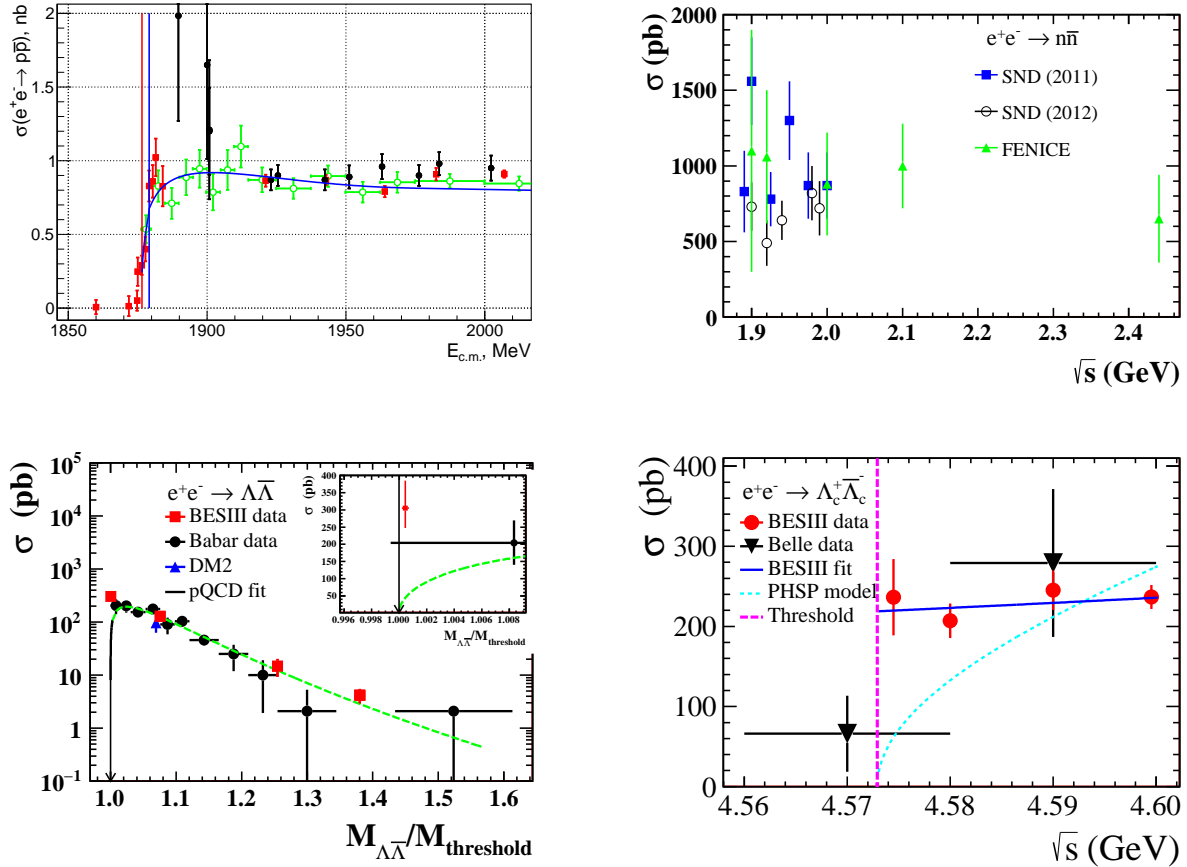


Figure 4.15: Top left: the $e^+e^- \rightarrow p\bar{p}$ Born cross sections measured with CMD-3 (black dots from Ref. [98], red squares from Ref. [123]) and BaBar [94] (green open circles). The solid curve shows the result of the prediction from Ref. [124]. The vertical lines show the $p\bar{p}$ and $n\bar{n}$ thresholds. Top right: world data on $e^+e^- \rightarrow n\bar{n}$ (blue and white points from SND [110], and green points from FENICE [100]). Bottom left: the $e^+e^- \rightarrow \Lambda\bar{\Lambda}$ cross sections near threshold, from BaBar [114] and BESIII [115]. Note that the scale on the y -axis is logarithmic. Bottom right: the $e^+e^- \rightarrow \Lambda_c^+\bar{\Lambda}_c^-$ cross sections from Belle [121] and BESIII [122].

$\Lambda\bar{\Lambda}$ decreases after its sharp rise [115]. This sharp rise, that is similar to the behavior of the $e^+e^- \rightarrow n\bar{n}$ [110], is difficult to explain with Eq. (4.9), since the Λ is neutral which means that $C = 1$ and hence β factor should cause the cross section to vanish at threshold. The nonzero cross section near threshold, as well as the wide plateau, have led to various interpretations, *e.g.*, final-state interactions [126], bound states or mesonlike resonances [127], and a gluon exchange contribution in the resummation factor [128].

4.3.3 Prospects with BESIII

BESIII is uniquely suited for nucleon and strange hyperon form factor studies. It is currently the only running or planned e^+e^- experiment that is optimized in the energy region where nucleon-antinucleon and strange hyperons are produced in abundance. The capability of detecting and identifying charged and neutral particles, including antineutron, is another advantage. Furthermore, the coming upgrade of the BEPCII collider up to cms energies of 4.9 GeV will enable structure studies of single-charm hyperons. The following topics can be addressed within BESIII in the near future:

- **EMFF phase measurements of octet hyperons**

Comparative studies of baryons with different isospin reveal the inner structure in terms of possible di-quark correlations [129]. For example, while the quark content of the Λ and the Σ^0 is the same, the isospin of the ud pair is different. As a consequence, the spin structure should be different. In the case of the Σ^+ , the isospin of the uu pair should be the same as that of the ud pair in the Λ . As a consequence, the cross sections of $e^+e^- \rightarrow \Lambda\bar{\Lambda}$ and $e^+e^- \rightarrow \Sigma^+\bar{\Sigma}^-$ should be similar, as observed by CLEO. However, measurements should be performed at energies that do not coincide with charmonium resonances in order to avoid interference effects. Furthermore, spin observables should be more sensitive to the underlying quark structure, and therefore, it would be illuminating to study the EMFF phase for different octet hyperons. For the Σ triplet, simulation studies show that $q = 2.5 \text{ GeV}/c$ is optimal in terms of cross section and reconstruction efficiency to collect a sample of the required size. The simulation studies show that 100 pb^{-1} would yield a sufficient amount of events to extract the phase of Σ^+ and Σ^0 . For the cascade doublet (Ξ^- and Ξ^0), the corresponding optimal point is located at $q = 2.8 \text{ GeV}/c$.

- **Energy dependence of the EMFF phase of the Λ hyperon**

Preliminary calculations of the energy dependence of the Λ EMFF phase have been performed [130] in an attempt to predict the spacelike EMFFs. However, the calculations call for measurements in more data points in order to constrain the predictions. Presently, the only conclusive measurement is obtained at $q = 2.396 \text{ GeV}/c$. The analysis of these data, as well as simulations at other energy points, show that data samples of $\approx 100 \text{ pb}^{-1}$ are required to achieve the necessary sample size. At low energies, collecting such data samples is time consuming and the points should therefore be chosen very carefully. The data samples at 2.5 GeV and 2.8 GeV, proposed in the previous bullet point, synergize well with the relevant criteria since the cross section at these points [114] should be sufficiently large for successful measurements.

- **Neutron EMFFs**

The analysis of energy scan data from BESIII, collected in 2015, shows that the methods for identifying neutron-antineutron final states have relatively low efficiencies. In order to determine the EMFFs with good precision, yet larger data samples are required. This is in line with the proposal of the previous point. In combination with the data collected in 2015, that are currently being analyzed, this will give a comprehensive picture of the neutron structure in the timelike region and enable comparative studies of proton and neutron EMFFs.

- **Energy dependence of Λ_c^+ EMFFs** With an upgraded BEPCII ring, it will be possible to perform a precision scan from the $\Lambda_c^+\bar{\Lambda}_c^-$ threshold and up to $q = 4.9 \text{ GeV}/c$. The observed discrepancy between Belle and BESIII can be investigated and the possible importance of the $Y(4630)$ resonance can be reviewed. Furthermore, it will be possible to study the EMFF ratio and phase, as outlined in the Charm chapter.

- **Threshold behavior of octet baryons**

In addition to the samples collected during 2015 at each baryon-antibaryon threshold, currently being analyzed, additional samples are needed just below and slightly above each threshold. In this way, possible systematic effects can be detected and taken into account and the observed behavior can be cross-checked. By comparing baryons of different charge, deeper insights can be gained and the relation to possible resonances or interactions at quark level can be established. In particular, a scan around the $\Sigma^+\bar{\Sigma}^-$ threshold with about 20 pb^{-1} per point would be very illuminating.

- **Contribution from two-photon exchange**

A contribution from two-photon exchange would show up as an asymmetry in the scattering angle distribution. This asymmetry has been measured in Ref. [119] and was found to be consistent with zero, though with a large uncertainty. Other baryon channels, for example $p\bar{p}$, where the sample sizes are larger for a given integrated luminosity, can reach a precision where possible effects from two-photon exchange can be revealed. This is particularly true if more data can be collected at some off-resonance energies.

- **Baryon form factor by ISR method**

The large amount of data that is planned to be collected at energies larger than 3.7 GeV enables studies of baryon EMFFs using the ISR method. This possibility is particularly valuable close to threshold. Special event selection techniques are required in the analysis of energy scan data, due to the low momenta of the outgoing particles. Due to the boost of the ISR photon, the respective baryons have larger momenta in the laboratory frame and can be detected more easily. Additionally, it is currently technically challenging to acquire energy scan data in the threshold region of nucleon production, due to the design of the accelerator. However, away from threshold, the statistical precision is generally better when using the energy scan method, as can be seen for example in a comparison of the proton EMFF studies

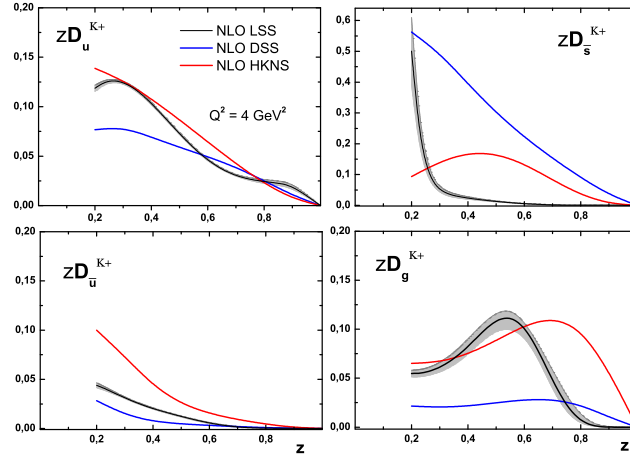


Figure 4.16: Comparison between NLO LSS, DSS and HKNS Kaon fragmentation functions at $Q^2 = 4 \text{ GeV}^2$, taken from Ref. [138].

using the ISR method [97] and the energy scan method [131]. Measurements of the form factor ratio and its relative phase benefit from data collected at well-defined energies with the scan method. The uncertainty in energy that is inevitable with the ISR method, propagates to the uncertainty in the ratio and the phase.

4.4 Fragmentation function

The fragmentation function $D_q^h(z)$ describes the probability of a hadron h to be found in the debris of a quark (or antiquark), carrying the fraction z of the quark energy. $D_q^h(z)$ is an inherently non-perturbative object governing hadronization. It cannot be deduced from first principles, but can be extracted from experimental data [132, 133]. Fragmentation functions are assumed to be universal, *i.e.*, they are not process dependent.

A large amount of data on inclusive hadron production from e^+e^- collisions has been collected in a wide energy range $10 \leq \sqrt{s} \leq 200 \text{ GeV}$ and $0.005 \leq z \leq 0.8$ [134]. These data sets, semi-inclusive deep-inelastic scattering (DIS) data and data sets from hadronic collisions are used to extract a fragmentation function by DSS [135], HKNS [136] and AKK08 [137]. However, the number of experimental data points is small, and the uncertainty of experimental data points is large at the few GeV energy region. Figure 4.16 compares the Kaon fragmentation function by different fragmentation function packages; the favored $D_s^{K^+}(z, Q^2)$ changes very rapidly between $z=0.2$ and $z=0.3$ [138].

A precise determination of fragmentation functions could help to understand the internal structure of the nucleon. The strange quark polarization puzzle, *i.e.*, the polarization of the strange quark is positive in the measured region of Bjorken x by semi-inclusive DIS analyses, where inclusive DIS yields significantly negative values of this quantity. It is pointed out in Ref. [139] that the polarization of the strange quark extracted from semi-inclusive DIS analyses is very sensitive to the input fragmentation functions. The

semi-inclusive DIS process is used to study the proton spin at the upgraded JLab-12 [140] and the future Electron-Ion Collider [141]. Thus, a better knowledge of fragmentation functions is needed.

DIS experiments have performed detailed studies of the transverse momentum dependence (TMD) by semi-inclusive processes. They describe cross sections in terms of TMD parton density functions (PDF) and fragmentation functions. The TMD fragmentation functions $D_q^h(z, P_{h\perp}^2, Q^2)$ describes a fragmentation process of an unpolarized parton q into an unpolarized hadron h , which carries the longitudinal-momentum fraction z and transverse momentum $P_{h\perp}$ in the process. In order to understand TMD PDFs, knowledge of the TMD fragmentation functions is needed. Unfortunately, the determination of unpolarized TMD fragmentation functions is still missing [142]. With data from the B factories and BESIII, we could extract these required TMD fragmentation functions.

The Collins fragmentation function describes spin-dependent effects in fragmentation processes [143]. It connects transverse quark spin with a measurable azimuthal asymmetry (so-called Collins effect) in the distribution of hadronic fragments along the initial quark's momentum. This azimuthal asymmetry has been reported in semi-inclusive DIS and e^+e^- annihilation [142], where the Collins effect is studied in e^+e^- annihilation by detecting simultaneously two hadrons, coming from fragmentation of quark and antiquark, in the process $e^+e^- \rightarrow h_1 h_2 + X$. In this case, the observable is associated with two Collins fragmentation functions.

The e^+e^- Collins asymmetries taken from Belle and BaBar correspond to higher Q^2 ($\approx 100 \text{ GeV}^2$) than the typical energy scale of existing DIS data (mostly $2-20 \text{ GeV}^2$), which is similar to that of BESIII. Therefore, the very low cms energies reached at BESIII allow to investigate energy scaling. The results are crucial to explore the Q^2 evolution of the Collins fragmentation function and further uncertainty of extracted transversity, thus improving our understanding of both the Collins fragmentation function and transversity [144].

The Collins asymmetries for pion pairs have been obtained at BESIII using data collected at $\sqrt{s} = 3.65 \text{ GeV}$ which correspond to an integrated luminosity of 62 pb^{-1} [145]. Figure 4.17 compares the Collins effect measured by BESIII, BaBar and Belle. The measured asymmetries are almost consistent with zero for low (z_1, z_2) , and rise with increasing z . The BESIII asymmetry in the last interval, is about two/three times larger compared to measurements from the B factories. Additional results are needed to confirm this observation with about 250 pb^{-1} data at 3.65 GeV . The Collins effect for strange quarks could be studied in $e^+e^- \rightarrow \pi K + X$ and $e^+e^- \rightarrow KK + X$. It is also interesting to study the Collins effect in $e^+e^- \rightarrow \pi^0\pi^0 + X$, $e^+e^- \rightarrow \eta\eta + X$ and $e^+e^- \rightarrow \pi^0\eta + X$ for neutral hadrons. These results are useful to extract TMD PDFs.

4.5 τ physics at BESIII

Since the discovery of τ lepton in 1975 at SPEAR e^+e^- storage ring [146], the study of τ lepton has been measured extensively. The properties of the τ lepton, including mass, lifetime and decays, have been tested sensibly [1]. As a member of the third fermion generation, it decays to the first and second generation fermions. The pure leptonic or semileptonic character of τ decays provides a clean laboratory to test the structure of the

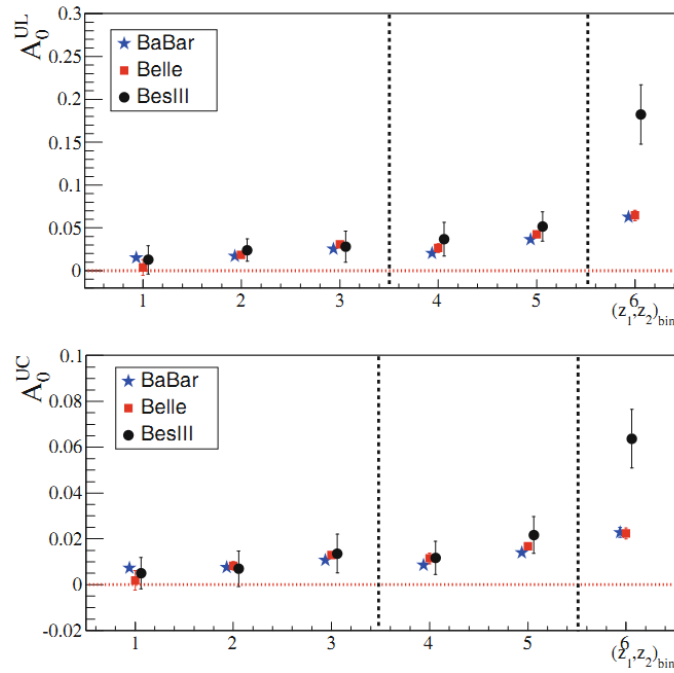


Figure 4.17: Comparison between the BESIII, BaBar and Belle measurements of the Collins effects. The detailed definition for the axis can be found in Ref. [145].

weak currents and the universality of their couplings to the gauge bosons. Moreover, τ being the only lepton massive enough to decay into hadrons, the semileptonic decays are an ideal tool for studying strong interactions.

The BEPCII is a τ -charm factory with a cms energy ranging from 2.0 to 4.9 GeV, and a design peak luminosity of $10^{33} \text{ cm}^{-2} \text{ s}^{-1}$ at the cms energy of 3.773 GeV. The great advantage of BEPCII lies in running near threshold of τ pair, which provides us an excellent opportunity for τ lepton physics. Comparing with other machines, the threshold region makes possible a much better control of background and systematic uncertainty for measurements.

There are three energy regions appreciated for researches. The first is below the τ pair production threshold, say 3.50 GeV, where the light quark background can be measured, and the result can be extrapolated to the other energy regions. The second is at the production threshold, such as 3.55 GeV, where τ lepton pair are produced at rest. It is an unique energy to study the τ decays. The third region is above the τ pair production threshold, which can be further classified into two cases. The one case is below the production of open charm, say 3.69 GeV, where the background is same as described at the below threshold region; the other is at 4.25 GeV, where the cross section of τ pair production is at the maximum, while charm background should be considered in addition to the light quarks background.

Figure 4.18 shows the production cross section and R ratio for τ pairs in the region of BEPCII. The luminosity at the τ lepton threshold is about $0.3 \times 10^{33} \text{ cm}^{-2} \text{ s}^{-1}$. Therefore several hundred thousand τ lepton pairs will be produced in a running year (about six months). In the past years, BESIII had taken about one month data near τ lepton

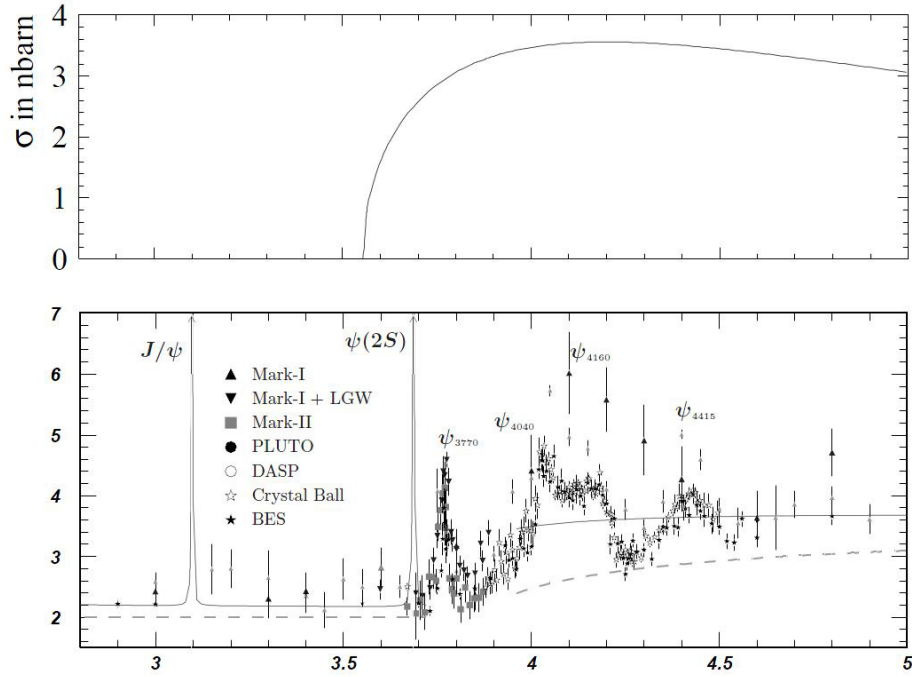


Figure 4.18: Top: Production cross section for τ pairs. Bottom: The R -ratio showing the expected background from quark production (from PDG). Cross section and R values are shown versus the cms energy in GeV on identical scales.

pair production threshold: about 150 pb^{-1} has been obtained. Comparing with the experiments at higher energy regions, such as B factories and LHC, BESIII does not have advantage at statistics. An immense amount of data have been obtained by high energy experiments, many measurements are performed pretty precisely. The running energy of BEPCII is low, the produced τ leptons are almost stationary, and the hardware does not allow us to measure the life time of the τ lepton accurately.

The advantages of BEPCII are the experimental condition: the machine runs near the threshold of τ pair production, the background is pretty simple and the systematic uncertainties can be controlled easily. The beam energy spread of BEPCII is small, about 1-2 MeV. Moreover, beam energy measurement system (BEMS) was built to determine the energy and energy spread accurately. Therefore, BESIII has unique advantage to perform the τ mass measurement.

4.5.1 Measurement of the τ mass

The τ is one of three charged elementary leptons in nature, and its mass is an important parameter of the Standard Model. The improvement of accuracy of τ mass (m_τ) is needed in its own right. Listed as follows are the measured mass values of three leptons according

to PDG2012 [147]:

$$\begin{aligned} m_e &= 0.510998910 \pm 0.000000013 \text{ MeV} & (\delta m_e/m_e &\approx 2.554 \times 10^{-8}) , \\ m_\mu &= 105.658367 \pm 0.000004 \text{ MeV} & (\delta m_\mu/m_\mu &\approx 3.786 \times 10^{-8}) , \\ m_\tau &= 1776.82 \pm 0.16 \text{ MeV} & (\delta m_\tau/m_\tau &\approx 9.568 \times 10^{-5}) . \end{aligned} \quad (4.15)$$

It can be seen that the accuracy of m_τ is almost four orders of magnitude lower than that of the other two leptons. The accuracy of electron and muon masses is already at the level of 10^{-8} .

One well-known motivation for obtaining an accurate value of m_τ is found in the test of lepton universality. Lepton universality, a basic ingredient of the Standard Model, requires that the charged-current gauge coupling strengths g_e, g_μ, g_τ are identical: $g_e = g_\mu = g_\tau$. Comparing the electronic branching fractions of τ and μ , lepton universality can be tested as:

$$\left(\frac{g_\tau}{g_\mu}\right)^2 = \frac{\tau_\mu}{\tau_\tau} \left(\frac{m_\mu}{m_\tau}\right)^5 \frac{B(\tau \rightarrow e\nu\bar{\nu})}{B(\mu \rightarrow e\nu\bar{\nu})} (1 + F_W)(1 + F_\gamma), \quad (4.16)$$

where F_W and F_γ are the weak and electromagnetic radiative corrections [148]. Note that $(g_\tau/g_\mu)^2$ depends on m_τ to the fifth power.

Furthermore, the precision of m_τ will also restrict the final sensitivity of m_{ν_τ} . The most sensitive bounds on the mass of the ν_τ is derived from the analysis of the invariant-mass spectrum of semi-hadronic τ decays. At present, the best limit of $m_{\nu_\tau} < 18.2 \text{ MeV}/c^2$ (95% confidence level) is based on the kinematics of 2939 (52) events of $\tau^- \rightarrow 2\pi^-\pi^+\nu_\tau$ ($\tau^- \rightarrow 3\pi^-2\pi^+(\pi^-\nu_\tau)$) [149]. This method depends on the determination of the kinematic end point of the mass spectrum, thus, high precision on m_τ is needed.

Another test also depends only on the accuracy of m_τ . An interesting formula related to the three leptons masses was discovered in 1981 [150]:

$$m_e + m_\mu + m_\tau = \frac{2}{3}(\sqrt{m_e} + \sqrt{m_\mu} + \sqrt{m_\tau})^2 . \quad (4.17)$$

According to the error propagation formula (f_m indicates the difference between the right and left sides of Eq. (4.17))

$$\delta f_m = \sqrt{\sum_{k=e,\mu,\tau} \left[m_k - \frac{2}{3} \left(\sum_{i=e,\mu,\tau} \sqrt{m_k m_i} \right) \right]^2} \cdot \left(\frac{\delta m_k}{m_k} \right)^2 \approx \frac{1}{3} \delta m_\tau , \quad (4.18)$$

which indicates that the test of Eq. (4.17) depends almost merely on the accuracy of m_τ .

The measurement of the τ mass has a history of more than forty years. In the first experimental paper on the τ lepton [146], m_τ is estimated to have a value in the range from 1.6 to 2.0 GeV/c^2 . Since then, many experiments have been performed measurements of m_τ [151–166], whose results are displayed in Fig. 4.19.

The results of m_τ measurements in the 21st century are summarized in Table 4.2, where two results were acquired using the method of pseudo-mass, while other experiments used the method of threshold scan. For the pseudo-mass method, the huge amount of data

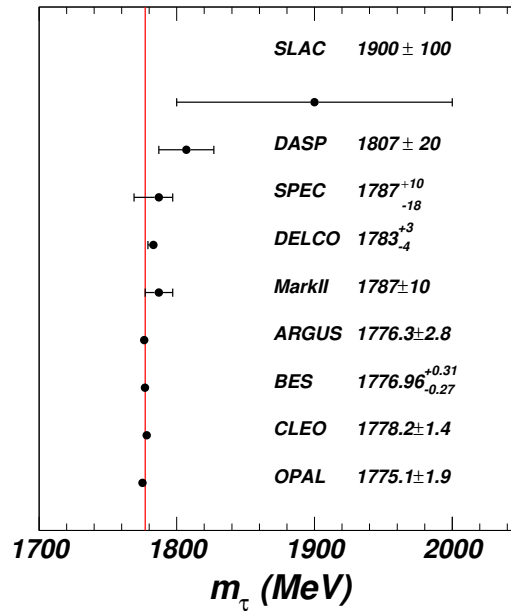
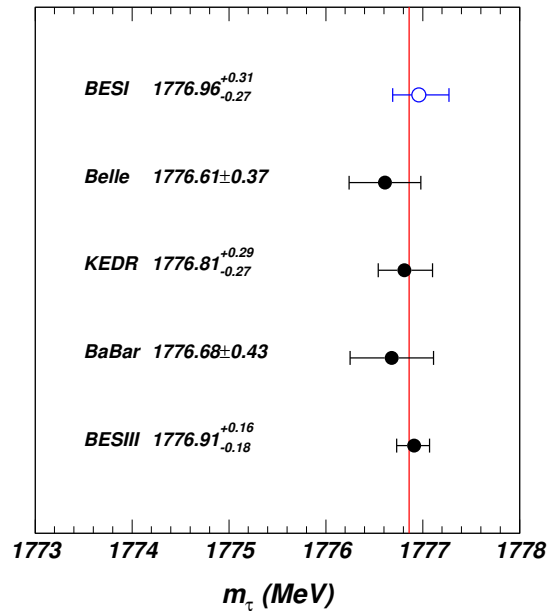
(a) m_τ measured in the 20 century(b) m_τ measured in the 21 century

Figure 4.19: m_τ measured in the last and this century. In (a) the red line indicates the average value of m_τ in PDG2000 [167]: $m_\tau = 1777.03^{+0.30}_{-0.26}$ MeV/ c^2 . For comparison, the measured value from BES in 1996 is also plotted in (b) but with blank blue circle for distinction. The average value of m_τ in PDG2015 [168]: $m_\tau = 1776.86 \pm 0.12$ MeV/ c^2 is also indicated by the red line in (b). It should be noted that since PDG1996 [169, 170], the results from experiments performed before 1990 were removed except for the result of DELCO.

Table 4.2: Measurement results of m_τ in the 21 century.

Measured m_τ (MeV/ c^2)	Year	Exp. Group	Data sample	Method
$1776.91 \pm 0.12^{+0.10}_{-0.13}$	2014	BESIII [166]	23.26 pb $^{-1}$	Threshold-scan
$1776.68 \pm 0.12 \pm 0.41$	2009	BaBar [165]	423 fb $^{-1}$	Pseudo-mass
$1776.81^{+0.25}_{-0.23} \pm 0.15$	2007	KEDR [164]	6.7 pb $^{-1}$	Threshold-scan
$1776.61 \pm 0.13 \pm 0.35$	2007	Belle [163]	414 fb $^{-1}$	Pseudo-mass

acquired at the B -factories is employed [163]. Good statistical accuracy is achieved, but large systematic uncertainty exists, which is mainly due to the absolute calibration of the particle momentum. For the threshold-scan method, the value of m_τ was extracted from the dependence of production cross section on the beam energy. In the KEDR experiment [164], both, the resonant depolarization technique and the Compton backscattering technique [171] are used to determine the beam energy. All these techniques greatly decrease the uncertainty of beam energy.

Although the accuracy of results from above two methods are at the comparable level, it is obvious that the pseudo-mass method is already dominated by systematic errors. Additional data taking will not improve the result. For the threshold-scan method, however, both the statistic and systematic errors still seem to have room for further improvements. Therefore, the BESIII collaboration adopted the threshold-scan method to measure the m_τ . In this approach it is of utmost importance to determine the beam energy and the beam energy spread precisely. For this purpose, starting from the year 2007, a high accuracy beam energy measurement system (BEMS) located at the north crossing point (NCP) of BEPCII was designed, constructed, and finally commissioned at the end of 2010 [172–176]. Two days were spent to perform a scan of the $\psi(3686)$ resonance. The mass difference between the PDG value in 2010 and the one measured by BEMS is 1 ± 36 keV, the deviation of which indicates that the relative accuracy of BEMS is at the level of 2×10^{-5} [175].

Prior to conducting the experiment, a study was carried out using Monte Carlo (MC) simulation and sampling to find out the scheme that can provide the highest precision on m_τ for a specified period of data taking time or equivalently for a given integrated luminosity. The main conclusions for the optimization study are summarized as follow [177–181]:

1. For N free parameters, N scan points are sufficient;
2. The optimal position can be obtained by single parameter scan;
3. Luminosity allocation can be determined analytically or by simulation method;
4. The uncertainty of m_τ is proportional to the inverse of square root of luminosity.

By virtue of these conclusions, the optimal scan strategy is designed as follows: firstly, a scan of the J/ψ resonance (scan points 1-7), then a scan in the vicinity of the τ -pair threshold (scan points 8-12), finally a scan of the $\psi(3686)$ resonance (scan points 13-19). After that, repeat (in τ -region, the data are taken only at scan points 9 and 10). The

Table 4.3: Scan plan and offline results. Superscript “plan” indicates the planned value for the scan; “exp” indicates the experimental measured value of scan plan; while “online” denotes the value from online record. E_{beam} and \mathcal{L} represent the beam energy and integrated luminosity respectively. (\dagger : the planned values are listed in last two columns; \ddagger : the measured values are little different from the expected ones due to the fluctuation of accelerator.)

Energy Region	order	$E_{\text{beam}}^{\text{plan}}$	$\mathcal{L}^{\text{plan}}$	$E_{\text{beam}}^{\text{exp}}$	$\mathcal{L}^{\text{online}}$	order	$E_{\text{beam}}^{\text{plan}}$ (MeV)	
		(MeV)	(pb^{-1})	(MeV)	(pb^{-1})		J/ψ	$\psi(3686)$
J/ψ	1-7	\dagger	—	\ddagger	32.6	1/13	1544.0	1838.0
τ	8	1771.0	14	1769.74	25.5	2/14	1547.8	1841.9
	9	1776.6	14+25	1776.43	42.6	3/15	1548.2	1842.5
	10	1777.0	14+12	1776.96	27.1	4/16	1548.6	1843.1
	11	1780.4	7	1780.18	8.3	5/17	1549.0	1843.8
	12	1792.0	14	1800.27	28.8	6/18	1549.4	1844.5
$\psi(3686)$	13-19	\dagger	—	\ddagger	67.2	7/19	1552.0	1847.0

two-round process is designed to understand the stability of accelerator and detector. The key issue here is to acquire 100 pb^{-1} data in τ -region to guarantee an uncertainty of m_τ of less than $0.1 \text{ MeV}/c^2$. The scan plan and parts of the offline results are summarized in Table 4.3.

Based on all these full preparations, the BESIII collaboration performed the finer τ mass scan experiment from April 14th to May 3rd, 2018. The actual data taking time is around 11.2 days (269 hours). The J/ψ and $\psi(3686)$ resonances were each scanned at seven and nine energy points respectively, and data were collected at five scan points near τ pair production threshold with cms energies of 3538.9, 3552.8, 3553.9, 3560.3, and 3599.5 MeV. The first τ scan point is below the mass of τ pair [147], while the other three are above*.

Using these data samples, the final goal of the finer scan is to obtain the τ lepton mass with high precision, namely 0.1 MeV , which includes the statistical error and systematical uncertainties. It is an unprecedented accuracy, and as indicated in the Ref. [182], this is a challenging task that needs a considerable effort, energy, and great patience.

So far, the statistical uncertainty of m_τ measurement is roughly equivalent to the systematic error. Only after finding a better way to reduce the systematic error, BESIII would collect more data to improve the precision of m_τ further.

4.5.2 Some τ -physics topics at BESIII

As mentioned above, τ is the only lepton heavy enough to decay into hadrons. Actually, its partial decay width involving hadrons in the final state is about 65%. The hadronic τ decays turn out to be a beautiful laboratory for studying the non-perturbative

*The original two-round process was designed mainly to understand the stability of accelerator and detector. During the period of m_τ scan, the status of accelerator and detector was fairly good, so two-round process degenerated into no-circle process.

regime of QCD, which will be useful to understand the hadronization of QCD currents, to study form factors and to extract resonance parameters.

Rare decays of the τ leptons are a very promising area because the interaction is suppressed and the sensitivity to new physics might eventually be enhanced. In SM, the suppression of rare τ decays might be due to several reasons: i) Cabbibo suppression: strange hadronic final states are suppressed with respect to non-strange ones since the $|V_{us}|$ element of the CKM matrix enters the description J^{PC} instead of $|V_{ud}|$; ii) phase space suppression: because of the larger masses of Kaon and η mesons in the final state, the phase space should always be suppressed; iii) second-class currents: in hadronic τ decays, the first-class currents have $J^{PC} = 0^{++}, 0^{-}, 1^{+-}$ or 1^{-+} and are expected to dominate. The second-class currents, which have $J^{PC} = 0^{+-}, 0^{-+}, 1^{++}$ or 1^{--} , are associated with a matrix element proportional to the mass difference between up and down quarks. They vanish in the limit of perfect isospin symmetry, but are not prohibited by SM, which indicates the branching fractions of such τ decays at the order of 10^{-5} .

The τ lepton provides a clean means to search for second-class currents, through the decay mode $\tau^- \rightarrow \pi^- \eta \nu_\tau$. The $\pi^- \eta$ final state must have either $J^{PC} = 0^{+-}$ or $J^{PC} = 1^{--}$, both of which can only be produced via second-class currents.

The CLEO collaboration analyzed 3.5 fb^{-1} data taken at the cms $\sqrt{s} = 10.6 \text{ GeV}$, had produced the most stringent limit on $\tau^- \rightarrow \pi^- \eta \nu_\tau$ decays, and set an upper limit of $\mathcal{B}(\tau^- \rightarrow \pi^- \eta \nu_\tau) < 1.4 \times 10^{-4}$ at the 95% confidence level [183]. Also the BaBar collaboration analyzed 470 fb^{-1} data taken at the cms $\sqrt{s} = 10.6 \text{ GeV}$, studied the decay $\tau^- \rightarrow \pi^- \eta \nu_\tau$, and set an upper limit of $\mathcal{B}(\tau^- \rightarrow \pi^- \eta \nu_\tau) < 0.99 \times 10^{-4}$ at the 95% confidence level [184].

The research on the second-class currents is both promising and challenging. On the one hand, the energy region of BEPCII is near the τ pair production threshold, and the background is relatively simple; on the other hand, since our luminosity is pretty low, even if the τ data are taken at the maximum cross section, say 4.25 GeV , to achieve considerable precision, 10^{-4} , BESIII has to run for ten years.

The decays of the τ lepton into three pseudoscalar particles can provide information on hadronic form factors, the Wess-Zumino anomaly, and also can be used for studies of CP violation in the leptonic sector. By studying decays into final states containing three Kaons, it can provide a direct determination of the strange quark mass and the Cabibbo-Kobayashi-Maskawa (CKM) matrix element $|V_{us}|$.

The BaBar collaboration [185] have studied the decay mode $\tau^- \rightarrow K^- K^+ K^- \nu_\tau$, and obtained the branching fraction $\mathcal{B}(\tau^- \rightarrow K^- K^+ K^- \nu_\tau) = (1.58 \pm 0.13 \pm 0.12) \times 10^{-5}$ by meas of analyzing the integrated luminosity of 342 fb^{-1} data at a cms energy near 10.58 GeV using the BaBar detector at the SLAC PEP-II asymmetric-energy e^+e^- storage ring. The Belle collaboration [186] also measured the branching fraction of this channel, their result is $(3.29 \pm 0.17 \pm 0.20) \times 10^{-5}$, based on a data sample of 666 fb^{-1} data collected with the Belle detector at the KEKB, asymmetric-energy e^+e^- collider of 10.58 GeV . The difference between the two measurements is larger than 3 standard deviations.

BESIII could perform this measurement if enough data are collected.

4.5.3 Measurement of branching fraction of $\psi(3686) \rightarrow \tau^+\tau^-$

The $\psi(3686)$ provides a unique opportunity to compare the three lepton generations by studying the leptonic decays $\psi(3686) \rightarrow e^+e^-$, $\mu^+\mu^-$, and $\tau^+\tau^-$. The sequential lepton hypothesis leads to a relationship between the branching fractions of these decays, $\mathcal{B}_{e^+e^-}$, $\mathcal{B}_{\mu^+\mu^-}$, and $\mathcal{B}_{\tau^+\tau^-}$ given by

$$\frac{\mathcal{B}_{e^+e^-}}{v_e(\frac{3}{2} - \frac{1}{2}v_e^2)} = \frac{\mathcal{B}_{\mu^+\mu^-}}{v_\mu(\frac{3}{2} - \frac{1}{2}v_\mu^2)} = \frac{\mathcal{B}_{\tau^+\tau^-}}{v_\tau(\frac{3}{2} - \frac{1}{2}v_\tau^2)} \quad (4.19)$$

with $v_l = [1 - (4m_l^2/M_{\psi(3686)}^2)]^{1/2}$, $l = e, \mu, \tau$. Substituting the mass values for the leptons and the $\psi(3686)$ yields

$$\mathcal{B}_{e^+e^-} = \mathcal{B}_{\mu^+\mu^-} = \frac{\mathcal{B}_{\tau^+\tau^-}}{0.3885} \equiv \mathcal{B}_{l^+l^-}. \quad (4.20)$$

BES once preformed such a study based on 3.96 million $\psi(3686)$ event sample at the cms $\sqrt{s} = 3686.36$ MeV [166]. Now with BESIII data sample, more detailed study can be expected.

In 2018, BESIII performed a fine $\psi(3686)$ scan at 10 points with totally 67 pb⁻¹ data. Exploiting with this large sample, instead of using Eq. (4.19), it is possible to measure each branching fraction separately and test the the relation between them. Further, unlike BES measurement at single energy point, with lots of scan points, the interference between the continuum and resonance parts can be measured directly, and even the phase angle between them. This will be a very technical and interesting work related to τ lepton.

4.5.4 Mass measurement for some hadrons

The mass of τ lepton can be determined precisely by means of BEMS. However not all masses of hadrons can be determined using BEMS. The details of BEMS can be found in Refs. [175, 187]. Generally speaking, the allowed region of beam energy for BEMS should not exceed 2 GeV. On the one hand, to a high-purity germanium detector, the energy of upper limit for the Compton backscattered photons is 10 MeV; on the other hand, there is no suitable radiation sources to calibrate the detector for such high energy backscattered photons. Moreover, the detection efficiency to high Compton backscattered photons is pretty low. Hence, it is better to measure the masses for hadrons, such as D_s^* , D_{s0} , D_{s1} , Λ_c , Σ_c using the invariant mass method if we have enough data.

4.5.5 Discussion

Experimentally speaking, measurements involving τ leptons can be divided into three categories: the mass of τ , the life time of τ and the measurements related to the determination of branching fraction of τ decay. Except for τ mass measurement, due to the limitation of data samples, BESIII lacks competitive power in other measurements.

4.6 Relative phase in vector charmonium decays

For many years, there has been evidence of an unexpected phenomenon in the decay of narrow charmonium resonances. A relative phase of $|\Delta\Phi| = 90^\circ$ between the strong and EM decay amplitudes of J/ψ is observed [188]. In case of the $\psi(3686)$, the available evidence is less compelling. However, $\psi(3686)$ scan data have been collected at BESIII and are being analyzed, *e.g.*, $e^+e^- \rightarrow \mu^+\mu^-, KK, \eta\pi^+\pi^-$ and baryon pairs. Concerning the $\psi(3770)$, the phase difference has been measured in a few cases and $\Delta\Phi = -90^\circ$ has been established [189, 190].

This phase difference, taking into account the aforementioned values, implies $\Gamma_P = \Gamma_{\text{EM}} + \Gamma_{\text{strong}}$, with Γ_P being the total width of the vector charmonium P . This relation might suggest the unconventional hypothesis that the J/ψ is a combination of two resonances, one decaying only through EM processes and another one decaying strongly (see [188], and references therein).

Currently available data are barely sufficient to determine the absolute value of $\Delta\Phi$ for J/ψ in a limited number of decay modes. The process $\eta\pi^+\pi^-$ is observed with low statistics in a J/ψ line shape scan of 16 energy points with a total integrated luminosity of about 100 pb^{-1} , where the fit procedure introduces 11% systematic uncertainty [188]. With ten times more of available scan data, we could obtain a more precise measurement of $\Delta\Phi$. In a few of those cases it might already be possible to determine also the sign of the relative phase of EM and strong amplitudes. However, in J/ψ decays into baryon pairs the “magnetic” and “electronic” amplitudes might have different phases.

An intriguing situation has been found in $J/\psi \rightarrow \pi\pi$. Due to G -parity violation a purely strong amplitude should be suppressed. However, the EM amplitude is not sufficient to explain the partial width of $J/\psi \rightarrow \pi\pi$. As a remedy, an amplitude has been suggested with two gluons and one virtual photon as an intermediate state [191]. In order to test the hypothesis, it is most interesting to determine the relative phase between the strong and EM decay amplitudes in the $J/\psi \rightarrow \pi\pi$ decay. The currently available data at BESIII, however, do not allow for such investigations yet.

In conclusion, much more data are needed to settle the question of the phase difference between the strong and EM decay amplitudes of vector charmonium states. If the aforementioned vector charmonium double nature is confirmed, something important has been missed in the understanding of the Zweig rule (see Ref. [192] and references therein).

4.7 Study of $\phi(2170)$ with the energy scan method

Quarkonia provide a unique platform to study QCD. Substantial progress has been made over the recent years from the investigation of charmonia ($c\bar{c}$) and bottomonia ($b\bar{b}$). A plethora of interesting new hadronic states were found. New types of hadronic matter, such as hybrids, multiquark states, and hadronic molecules with (hidden) charm and bottom quarks are considered in the interpretation [193–195].

The multitude of results from heavier quarkonia leads to the obvious question whether similar states should exist in the strange sector. However, experimental evidence for a rich spectrum of strangeonium ($s\bar{s}$) or new types of hadronic matter with strange quarks

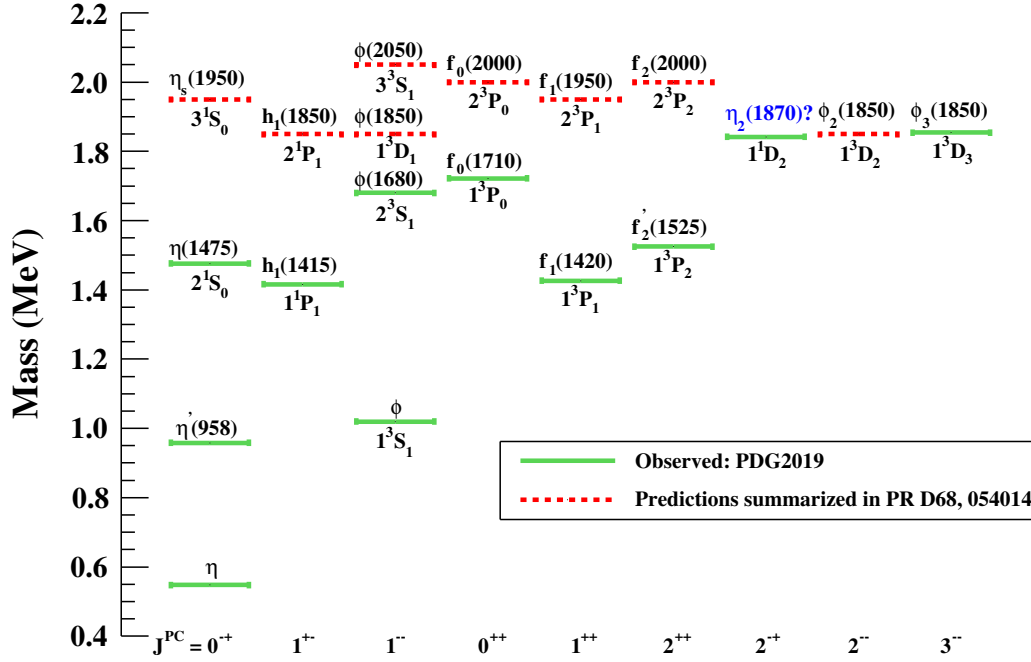
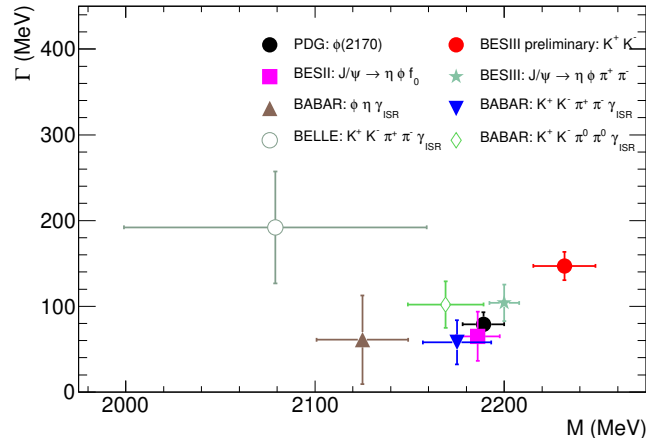


Figure 4.20: The strangeonium spectroscopy. The red dotted line corresponds to predicted strangeonium states summarized in Ref. [196], and the green line corresponds to observed $s\bar{s}$ resonances, taken from PDG [24].

is scarce. Figure 4.20 shows predicted strangeonium states [196] with identified $s\bar{s}$ resonances [24]. Only 10 probable $s\bar{s}$ resonances out of the 22 expected below 2.2 GeV are established. A candidate for an exotic type of hadronic matter containing strange quarks is the $\phi(2170)$. At BESIII the $\phi(2170)$ can be studied as an intermediate state in charmonium decays, exploiting the unique statistics of the J/ψ data set, and by performing a dedicated energy scan around the mass of the $\phi(2170)$. Both methods provide unique opportunities in terms of precision and accuracy necessary to understand the nature of the $\phi(2170)$.

The $\phi(2170)$, previously referred to as the $Y(2175)$, has been observed in $e^+e^- \rightarrow \phi f_0(980)$ at B factories using the ISR method [197, 198], in the charmonium decay $J/\psi \rightarrow \eta \phi f_0(980)$ [199], and in $e^+e^- \rightarrow \eta \phi f_0(980)$ at cms energies between 3.7 and 4.6 GeV [200]. Theorists explain it as a traditional $3^3S_1 s\bar{s}$ or $2^3D_1 s\bar{s}$ state [201–204], as a $1^{--} s\bar{s}g$ hybrid [205], as a tetraquark state [206–209], as a $\Lambda\bar{\Lambda}(^3S_1)$ bound state [210–212], and as a $\phi K\bar{K}$ resonance state [213]. According to PDG [24], the $\phi(2170)$ has been observed in the final states $\phi f_0(980)$, $\phi\eta$, $\phi\pi\pi$, and $K^+K^-f_0(980)$. For the final state $K^{*0}\bar{K}^{*0}$ only an upper limit has been reported [214]. Hence, the number of experimentally established decay modes of $\phi(2170)$ is limited. Additionally, as shown in Fig. 4.21, there is a large scatter of the measured values of mass and width of the $\phi(2170)$. So far, none of above theory models are either estimated or ruled out by experimental results.

Figure 4.21: Mass and width of the $\phi(2170)$.

Describing the $\phi(2170)$ as a $3^3S_1s\bar{s}$ or $2^3D_1s\bar{s}$ state favors the decay modes $K^*\bar{K}^*$, $K\bar{K}(1460) + c.c.$, and $\eta h_1(1380)$, while these modes are forbidden for a $1^{--}s\bar{s}g$ state. Instead, the $K\bar{K}_1(1400) + c.c.$ and $K\bar{K}_1(1270) + c.c.$ are favored for $1^{--}s\bar{s}g$ state [196, 201, 205]. However, all of the four previously mentioned decays produce the same final state: $K\bar{K}\pi\pi$. Originally, the $\phi(2170)$ was observed in the $\phi\pi\pi$ final state, an intermediate state of $K\bar{K}\pi\pi$. The fitted $\phi(2170)$ resonance parameters $m = (2079 \pm 13) \text{ MeV}/c^2$ and $\Gamma = (192 \pm 23) \text{ MeV}$ in the $\phi\pi\pi$ mode are slightly lower than $m = (2163 \pm 32) \text{ MeV}/c^2$ and $\Gamma = (125 \pm 40) \text{ MeV}$ in the $\phi f_0(980)$ mode [198], which is consistent with available measurements in the $\phi f_0(980)$ mode (see Fig. 4.21). A PWA analysis of $e^+e^- \rightarrow K\bar{K}\pi\pi$ at BESIII is useful to distinguish $s\bar{s}$ and $s\bar{s}g$, and understand results obtained from the $\phi\pi\pi$ and $\phi f_0(980)$ modes.

The $e^+e^- \rightarrow \phi\eta$ and $e^+e^- \rightarrow \phi\eta'$ processes are well suited to study excited ϕ states, and useful to estimate mass and width of strange quarkonia due to the OZI rule. The main decay modes in tetraquark pictures [208] are $\phi\eta$ and $\phi\eta'$ modes; the predicted decay width of a $1^{--}s\bar{s}g$ state to $\phi\eta$ is much larger than that of $\phi\eta'$ [205, 215], whereas $\phi\eta$ is forbidden for $2^3D_1s\bar{s}$ states [201]. However, the uncertainty of the cross section of $\phi\eta$ around $\sqrt{s} = 2.2 \text{ GeV}$ measured by BaBar is at the 50% level [216]. A clear signal of $\phi\eta'$ is observed by BaBar in Ref. [217]. A precise measurement of $\phi\eta$ and $\phi\eta'$ modes at BESIII is useful to distinguish tetraquark, hybrid and 2^3D_1 pictures of the $\phi(2170)$. Besides $\phi(2170)$, there is another possible structure for $\phi f_0(980)$ and $K^+K^- f_0(980)$ around 2.4 GeV [197–199]. BaBar determined its mass and width as $(2.37 \pm 0.07) \text{ GeV}/c^2$ and $(77 \pm 65) \text{ MeV}$, while Ref. [218] obtained $(2436 \pm 34) \text{ MeV}/c^2$ and $(99 \pm 105) \text{ MeV}$, respectively, whose statistical significance is smaller than 3σ . A QCD sum rule also predicts two $J^{PC} = 1^{--}$ resonances $2.34 \pm 0.17 \text{ GeV}$ and $2.41 \pm 0.25 \text{ GeV}$, both around 2.4 GeV [219]. In the ϕK^+K^- mode two broad structures were observed at 2.3 GeV and 2.7 GeV , respectively, albeit in a different $m(K^+K^-)$ range [197]. A scan in 40 MeV steps in the range of $[2.35, 2.83] \text{ GeV}$ with integrated luminosities of 20 pb^{-1} at each energy point, is called for to search for (possible) new resonances.

Last but not least, Refs. [202, 220] predict a broad resonance with mass around 1.9 GeV regarded as the $1D$ state of the ϕ family. A new scan measurement between 1.8 and

2.0 GeV is needed to search for $1^3D_1 s\bar{s}$ (shown in Fig. 4.20), to investigate the threshold production of nucleon pairs and a structure around 1.9 GeV, shown in Ref. [221]. The scan should be performed with 10 MeV steps between 1.8 and 2.0 GeV and an integrated luminosity 4 pb^{-1} at each energy point.

Based on collected data for R values in the energy range between 2.0 and 3.08 GeV, we already studied the final states K^+K^- , ϕK^+K^- , and $K^+K^-\pi^0\pi^0$, and the investigation of further possible decay modes is ongoing. However, more data at additional energy points are needed, which are listed in Table 4.4.

4.8 Prospects

The different physics aspects addressed in this chapter cannot be studied from a single data set. While studies based on ISR or two-photon collisions require large data samples, taken at masses well above the actual mass range of interest, precise studies of line shapes or threshold effects are best performed on several smaller data sets in an energy scan.

The existing ISR studies were mostly performed on 2.9 fb^{-1} taken at the $\psi(3770)$ peak. The results are already competitive with previous measurements of hadronic cross sections. However, one of the key issues, the hadronic contributions to a_μ , is still unsettled. The published BESIII result on the dominating $\pi^+\pi^-$ contribution is currently dominated by systematics, where the largest contributions stem from the uncertainties of the luminosity determination and the theoretical uncertainty of the radiator function. An alternative approach to the normalization of the cross section can reduce the systematic uncertainty. Using the ratio to the muon cross section cancels the two uncertainties mentioned above. However, due to an insufficient muon yield in the current data set, the statistical uncertainty becomes dominant. Based on the performance of the published work, it is estimated that an additional data set of 20 fb^{-1} , taken at the $\psi(3770)$ peak, and data set listed in Chapter 3 for XYZ physics, will allow to collect sufficient statistics to perform the normalization of the hadronic cross sections with respect to the muon yield. The systematic uncertainty of the pion form factor measurement could be reduced to $\mathcal{O}(0.5\%)$, making the BESIII result not only comparable, but competitive to the KLOE, the BaBar, and the announced CMD-3 measurements as well as potential future analyses at Belle II.

At the same time, the data can be used to study TFFs in two-photon collisions. While π^0 , η , η' , as well as pion pairs can be studied very well in a single-tag measurement using the existing data, the statistics is rather scarce for higher mass resonances, or a double-tagged measurement of the lightest pseudoscalar mesons. However, the latter two are of special interest in order to understand the hadronic light-by-light contribution to a_μ at the level of the new direct measurements at FNAL and J-PARC. An additional data set of 20 fb^{-1} at $\sqrt{s}=3.773 \text{ GeV}$ is most beneficial for the TFF measurements at BESIII for two reasons, On the one hand it increases the statistics at large invariant masses of the produced hadronic systems, and on the other hand it will allow to perform the first measurement of the doubly-virtual TFF, in the energy region most relevant for the a_μ calculations, with sufficient statistical precision to scrutinize hadronic models and provide valuable input to the new, data-driven theory approaches to a_μ^{hLBL} .

Table 4.4: Proposed data for τ -QCD study.

Energy	Physics highlight	Current data	Expected final data	time (day)
1.8-2.0 GeV	R , nucleon, resonances	N/A	96 pb ⁻¹ at 23 points	66
around 2.2324 GeV	$\Lambda\bar{\Lambda}$ threshold	one point	40 pb ⁻¹ at 4 points	17
2.35-2.83 GeV	R & resonances	few points	260 pb ⁻¹ at 13 points	60
2.5 GeV	hyperon	1 pb ⁻¹ data	100 pb ⁻¹	26
J/ψ scan	phase	100 pb ⁻¹ data	1000 pb ⁻¹	150

The scan measurements performed at BESIII have successfully allowed to determine baryon EM FFs at the respective thresholds and revealed puzzling features. In order to shed more light on these aspects, further detailed studies on enhanced data sets around the nucleon threshold at cms energies between $\sqrt{s} = (1.8, 2.0)$ GeV, the $\Lambda\bar{\Lambda}$ threshold at 2.2 GeV, and the $\Lambda_c\bar{\Lambda}_c$ threshold at 4.58 GeV are necessary.

So far, most emphasis has been put on the investigation of EM FFs of nucleons and the Λ hyperon. An additional integrated luminosity of 100 pb⁻¹ at ≈ 2.5 GeV allows not only precision studies of the Λ , but also of Σ^0 with 6% statistical uncertainty, and Σ^\pm with 4% statistical uncertainty, including the measurement of their effective form factors, their $|G_E/G_M|$ ratios, and the phase angle between G_E and G_M for Λ and Σ^+ hyperons.

A high-statistics data set taken at 2.2 GeV in order to improve the understanding of the $\Lambda\bar{\Lambda}$ threshold behavior is also beneficial for studies of the $\phi(2170)$. It would allow us to perform PWAs of the $\phi\pi\pi$ final state. Around 2.4 GeV, a structure has been observed in the $\phi\pi\pi$ system. The existing data taken at BESIII at this energy suffer from small statistics. In order to shed light on the nature of this structure, it is necessary to collect more data with 20 pb⁻¹ for each energy point around 2.4 GeV with 8% uncertainty.

In summary, Table 4.4 summarizes proposed data in this chapter.

Bibliography

- [1] D. M. Asner *et al.*, Int. J. Mod. Phys. A **24**, S1 (2009).
- [2] J. B. Guimarães da Costa *et al.* (CEPC Study Group), arXiv:1811.10545 [hep-ex].
- [3] A. Abada *et al.* (FCC Collaboration), Eur. Phys. J. ST **228**, 261 (2019).
- [4] F. Jegerlehner, Springer Tracts Mod. Phys. **274**, 1 (2017).
- [5] A. Keshavarzi, D. Nomura and T. Teubner, Phys. Rev. D **97**, 114025 (2018).
- [6] G. W. Bennet *et al.* (Muon $(g - 2)$ Collaboration), Phys. Rev. D **73**, 072003 (2006).
- [7] M. Davier, A. Hoecker, B. Malaescu and Z. Zhang, Eur. Phys. J. C **77**, 827 (2017).
- [8] B. L. Roberts, Chin. Phys. C **34**, 741 (2010).
- [9] J. Grange *et al.*, arXiv:1501.06858.
- [10] Tsutomu Mibe, Chin. Phys. C **34**, 745 (2010).
- [11] D. W. Hertzog *et al.*, arXiv:0705.4617.
- [12] J. Prades, E. de Rafael and A. Vainshtein, Adv. Ser. Direct. High Energy Phys. **20**, 303 (2009).
- [13] G. Colangelo, M. Hoferichter, M. Procura and P. Stoffer, JHEP **1409**, 091 (2014).
- [14] G. Colangelo, M. Hoferichter, B. Kubis, M. Procura and P. Stoffer, Phys. Lett. B **738**, 6 (2014).
- [15] G. Colangelo, M. Hoferichter, M. Procura and P. Stoffer, JHEP **1509**, 074 (2015).
- [16] G. Colangelo, M. Hoferichter, M. Procura and P. Stoffer, JHEP **1704**, 161 (2017).
- [17] G. Colangelo, M. Hoferichter, M. Procura and P. Stoffer, Phys. Rev. Lett. **118**, 232001 (2017).
- [18] V. Pauk and M. Vanderhaeghen, Phys. Rev. D **90**, 113012 (2014).
- [19] V. Pauk and M. Vanderhaeghen, arXiv:1403.7503.
- [20] A. Nyffeler, Phys. Rev. D **94**, 053006 (2016)

- [21] T. Blum, A. Denig, I. Logashenko, E. de Rafael, B. Lee Roberts, T. Teubner and G. Venanzoni, arXiv:1311.2198.
- [22] G. Colangelo, M. Hoferichter and P. Stoffer, JHEP **1902**, 6 (2019).
- [23] Second Plenary Workshop of the $g - 2$ Theory Initiative, <https://wwwth.kph.uni-mainz.de/g-2/> .
- [24] M. Tanabashi *et al.* (Particle Data Group), Phys. Rev. D **98**, 030001 (2018).
- [25] S. Binner, J. H. Kühn, K. Melnikov, Phys. Lett. B **459**, 279 (1999).
- [26] M. Benayoun, S. I. Eidelman, V. N. Ivanchenko and Z. K. Silagadze, Mod. Phys. Lett. A **14**, 2605 (1999).
- [27] V. P. Druzhinin, S. I. Eidelman, S. I. Serednyakov and E. P. Solodov, Rev. Mod. Phys. **83**, 1545 (2011).
- [28] G. Rodrigo *et al.*, Eur. Phys. J. C **24**, 71 (2002).
- [29] H. Czyż, J. H. Kühn and A. Wapientnik, Phys. Rev. D **77**, 114005 (2008).
- [30] H. Czyż and J. H. Kühn, Phys. Rev. D **80**, 034035 (2009).
- [31] M. Ablikim *et al.* (BESIII Collaboration), Phys. Lett. B **753**, 629 (2016).
- [32] A. Hoecker, P. Speckmayer, J. Stelzer, J. Therhaag, E. von Toerne, and H. Voss, PoS A CAT 040 (2007). [physics/0703039].
- [33] F. Campanario, H. Czyż, J. Gluza, M. Gunia, T. Riemann, G. Rodrigo and V. Yundin, JHEP **1402**, 114 (2014).
- [34] F. Ambrosino *et al.* (KLOE Collaboration), Phys. Lett. B **670**, 285 (2009).
- [35] F. Ambrosino *et al.* (KLOE collaboration), Phys. Lett. B **700**, 102 (2011).
- [36] F. Ambrosino *et al.* (KLOE collaboration), Phys. Lett. B **720**, 336 (2013).
- [37] B. Aubert *et al.* (BaBar collaboration), Phys. Rev. Lett. **103**, 231801 (2009).
- [38] M. Ablikim *et al.* (BESIII Collaboration), Phys. Lett. B **761**, 98 (2016).
- [39] M. Ablikim *et al.* (BESIII Collaboration), Phys. Lett. B **774**, 252 (2017).
- [40] R. R. Akhmetshin *et al.* (CMD-2 Collaboration), Phys. Lett. B **476**, 33 (2000).
- [41] M. N. Achasov, K. I. Beloborodov, A. V. Berdyugin, A. G. Bogdanchikov, A. V. Bozhenok, A. D. Bukin, D. A. Bukin and T. V. Dimova *et al.*, Phys. Rev. D **68**, 052006 (2003).
- [42] B. Aubert *et al.* (BaBar collaboration), Phys. Rev. D **70**, 072004 (2004).

- [43] A. Antonelli *et al.* (DM2 collaboration), *Z. Phys. C* **56**, 15 (1992).
- [44] R. R. Akhmetshin *et al.* (CMD-2 Collaboration), *Phys. Lett. B* **466**, 392 (1999).
- [45] M. N. Achasov *et al.* (SND Collaboration), BUDKER-INP-2001-34.
- [46] J. P. Lees *et al.* (BaBar Collaboration), *Phys. Rev. D* **96**, 092009 (2017).
- [47] J. Z. Bai *et al.* (BES Collaboration), *Phys. Rev. Lett.* **84**, 594 (2000); J. Z. Bai *et al.* (BES Collaboration), *Phys. Rev. Lett.* **88**, 101802 (2004); M. Ablikim *et al.* (BES Collaboration), *Phys. Lett. B* **641**, 145 (2006); M. Ablikim *et al.* (BES Collaboration), *Phys. Lett. B* **660**, 315 (2008); M. Ablikim *et al.* (BES Collaboration), *Phys. Lett. B* **677**, 239 (2009).
- [48] V. V. Anashin *et al.* (KEDR Collaboration), *Phys. Lett. B* **753**, 533 (2016); V. V. Anashin *et al.* (KEDR Collaboration), *Phys. Lett. B* **770**, 174 (2017).
- [49] V. V. Anashin *et al.* (KEDR Collaboration), *Phys. Lett. B* **788**, 42 (2019).
- [50] B. Andersson and H. M. Hu, arXiv:hep-ph/9910285.
- [51] Ronggang Ping *et al.* *Chin. Phys. C* **40**, 113002 (2016).
- [52] F. Jegerlehner, *Acta Phys. Polon. B* **44**, 2257 (2013).
- [53] B. Aubert *et al.* (BaBar Collaboration), *Phys. Rev. D* **74**, 012002 (2006).
- [54] J. P. Lees *et al.* (BaBar Collaboration), *Phys. Rev. D* **98**, 112002 (2018).
- [55] T. Feldmann, P. Kroll, B. Stech, *Phys. Rev. D* **58**, 114006 (1998); T. Feldmann, *Int. J. Mod. Phys. A* **15**, 159 (2000).
- [56] J. F. Donoghue, B. R. Holstein, Y. C. R. Lin, *Phys. Rev. Lett.* **55**, 2766 (1985).
- [57] H. Leutwyler, *Nucl. Phys. Proc. Suppl.* **64**, 223 (1998); R. Kaiser and H. Leutwyler, *Eur. Phys. J. C* **17**, 623 (2000).
- [58] H. J. Behrend *et al.* (CELLO Collaboration), *Z. Phys. C* **49**, 401 (1991).
- [59] J. Gronberg *et al.* (CLEO Collaboration), *Phys. Rev. D* **57**, 33 (1998).
- [60] B. Aubert *et al.* (BaBar Collaboration), *Phys. Rev. D* **80**, 052002 (2009).
- [61] S. Uehara *et al.* (Belle Collaboration), *Phys. Rev. D* **86**, 092007 (2012).
- [62] M. Hoferichter, B. L. Hoid, B. Kubis, S. Leupold and S. P. Schneider, *Phys. Rev. Lett.* **121**, 112002 (2018); M. Hoferichter, B. L. Hoid, B. Kubis, S. Leupold and S. P. Schneider, *JHEP* **1810**, 141 (2018).
- [63] A. Gérardin, H. B. Meyer and A. Nyffeler, *Phys. Rev. D* **100**, 034520 (2019).

- [64] I. Danilkin, C. F. Redmer and M. Vanderhaeghen, *Prog. Part. Nucl. Phys.* **107**, 20 (2019).
- [65] H. Czyz and P. Kiswa, *Comput. Phys. Commun.* **234**, 245 (2019).
- [66] M. Hoferichter and P. Stoffer, *JHEP* **1907**, 073 (2019).
- [67] I. Danilkin, O. Deineka and M. Vanderhaeghen, arXiv:1909.04158 [hep-ph].
- [68] M. Masuda *et al.* (Belle Collaboration), *Phys. Rev. D* **93**, 032003 (2016).
- [69] N. Isgur, Proceedings of NSTAR 2000, JLAB-THY-00-20 (2000).
- [70] J. Ashman *et al.*, *Phys. Lett. B.* **206**, 206 (1988).
- [71] C. A. Aidala *et al.*, *Rev. Mod. Phys.* **85**, 655 (2013).
- [72] G. A. Miller, *Phys. Rev. Lett.* **99**, 112001 (2007).
- [73] S. Weinberg, *Nucl. Phys. B* **363**, 3 (1991).
- [74] R. Machleidt and D. R. Entem, *Phys. Rep.* **503**, 1 (2011).
- [75] K. G. Wilson, *Phys. Rev. D* **10**, 2445 (1974).
- [76] T. Skyrme, *Proc. Roy. Soc. Lond. A* **260**, 237 (1961).
- [77] G. S. Adkins, C. R. Nappi and E. Witten, *Nucl. Phys. B* **228**, 552 (1982).
- [78] V. Punjabi, C. F. Perdrisat and M. K. Jones, *Eur. Phys. J. A* **51**, 79 (2015).
- [79] C. Granados, S. Leupold and E. Perotti, *Eur. Phys. J. A* **53**, 17 (2017).
- [80] M. A. Belushkin *et al.*, *Phys. Rev. C* **75**, 035202 (2007).
- [81] E. C. Titchmarsh, *The Theory of Functions*, Oxford University Press (1939).
- [82] A. D. Sakharov, *Sov. Phys. Usp* **34**, 375 (1991).
- [83] A. Sommerfeld, *Ann. Phys.* **403**, 257 (1931).
- [84] G. Fäldt, *Eur. Phys. J. A* **52**, 141 (2016).
- [85] G. Fäldt and A. Kupsc, *Phys. Lett. B* **772**, 16 (2017).
- [86] G. I. Gakh and E. Tomasi-Gustafsson, *Nucl. Phys. A* **761**, 120 (2005).
- [87] E. Tomasi-Gustafsson *et al.*, *Phys. Lett. B* **659**, 197 (2008).
- [88] A. I. Akhiezer and M. P. Rekalov, *Sov. Phys. Dokl.* **13**, 572 (1968); A. Akhiezer, M. P. Rekalov, *Sov. J. Part. Nucl.* **4**, 277 (1974).
- [89] A. J. R. Puckett *et al.* *Phys. Rev. C* **85**, 045203 (2012).

- [90] M. Rosenbluth, Phys. Rev. **79**, 615 (1950).
- [91] P. A. M. Guichon and M. Vanderhaeghen, Phys. Rev. Lett. **91** 142303 (2003).
- [92] P. G. Blunden, W. Melnitchouk and J. A. Tjon, Phys. Rev. Lett. **91** 142304 (2003).
- [93] S. Pacetti, R. Baldini Ferroli and E. Tomasi-Gustafsson, Phys. Rept. **550**, 1 (2015), and references therein.
- [94] J. P. Lees *et al.* (BaBar Collaboration), Phys. Rev. D **87**, 092005 (2007).
- [95] G. Bardin *et al.* (PS170 Collaboration) Nucl. Phys. B **411**, 3 (1994).
- [96] M. Ablikim *et al.* (BESIII Collaboration), Phys. Rev. D **91**, 112004 (2015).
- [97] M. Ablikim *et al.* (BESIII Collaboration), Phys. Rev. D **99**, 092002 (2019).
- [98] R. R. Akhmetshin *et al.* (CMD-2 Collaboration), Phys. Lett. B **759**, 634 (2016).
- [99] M. Ablikim *et al.* (BES Collaboration), Phys. Lett. B **630**, 14 (2005).
- [100] A. Antonelli *et al.* (FENICE Collaboration), Nucl. Phys. B **517**, 3 (1998).
- [101] T. A. Armstrong *et al.* (E760 Collaboration), Phys. Rev. Lett. **70**, 1212 (1993).
- [102] M. Ambrogiani *et al.* (E835 Collaboration), Phys. Rev. D **60**, 032002 (1999); M. Andreotti *et al.* (E835 Collaboration), Phys. Lett. B **559**, 20 (2003).
- [103] D. Bisello *et al.* (DM2 Collaboration), Nucl. Phys. B **224**, 379 (1983); Z. Phys. C **48**, 23 (1990).
- [104] A. Bianconi and E. Tomasi-Gustafsson, Phys. Rev. Lett. **114**, 232301 (2015).
- [105] J. Haidenbauer *et al.*, Nucl. Phys. A **929**, 102 (2014).
- [106] J. R. Green *et al.* Phys. Rev. D **90**, 074507 (2014); B. Jäger *et al.*, PoS LATTICE **2013**, 272 (2014)
- [107] R. Bijker and F. Iachello, Phys. Rev. C **69**, 068201 (2004).
- [108] T. Melde *et al.*, Phys. Rev. D **76**, 074020 (2007).
- [109] S. J. Brodsky and G. R. Farrar, Phys. Rev. D **11**, 1309 (1975).
- [110] M. N. Achasov *et al.*, Phys. Rev. D **90**, 112007 (2014).
- [111] J. R. Ellis and M. Karliner, New J. Phys. **4**, 18 (2002).
- [112] M. Karliner and S. Nussinov, Phys. Lett. B **538**, 321-326 (2002).
- [113] D. Bisello *et al.* (DM2 Collaboration), Z. Phys. C **48**, 23 (1990).
- [114] B. Aubert *et al.* (BaBar Collaboration), Phys. Rev. D **76**, 092006 (2007).

- [115] M. Ablikim *et al.* (BESIII Collaboration), Phys. Rev. D **97**, 032013 (2018).
- [116] S. Dobbs *et al.* Phys. Lett. B **739**, 90 (2014); *ibid.* Phys. Rev. D **96**, 092004 (2017).
- [117] M. Anselmino *et al.*, Rev. Mod. Phys. **65**, 1199 (1993).
- [118] R. Jaffe and F. Wilczek, Phys. Rev. Lett. **91**, 232003 (2003).
- [119] M. Ablikim *et al.* (BESIII Collaboration) Phys. Rev. Lett. **123**, 122003 (2019).
- [120] J. Haidenbauer and U.-G. Meißner, Phys. Lett. B **761**, 456 (2016).
- [121] G. Pakhlova *et al.* (Belle Collaboration), Phys. Rev. Lett. **101** 172001 (2008).
- [122] M. Ablikim *et al.* (BESIII Collaboration), Phys. Rev. Lett. **120**, 132001 (2018).
- [123] R. R. Akhmetshin *et al.* (CMD-3 Collaboration), Phys. Lett. B **794**, 64-68 (2019).
- [124] V. F. Dmitriev, A. I. Milstein and S. G. Salnikov, Phys. Rev. D **93**, 034033 (2016);
A. I. Milstein, S. G. Salnikov, Nucl. Phys. A **966**, 54 (2017); A. I. Milstein and
S. G. Salnikov, Nucl. Phys. A **977**, 60 (2018).
- [125] L.-Y. Dai *et al.*, Phys. Rev. D **96** (2017) 116001.
- [126] O. D. Dalkarov, P. A. Khakhulin, and A. Yu. Voronin, Nucl. Phys. A **833**, 104
(2010).
- [127] B. El-Bennich *et al.*, Phys. Rev. C **79**, 054001 (2009); J. Haidenbauer *et al.*, Phys.
Lett. B **643**, 29 (2006).
- [128] R. Baldini *et al.*, Eur. Phys. J. A **39**, 315 (2009); R. Baldini *et al.*, Eur. Phys. J. A
48, 33 (2012).
- [129] M. Anselmino *et al.*, Rev. Mod. Phys. **65**, 1199 (1993), and references therein.
- [130] S. Pacetti, talk presented at the Int. Workshop on Baryon Production in BESIII,
Hefei, China, 2019.
- [131] M. Ablikim *et al.* (BESIII Collaboration), Phys. Rev. Lett. **124**, 042001 (2020).
- [132] S. Albino, Rev. Mod. Phys. **82**, 2489 (2010), and references therein.
- [133] M. Radici, Nuovo Cim. C **035**, 69 (2012).
- [134] F. Arleo, Eur. Phys. J. C **61**, 603 (2009).
- [135] D. De Florian, R. Sassot and M. Stratmann, Phys. Rev. D **75**, 114010 (2007); D **76**
074033 (2007).
- [136] M. Hirai, S. Kumano, T. H. Nagai and K. Sudoh, Phys. Rev. D **75**, 094009 (2007).
- [137] S. Albino, B. A. Kniehl and G. Kramer, Nucl. Phys. B **803**, 42 (2008).

- [138] E. Leader *et al.*, talk presented at 20th International Symposium on Spin Physics (SPIN2012) JINR, Dubna, Russia, 2012.
- [139] E. Leader *et al.*, Phys. Rev. D **91**, 054017 (2015); Phys. Rev. D **84**, 014002 (2011).
- [140] Jozef Dudek *et al.*, Eur. Phys. J. A **48**, 187 (2012).
- [141] A. Accardi *et al.*, Eur. Phys. J. A **62**, 218 (2016).
- [142] Isabella Garzia and Francesca Giordano, Eur. Phys. J. A **52**, 152 (2016).
- [143] J. C. Collins, Nucl. Phys. B **396**, 161 (1993).
- [144] P. Sun and F. Yuan, Phys. Rev. D **88**, 034016 (2013).
- [145] M. Ablikim *et al.* (BESIII Collaboration), Phys. Rev. Lett. **116**, 042001 (2016).
- [146] M. L. Perl *et al.*, Phys. Rev. Lett. **35**, 1489 (1975).
- [147] J. Beringer *et al.* (Particle Data Group), Phys. Rev. D **86**, 010001 (2012).
- [148] W.J. Marciano and A. Sirlin, Phys. Rev. Lett. **61**, 1815 (1988).
- [149] R. Barate *et al.*, Eur. Phys. J. C **2**, 395 (1998).
- [150] Y. Koide, Phys. Rev. D **28**, 252 (1983); Mod. Phys. Lett. A **5**, 2319 (1990).
- [151] M. L. Perl *et al.*, Phys. Lett. B **70**, 487 (1977).
- [152] R. Brandelik *et al.* (DASP Collaboration), Phys. Lett. B **73**, 109 (1978).
- [153] W. Bartel *et al.*, Phys. Lett. B **77**, 331 (1978).
- [154] W. Bacino *et al.*, Phys. Rev. Lett. **41**, 13 (1978).
- [155] C. A. BLOCKER *et al.*, Phys. Lett. B **109**, 119 (1978).
- [156] H. Albrecht *et al.* (ARGUS Collaboration), Phys. Lett. B **292**, 221 (1992).
- [157] J. Z. Bai *et al.* (BES Collaboration), Phys. Rev. Lett. **69**, 3021 (1992).
- [158] J. Z. Bai *et al.* (BES Collaboration), Phys. Rev. D **53**, 20 (1996).
- [159] J. Z. Bai *et al.* (BES Collaboration), HEP&NP **16**, 343 (1992).
- [160] R. Balest *et al.* (CLEO Collaboration), Phys. Rev. D **47**, 3671 (1993).
- [161] A. Anastassov *et al.* (CLEO Collaboration), Phys. Rev. D **55**, 2559 (1997); Erratum: [Phys. Rev. D **58**, 119904 (1998)].
- [162] G. Abbiendi *et al.* (OPAL Collaboration), Phys. Lett. B **492**, 23 (2000).
- [163] K. Belous *et al.* (Belle Collaboration), Phys. Rev. Lett. **99**, 011801 (2007).

- [164] V. V. Anashin *et al.* (KEDR Collaboration), J. Exp. The. Phys. Lett. **85**, 347 (2007).
- [165] B. Aubert *et al.* (BaBar Collaboration), Phys. Rev. D **80**, 092005 (2009).
- [166] M. Ablikim *et al.* (BESIII Collaboration), Phys. Rev. D **90**, 012001 (2014).
- [167] D. E. Groom *et al.* (Particle Data Group), Eur. Phys. J. C, **15**, 1 (2000).
- [168] K. A. Olive *et al.* (Particle Data Group), Chin. Phys. C, **38**, 090001 (2014).
- [169] R. M. Barnett *et al.* (Particle Data Group), Phys. Rev. D, **54**, 1 (1996).
- [170] L. Montanet *et al.* (Particle Data Group), Phys. Rev. D, **50**, 1173 (1994).
- [171] A. Bogomyagkov *et al.*, the 9th European Particle Accelerator Conference (EPAC 2004), Lucerne, Switzerland, 2004.
- [172] Xiao-Hu Mo *et al.*, Chin. Phys. C **32**, 995 (2008).
- [173] M. N. Achasov *et al.*, Nucl. Phys. B (Proc. Suppl.) **189**, 366 (2009).
- [174] X. H. Mo, E.V. Abakumova, M.N. Achasov *et al.*, Chin. Phys. C **34**, 912 (2010).
- [175] E.V. Abakumova *et al.*, Nucl. Instrum. Methods Phys. Res., Sect. A **659**, 21 (2011).
- [176] J. Y. Zhang *et al.*, Nucl. Phys. B (Proc. Suppl.) **225**, 309 (2012).
- [177] X. H. Mo, Int. J. Mod. Phys. A **30**, 1550149 (2015).
- [178] Y. K. Wang, X.H. Mo, C.Z. Yuan, J.P. Liu, Nucl. Instrum. Methods Phys. Res., Sect. A **583**, 479 (2007).
- [179] Y. K. Wang, J.Y. Zhang, X.H. Mo, C.Z. Yuan, Chin. Phys. C **33**, 501 (2009).
- [180] B. Q. Wang, X.H. Mo, C.Z. Yuan, Int. J. Mod. Phys. A **27**, 1250150 (2012).
- [181] B. Q. Wang, X.H. Mo, Chin. Phys. C **37**, 026202 (2013).
- [182] X. H. Mo, Mod. Phys. Lett. A **31**, 1650196 (2016).
- [183] J. Bartelt *et al.* (CLEO Collaboration), Phys. Rev. Lett. **76**, (1996) 4119.
- [184] P. del Amo Sanchez *et al.* (BaBar Collaboration), Phys. Rev. D **83**, 032002 (2011).
- [185] B. Aubert *et al.* (BaBar Collaboration), Phys. Rev. Lett. **100**, 011801 (2008).
- [186] M. J. Lee *et al.* (Belle Collaboration), Phys. Rev. D **81**, 113007 (2010).
- [187] J. Y. Zhang *et al.*, Chin. Phys. C **40**, 076001 (2016).
- [188] M. Ablikim *et al.* (BESIII Collaboration), Phys. Lett. B **791**, 375 (2019).

- [189] K. K. Seth, S. Dobbs, A. Tomaradze, T. Xiao and G. Bonvicini, *Phys. Lett. B* **730**, 332 (2014).
- [190] K. K. Seth, S. Dobbs, Z. Metreveli, A. Tomaradze, T. Xiao and G. Bonvicini, *Phys. Rev. Lett.* **110**, 022002 (2013).
- [191] R. B. Ferroli, A. Mangoni and S. Pacetti, *Phys. Rev. C* **98**, 045210 (2018).
- [192] K. Zhu, X. H. Mo, C. Z. Yuan, *Int. J. Mod. Phys. A* **30**, 1550148 (2015).
- [193] Shi-Lin Zhu, *Int. J. of Mod. Phys. E* **17**, 283 (2008), and references therein.
- [194] Hua-Xing Chen *et al.*, *Phys. Rept.* **639**, 1 (2016), and references therein.
- [195] Stephen Lars Olsen *et al.*, *Rev. Mod. Phys.* **90**, 015003 (2018), and references therein.
- [196] T. Barnes, *et al.*, *Phys. Rev. D* **68**, 054014 (2003).
- [197] J. P. Lees *et al.* (BaBar Collaboration), *Phys. Rev. D* **86**, 012008 (2012); B. Aubert *et al.* (BaBar Collaboration), *Phys. Rev. D* **76**, 012008 (2007).
- [198] C. P. Shen *et al.* (Belle Collaboration), *Phys. Rev. D* **80**, 031101(R) (2009).
- [199] M. Ablikim *et al.* (BES Collaboration), *Phys. Rev. Lett.* **100**, 012003 (2008); M. Ablikim *et al.* (BESIII Collaboration), *Phys. Rev. D* **95**, 052017 (2015).
- [200] M. Ablikim *et al.* (BESIII Collaboration), *Phys. Rev. D* **99**, 012014 (2019).
- [201] G. J. Ding and M. L. Yan, *Phys. Lett. B* **657**, 49 (2007).
- [202] X. Wang *et al.*, *Phys. Rev. D* **85**, 074024 (2012).
- [203] S. S. Afonin and I. V. Pusenkov, *Phys. Rev. D* **90**, 094020 (2014).
- [204] Cheng-Qun Pang, *Phys. Rev. D* **99**, 074015 (2019).
- [205] G. J. Ding and M. L. Yan, *Phys. Lett. B* **650**, 390 (2007).
- [206] Z. G. Wang, *Nucl. Phys. A* **791**, 106 (2007).
- [207] H. X. Chen *et al.*, *Phys. Rev. D* **78**, 034012 (2008).
- [208] N. V. Drenska, R. Faccini and A. D. Polosa, *Phys. Lett. B* **669**, 160 (2008).
- [209] Hong-Wei Ke and Xue-Qian Li, *Phys. Rev. D* **99**, 036014 (2019).
- [210] L. Zhao *et al.*, *Phys. Rev. D* **87**, 054034 (2013).
- [211] C. Deng *et al.*, *Phys. Rev. D* **88**, 074007 (2013).
- [212] Yubing Dong *et al.*, *Phys. Rev. D* **96**, 074027 (2017).

- [213] A. Martinez Torres *et al.*, Phys. Rev. D **78**, 074031 (2008); S. Gomez-Avila, M. Napsuciale and E. Oset, Phys. Rev. D **79**, 034018 (2009).
- [214] M. Ablikim *et al.* (BES Collaboration), Phys. Lett. B **685**, 27 (2010).
- [215] Philip R. Page *et al.*, Phys. Rev. D **59**, 034016 (1999).
- [216] B. Aubert *et al.* (BaBar Collaboration), Phys. Rev. D **77**, 092002 (2007).
- [217] B. Aubert *et al.* (BaBar Collaboration), Phys. Rev. D **76**, 092005 (2007).
- [218] C. P. Shen and C. Z. Yuan, Chin. Phys. C **34**, 1045 (2010).
- [219] H. X. Chen *et al.*, Phys. Rev. D **98**, 014011 (2018).
- [220] M. Piotrowska *et al.* Phys. Rev. D **96**, 054033 (2017).
- [221] Peter Lichard, Phys. Rev. D **98**, 113011 (2018).

Chapter 5

Charm Physics

5.1 Introduction

The ground states of charmed hadrons, *e.g.*, $D^{0(+)}$, D_s^+ , and Λ_c^+ , can only decay weakly and so precision studies of these charm decays provide important constraints on the weak interaction [1]. Furthermore, as the strong force is always involved in the decays of the charmed hadrons and the formation of the final-state hadrons, precise measurements of the decay properties allow tests of non-perturbative quantum chromodynamics (QCD) calculations. The decay rates of the ground states of charmed hadrons are dominated by the weak decay of the charm quark. For comparison, the lifetimes of the charmed hadrons are shown in Fig. 5.1(a); it is surprising that their individual lifetimes differ by up to a factor of 10. As shown in Fig. 5.1(b), the ratio of $\tau(D^+)/\tau(D^0) = 2.54 \pm 0.01$ is very different from that for the corresponding lifetimes in the beauty sector, $\tau(B^+)/\tau(B^0) = 1.076 \pm 0.004$. From these observations one can infer that deviations of the lifetime ratios from unity decrease with increasing heavy-flavor quark mass m_Q . Heavy flavor decays thus constitute an intriguing lab to study QCD. According to the data, the non-perturbative effects in the decays of the charmed hadrons are much more important than those in the beauty sector. Comprehensive studies of the decays of charmed mesons and baryons will play an essential role in furthering our understanding of strong interactions. In particular, understanding the different decay mechanisms, such as weak-annihilation, W -exchange and final-state scattering, is essential for developing a complete theory of charmed hadron decays. Therefore, the data at the BESIII experiment will have a leading role in understanding non-perturbative QCD.

BEPCII/BESIII produces charmed hadrons near their mass threshold; this allows exclusive reconstruction of their decay products with well-determined kinematics. Up to now, BESIII has collected data corresponding to the integrated luminosities of 2.9 fb^{-1} , 0.5 fb^{-1} , 3.2 fb^{-1} , and 0.6 fb^{-1} at $\sqrt{s} = 3.773, 4.009, 4.178, \text{ and } 4.600 \text{ GeV}$, respectively, as well as data at $\sqrt{s} = 4.23, 4.26, \text{ and } 4.36 \text{ GeV}$. Based on these data sets, many world-leading results have been published. These include the first absolute branching fraction (BF) measurements of the Λ_c^+ baryon to hadronic and semi-leptonic (SL) final states, which are important milestones in the investigation of the charmed baryon sector; the most accurate measurements of the Cabibbo-Kobayashi-Maskawa (CKM) matrix elements $|V_{cs}|$ and $|V_{cd}|$, which are essential inputs in tests of the CKM matrix unitarity; and the

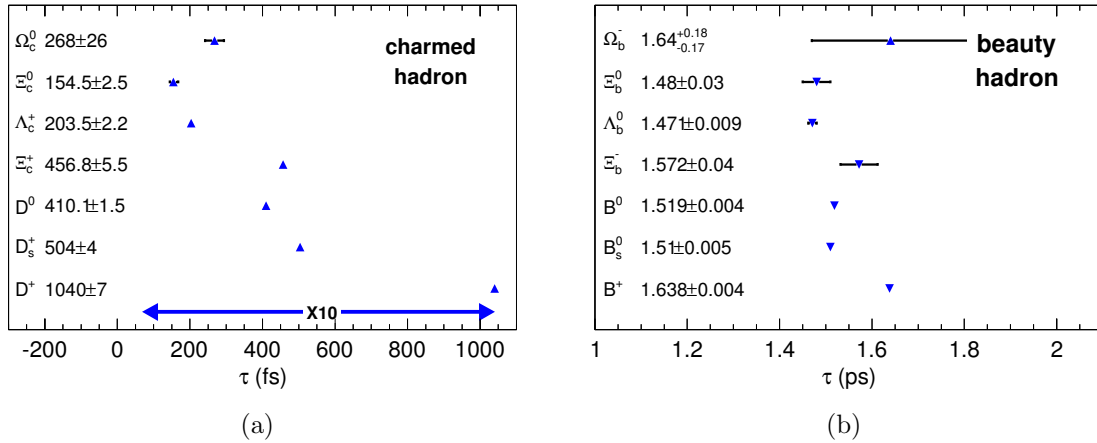


Figure 5.1: (a) Comparison of the lifetimes for the charmed hadrons [2]. For the lifetimes of Ω_c^0 , Ξ_c^0 and Ξ_c^+ , we take the recent measurement from LHCb [3]. (b) Comparison of the lifetimes for the beauty hadrons. In the left figure, “10 \times ” means that lifetimes differ by about one order of magnitude.

most precise measurements of the decay constants in leptonic decays, as well as the form factors in SL decays, which are crucial measurements with which to calibrate LQCD for heavy quark studies. Also, it is important to test lepton-flavor universality (LFU) by using the leptonic and SL charmed hadron decays.

However, improved knowledge of these charmed hadron decays is required to match the significantly improved LQCD calculations and to better understand the strong-force dynamics in the charm region. In addition, more precise measurements of the strong-phase difference between D^0 and \bar{D}^0 decays to final states used to measure the γ angle (also known as ϕ_3) of the CKM unitary triangle in $B^+ \rightarrow DK^+$ decays are necessary (D denotes either D^0 or \bar{D}^0); such improved measurements will prevent the γ measurements at LHCb and Belle II from becoming systematically limited due to neutral D strong-phase uncertainties.

This section describes the future pursuit of this rich charm programme. Specifically, we focus our discussions on the most important measurements that can be made with the proposed future data taking: $D^{0(+)}$, D_s^+ , and Λ_c^+ samples accumulated at $\sqrt{s} = 3.773$, 4.178, and 4.64 GeV corresponding to integrated luminosities of 20 fb $^{-1}$, 6 fb $^{-1}$, and 5 fb $^{-1}$, respectively. Furthermore, it will be interesting to study the baryons Λ_c and Σ_c for the first time at threshold and at higher cms energies, for example, $e^+e^- \rightarrow \Lambda_c^+\bar{\Sigma}_c^-$ and $\Lambda_c^+\bar{\Sigma}_c^-\pi$. We also discuss possible energy upgrade of the BEPCII up to 5 GeV, so that the thresholds will be open for baryon pair productions of $e^+e^- \rightarrow \Sigma_c\bar{\Sigma}_c$ and $\Xi_c\bar{\Xi}_c$.

5.2 $D^{0(+)}$ and D_s^+ physics

5.2.1 Leptonic decays

In the standard model (SM), the partial widths of the leptonic decays $D_{(s)}^+ \rightarrow \ell^+ \nu_\ell$ can be written as

$$\Gamma(D_{(s)}^+ \rightarrow \ell^+ \nu_\ell) = \frac{G_F^2 f_{D_{(s)}^+}^2}{8\pi} |V_{cd(s)}|^2 m_\ell^2 m_{D_{(s)}^+} \left(1 - \frac{m_\ell^2}{m_{D_{(s)}^+}^2}\right)^2, \quad (5.1)$$

where G_F is the Fermi coupling constant, $f_{D_{(s)}^+}$ is the $D_{(s)}^+$ decay constant, $|V_{cd(s)}|$ is the CKM matrix element [2], and m_ℓ [$m_{D_{(s)}^+}$] is the lepton [$D_{(s)}^+$ meson] mass. Using the lifetimes and the measured BFs of these decays, one can determine the product $f_{D_{(s)}^+} |V_{cd(s)}|$. By taking as input $f_{D_{(s)}^+}$ as calculated in LQCD, the value of $|V_{cd(s)}|$ can then be obtained. Alternatively, $|V_{cd(s)}|$ can be taken from global fits to other CKM matrix elements and $f_{D_{(s)}^+}$ instead can be determined.

With the data sets in hand, BESIII has reported the improved measurements of the BFs of $D^+ \rightarrow \mu^+ \nu_\mu$, $D^+ \rightarrow \tau^+ \nu_\tau$, and $D_s^+ \rightarrow \mu^+ \nu_\mu$, as well as $f_{D_{(s)}^+}$ and $|V_{cs(d)}|$ [4–6]. The achieved precision is summarized in Table 5.1. Experimental studies of $D_s^+ \rightarrow \tau^+ \nu_\tau$ with $\tau^+ \rightarrow \pi^+ \nu_\tau$, $\tau^+ \rightarrow e^+ \nu_\tau \nu_e$, $\tau^+ \rightarrow \mu^+ \nu_\tau \nu_\mu$, and $\tau^+ \rightarrow \rho^+ \nu_\tau$ are still ongoing. Based on existing measurements at CLEO-c [7–9], BaBar [10], and Belle [11], the expected signal yield of $D_s^+ \rightarrow \tau^+ \nu_\tau$ will be larger than that of $D_s^+ \rightarrow \mu^+ \nu_\mu$, but will have more background and significant systematic uncertainties. After weighting the measurements performed with different τ^+ decays, the sensitivity of the result for $D_s^+ \rightarrow \tau^+ \nu_\tau$ will be comparable to that made with $D_s^+ \rightarrow \mu^+ \nu_\mu$. Thus, the measurement precision with $D_s^+ \rightarrow \tau^+ \nu_\tau$ can be estimated, as summarized in Table 5.1.

There are four reasons why the improved measurements of $D_{(s)}^+ \rightarrow \ell^+ \nu_\ell$ with 20 fb⁻¹ of data at 3.773 GeV and 6 fb⁻¹ of data at 4.178 GeV are desirable.

1. *Constraints on LQCD calculations:*

Figure 5.2 shows a comparison of $f_{D_{(s)}^+}$ measurements by various experiments and the values evaluated in LQCD. Focusing initially on f_{D^+} , it may be seen that BESIII currently supplies the most precise individual measurement, which itself has a statistical uncertainty of around 2.5%. In contrast to the LQCD uncertainty of 0.2%, there is much room to be improved in experiment. With 20 fb⁻¹ of data at 3.773 GeV, the relative statistical uncertainty on f_{D^+} can be reduced to approximately 1%, which is still larger than the current systematic uncertainty.

2. *Determinations of $|V_{cs(d)}|$:*

Alternatively, the LQCD calculations for $f_{D_{(s)}^+}$ may be taken as input, and the leptonic BF measurements used to confront weak physics. In the SM, quark-flavor

Table 5.1: Expected precision of measurements of $D_{(s)}^+ \rightarrow \ell^+ \nu_\ell$ and those at Belle II. For BESIII, some systematic uncertainties, which are statistically limited by control samples, are expected to be improved. The total systematic uncertainty is assumed to be comparable to the corresponding statistical uncertainty. For $D^+ \rightarrow \tau^+ \nu_\tau$, only $\tau^+ \rightarrow \pi \nu$, $e \nu \nu$, $\mu \nu \nu$, and $\rho \nu$. Considering that the LQCD uncertainty of f_{D^+} has been reduced from 1.9% to 0.2%, the $|V_{cd}|$ measured at BESIII has been re-calculated, and is marked with *. Preliminary results are marked with †. For Belle II, we assume that the systematic uncertainties can be reduced by a factor of 2 compared to Belle's results, and the systematic uncertainty for $D^+ \rightarrow \mu^+ \nu_\mu$ is the same as that of $D_s^+ \rightarrow \mu^+ \nu_\mu$.

	BESIII	BESIII	Belle	Belle II
Luminosity	2.9 fb ⁻¹ at 3.773 GeV	20 fb ⁻¹ at 3.773 GeV	1 ab ⁻¹ at $\mathcal{I}(nS)$	50 ab ⁻¹ at $\mathcal{I}(nS)$
$\mathcal{B}(D^+ \rightarrow \mu^+ \nu_\mu)$	5.1% _{stat.} 1.6% _{sys.} [4]	1.9% _{stat.} 1.3% _{sys.}	–	3.0% _{stat.} 1.8% _{sys.} [54]
f_{D^+} (MeV)	2.6% _{stat.} 0.9% _{sys.} [4]	1.0% _{stat.} 0.8% _{sys.}	–	–
$ V_{cd} $	2.6% _{stat.} 1.0% _{sys.} * [4]	1.0% _{stat.} 0.8% _{sys.} *	–	–
$\mathcal{B}(D^+ \rightarrow \tau^+ \nu_\tau)$	20% _{stat.} 10% _{sys.} [5]	8% _{stat.} 5% _{sys.}	–	–
$\mathcal{B}(D^+ \rightarrow \mu^+ \nu_\mu)$	20% _{stat.} 13% _{sys.} [5]	8% _{stat.} 5% _{sys.}	–	–
Luminosity	3.2 fb ⁻¹ at 4.178 GeV	6 fb ⁻¹ at 4.178 GeV	1 ab ⁻¹ at $\mathcal{I}(nS)$	50 ab ⁻¹ at $\mathcal{I}(nS)$
$\mathcal{B}(D_s^+ \rightarrow \mu^+ \nu_\mu)$	2.8% _{stat.} 2.7% _{sys.} [6]	2.1% _{stat.} 2.2% _{sys.}	5.3% _{stat.} 3.8% _{sys.}	0.8% _{stat.} 1.8% _{sys.}
$f_{D_s^+}$ (MeV)	1.5% _{stat.} 1.6% _{sys.} [6]	1.0% _{stat.} 1.2% _{sys.}	–	–
$ V_{cs} $	1.5% _{stat.} 1.6% _{sys.} [6]	1.0% _{stat.} 1.2% _{sys.}	–	–
$f_{D_s^+}/f_{D^+}$	3.0% _{stat.} 1.5% _{sys.} [6]	1.4% _{stat.} 1.4% _{sys.}	–	–
$\mathcal{B}(D_s^+ \rightarrow \tau^+ \nu_\tau)$	2.2% _{stat.} 2.6% _{sys.} †	1.6% _{stat.} 2.4% _{sys.}	3.7% _{stat.} 5.4% _{sys.}	0.6% _{stat.} 2.7% _{sys.}
$f_{D_s^+}$ (MeV)	1.1% _{stat.} 1.5% _{sys.} †	0.9% _{stat.} 1.4% _{sys.}	–	–
$ V_{cs} $	1.1% _{stat.} 1.5% _{sys.} †	0.9% _{stat.} 1.4% _{sys.}	–	–
$\overline{V}_{cs}^{\mu\kappa\tau}$ (MeV)	0.9% _{stat.} 1.0% _{sys.} †	0.6% _{stat.} 0.9% _{sys.}	1.6% _{stat.} 2.0% _{sys.}	0.3% _{stat.} 1.0% _{sys.}
$ V_{cs}^{\mu\kappa\tau} $	0.9% _{stat.} 1.0% _{sys.} †	0.6% _{stat.} 0.9% _{sys.}	–	–
$\mathcal{B}(D_s^+ \rightarrow \tau^+ \nu_\tau)$	3.6% _{stat.} 3.0% _{sys.} †	2.6% _{stat.} 2.8% _{sys.}	6.4% _{stat.} 5.2% _{sys.}	0.9% _{stat.} 3.2% _{sys.}

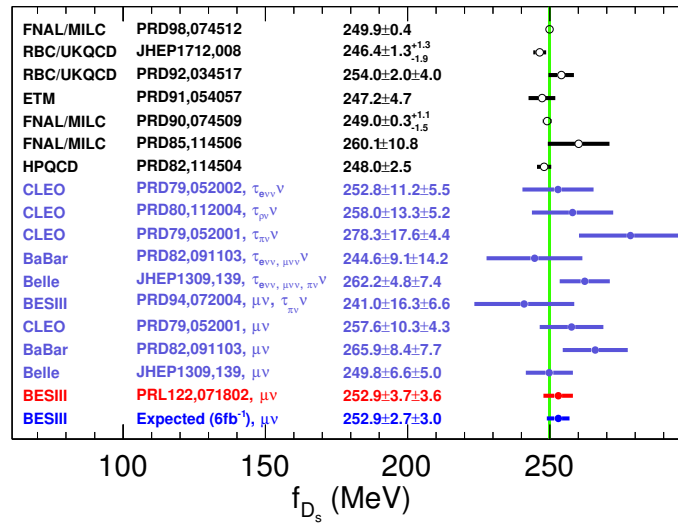
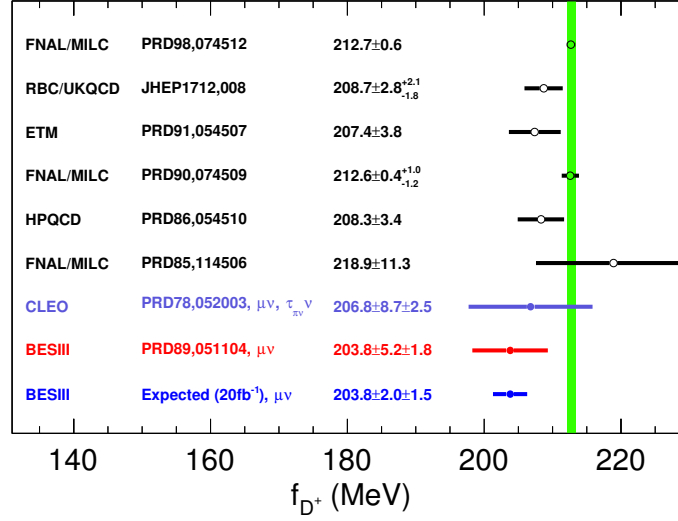


Figure 5.2: Expected precision of the measurements of (a) f_{D^+} using $D^+ \rightarrow \mu^+ \nu_\mu$ with 20 fb⁻¹ of data at 3.773 GeV and (b) $f_{D_s^+}$ using $D_s^+ \rightarrow \mu^+ \nu_\mu$ with 6 fb⁻¹ of data at 4.178 GeV. The green bands present the LQCD uncertainties [12]. The circles and dots with error bars are the LQCD calculations and experimental measurements, respectively. The value marked in red denotes the best measurement, and the value marked in light blue denotes the expected precision.

mixing is described by the unitary 3×3 CKM matrix

$$V_{\text{CKM}} = \begin{pmatrix} V_{ud} & V_{us} & V_{ub} \\ V_{cd} & V_{cs} & V_{cb} \\ V_{td} & V_{ts} & V_{tb} \end{pmatrix}. \quad (5.2)$$

Any deviation from unitarity would indicate new physics beyond the SM. Improving the accuracy with which CKM matrix elements are determined is one of the principal goals in flavor physics, as it will test the unitarity of the CKM matrix with higher accuracy.

In the past decade, much progress has been achieved in LQCD calculations of $f_{D_{(s)}^+}$. The uncertainties of $f_{D_{(s)}^+}$ calculated in LQCD have been reduced from (1-2)% to the 0.2% level [12, 13], thus providing precise information to measure $|V_{cs}|$ and $|V_{cd}|$. Comparison of the measured $|V_{cs(d)}|$ with different methods and experiments are shown in Fig. 5.3. In the figure, the BESIII result of $|V_{cd}|$ has been recalculated with the latest LQCD calculation of $f_{D^+} = 212.7 \pm 0.6$ MeV [12]. Currently, the average is dominated by the BESIII measurements of $D_{(s)}^+ \rightarrow \ell^+ \nu_\ell$ decays, which have an uncertainty of 2.5% (1.5%) for $|V_{cd(s)}|$. The statistical uncertainty of $|V_{cd}|$ is dominant, whereas the statistical and systematic uncertainties of $|V_{cs}|$ are comparable.

The recalculated value of $|V_{cd}|$ is consistent with the value of $|V_{cd}| = 0.22522 \pm 0.00061$, obtained from a global fit to other CKM matrix element measurements that assumes unitarity in the SM, within 1.7σ . With 20 fb^{-1} of data at 3.773 GeV and 6 fb^{-1} of data at 4.178 GeV, the relative precision of the measurements of $|V_{cs}|$ and $|V_{cd}|$ with leptonic decays will both reach 1.0%.

3. Tests on lepton flavor universality:

In recent years, some hints of LFU violation have emerged in some SL B -meson decays [14–23]. Ref. [24] argues that LFU violation may happen in $c \rightarrow s$ transitions due to an amplitude that includes a charged Higgs boson, that arises in a two-Higgs-doublet model, interfering with the SM amplitude involving a W^\pm boson. Therefore, it is important to test LFU with $D_{(s)}^+ \rightarrow \ell^+ \nu_\ell$ decays.

In the SM, the ratio of the partial widths of $D_{(s)}^+ \rightarrow \tau^+ \nu_\tau$ and $D_{(s)}^+ \rightarrow \mu^+ \nu_\mu$ is predicted to be

$$R_{D_{(s)}^+} = \frac{\Gamma(D_{(s)}^+ \rightarrow \tau^+ \nu_\tau)}{\Gamma(D_{(s)}^+ \rightarrow \mu^+ \nu_\mu)} = \frac{m_{\tau^+}^2 \left(1 - \frac{m_{\tau^+}^2}{m_{D_{(s)}^+}^2}\right)^2}{m_{\mu^+}^2 \left(1 - \frac{m_{\mu^+}^2}{m_{D_{(s)}^+}^2}\right)^2}.$$

With the world average values of the masses of lepton and $D_{(s)}^+$ [2], one obtains $R_{D^+} = 2.67$ and $R_{D_s^+} = 9.74$ with negligible uncertainties. The measured values of $R_{D_{(s)}^+}$ reported by BESIII are $3.21 \pm 0.64 \pm 0.43$ (9.98 ± 0.52), which agree with

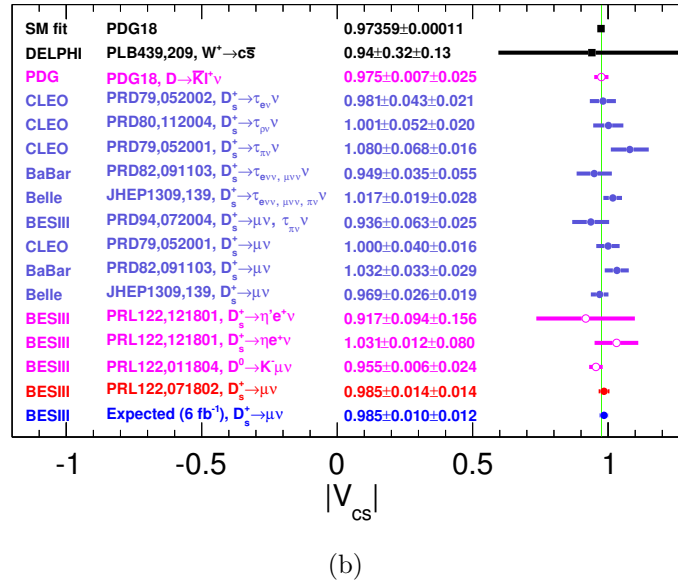
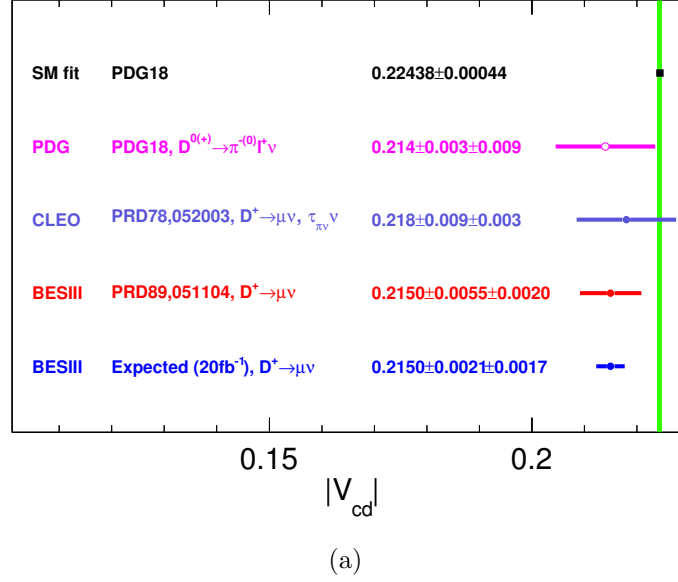


Figure 5.3: Expected precision of the measurements of (a) $|V_{cd}|$ using $D^+ \rightarrow \mu^+ \nu_\mu$ with 20 fb⁻¹ of data at 3.773 GeV and (b) $|V_{cs}|$ using $D_s^+ \rightarrow \mu^+ \nu_\mu$ with 6 fb⁻¹ of data at 4.178 GeV. The green bands present the uncertainties of the average values from the global fit in the SM [2]. The circles, dots and rectangles with error bars are the values based on SL D decays, leptonic D decays and other methods, respectively. The value marked in red denotes the best measurement, and the value marked in light blue denotes the expected precision.

the SM predicted values. However, as previously noted, these measurements are statistically limited. With 20 fb^{-1} of data at 3.773 GeV the precision on R_{D^+} will be statistically limited to about 8%. With 6 fb^{-1} of data at 4.178 GeV the precision on $R_{D_s^+}$ will be systematically limited to about 3%.

4. Comparison with other experiments:

The leptonic decays reconstructed at BESIII and CLEO-c come from data sets accumulated just above the open-charm threshold, where the $D^0\bar{D}^0$ or D^+D^- mesons are produced as a pair. The BF's can be determined by considering the yields for both the single-tagged and double-tagged events. With this method, the background level and systematic uncertainties are lower than for the measurements at B factories.

Currently, the best measurements of $D^+ \rightarrow \ell^+\nu_\ell$ are from BESIII. So far, no studies of $D^+ \rightarrow \ell^+\nu_\ell$ have been reported by BaBar, Belle, and LHCb, which may be due to the higher level of background any measurement at these experiments would encounter. BESIII is expected to provide unique data to improve the knowledge of f_{D^+} , $|V_{cd}|$, and tests of LFU in $D^+ \rightarrow \ell^+\nu_\ell$ decays in the next decade.

BaBar [10] and Belle [11] have reported the measurement of $D_s^+ \rightarrow \ell^+\nu_\ell$ using $e^+e^- \rightarrow c\bar{c} \rightarrow DKXD_s^{*-}$ with $D_s^{*-} \rightarrow D_s^-\gamma$, performed with about 0.5 and 1.0 ab^{-1} of data taken around the $\Upsilon(4S)$, respectively. The statistical and systematic uncertainties of these measurements of $f_{D_s^+}$ and $|V_{cs}|$ at Belle are 1.6% and 2.5%, respectively. The dominant systematic uncertainties are from normalization, tag bias, particle identification, fit model and D_s^+ background. With 50 ab^{-1} of data at Belle II, the statistical uncertainties of these measurements are expected to be reduced to 0.25%, however it will be extremely challenging to reduce the systematics uncertainties to match this level. Hence it is expected that a measurement of $D_s^+ \rightarrow \ell^+\nu_\ell$ performed at BESIII with 6 fb^{-1} of data at 4.178 GeV will have very significant weight in a future world average.

BESIII measurements of purely leptonic D_s^+ decays will be limited by systematic uncertainties to a large degree. This motivates the exploration of taking data at $\sqrt{s} = 4.009 \text{ GeV}$ where only $D_s^+D_s^-$ production is possible; such a data set will have much reduced backgrounds in the double-tag method, thus improving the systematic uncertainties on the measurements. The drawback is the reduction in cross section by a factor of three with respect to operation at 4.178 GeV. Therefore, a data set of 20 fb^{-1} would be required to match the statistical precision of 6 fb^{-1} of data at 4.178 GeV across all measurements of D_s^+ decay. Such a large set corresponds to many years of data taking and as such cannot be considered as the highest priority among the various charm-physics data sets requested.

5.2.2 Semileptonic decays

In the SM, the weak and strong effects in SL $D^{0(+)}$ decays can be well separated [25]. Among them, the simplest case is $D^{0(+)} \rightarrow \bar{K}(\pi)\ell^+\nu_\ell$, for which the differential decay rate

can be simply written as

$$\frac{d\Gamma}{dq^2} = \frac{G_F^2}{24\pi^3} |V_{cs(d)}|^2 p_{K(\pi)}^3 |f_+^{K(\pi)}(q^2)|^2, \quad (5.3)$$

where G_F is the Fermi coupling constant, and $p_{K(\pi)}$ is the kaon (pion) momentum in the D rest frame, $f_+^{K(\pi)}(q^2)$ is the form factor of the hadronic weak current depending on the square of the transferred four-momentum $q = p_D - p_{K(\pi)}$. From analyses of the dynamics in these decays, one can obtain the product $f_+^{K(\pi)}(0)|V_{cs(d)}|$. By taking the $f_+^{K(\pi)}(0)$ calculated in LQCD or $|V_{cd(s)}|$ from a global fit assuming unitarity in the SM, the value of either $|V_{cd(s)}|$ or $f_+^{K(\pi)}(0)$ can be obtained.

- *Form factors of SL decays:*

With the data sets in hand, BESIII has reported improved measurements of the absolute BFs and the form factors of the SL decays $D^{0(+)} \rightarrow \bar{K}e^+\nu_e$, $D^{0(+)} \rightarrow \pi e^+\nu_e$ [26, 27], $D^0 \rightarrow K^-\mu^+\nu_\mu$ [28], $D^+ \rightarrow \eta e^+\nu_e$ [29], $D^+ \rightarrow \bar{K}^{*0}e^+\nu_e$ [30], $D^{0(+)} \rightarrow \rho^{-(0)}e^+\nu_e$ [31], $D^+ \rightarrow \omega e^+\nu_e$ [32], $D_s^+ \rightarrow K^{(*)0}e^+\nu_e$ [33] and $D_s^+ \rightarrow \eta^{(\prime)}e^+\nu_e$ [34]. Figure 5.4 shows comparison of the form factors $f_+^K(0)$, and $f_+^\pi(0)$ measured by various experiments and those calculated in LQCD. The BESIII measurement of $f_+^K(0)$ is dominated by systematic uncertainties, whereas other measurements are dominated by statistical uncertainties. The measurements of the form factors of $D^0 \rightarrow K^{*-}e^+\nu_e$, $D^+ \rightarrow \eta\mu^+\nu_\mu$, $D_s^+ \rightarrow \phi e^+\nu_e$, $D_s^+ \rightarrow f_0(980)e^+\nu_e$ and $D_s^+ \rightarrow \eta\mu^+\nu_\mu$ are still ongoing, but all will be statistically limited with the current data sets.

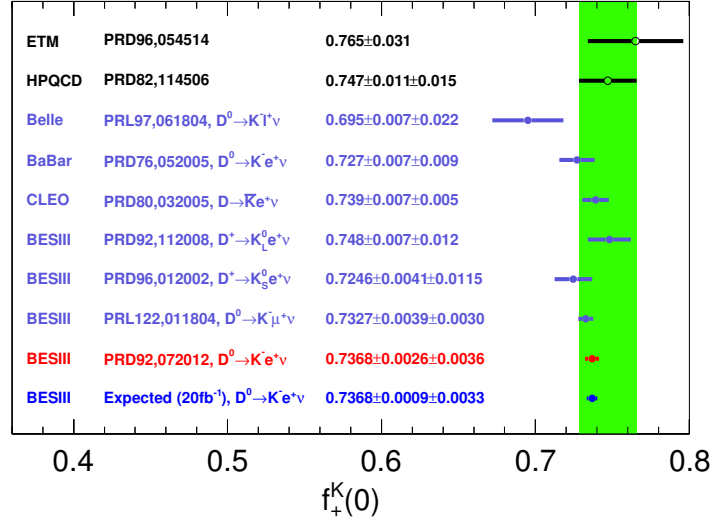
Measurements of SL $D^{0(+)}$ decays that contain a scalar or axial-vector meson in the final state, *e.g.*, $D^{0(+)} \rightarrow \bar{K}_1(1270)e^+\nu_e$ [35] and $D^{0(+)} \rightarrow a_0(980)e^+\nu_e$ [36], have been reported by CLEO-c and BESIII. However, these decay samples are up to about 100 events, which are insufficient to perform form-factor measurements.

With 20 fb^{-1} of data at 3.773 GeV, all the form-factor measurements which are currently statistically limited will be statistically improved by a factor of up to 2.6. We also have opportunities to determine the form factors of $D^0 \rightarrow K_1^-(1270)e^+\nu_e$, $D^+ \rightarrow \bar{K}_1^0(1270)e^+\nu_e$, $D^+ \rightarrow \eta'e^+\nu_e$, $D^0 \rightarrow a_0^-(980)e^+\nu_e$, and $D^+ \rightarrow a_0^0(980)e^+\nu_e$ for the first time. In addition, studies of the semi-muonic decays of $D^{0(+)} \rightarrow \bar{K}\mu^+\nu_\mu$ and $D^{0(+)} \rightarrow \pi\mu^+\nu_\mu$ will further improve the knowledge of $f_+^K(0)$ and $f_+^\pi(0)$.

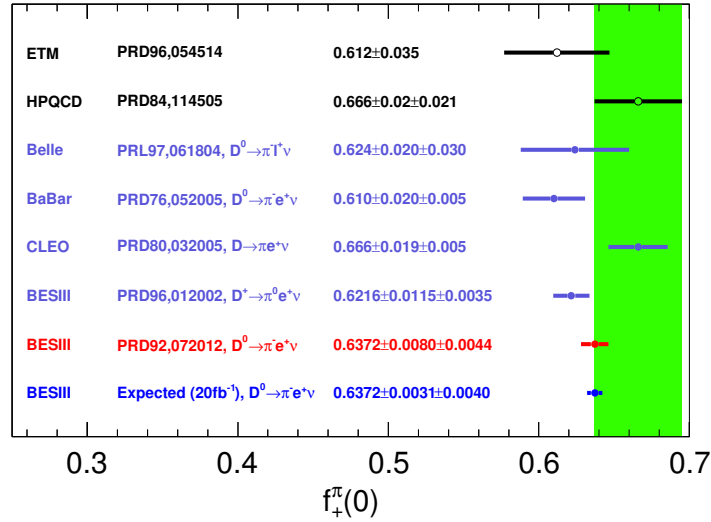
With 3.2 fb^{-1} of data at 4.178 GeV, the expected yield for each of the Cabibbo-favored (CF) SL D_s^+ decays is about 1000, while that for each of the singly Cabibbo-suppressed (SCS) SL D_s^+ decays is not more than 200. In this case, all studies of the dynamics of SL D_s^+ decays are restricted due to the limited data sets. The measurements of the form factors in these decays will be improved by a factor of up to 1.4 with 6 fb^{-1} of data at 4.178 GeV.

- *Determinations of $|V_{cs(d)}|$:*

The CKM elements $|V_{cs}|$ and $|V_{cd}|$ can also be determined from analyses of the SL decays of $D^{0(+)} \rightarrow \bar{K}\ell^+\nu_\ell$ and $D^{0(+)} \rightarrow \pi\ell^+\nu_\ell$, when the values of the form factors are taken from LQCD. Results using this approach are included in Fig. 5.3. At



(a)



(b)

Figure 5.4: Expected precision of the measurements of (a) $f_+^K(0)$ and (b) $f_+^\pi(0)$ with 20 fb^{-1} of data at 3.773 GeV . The green bands present the LQCD uncertainties [37, 38]. The PDG value is combined from the results of from Belle, CLEO, BaBar and BESIII. The circles and dots with error bars are the LQCD calculations and experimental measurements, respectively. The value marked in red denotes the best measurement, and the value marked in light blue denotes the expected precision.

present, the LQCD uncertainties are 2.4% for $f_+^K(0)$ [37] and 4.4% for $f_+^\pi(0)$ [38], which are significantly larger than the associated experimental uncertainties, and therefore limit the determinations of $|V_{cs}|$ and $|V_{cd}|$ from this method.

In the coming decade, however, the uncertainties of $f_+^K(0)$ and $f_+^\pi(0)$ calculated in LQCD are expected to be reduced to the level of 1.0% and 0.5% [39], respectively. Therefore, further improved measurements of $f_+^K(0)$ and $f_+^\pi(0)$ will play key roles in the determinations of $|V_{cs}|$ and $|V_{cd}|$. With 20 fb^{-1} of $\psi(3770)$ data, the experimental uncertainties of the measurements of $|V_{cs}|$ and $|V_{cd}|$ with SL $D^{0(+)}$ decays in electron channels are expected to reach the 0.5% level. Studies of $D^{0(+)} \rightarrow \bar{K}\mu^+\nu_\mu$ and $D^{0(+)} \rightarrow \pi\mu^+\nu_\mu$ will provide additional sensitivity.

In SL D_s^+ decays, analyses of the dynamics of $D_s^+ \rightarrow \eta^{(\prime)}e^+\nu_e$ decays with 6 fb^{-1} of data at 4.178 GeV, where the $\eta - \eta'$ mixing is involved, will provide complementary measurements of $|V_{cs}|$. The statistical uncertainty is expected to reach the 2.0% level; this will further improve the measurement precision of $|V_{cs}|$ at BESIII.

- *Tests of lepton flavor universality:* Previous measurements of the BFs of $D^0 \rightarrow \pi^-\mu^+\nu_\mu$ and $D^0 \rightarrow \pi^-e^+\nu_e$ [2], resulted in the ratio of BFs $\mathcal{B}(D^0 \rightarrow \pi^-\mu^+\nu_\mu)/\mathcal{B}(D^0 \rightarrow \pi^-e^+\nu_e) = 0.82 \pm 0.08$, which deviates from the SM prediction of 0.985 ± 0.002 [40] by 2.1σ . This possible hint of LFU violation has motivated BESIII to report more precise BF measurements to obtain the ratios $\mathcal{B}(D^0 \rightarrow \pi^-\mu^+\nu_\mu)/\mathcal{B}(D^0 \rightarrow \pi^-e^+\nu_e) = 0.922 \pm 0.030 \pm 0.022$ and $\mathcal{B}(D^+ \rightarrow \pi^0\mu^+\nu_\mu)/\mathcal{B}(D^+ \rightarrow \pi^0e^+\nu_e) = 0.964 \pm 0.037 \pm 0.026$ [41]. These results are consistent with the SM predictions, within 1.7σ and 0.5σ , respectively. Much more accurate studies will be possible with 20 fb^{-1} of data at 3.773 GeV, besides optimizations on the systematic uncertainties.

As Ref. [24] pointed out, due to the mediation of charged Higgs bosons in the two-Higgs-doublet model, LFU in $c \rightarrow s$ transitions may be violated. In charm decays, the semi-tauonic decays involving a kaon in the final states are kinematically forbidden. Measurements of the ratios of the partial widths of $D^{0(+)} \rightarrow \bar{K}\mu^+\nu_\mu$ over those of $D^{0(+)} \rightarrow \bar{K}e^+\nu_e$ in different q^2 intervals constitute a complementary test of LFU to those using semi-tauonic decays. These measurements are currently statistically limited [28, 41], and will be significantly improved with 20 fb^{-1} of data at 3.773 GeV.

- *Studies on meson spectroscopy:* Studies on intermediate resonances in hadronic final states in SL decays provide a clean environment to explore meson spectroscopy, as no other particles interfere. This corresponds to a much simpler treatment than those studies in $D_{(s)}^{0(+)}$ hadronic decays or charmonium decays. For instance, in $D^0 \rightarrow K_1^-(1270)e^+\nu_e$ and $D^+ \rightarrow \bar{K}_1^0(1270)e^+\nu_e$, the single hadronic current allows the production of the axial-meson to be factorized, which provides unique information on the structure of this lightest strange axial-vector mesons. At present, the world average values of the mass, $1272 \pm 7 \text{ MeV}$, and width, $90 \pm 20 \text{ MeV}$, of the $\bar{K}_1(1270)$ have large uncertainties [2]. Furthermore, different analysis channels produce conflicting resonance parameters. Based on the future BESIII data set, the precision of these parameters is expected to be improved by a factor of two to

three. Also, we have the opportunity to study the properties of other particles, *e.g.*, $a_0^-(980)$ and $a_0^0(980)$ in SL decays. In addition, it is possible to search for various SL $D_{(s)}^{0(+)}$ transitions into other scalar or axial-vector mesons, as listed in Ref. [42].

- *Comparison with other experiments:* BaBar studied the SL decays $D^0 \rightarrow K^- e^+ \nu_e$ [43] and $D^0 \rightarrow \pi^- e^+ \nu_e$ [44] using the decay $D^0 \rightarrow K^- \pi^+$ to normalize the measurements. However, the BF of $D^0 \rightarrow K^- \pi^+$ has an uncertainty of 1% that is larger than the systematic uncertainties in the measurements of $D^0 \rightarrow K^- e^+ \nu_e$ and $D^0 \rightarrow \pi^- e^+ \nu_e$ at BESIII. Belle made absolute measurements of $D^0 \rightarrow K^- \ell^+ \nu_\ell$ and $D^0 \rightarrow \pi^- \ell^+ \nu_\ell$ by using the decay chain of $D_{\text{tag}}^{(*)} D_{\text{sig}}^{*-} X$ with 282 fb^{-1} of data taken around $\Upsilon(4S)$ [45], with precision summarized in Table 5.2. So far, no other SL measurements have been reported by Belle.

BESIII has the advantage of low background and small systematic uncertainty ($< 1\%$) for measurements of semi-electronic $D^{0(+)}$ decays, and with 20 fb^{-1} of data at 3.773 GeV , will be competitive with Belle II. On the other hand, the momenta of most muons in semi-muonic $D^{0(+)}$ decays produced at threshold are lower than $0.5 \text{ GeV}/c$, which lies outside the detection ability of the muon counter, and hence makes the study of semi-muonic $D^{0(+)}$ decays challenging at BESIII. However, improved and comprehensive measurements of dynamics of as many as semi-muonic $D^{0(+)}$ decays into a pseudoscalar meson are workable, as done in Refs. [28, 41], but will be challenging for those semi-muonic $D^{0(+)}$ transitions into a vector, scalar or axial-vector meson.

The SL decays can also be studied at LHCb and its upgrades, particularly in the muon channels. However, the studies of the SL $D_{(s)}^{0(+)}$ decays involving electron and photon(s) in the final states are more difficult in the environment of a hadron collider due to larger backgrounds.

5.2.3 Quantum-correlated measurements of D^0 hadronic decays

The quantum correlation of the $D^0 \bar{D}^0$ meson pair produced at $\psi(3770)$ provides a unique way to probe the amplitudes of the D decays, the $D^0 \bar{D}^0$ mixing parameters and potential CP violation in D^0 decays [46]. Furthermore, the determination of the strong-phase difference between the CF and doubly Cabibbo-suppressed (DCS) amplitudes in the decay of quantum-correlated $D^0 \bar{D}^0$ meson pairs has several motivations: understanding the non-perturbative QCD effects in the charm sector; serving as essential inputs to extract the angle γ of the CKM unitarity triangle (UT); and relating the measured mixing parameters in hadronic decay (x', y') to the mass and width difference parameters (x, y) [29].

The measurements of the CKM UT angles α , β , and γ in B decays are important to test CKM unitarity and search for CP violation beyond the SM. Any discrepancy in the measurements of the unitarity triangle involving tree and loop dominated processes would indicate high-mass new physics within the loops. Among the three CKM angles, γ , where the current world-best measurement from LHCb is $(74.0_{-5.8}^{+5.0})^\circ$ [48], has particular

Table 5.2: Form-factor measurements of SL $D^{0(+)}$ decays. For the decays involving a pseudoscalar or scalar meson, the decay rate is parameterized by one form factor $f_+(0)$. For the decays involving a vector or axial-vector meson, the decay rate is parameterized by three form factors, $V(0)$, $A_1(0)$, and $A_2(0)$, which has relations $r_V = V(0)/A_1(0)$ and $r_A = A_2(0)/A_1(0)$. The $A_1(0)$ for $D^+ \rightarrow \bar{K}^{*0} e^+ \nu_e$ decay is reported due to low background and enough signals at BESIII. For Belle II, we assume that the systematic uncertainties can be reduced by a factor of 2 compare to Belle's results. The results marked in * for Belle (II) are based on both semi-electronic and semi-muonic decays.

	BESIII		Belle		Belle II	
	2.9 fb ⁻¹ @3.773 GeV	20 fb ⁻¹ @3.773 GeV	0.28 ab ⁻¹	50 ab ⁻¹		
Luminosity						
$D^0 \rightarrow K^- e^+ \nu_e$	0.4% _{stat.} 0.5% _{sys.}	0.2% _{stat.} 0.4% _{sys.}	1.0% _{stat.} 3.2% _{stat.} * 0.1% _{stat.} 1.6% _{stat.} *			
$D^0 \rightarrow K^- \mu^+ \nu_\mu$	0.5% _{stat.} 0.4% _{sys.}	0.2% _{stat.} 0.4% _{sys.}				
$D^0 \rightarrow \pi^- e^+ \nu_e$	1.3% _{stat.} 0.7% _{sys.}	0.5% _{stat.} 0.4% _{sys.}	3.2% _{stat.} 4.8% _{stat.} * 0.2% _{stat.} 2.4% _{stat.} *			
$D^0 \rightarrow \pi^- \mu^+ \nu_\mu$	NA	0.8% _{stat.} 0.8% _{sys.}				
$D^0 \rightarrow K^{*-} e^+ \nu_e$						
r_V	5.0% _{stat.} 2.0% _{sys.}	2.0% _{stat.} 2.0% _{sys.}				
r_A	10.% _{stat.} 2.0% _{sys.}	4.0% _{stat.} 2.0% _{sys.}				
$D^0 \rightarrow a_0^- (980) e^+ \nu_e$	NA	10.% _{stat.} 5.0% _{sys.}				
$D^0 \rightarrow K_1^- (1270) e^+ \nu_e$	NA	10.% _{stat.} 5.0% _{sys.}				
$D^+ \rightarrow \bar{K}^0 e^+ \nu_e$	0.6% _{stat.} 1.7% _{sys.}	0.2% _{stat.} 1.0% _{sys.}				
$D^+ \rightarrow \bar{K}_1^0 e^+ \nu_e$	0.9% _{stat.} 1.6% _{sys.}	0.4% _{stat.} 1.0% _{sys.}				
$D^+ \rightarrow \bar{K}^0 \mu^+ \nu_\mu$	NA	0.3% _{stat.} 1.0% _{sys.}				
$D^+ \rightarrow \bar{K}^{*0} e^+ \nu_e$						
$A_1(0)$	1.7% _{stat.} 2.0% _{sys.}	0.7% _{stat.} 1.0% _{sys.}				
r_V	4.0% _{stat.} 0.5% _{sys.}	1.6% _{stat.} 0.5% _{sys.}				
r_A	5.0% _{stat.} 1.0% _{sys.}	2.0% _{stat.} 1.0% _{sys.}				
$D^+ \rightarrow \pi^0 e^+ \nu_e$	1.9% _{stat.} 0.5% _{sys.}	0.7% _{stat.} 0.5% _{sys.}				
$D^+ \rightarrow \pi^0 \mu^+ \nu_\mu$	NA	1.0% _{stat.} 1.0% _{sys.}				
$D^+ \rightarrow \eta e^+ \nu_e$	4.5% _{stat.} 2.0% _{sys.}	2.0% _{stat.} 2.0% _{sys.}				
$D^+ \rightarrow \eta' e^+ \nu_e$	NA	10.% _{stat.} 5.0% _{sys.}				
$D^+ \rightarrow \omega e^+ \nu_e$						
r_V	7.2% _{stat.} 4.8% _{sys.}	3.0% _{stat.} 2.0% _{sys.}				
r_A	14% _{stat.} 5.0% _{sys.}	3.0% _{stat.} 2.0% _{sys.}				
$D^+ \rightarrow a_0^0 (980) e^+ \nu_e$	NA	10.% _{stat.} 5.0% _{sys.}				
$D^+ \rightarrow K_1^0 (1270) e^+ \nu_e$	NA	10.% _{stat.} 5.0% _{sys.}				
$D^{0(+)} \rightarrow \rho^{-(0)} e^+ \nu_e$						
r_V	5.0% _{stat.} 4.0% _{sys.}	2.0% _{stat.} 2.0% _{sys.}				
r_A	8.0% _{stat.} 4.0% _{sys.}	3.0% _{stat.} 2.0% _{sys.}				

importance, being the only CP-violating observable that can be determined using tree-level decays. Degree-level precision on γ will allow a rigorous comparison of the loop and tree-level determinations of the UT. The independence from loop diagrams means that the measurement of γ has negligible theoretical uncertainty [49]. The precision measurement of γ is one of the top priorities for the LHCb upgrade(s) and Belle II experiments.

The most precise method to measure γ is based upon the interference between $B^+ \rightarrow \bar{D}^0 K^+$ and $B^+ \rightarrow D^0 K^+$ decays [50–52]. In the future, the statistical uncertainties of these measurements will be greatly reduced by using the large B meson samples recorded by LHCb and Belle II, and by extending these measurements to other similar B modes such as $B^0 \rightarrow DK^{*0}$, where D implies either D^0 or \bar{D}^0 , $B^+ \rightarrow D^* K^+$, $B^+ \rightarrow DK\pi\pi$, and $B^+ \rightarrow DK^{*+}$ [53, 54]. However, with increased statistical precision, limited knowledge of the strong phases of the D decays will systematically restrict the overall sensitivity. Consequently, improved knowledge of the strong-phase related parameters in D decays is essential to make measurements of γ to degree-level precision. Strong-phase information in the following D decay modes has been obtained from the CLEO-c experiment and has been used in the most recent γ measurements:

- measurement of the amplitude weighted average cosine and sine of the strong-phase difference, c_i and s_i , where the index i refers to the phase-space region of self-conjugate multi-body decays, such as $D \rightarrow K_S^0 \pi^+ \pi^-$ and $D \rightarrow K_S^0 K^+ K^-$ [55];
- measurement of the coherence factor and average strong-phase difference in $D \rightarrow K^\pm \pi^\mp \pi^+ \pi^-$ and $D \rightarrow K^\pm \pi^\mp \pi^0$ [56];
- measurement of the coherence factor and average strong-phase difference in $D \rightarrow K_S^0 K^\pm \pi^\mp$ [57];
- measurement of the CP-even content of $D \rightarrow \pi^+ \pi^- \pi^+ \pi^-$, $D \rightarrow \pi^+ \pi^- \pi^0$, and $D \rightarrow K^+ K^- \pi^0$ [58];
- measurement of the strong-phase difference in $D \rightarrow K^\pm \pi^\mp$ [59];
- measurement of the CP-even content and strong-phase difference c_i and s_i in $D \rightarrow K_S \pi^+ \pi^- \pi^0$ [60].

Complementary constraints on the strong phase in $D \rightarrow K^\pm \pi^\mp \pi^+ \pi^-$ decays have come from charm-mixing measurements at LHCb [61]. It should be noted that the precision on the $D \rightarrow K^\pm \pi^\mp$ phase is dominated by the combination of charm-mixing measurements at the LHCb, CDF experiments and the B factories [29] and so here the role of threshold data is less important. Recently, BESIII reported the strong-phase measurement of $D \rightarrow K^\pm \pi^\mp$ decays [62] and the preliminary results of the strong-phase measurements of $D \rightarrow K_S^0 \pi^+ \pi^-$ decays [63] from current $\psi(3770)$ data with an integrated luminosity of 2.93 fb^{-1} . The precision of these measurements demonstrated the powerful capabilities of BESIII to determine strong-phase parameters accurately. However, all the current strong-phase measurements are still limited by the size of the $\psi(3770)$ data. Therefore, one of the most important goals of the BESIII charm physics program is to improve the strong-phase measurements with a larger $\psi(3770)$ data.

Table 5.3: Expected γ/ϕ_3 precision in the LHCb [53] and Belle II [54] experiments along with the timescales.

Runs	Collected / Expected integrated luminosity	Year attained	γ/ϕ_3 sensitivity
LHCb Run-1 [7, 8 TeV]	3 fb ⁻¹	2012	8°
LHCb Run-2 [13 TeV]	6 fb ⁻¹	2018	4°
Belle II Run	50 ab ⁻¹	2025	1.5°
LHCb upgrade I [14 TeV]	50 fb ⁻¹	2030	< 1°
LHCb upgrade II [14 TeV]	300 fb ⁻¹	(>)2035	< 0.4°

For the existing determination of γ that is made by combining the CP-violation sensitive observables from different D modes in $B \rightarrow D^{(*)}K^{(*)}$ decays, the uncertainty arising from the CLEO-c inputs has been found to be about 2° for LHCb. The current BESIII $\psi(3770)$ data is approximately four times larger than that of CLEO-c. The full analysis based on it gives in general a factor of 2.5(1.9) more precise results for $c_i(s_i)$, which reduces its contribution to the uncertainty on γ to 0.7° [63] at most. As evident from Table 5.3, this precision should be adequate for the LHCb Run-2 measurement, but will not be sufficient for the future LHCb upgrade and Belle II era, in particular because these strong-phase uncertainties will be largely correlated between the two experiments for each mode. To minimize the impact of the strong-phase measurement uncertainties for these next generation experiments, a much larger $\psi(3770)$ data at BESIII, ideally corresponding to an integrated luminosity of 20 fb⁻¹, is essential, as BEPCII is the only machine working at the charm-threshold energy region. Furthermore, determining these parameters with radiative return events to the $\psi(3770)$ at Belle II will not be achievable with suitable precision even with a data set of 50 ab⁻¹. A 20 fb⁻¹ sample of $\psi(3770)$ data would lead to an uncertainty of approximately 0.4° for the γ measurement, which will be necessary for the goals of LHCb upgrade I and Belle II. Moreover, this improved precision will be essential to allow the even larger data of LHCb upgrade II [64] to be fully exploited in improving further the knowledge of γ and allowing detailed comparison of the results obtained with different decay modes. A reasonable time frame for taking the $\psi(3770)$ data of 20 fb⁻¹ would be by 2025, when Belle II will have completed accumulation of its 50 ab⁻¹ of data and LHCb upgrade I will be mid-way through its period of operation.

A synergy between the BESIII, LHCb, and Belle II experiments is the best way to accurately determine γ in a manner that results in the uncertainty on γ being statistically rather than systematically limited. Table 5.4 lists the decay modes of interest that can be measured at BESIII. Furthermore, for the multi-body D final states the phase-space binning schemes that could be employed are mentioned; increasing the number of bins improves the statistical sensitivity of the measurements as the amount of information loss relative to an unbinned method is reduced. The modes are listed in their approximate order of importance for LHCb measurements. For the Belle II experiment those modes with neutrals are more important due to the larger neutral reconstruction efficiency compared to LHCb; LHCb will have an advantage for two- and four-body D decays containing only prompt charged pions and kaons in the final state.

In addition, it is worth noting the ability of BESIII to efficiently reconstruct D modes

Table 5.4: A priority-ordered list of strong-phase related measurements that are important for precision measurements of γ and indirect CP violation in charm mixing [53]. For states that are not self-conjugate, the coherence factor, R , and average strong-phase difference, δ , can be measured [65]. For self-conjugate states there are two choices: either a measurement of the CP-even fraction, F_+ [66], or a measurement of the amplitude weighted average cosine and sine of the strong-phase difference, c_i and s_i , where the index i refers to the phase-space region of the given multi-body decay [67].

Decay mode	Quantity of interest	Comments
$D \rightarrow K_S^0 \pi^+ \pi^-$	c_i and s_i	Binning schemes as those used in the CLEO-c analysis. With 20 fb^{-1} of data at 3.773 GeV, it might be worthwhile to explore alternative binning.
$D \rightarrow K_S^0 K^+ K^-$	c_i and s_i	Binning schemes as those used in the CLEO-c analysis. With 20 fb^{-1} of data at 3.773 GeV, it might be worthwhile to explore alternative binning.
$D \rightarrow K^\pm \pi^\mp \pi^+ \pi^-$	R, δ	In bins guided by amplitude models, currently under development by LHCb.
$D \rightarrow K^+ K^- \pi^+ \pi^-$	c_i and s_i	Binning scheme guided by the CLEO-c model [68] or potentially an improved model in the future.
$D \rightarrow \pi^+ \pi^- \pi^+ \pi^-$	F_+ or c_i and s_i	Unbinned measurement of F_+ . Measurements of F_+ in bins or c_i and s_i in bins could be explored.
$D \rightarrow K^\pm \pi^\mp \pi^0$	R, δ	Simple 2-3 bin scheme could be considered.
$D \rightarrow K_S^0 K^\pm \pi^\mp$	R, δ	Simple 2 bin scheme where one bin encloses the K^* resonance.
$D \rightarrow \pi^+ \pi^- \pi^0$	F_+	No binning required as $F_+ \sim 1$.
$D \rightarrow K_S^0 \pi^+ \pi^- \pi^0$	F_+ or c_i and s_i	Unbinned measurement of F_+ required. Additional measurements of F_+ or c_i and s_i in bins could be explored.
$D \rightarrow K^+ K^- \pi^0$	F_+	Unbinned measurement required. Extensions to binned measurements of either F_+ or c_i and s_i .
$D \rightarrow K^\pm \pi^\mp$	δ	Of low priority due to good precision available through charm-mixing analyses.

containing a K_L^0 meson in the final state and determine the relevant strong-phases. These K_L^0 modes provide additional tags (for example Ref. [66]) that increase the precision of other strong-phase parameter measurements at the $\psi(3770)$. Furthermore, it may be possible to use K_L^0 modes at Belle II to reconstruct $B^+ \rightarrow DK^+$ given the anticipated improvements in K_L^0 reconstruction. Evidence of this is given by the fact that the determination of the UT angle β at the B factories benefited from included $B^0 \rightarrow J/\psi K_L^0$ decays in the measurement.

The measurements of strong phases using quantum-coherent analyses [69] at BESIII provide important inputs to the LHCb and Belle II experiments to measure the $D^0 \bar{D}^0$ mixing parameters and indirect CP violation in charm mixing. The measurement methods, as described in Refs. [70–72], all use the charm strong-phase parameters. For example, using the c_i and s_i results as inputs to time-dependent measurements of $D^0 \rightarrow K_S \pi^+ \pi^-$, the charm mixing parameters x and y can be determined in a model-independent way [73].

More precise strong-phase measurements listed in Table 5.4 performed with the current and future $\psi(3770)$ data at BESIII, will prevent these studies from being limited by strong-phase related uncertainties. Furthermore, the strong-phase measurements have recently been used in time-dependent CP-violation measurements of $B^0 \rightarrow D^{(*)0}\pi^0$ decays by Belle [74] to make measurements of β/ϕ_1 that are free of uncertainties related to penguin processes. Such measurements are very attractive at Belle II, so that they can be compared to the “golden modes” $B^0 \rightarrow J/\psi K^0$ to empirically determine the pollution with penguin diagrams in the determination of β/ϕ_1 .

5.2.4 Impact on CKM measurements

In the SM, quark-flavor mixing is described by the 3×3 CKM matrix V_{CKM} as shown in Eq. (5.2) in Sec. 5.2.1. Unitarity is the only, albeit powerful, constraint on V_{CKM} . Without loss of generality, the V_{CKM} can be parameterized in terms of three mixing angles and one phase [75]

$$V_{\text{CKM}} = \begin{pmatrix} c_{12}c_{13} & s_{12}c_{13} & s_{13}e^{-i\delta} \\ -s_{12}c_{23} - c_{12}s_{23}s_{13}e^{i\delta} & c_{12}c_{23} - s_{12}s_{23}s_{13}e^{i\delta} & s_{23}c_{13} \\ s_{12}s_{23} - c_{12}c_{23}s_{13}e^{i\delta} & -c_{12}s_{23} - s_{12}c_{23}s_{13}e^{i\delta} & c_{23}c_{13} \end{pmatrix}, \quad (5.4)$$

where $c_{ij} \equiv \cos \theta_{ij}$ and $s_{ij} \equiv \sin \theta_{ij}$ (for $ij = 12, 23$ and 13). The irremovable phase δ is the unique source of CP-violation in quark flavor-changing processes within the SM. Following the observation of a hierarchy between the different matrix elements, Wolfenstein [76] proposed an expansion of the CKM matrix in terms of the four parameters λ , A , ρ , and η , which are widely used in contemporary literature, and which is the parameterization employed in CKMfitter [77].

The allowed region in the ρ and η space can be elegantly displayed by means of the UT described by the rescaled unitarity relation between the first and the third column of the CKM matrix (*i.e.*, corresponding to the b -meson system). The UT can be described in the complex $(\bar{\rho}, \bar{\eta})$ plane, where the apex is given by the following phase-convention independent definition [78]

$$\bar{\rho} + i\bar{\eta} \equiv -\frac{V_{ud}V_{ub}^*}{V_{cd}V_{cb}^*}. \quad (5.5)$$

We also propose to represent the combination of the CKM constraints in the plane that is relevant to the D meson UT. In analogy with the exact and rephasing-invariant expression of $(\bar{\rho}, \bar{\eta})$ we define the coordinates of the apex of the D meson UT [1]

$$\bar{\rho}_{cu} + i\bar{\eta}_{cu} \equiv -\frac{V_{ud}V_{cd}^*}{V_{us}V_{cs}^*}, \quad (5.6)$$

where $\bar{\rho}_{cu} = 1 + \mathcal{O}(\lambda^4)$ and $\bar{\eta}_{cu} = \mathcal{O}(\lambda^4)$. One can see that this triangle has two sides with length very close to 1 and a small side of order $\mathcal{O}(\lambda^4)$, with angles $\alpha_{cu} = -\gamma$, $\beta_{cu} = \gamma + \pi + \mathcal{O}(\lambda^4)$ and $\gamma_{cu} = \mathcal{O}(\lambda^4)$.

To constrain these parameters, we consider a prospective exercise when BESIII will complete the taking of 20 fb^{-1} data accumulated at the $D\bar{D}$ threshold [1] and 6 fb^{-1} data at 4.178 GeV around 2025 (Phase I). At that time, the collected data amount for LHCb

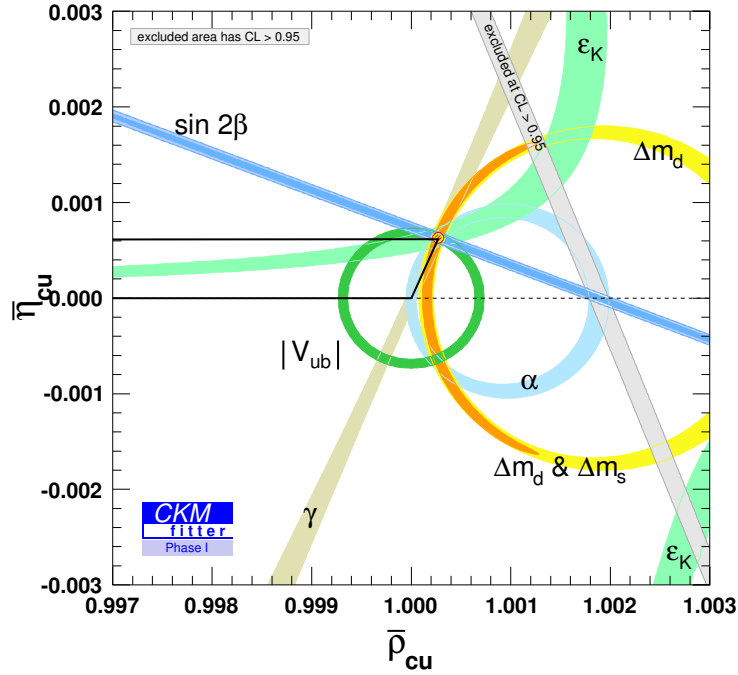


Figure 5.5: Individual constraints and the global CKM fit on the $(\bar{\rho}_{cu}, \bar{\eta}_{cu})$ plane according to our projections of the experimental status in 2025 (Phase I). The shaded areas have 95% CL. Only a part of the D meson UT is visible (in black solid lines): the two apices associated with large angles are shown, whereas the missing corner is situated at the origin, far away on the left.

will be 23 fb^{-1} [79] and for CMS/ATLAS 300 fb^{-1} , which is after Run 3 and prior to the start of the HL-LHC. We also take into account the prospective accuracies for Belle II at 50 ab^{-1} [54] already at Phase I. The individual constraints as well as the combination from the usual observables are shown for 2025 in the $(\bar{\rho}_{cu}, \bar{\eta}_{cu})$ plane in Fig. 5.5. One can also transfer the constraints to the $(|V_{cs}|, |V_{cd}|)$ plane as shown in Fig. 5.6, which clearly shows the direct contribution from the BESIII measurements of $|V_{cs}|$ and $|V_{cd}|$, and allows precise tests of the consistency of CKM determination from different quark sectors.

In the further Phase II beyond 2035, we assume larger data sets of 300 fb^{-1} for LHCb and 3000 fb^{-1} for CMS/ATLAS. The corresponding perspectives of individual constraints and the global CKM fit on the $(\bar{\rho}, \bar{\eta})$ plane are shown in Fig. 5.7, which involve both LHC and Belle II experiments for the CKM measurements related to B and B_s mesons. We use available resources for the uncertainties [54, 79] assuming that all the measurements agree perfectly well within the SM. As mentioned in Sec. 5.2.3, thanks to the critical input with 20 fb^{-1} data accumulated at the $D\bar{D}$ threshold [1] from BESIII on charm strong phases, the knowledge of the angle γ will be improved to 0.4° or better, allowing for extremely precise tests of the CKM paradigm, and providing a sensitive probe for possible new physics contributions.

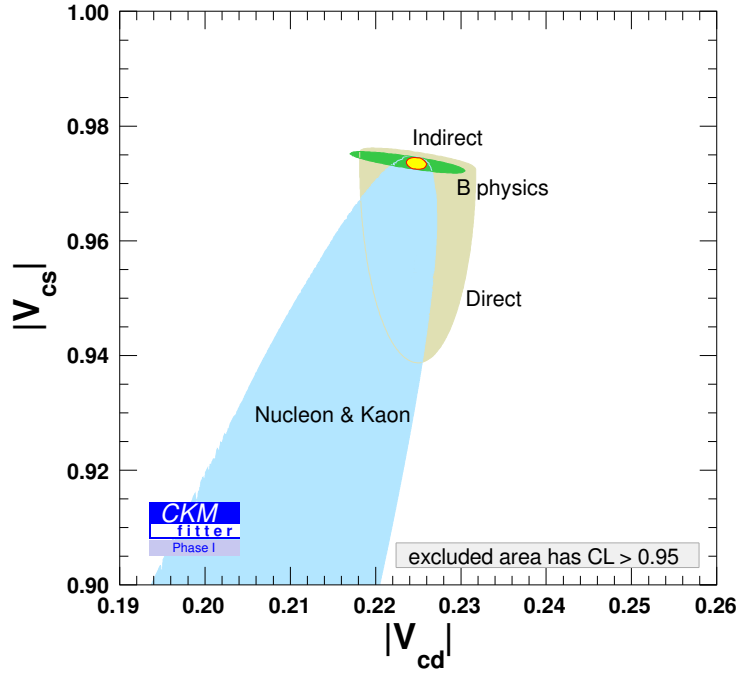


Figure 5.6: Constraints in the $(|V_{cd}|, |V_{cs}|)$ plane for the Phase I data. The indirect constraints (coming from b transitions) are related to $|V_{cd}|$ and $|V_{cs}|$ through unitarity. The direct constraints combine leptonic and SL D and D_s decays from BESIII experiment. The red hashed region of the global combination corresponds to 68% CL.

5.2.5 CP violation and D mixing

It is not competitive to search for CP violation and charm mixing parameters at BESIII, since the achievable D^0 and \bar{D}^0 samples are less than those at LHCb and Belle II by more than 2-4 orders of magnitudes. However, BESIII can uniquely explore the quantum coherence of the initial $D^0\bar{D}^0$ state produced at $\psi(3770)$ to provide constraints [80] on mixing and CP-violating parameters [81, 82] that have completely different systematic uncertainties than those of LHCb or Belle II. For example, decays of each D in the $D^0\bar{D}^0$ state into final states of the same CP would immediately indicate CP-violation in charm, as the D -states produced at $\psi(3770)$ have opposite CP,

$$\Gamma_{D^0\bar{D}^0}^{++} = [(x^2 + y^2) (\cosh^2 a_m - \cos^2 \phi)] \Gamma^2(D \rightarrow f_+), \quad (5.7)$$

where we employ two $CP = +$ states f , such as $f = \pi^+\pi^-$. Also, $\phi = \arg(p/q)$, $R_m = |p/q|$, and $a_m = \log R_m$ [81]. In addition, superb kinematical constraints might make BESIII competitive in studies of CP-asymmetries in some multi-body D decays [83].

5.2.6 CPT violation in charm mixing

CPT is conserved in all local Lorentz-invariant theories, including SM and all its commonly-discussed extensions. Yet, CPT violation might arise in string theory or some

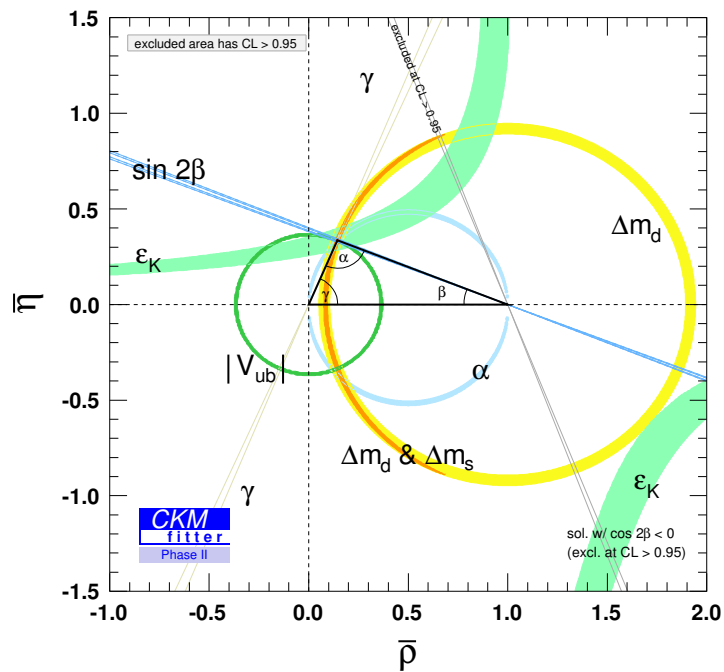


Figure 5.7: Evolving constraints and the global fit in the $(\bar{\rho}, \bar{\eta})$ plane with the anticipated improvements for the Phase II data (300 fb^{-1} from LHCb [79], 3000 fb^{-1} from CMS/ATLAS, and 50 ab^{-1} from Belle II [54]). The γ is expected to have an accuracy around 0.4 degrees (shown in Table 5.3), thanks to BESIII charm inputs with 20 fb^{-1} data accumulated at the $D\bar{D}$ threshold [1]. The shaded areas have 95% CL.

extra-dimensional models with Lorentz-symmetry violations in four dimensions. Time evolution studies of CP-correlated $D^0\bar{D}^0$ states are complementary to CPT-violation studies at B -factories and the LHC. While studies of those models are not particularly well motivated at charm threshold, CPT-violating effects can still be probed with the quantum-correlated $D^0\bar{D}^0$ states at $\psi(3770)$ [84].

5.2.7 Absolute measurement of hadronic decays

The hadronic decay of charmed hadrons provides important information on not only the charmed hadron itself, but also on the light daughters of the hadron. Therefore, studying charm multi-body hadronic decays is a powerful tool for light hadron spectroscopy. Analogously, studying high-statistics hadronic decays of the charmed baryon Λ_c^+ with a data set of 5 fb^{-1} produced at 4.64 GeV, as discussed in Sec. 5.3.1, is useful for improved understanding of light meson and baryon spectroscopy.

Experimental studies of two-body hadronic decays of D^0 , D^+ , and D_s^+ mesons are very important for calibrating theoretical models. There are different final-state possibilities, namely PP , VP , VV , SP , AP , and TP , where P , V , S , A , and T represent pseudoscalar, vector, scalar, axial vector, and tensor mesons, respectively. The simplest cases of the PP decays of D^0 , D^+ , and D_s^+ have been well investigated experimentally in recent years. However, some of these measurements, particularly of DCS decays, are still statistically limited. Studies of non- PP final states require sophisticated amplitude analyses of multi-body decays of charmed mesons that are not well developed because of either the limited statistics or the high background level. Larger $D^{0(+)}$ and D_s data samples are necessary to guarantee clean signal samples with sufficient yields to perform reliable amplitude analyses, so that all types of two-body process can be well understood.

At present, the sums of the BF's for the known exclusive decays of D^0 , D^+ , and D_s^+ are all more than 80% [2]. However, there is still significant room to explore many unknown hadronic decays. A 20 fb^{-1} sample of data at the $\psi(3770)$ will allow the determination of many BF's of these missing decays to $K\pi\pi\pi$, $KK\pi\pi$, and $KK\pi\pi\pi$, as well as further exploration of the sub-structures in these decays. Some of them, for example $D^0 \rightarrow K^-\pi^+\pi^0\pi^0$ and $D^+ \rightarrow \bar{K}^0\pi^+\pi^0\pi^0$, are expected to have a BF in the range 5 to 10% [85], which can be improved a lot with the advantage of BESIII in precise π^0 and photon detections.

LHCb has the ability to measure a large number of relative BF's of charm and beauty hadrons, on account of the high yields that result from the large cross section for heavy-flavor production in the forward region. Converting from the BF ratio to the absolute BF incurs an additional uncertainty from the BF of the reference mode, such as $D^0 \rightarrow K^-\pi^+$, $D^0 \rightarrow K^-\pi^+\pi^+\pi^-$, $D^+ \rightarrow K^-\pi^+\pi^+$, $D_s^+ \rightarrow K^-K^+\pi^+$, and $\Lambda_c^+ \rightarrow pK^-\pi^+$. Absolute BF measurements of the other charmed baryons, Ξ_c^0 and Ξ_c^+ are also strongly desired. Although it is acknowledged that these modes would be very hard to measure with the current energy of the collisions at BESIII, the importance of these measurements is stressed here in case future developments could make them possible. Relevant discussions on the prospects for measurements of charmed baryons are given in Sec. 5.3.1.

With 20 fb^{-1} of data at 3.773 GeV and 6 fb^{-1} around 4.178 GeV at BESIII, many $D_{(s)}$ decays are expected to be measured with an uncertainty of about 1%, which will then be

limited by the systematic uncertainties related to particle reconstruction in the different final states. Improved measurements of these absolute BF's at BESIII will be highly beneficial to some key measurements at LHCb, since it is expected that the uncertainty of the reference mode will become the dominant uncertainty in several measurements. One prime example is the LHCb measurement of $B \rightarrow D^* \tau^+ \nu_\tau$, which is used to test lepton universality [53]. BESIII can make precise measurements of the BF's for D^0 , D_s^+ , and D^+ inclusive decays to three charged pions and to the neutral particles, and exclusive decays to final states with neutral kaons and pions (*e.g.*, $D_s^+ \rightarrow \eta' \pi^+ \pi^0$, $D^+ \rightarrow \bar{K}^0 \pi^+ \pi^+ \pi^- \pi^0$, and $D^{0(+)} \rightarrow \eta X$, X denotes any possible particle combinations), which will have a significant impact on optimizing the background models. Another example is the determination of the CKM matrix elements $|V_{c(u)b}|$ via inclusive or exclusive SL B decays, such as $B \rightarrow D^* \ell^- \nu_\ell$ or $\Lambda_b^0 \rightarrow \Lambda_c^+ \bar{\ell}^- \nu_\ell$. Precise measurements of absolute BF's of both $D_{(s)}^{0(+)}$ and Λ_c^+ decays (Sec. 5.3.1) are crucial for improvement of the $|V_{c(u)b}|$ measurements.

Due to interference effects between the CF and DCS contributions, the BF's of $D_{(s)} \rightarrow K_S^0 X$ and $D_{(s)} \rightarrow K_L^0 X$ are not expected to be equal. The recoil-mass method, or that developed in Ref. [86], allows the efficient reconstruction of $D_{(s)} \rightarrow K_L^0 X$ decays at BESIII. A difference of about 10% has been observed in $D^0 \rightarrow K_{S,L}^0 \pi^0$ decays at CLEO-c [86] and has been confirmed at BESIII [87]. The two-body decays $D^0 \rightarrow K_{S,L}^0 X$ ($X = \pi^0, \eta, \eta', \omega, \phi$) are expected to have an asymmetry under the same mechanism [88], which can be tested with the current $\psi(3770)$ data, but the uncertainties will be dominated by statistical uncertainties. Furthermore, measurements of these modes are of interest in understanding the width difference in the neutral D system [89]. With the future 20 fb^{-1} and 6 fb^{-1} of data taken at $\sqrt{s} = 3.773$ and 4.178 GeV, these measurements will be performed with much better precision.

5.3 Charmed baryons

5.3.1 Λ_c^+ physics

Studies of charm baryons have been ongoing since 1975 [90], with all ground states of singly charmed baryons, as well as some excited states, having been observed. The constituents of the lightest charmed baryon (Λ_c^+) are one diquark (ud) and one heavy charm quark (c), where, relative to the heavy quark, the light diquark is in a net quantum state of spin zero and isospin zero. In a naive spectator model the Λ_c^+ decays dominatedly through the weak amplitudes $c \rightarrow W^+s$ and $c \rightarrow W^+d$ at leading order, which leads to a simpler theoretical description in non-perturbative models than in the case of charmed mesons. Hence, studying Λ_c^+ decays allows a deeper understanding of strong and weak interactions in the charm sector, which is complementary to that provided by charmed mesons. In addition, the Λ_c^+ is the cornerstone of the charmed baryon spectra. Improved knowledge of Λ_c^+ decays is essential to the studies of the whole charmed baryon family. Furthermore, this knowledge will provide important information to the studies of beauty baryons that decay into final states involving Λ_c^+ .

Compared to the significant progress in the studies of charmed mesons (D^0 , D^+ , and D_s^+) in both theory and experiment, the advancement of our understanding of charmed baryons has been relatively slow during the past 40 years. Until 2014, no absolute measurements of the decay rates of the Λ_c^+ had been performed, with almost all these rates having been measured relative to the normalization mode $\Lambda_c^+ \rightarrow pK^-\pi^+$, whose BF suffered from a large uncertainty of 25%. This overall situation has changed since 2014, when BESIII collected a data set of e^+e^- annihilation at $\sqrt{s} = 4.6$ GeV, corresponding to an integrated luminosity of 567 pb^{-1} . At this energy, the $\Lambda_c^+\bar{\Lambda}_c^-$ pairs are produced in pairs with no accompanying hadrons. The total number of $\Lambda_c^+\bar{\Lambda}_c^-$ pairs produced is approximately 100,000. This threshold data set provides a clean environment to systematically investigate the production and decays of the Λ_c^+ . Precise BF measurements of $\Lambda_c^+ \rightarrow pK^-\pi^+$ were reported by Belle [91] and BESIII [92]; the combined precision of the $\Lambda_c^+ \rightarrow pK^-\pi^+$ BF is 5.2%, a five-fold reduction of the uncertainty with respect to the previous result. In addition, more analyses were implemented at BESIII, Belle, and LHCb. At BESIII a series of BF measurements have been reported, including

- absolute BF measurement of $\Lambda_c^+ \rightarrow \Lambda\ell^+\nu_\ell$ [93, 94], which motivated the first LQCD calculation of this channel [95];
- absolute BF measurements of 12 Cabibbo-favored (CF) decays of the Λ_c^+ [92], including $\Lambda_c^+ \rightarrow pK_S^0, pK^-\pi^+, pK_S^0\pi^0, pK_S^0\pi^+\pi^-, \Lambda\pi^+, \Lambda\pi^+\pi^0, \Lambda\pi^+\pi^+\pi^-, pK^-\pi^+\pi^0, \Sigma^0\pi^+, \Sigma^+\pi^0, \Sigma^+\pi^+\pi^-,$ and $\Sigma^+\omega$;
- studies of singly-Cabibbo-suppressed (SCS) decays $\Lambda_c^+ \rightarrow p\pi^+\pi^-, pK^+K^-, p\eta,$ and $p\pi^0$ [96, 97];
- observation of modes with a neutron in the final state, $\Lambda_c^+ \rightarrow nK_S^0\pi^+$ [98] and $\Sigma^-\pi^+\pi^+\pi^0$ [99].
- measurements of the absolute BFs of $\Lambda_c^+ \rightarrow \Xi^0K^+, \Xi^{*0}K^+$ [100], $\Sigma^+\eta, \Sigma^+\eta'$ [101], $\Sigma(1385)^+\eta$ and $\Lambda\eta\pi^+$ [102].

- studies of inclusive ΛX decay [103] and inclusive electronic decay [104].

Although much progress has been made since 2014, the knowledge of Λ_c^+ decays is still very limited in comparison to that of charmed mesons. Firstly, only a single SL decay mode $\Lambda_c^+ \nu_\ell$ has been observed. Secondly, the DCS modes have not been systematically studied. Thirdly, the known exclusive decays of the Λ_c^+ account for only about 60% of the total BF. Many channels are still unobserved. In particular, information about decays that involve a neutron is minimal considering such decays should account for nearly half of the Λ_c^+ decay rate. A thorough investigation of these channels requires a much larger data set taken in the low-multiplicity environment obtained at threshold in e^+e^- collisions.

5.3.2 Prospects in Λ_c^+ physics

The approved energy upgrade project of BEPCII will increase the collision energy up to 4.9 GeV. Together with commissioning of the top-up mode, we will be able to take 5 fb^{-1} of data at 4.64 GeV, which corresponds to the energy point with the expected peaking cross section of the $\Lambda_c^+ \bar{\Lambda}_c^-$ pairs. This data set will have more than 16 times the statistics of the current BESIII data set at 4.6 GeV, and will allow to improve the precision of the Λ_c^+ decay rates to a level comparable to those of the charmed mesons, as listed in Table 5.5. In addition, it will provide an opportunity to study many unexplored physics observables related to Λ_c^+ decays. In particular, this advancement will boost our understanding of the non-perturbative effects in the charmed baryon sector.

A larger data set will guarantee the first absolute measurement of the form factors in the SL decay $\Lambda_c^+ \rightarrow \Lambda \ell^+ \nu_\ell$, which is crucial for calibrating the various theoretical calculations. Besides $\Lambda_c^+ \rightarrow \Lambda \ell^+ \nu_\ell$, more SL modes can be identified, such as those listed in Table 5.6. According to the predicted rates in model calculations, the new CF modes $\Lambda_c^+ \rightarrow p K^- e^+ \nu_e$ and $\Sigma \pi e^+ \nu_e$ will be established for the first time with the double-tag technique. For the SCS mode, studying $\Lambda_c^+ \rightarrow n e^+ \nu_e$ will be challenging due to the presence of two missing particles in the final state and the dominant $\Lambda_c^+ \rightarrow \Lambda e^+ \nu_e$ backgrounds. However, we still have the opportunity to identify the decay by taking advantage of the well constrained kinematics, the clean reaction environment and neutron shower information inside the electromagnetic calorimeter. Meanwhile, another SCS mode $\Lambda_c^+ \rightarrow p \pi^- e^+ \nu_e$ can be searched for in the enlarged data set.

The hadronic weak decay of a singly charmed baryon is expected to violate parity conservation. For instance, the two-body decay, $\Lambda_c^+ \rightarrow \Lambda \pi^+$, proceeds via a W -interaction, $c \rightarrow W^+ + s$, in which parity is not conserved. The Λ and π^+ particles are allowed to be in an S - or P -wave state. The effects of parity violation are determined from the polarization of the charmed baryons, which is characterized by the angular distribution of the Λ in the Λ_c^+ rest frame, taking the form of $\frac{dN}{d \cos \theta_\Lambda} \propto 1 + \alpha_{\Lambda\pi} \cos \theta_\Lambda$, where $\alpha_{\Lambda\pi}$ is the decay asymmetry parameter [111, 112]. In addition the decay asymmetry allows discrimination between different theoretical models, as listed in Ref. [112]. Some decay asymmetry parameters, *e.g.*, $\alpha_{\Lambda\pi}$ for $\Lambda_c^+ \rightarrow \Lambda \pi^+$, $\alpha_{\Sigma^+\pi^0}$ for $\Lambda_c^+ \rightarrow \Sigma^+ \pi^0$, and $\alpha_{\Xi^-\pi^+}$ for $\Xi_c^0 \rightarrow \Xi^- \pi^+$, have been studied previously, but with limited precision [2]. Therefore, improved measurements are desirable, as they will shed light on the decay mechanism and allow searches for CP asymmetries in the charmed baryon sector. In addition, more decay

Table 5.5: Measured or projected precisions of charmed hadrons, along with the relative precision in parenthesis. For the future Λ_c^+ precision, it is estimated for 5 fb^{-1} of data at $\sqrt{s} = 4.64 \text{ GeV}$.

	Leading hadronic decay	Typical two-body decay	Leading SL decay
Λ_c^+	$\mathcal{B}(K^- p \pi^+) =$	$\mathcal{B}(K_S^0 p) =$	$\mathcal{B}(\Lambda c^+ \nu_e) =$
	2014: $(5.0 \pm 1.3)\%$ (26%)	2014: $(1.2 \pm 0.3)\%$ (26%)	2014: $(2.1 \pm 0.6)\%$ (29%)
	2017(w/ BESIII): $(6.35 \pm 0.33)\%$ (5.2%)	BESIII: $(1.52 \pm 0.08)\%$ (5.6%)	BESIII: $(3.63 \pm 0.43)\%$ (12%)
	$5 \text{ fb}^{-1}; \frac{\delta \mathcal{B}}{\mathcal{B}} < 2\%$	$5 \text{ fb}^{-1}; \frac{\delta \mathcal{B}}{\mathcal{B}} < 2\%$	$5 \text{ fb}^{-1}; \frac{\delta \mathcal{B}}{\mathcal{B}} \sim 3.3\%$
D^0	$\mathcal{B}(K^- \pi^+) = (3.89 \pm 0.04)\%$ (1.0%)	$\mathcal{B}(K_S^0 \pi^0) = (1.19 \pm 0.04)\%$ (3.4%)	$\mathcal{B}(K^- e^+ \nu_e) = (3.53 \pm 0.03)\%$ (0.8%)
D^+	$\mathcal{B}(K^- \pi^+ \pi^+) = (8.98 \pm 0.28)\%$ (3.1%)	$\mathcal{B}(K_S^0 \pi^+) = (1.47 \pm 0.08)\%$ (5.4%)	$\mathcal{B}(K_S^0 e^+ \nu_e) = (4.41 \pm 0.07)\%$ (1.5%)
D_s^+	$\mathcal{B}(K^- K^+ \pi^+) = (5.45 \pm 0.17)\%$ (3.8%)	$\mathcal{B}(K_S^0 K^+) = (1.40 \pm 0.05)\%$ (3.6%)	$\mathcal{B}(\phi e^+ \nu_e) = (2.39 \pm 0.23)\%$ (9.6%)

Table 5.6: Expected rates of the SL modes and estimated precision for 5 fb^{-1} of data at $\sqrt{s} = 4.64 \text{ GeV}$.

Mode	Expected rate (%)	Relative uncertainty (%)
$\Lambda_c^+ \rightarrow \Lambda \ell^+ \nu_\ell$	3.6 [95, 105]	3.3
$\Lambda_c^+ \rightarrow \Lambda^* \ell^+ \nu_\ell$	0.7 [106, 107]	10
$\Lambda_c^+ \rightarrow N K e^+ \nu_e$	0.7 [106]	10
$\Lambda_c^+ \rightarrow \Sigma \pi \ell^+ \nu_\ell$	0.7 [106]	10
$\Lambda_c^+ \rightarrow n e^+ \nu_e$	0.2 [105, 108, 109]; 0.4 [110]	17

asymmetry parameters in $\Lambda_c^+ \rightarrow \Sigma^0 \pi^+$, $p \bar{K}^0$, and $\Xi_c^0 \rightarrow \Xi^- \pi^+$ can be accessed. Based on the sensitivity with the current BESIII data set, a $16\times$ larger data set would result in an approximate precision of 4% and 6% for measuring $\alpha_{\Lambda\pi^+}$ and $\alpha_{\Sigma^0\pi^+}$, respectively.

The weak radiative decay $\Lambda_c^+ \rightarrow \gamma \Sigma^+$ is predicted to have a BF of 10^{-5} to 10^{-4} . The new data set will push the experimental sensitivity to 10^{-5} , which provides an opportunity to measure this process for the first time. Moreover, the SCS radiative decay $\Lambda_c^+ \rightarrow \gamma p$ can be searched for.

We will have better sensitivity to explore the SCS modes, which at present have limited precision or have not been studied before. Meanwhile, more modes with the neutron or Σ^- in the final state can be accessed. This will significantly enhance our knowledge of the less well known decays, and will allow improved studies of $\Lambda_c^+ \rightarrow p \pi^0$ and first searches for $n \pi^+$ and $n K^+$.

Thorough analysis of the involved intermediate states can be carried out in the decays to multi-body final states. This can be achieved by implementing amplitude analyses of the copious hadronic decays, such as $\Lambda_c^+ \rightarrow p K^- \pi^+$, $p K_S^0 \pi^0$, $p K_S^0 \pi^+ \pi^-$, $\Lambda \pi^+ \pi^0$, $\Lambda \pi^+ \pi^+ \pi^-$, $p K^- \pi^+ \pi^0$, and $\Sigma^+ \pi^+ \pi^-$. From these analyses, more two-body decay patterns of $\Lambda_c^+ \rightarrow B^{\frac{3}{2}} P$ and $B^{\frac{1}{2}} V$ can be extracted. Here, $B^{\frac{3}{2}}$ and $B^{\frac{1}{2}}$ denote baryon states with isospin $\frac{3}{2}$ and $\frac{1}{2}$, respectively. Also, the Λ_c^+ decays, acting as an isospin filter, provide a good place to study light-hadron spectroscopy, such as the study of Λ^* and scalar meson states via the weak decays $\Lambda_c^+ \rightarrow \Sigma \pi \pi$, $N K \pi$, and $\Lambda \pi^+ \eta$ [102, 113–115].

5.3.3 Σ_c and Ξ_c physics

Above 4.88 GeV, the Σ_c baryon can be produced via $e^+ e^- \rightarrow \Sigma_c \bar{\Lambda}_c^- \pi$. The width of the $\Sigma_c^{0(++)}$ has been well determined by Belle, while only an upper limit on the width of the Σ_c^+ was determined. BESIII will provide an improved width measurement of the Σ_c^+ via the dominant decay $\Sigma_c^+ \rightarrow \Lambda_c^+ \pi^0$, which is useful to test the overall understanding of the decay dynamics. Moreover, BESIII can also search for the decay of $\Sigma_c \rightarrow \Lambda_c^+ \gamma$, which is theoretically expected to occur with a BF of approximately 1%. Above 4.74 GeV, the sum of the Λ_c^+ and Σ_c^+ masses, the isospin-violating EM reaction $e^+ e^- \rightarrow \Sigma_c^+ \bar{\Lambda}_c^-$ happens. It is interesting to measure its cross section near threshold, whose ratio to the cross section of $e^+ e^- \rightarrow \Lambda_c^+ \bar{\Lambda}_c^-$ will provide insight of the vacuum productions of $c\bar{c}$ and $s\bar{s}$ pairs. In addition, it is possible to study the Σ_c baryon pair production at 4.91 GeV through $e^+ e^- \rightarrow \Sigma_c \bar{\Sigma}_c$. Relative to the production rate of $e^+ e^- \rightarrow \Lambda_c^+ \bar{\Lambda}_c^-$, one can explore the mechanism of generating ‘good’ spin-0 and ‘bad’ spin-1 u - d diquarks inside the Λ_c

and Σ_c , respectively, near threshold.

For the charmed baryons Ξ_c^0 and Ξ_c^+ , the relative uncertainties of the measured BFs are large, and most of the decays have not yet been studied experimentally [2]. Belle performed first measurements of the absolute BFs of Ξ_c^0 and Ξ_c^+ decays in $\bar{B}^{-(0)} \rightarrow \bar{\Lambda}_c^- \Xi_c^{0(+)}$ [116, 117]. Their results are given as

$$\begin{aligned}\mathcal{B}(\Xi_c^0 \rightarrow \Xi^- \pi^+) &= (1.80 \pm 0.50 \pm 0.14)\%, \\ \mathcal{B}(\Xi_c^0 \rightarrow \Lambda K^- \pi^+) &= (1.17 \pm 0.37 \pm 0.09)\%, \\ \mathcal{B}(\Xi_c^0 \rightarrow p K^- K^- \pi^+) &= (0.58 \pm 0.23 \pm 0.05)\%, \\ \mathcal{B}(\Xi_c^+ \rightarrow \Xi^- \pi^+ \pi^+) &= (2.86 \pm 1.21 \pm 0.38)\%, \\ \mathcal{B}(\Xi_c^+ \rightarrow p K^- \pi^+) &= (0.45 \pm 0.21 \pm 0.07)\%.\end{aligned}$$

So far, their statistical uncertainties are about 30~40% and their systematic uncertainties are about 10%. The statistical uncertainties can be suppressed to about 5% at Belle II with 50 times more data set by 2025. However, the systematic uncertainties have less potential to be improved further. So the overall uncertainties will be below 10%.

If BEPCII has the possibility of increasing the cms energy above 4.95 GeV, which is just above the mass of Ξ_c pairs, we will be able to perform absolute BF measurements of Ξ_c decays in the same fashion as is done for the Λ_c^+ . If we assume their production cross sections of $e^+e^- \rightarrow \Lambda_c^+ \bar{\Lambda}_c^-$ and $\Xi_c \bar{\Xi}_c$ are at the same level near mass threshold, the precisions at BESIII are expected to be competitive or superior to the Belle II results, depending on different modes. These precise absolute BF measurements will be extremely useful inputs for studying the b -baryon decays [53]. Furthermore, many of the missing hadronic and SL decays of Ξ_c can be studied for the first time. The data set taken at this energy can also be used to study the triplet states Σ_c^{++} , Σ_c^+ , and Σ_c^0 .

5.3.4 The EM structure of charmed baryons

As discussed in Chapter 4 of this White Paper, the BESIII experiment is perfectly suited to perform precision studies of hyperon structure. The coming upgrades of BEPCII opens up new avenues to study single-charm hyperons. In this section, we will discuss these possibilities and the prospects of performing tests of CP violation in hyperon decays.

Let's consider a hyperon-antihyperon pair $Y\bar{Y}$, where Y and \bar{Y} have spin 1/2, produced in e^+e^- annihilation. The differential cross section can be parameterized in terms of electric and magnetic form factors, $G_E(q^2)$ and $G_M(q^2)$, which are related to helicity flip and non-flip amplitudes, respectively. These are linear combinations constructed from Dirac and Fermi unconstrained form factors F_1 and F_2 : $G_E = F_1 + F_2$ and $G_M = F_1 + \tau F_2$, where $\tau = \frac{q^2}{4m_Y^2}$, and m_Y is the Y mass. The differential cross section can be expressed as

$$\frac{d\sigma}{d\cos\theta} \propto 1 + \eta \cos^2\theta, \quad (5.8)$$

where θ is the polar angle of Λ_c^+ in the e^+e^- center-of-mass system, $-1 \leq \eta \leq 1$ and is related to the form-factor ratio $R = |G_E/G_M|$ in the following way

$$R = \sqrt{\tau} \sqrt{\frac{1-\eta}{1+\eta}}. \quad (5.9)$$

The form factors are complex in the time-like region, *i.e.*, they can be written as $G_M(q^2) = |G_M(q^2)|e^{i\Phi_M}$ and $G_E(q^2) = |G_E(q^2)|e^{i\Phi_E}$, from which the relative phase can be defined: $\Delta\Phi = \Phi_E - \Phi_M$. This non-trivial relative phase has an impact on spin projections and spin correlations of the produced hyperons and could be detected experimentally via the weak decay of hyperons.

The challenge in charmed baryon studies is the lack of prominent decay modes with large BFs. All two-body decay channels have a BF of (1-2)% [2]. Consequently, even a large data set yields only a few hundred reconstructed events per channel. In particular, only the single-tag method can be applied to produce an adequate sample.

The most straightforward mode to study the Λ_c^+ polarization is the $\Lambda_c^+ \rightarrow K_S^0 p$ channel. Then, the formalism outlined in Ref. [118] can be used, adapted for single-tag $\Lambda_c^+ \rightarrow K_S^0 p$ measurements by integrating over the antiproton angles:

$$\mathcal{W}(\boldsymbol{\xi}) = 4\pi(1 + \eta \cos^2 \theta + \alpha_{K_S^0 p} \sqrt{1 - \eta^2} \sin(\Delta\Phi)(\sin \theta \cos \theta \sin \theta_1 \sin \phi_1)), \quad (5.10)$$

where $\boldsymbol{\xi}$ is a vector of the involved parameters and variables, θ is the polar angle of Λ_c^+ in the e^+e^- center-of-mass system, θ_1 (ϕ_1) is the solid angle in the Λ_c^+ ($\bar{\Lambda}_c^-$) helicity system, and $\alpha_{K_S^0 p}$ is the decay-asymmetry parameter. The disadvantage is that the decay asymmetry $\alpha_{K_S^0 p}$ is not known, so only the product $\alpha_{K_S^0 p} \sin(\Delta\Phi)$ can be determined. However, if one studies sequential decays such as $\Lambda_c^+ \rightarrow \Lambda \pi^+$, $\Lambda \rightarrow p \pi^-$, using the formalism outlined in Ref. [119], the asymmetry parameters β and γ are also accessible.

A measurement [120] of $\Delta\Phi$ has been made using a data set collected by the BESIII detector at $\sqrt{s} = 4.6$ GeV (corresponding to $\tau = 1.012$), using an integrated luminosity of $\mathcal{L}_{\text{int}} = 0.6 \text{ fb}^{-1}$. The value reported is $\sin(\Delta\Phi) = -0.28 \pm 0.13 \pm 0.03$. It is expected that the phase initially increases when \sqrt{s} goes higher but the most important improvement should come from larger statistics. Therefore, this motivates a high statistics study of the process $e^+e^- \rightarrow \Lambda_c^+ \bar{\Lambda}_c^-$ at the energy providing the highest yield of Λ_c . In particular, the reaction has maximum cross section at about 4.64 GeV, as expected from Belle data. This energy corresponds to a kinematic factor of $\tau = 1.034$.

Another interesting study of the Λ_c^+ form factor would be with a kinematic factor of approximately $\tau = 1.058$, which is the value at which the BESIII measurement of the Λ was made and yielded the result $\Delta\Phi = (37 \pm 12 \pm 7)^\circ$. Such a measurement will enable the first complete extraction of the EM form factor of a charmed hyperon, thus shedding light on the role of strangeness and charm in hadron structure, and provide a systematic comparison with the strange partner.

Several three-body decay channels have BFs five to seven times larger relative to the two-body decays [2]. In Ref. [121], it was found that for an integrated luminosity of 567 pb^{-1} the number of tagged $\Lambda_c^+ \rightarrow p K^- \pi^+$ was around 3000, and similarly for the charge-conjugate $\bar{\Lambda}_c^- \rightarrow \bar{p} K^+ \pi^-$. It may therefore be a better strategy to construct an angular observable for a three-body decay that is sensitive to the EM phase $\Delta\Phi$ [118, 122, 123]. With the data set proposed, such strategies can be pursued to give complementary measurements of $\Delta\Phi$.

Tests of CP violation can be made for two-body decays of charm hyperons as for strange hyperons; suitable observables for CP tests have been derived, *e.g.*, in Ref. [124]. These asymmetries are common in terms of the asymmetry parameters measured sepa-

rately for Λ_c^+ and $\bar{\Lambda}_c^-$, which can be done in the large data proposed above the threshold for production.

5.4 Summary

In this chapter we have presented the physics studies that are possible with data corresponding to integrated luminosities of 20 fb^{-1} at $\sqrt{s} = 3.773 \text{ GeV}$, 6 fb^{-1} at $\sqrt{s} = 4.178 \text{ GeV}$, and 5 fb^{-1} at $\sqrt{s} = 4.64 \text{ GeV}$; these cms energies correspond to the optimal values to accumulate samples of $D\bar{D}$, $D_s^{*+}D_s^-$, and $\Lambda_c^+\bar{\Lambda}_c^-$ events at threshold, respectively. Such samples at threshold allow a double-tag technique to be employed where the full event can be reconstructed, even if it contains one undetected particle such as a ν or K_L^0 meson. These samples provide a unique environment to measure the absolute BF's of charmed hadrons to leptonic, SL and hadronic final states, with very low levels of background. Such measurements provide rigorous tests of QCD, CKM unitarity and LFU that complement similar studies of beauty hadrons. Furthermore, the 20 fb^{-1} of data of coherent $\psi(3770) \rightarrow D^0\bar{D}^0$ events allow measurements of the strong-phase difference between the D^0 and \bar{D}^0 that are essential inputs to determining the UT angle γ in a model-independent fashion from B decays at LHCb and its upgrades, as well as at Belle II. These strong-phase differences can only be determined using this data set to the required level of precision. In addition, these strong-phase measurements are important ingredients of model-independent measurements of $D^0\bar{D}^0$ mixing and searches for indirect CP violation in D^0 decay. Finally, there are additional studies of charmed baryons that can be performed related to their electromagnetic form factors and, if the BEPCII cms energy is upgraded, studies of the absolute BF's of Σ_c and Ξ_c . Table 5.7 presents the precision prospects on some key measurements in $D^{0(+)}$, D_s^+ , and Λ_c^+ based on the proposed data set, and a comparison with Belle II.

Table 5.7: Prospects on some key measurements at the future BESIII, and comparison with Belle II. ‘NA’ means ‘not available’ and ‘-’ means ‘no estimation’.

Observable	Measurement	BESIII	Belle II
$\mathcal{B}(D^+ \rightarrow \ell^+\nu)$	$f_{D^+} V_{cd} $	1.1%	1.4%
$\mathcal{B}(D_s^+ \rightarrow \ell^+\nu)$	$f_{D_s^+} V_{cs} $	1.0%	1.0%
$d\Gamma(D^{0(+)} \rightarrow \bar{K}\ell^+\nu)/dq^2$	$f_+^K(0) V_{cs} $	0.5%	0.9%
$d\Gamma(D^{0(+)} \rightarrow \pi\ell^+\nu)/dq^2$	$f_+^\pi(0) V_{cd} $	0.6%	1.0%
$d\Gamma(D_s^+ \rightarrow \eta\ell^+\nu)/dq^2$	$f_+^\eta(0) V_{cs} $	0.8%	-
Strong phases in $D^0\bar{D}^0$	Constraint on γ	$< 0.4^\circ$	N/A
$\Lambda_c^+ \rightarrow pK^-\pi^+$	\mathcal{B}	2%	3%
$\Lambda_c^+ \rightarrow \Lambda\ell^+\nu$	\mathcal{B}	3.3%	-

Bibliography

- [1] D. M. Asner *et al.*, Int. J. Mod. Phys. A **24**, S1 (2009).
- [2] M. Tanabashi *et al.* (Particle Data Group), Phys. Rev. D **98**, 030001 (2018).
- [3] R. Aaij *et al.* (LHCb Collaboration), Phys. Rev. Lett. **121**, 092003 (2018).
- [4] M. Ablikim *et al.* (BESIII Collaboration), Phys. Rev. D **89**, 051104 (2014).
- [5] M. Ablikim *et al.* (BESIII Collaboration), Phys. Rev. Lett. **123**, 211802 (2019).
- [6] M. Ablikim *et al.* (BESIII Collaboration), Phys. Rev. Lett. **122**, 071802 (2019).
- [7] J. P. Alexander *et al.* (CLEO Collaboration), Phys. Rev. D **79**, 052001 (2009).
- [8] P. U. E. Onyisi *et al.* (CLEO Collaboration), Phys. Rev. D **79**, 052002 (2009).
- [9] P. Naik *et al.* (CLEO Collaboration), Phys. Rev. D **80**, 112004 (2009).
- [10] P. del Amo Sanchez *et al.* (BaBar Collaboration), Phys. Rev. D **82**, 091103 (2010).
- [11] A. Zupanc *et al.* (Belle Collaboration), JHEP **1309**, 139 (2013).
- [12] A. Bazavov *et al.* (Fermilab Lattice and MILC Collaboration), Phys. Rev. D **98**, 074512 (2018).
- [13] N. Carrasco *et al.* (ETM Collaboration), Phys. Rev. D **91**, 054507, (2015).
- [14] J. P. Lees *et al.* (BaBar Collaboration), Phys. Rev. Lett. **109**, 101802 (2012).
- [15] J. P. Lees *et al.* (BaBar Collaboration), Phys. Rev. D **88**, 072012 (2013).
- [16] A. Matyja *et al.* (Belle Collaboration), Phys. Rev. Lett. **99**, 191807 (2007).
- [17] I. Adachi *et al.* (Belle Collaboration), arXiv:0910.4301 [hep-ex].
- [18] A. Bozek *et al.* (Belle Collaboration), Phys. Rev. D **82**, 072005 (2010).
- [19] R. Aaij *et al.* (LHCb Collaboration), Phys. Rev. Lett. **115**, 111803 (2015).
- [20] R. Aaij *et al.* (LHCb Collaboration), JHEP **1602**, 104 (2016).
- [21] R. Aaij *et al.* (LHCb Collaboration), JHEP **1509**, 179 (2015).

- [22] R. Aaij *et al.* (LHCb Collaboration), Phys. Rev. Lett. **113**, 151601 (2014).
- [23] S. Wehle *et al.* (Belle Collaboration), Phys. Rev. Lett. **113**, 111801 (2017).
- [24] S. Fajfer, I. Nisandzic, and U. Rojec, Phys. Rev. D **91**, 094009 (2015).
- [25] M. A. Ivanov, J. G. Krner, J. N. Pandya, P. Santorelli, N. R. Soni and C. T. Tran, Front. Phys. (Beijing) **14**, 64401 (2019).
- [26] M. Ablikim *et al.* (BESIII Collaboration), Phys. Rev. D **92**, 072012 (2015).
- [27] M. Ablikim *et al.* (BESIII Collaboration), Phys. Rev. D **96**, 012002 (2016).
- [28] M. Ablikim *et al.* (BESIII Collaboration), Phys. Rev. Lett. **122**, 011804 (2019).
- [29] M. Ablikim *et al.* (BESIII Collaboration), Phys. Rev. D **97**, 092009 (2018).
- [30] M. Ablikim *et al.* (BESIII Collaboration), Phys. Rev. D **94**, 032001 (2016).
- [31] M. Ablikim *et al.* (BESIII Collaboration), Phys. Rev. Lett. **122**, 062001 (2019).
- [32] M. Ablikim *et al.* (BESIII Collaboration), Phys. Rev. D **92**, 071101 (2015).
- [33] M. Ablikim *et al.* (BESIII Collaboration), Phys. Rev. Lett. **122**, 061801 (2019).
- [34] M. Ablikim *et al.* (BESIII Collaboration), Phys. Rev. Lett. **122**, 121801 (2019).
- [35] M. Artuso *et al.* (Belle Collaboration), Phys. Rev. Lett. **99**, 191801 (2007).
- [36] M. Ablikim *et al.* (BESIII Collaboration), Phys. Rev. Lett. **121**, 081802 (2018).
- [37] H. Na *et al.* (HPQCD Collaboration), Phys. Rev. D **82**, 114506 (2010).
- [38] H. Na *et al.* (HPQCD Collaboration), Phys. Rev. D **84**, 114505 (2011).
- [39] Aida X. El-Khadra, talk presented at Beauty2014.
- [40] L. Riggio, G. Salerno, and S. Simula, Eur. Phys. J. C **78** 501 (2018).
- [41] M. Ablikim *et al.* (BESIII Collaboration), Phys. Rev. Lett. **121**, 171803 (2018).
- [42] H. Y. Cheng and X. W. Kang, Eur. Phys. J. C **77**, 587 (2017) [Erratum: Eur. Phys. J. C **77**, 863 (2017)].
- [43] B. Aubert *et al.* (BaBar Collaboration), Phys. Rev. D **76**, 052005 (2007).
- [44] J. P. Lees *et al.* (BaBar Collaboration), Phys. Rev. D **91**, 052022 (2015).
- [45] L. Widhalm *et al.* (Belle Collaboration), Phys. Rev. Lett. **97**, 061804 (2006).
- [46] Z. Z. Xing, Phys. Rev. D **55**, 196 (1997).
- [47] Y. Amhis *et al.* (HFLAV Collaboration), Eur. Phys. J. C **77**, 895 (2017).

- [48] LHCb Collaboration, Technical Report, LHCb-CONF-2018-002 (2018).
- [49] J. Brod and J. Zupan, JHEP **1401**, 051 (2014).
- [50] M. Gronau and D. London, Phys. Lett. B **253**, 483 (1991); M. Gronau and D. Wyler, Phys. Lett. B **265**, 172 (1991).
- [51] D. Atwood, I. Dunietz, and A. Soni, Phys. Rev. Lett **78**, 3257 (1997); Phys. Rev D **63**, 036005 (2001).
- [52] A. Giri, Y. Grossman, A. Soffer, and J. Zupan, Phys. Rev. D **68** (2003).
- [53] S. S. Malde, Technical Report, LHCb-PUB-2016-025 (2016).
- [54] E. Kou *et al.* (Belle II Collaboration), PTEP **2019**, 123C01 (2019).
- [55] J. Libby *et al.* (CLEO collaboration), Phys. Rev. D **82**, 112006 (2010).
- [56] T. Evans *et al.*, Phys. Lett. B **757**, 520 (2016); Erratum: [Phys. Lett. B **765**, 402 (2017)].
- [57] J. Insler *et al.* (CLEO Collaboration), Phys. Rev. D **85**, 092016 (2012).
- [58] S. Malde *et al.*, Phys. Lett. B **747**, 9 (2015).
- [59] D. M. Asner *et al.* (CLEO Collaboration), Phys. Rev. D **86**, 112001 (2012).
- [60] P. K. Resmi, J. Libby, S. Malde and G. Wilkinson, JHEP **1801**, 082 (2018).
- [61] R. Aaij *et al.* (LHCb Collaboration), Phys. Rev. Lett. **116**, 241801 (2016).
- [62] M. Ablikim *et al.* (BESIII Collaboration), Phys. Lett. B **734**, 227 (2014).
- [63] M. Ablikim *et al.*, arXiv:2003.00091 [hep-ex].
- [64] R. Aaij *et al.* (LHCb Collaboration), Technical Report, CERN-LHCC-2017-003 (2017).
- [65] D. Atwood, I. Dunietz, and A. Soni, Phys. Rev. D **63**, 036005 (2001).
- [66] M. Nayak *et al.*, Phys. Lett. B **740**, 1 (2015).
- [67] A. Giri, Y. Grossman, A. Soffer, and J. Zupan, Phys. Rev. D **68**, 054018 (2003).
- [68] M. Artuso *et al.* (CLEO Collaboration), Phys. Rev. D **85**, 122002 (2012).
- [69] M. Gronau, Y. Grossman and J. L. Rosner, Phys. Lett. B **508**, 37 (2001).
- [70] C. Thomas and G. Wilkinson, JHEP **1210**, 185 (2012).
- [71] S. Malde, C. Thomas, and G. Wilkinson, Phys. Rev. D **91**, 094032 (2015).
- [72] S. Malde and G. Wilkinson, Phys. Lett. B **701**, 353 (2011).

- [73] R. Aaij *et al.* (LHCb Collaboration), JHEP **1604**, 033 (2016)
- [74] V. Vorobiev *et al.* (Belle Collaboration), Phys. Rev. D **94**, 052004 (2016).
- [75] L. L. Chau and W. Y. Keung, Phys. Rev. Lett. **53**, 1802 (1984).
- [76] L. Wolfenstein, Phys. Rev. Lett. **51**, 1945 (1983).
- [77] J. Charles *et al.* (CKMfitter Group), Eur. Phys. J. C **41**, 1 (2005).
- [78] A. J. Buras, M. E. Lautenbacher, and G. Ostermaier, Phys. Rev. D **50**, 3433 (1994).
- [79] I. Bediaga *et al.* (LHCb Collaboration), arXiv:1808.08865 [hep-ex].
- [80] M. Ablikim *et al.* (BESIII Collaboration), Phys. Lett. B **744**, 339 (2015).
- [81] D. Atwood and A. A. Petrov, Phys. Rev. D **71**, 054032 (2005).
- [82] D. M. Asner and W. M. Sun, Phys. Rev. D **73**, 034024 (2006); [Erratum: Phys. Rev.D **77**, 019901 (2008)].
- [83] I. I. Bigi and A. Paul, JHEP **03**, 021 (2012).
- [84] V. A. Kostelecky, Phys. Rev. D **64**, 076001 (2001).
- [85] S. Barlag *et al.* (ACCMOR Collaboration), Z. Phys. C **55**, 383 (1992).
- [86] Q. He *et al.* (CLEO Collaboration), Phys. Rev. Lett. **100**, 091801 (2008).
- [87] Wenjing Zheng (for the BESIII Collaboration), PoS CHARM2016 (2016) 075.
- [88] Fusheng Yu, presented at 2016 workshop of BESIII Charm Hadron physics, Dec. 27-28, 2016, Beijing, China.
- [89] T. Gershon, J. Libby, and G. Wilkinson, Phys. Lett. B **750**, 338 (2015).
- [90] E. G. Cazzoli *et al.*, Phys. Rev. Lett. **34**, 1125 (1975).
- [91] A. Zupanc *et al.* (Belle Collaboration), Phys. Rev. Lett. **113**, 042002 (2014).
- [92] M. Ablikim *et al.* (BESIII Collaboration), Phys. Rev. Lett. **116**, 052001 (2016).
- [93] M. Ablikim *et al.* (BESIII Collaboration), Phys. Rev. Lett. **115**, 221805 (2015).
- [94] M. Ablikim *et al.* (BESIII Collaboration), Phys. Lett. B **767**, 42 (2017).
- [95] S. Meinel, Phys. Rev. Lett. **118**, 082001 (2017).
- [96] M. Ablikim *et al.* (BESIII Collaboration), Phys. Rev. Lett. **117**, 232002 (2016).
- [97] M. Ablikim *et al.* (BESIII Collaboration), Phys. Rev. D **95**, 111102 (2017).
- [98] M. Ablikim *et al.* (BESIII Collaboration), Phys. Rev. Lett. **118**, 112001 (2017).

- [99] M. Ablikim *et al.* (BESIII Collaboration), Phys. Lett. B **772**, 388 (2017).
- [100] M. Ablikim *et al.* (BESIII Collaboration), Phys. Lett. B **783**, 200 (2018).
- [101] M. Ablikim *et al.* (BESIII Collaboration), Chin. Phys. C **43**, 083002 (2019).
- [102] M. Ablikim *et al.* (BESIII Collaboration), Phys. Rev. D **99**, 032010 (2019).
- [103] M. Ablikim *et al.* (BESIII Collaboration), Phys. Rev. Lett. **121**, 062003 (2018).
- [104] M. Ablikim *et al.* (BESIII Collaboration), Phys. Rev. Lett. **121**, 251801 (2018).
- [105] R. N. Faustov and V. O. Galkina, Eur. Phys. J. C **76**, 628 (2016).
- [106] M. Pervin *et al.*, Phys. Rev. C **72**, 035201 (2005).
- [107] N. Ikeno and E. Oset, Phys. Rev. D **93**, 014021 (2016).
- [108] T. Gutsche *et al.*, Phys. Rev. D **90**, 114033 (2014).
- [109] Cai-Dian Lü, Wei Wang, and Fu-Sheng Yu, Phys. Rev. D **93**, 056008 (2016).
- [110] S. Meinel, Phys. Rev. D **97**, 034511 (2018).
- [111] D. Wang, R. G. Ping, L. Li, X. R. Lyu, and Y. H. Zheng, Chin. Phys. C **41**, 023106 (2017).
- [112] H. Y. Cheng, Front. Phys. (Beijing) **10**, 101406 (2015).
- [113] T. Hyodo and M. Oka, Phys. Rev. C **84**, 035201 (2011).
- [114] K. Miyahara, T. Hyodo, and E. Oset, Phys. Rev. C **92**, 055204 (2015).
- [115] J. J. Xie and L. S. Geng, Eur. Phys. J. C **76**, 496 (2016).
- [116] Y. B. Li *et al.* (Belle Collaboration), Phys. Rev. Lett. **122**, 082001 (2019).
- [117] Y. B. Li *et al.* (Belle Collaboration), Phys. Rev. D **100**, 031101 (2019).
- [118] G. Fäldt and A. Kupsc, Phys. Lett. B **772**, 16 (2017).
- [119] G. Fäldt, Phys. Rev. D **97**, 053002 (2018).
- [120] M. Ablikim *et al.* (BESIII Collaboration), Phys. Rev. D **100**, 072004 (2019).
- [121] M. Ablikim *et al.* (BESIII Collaboration), Phys. Rev. Lett. **120**, 132001 (2018).
- [122] S. Leupold, private communication (2017).
- [123] S. Bianco *et al.*, Nuovo Cim. **26N7**, 1 (2003).
- [124] N. Hamann *et al.*, Technical Report, CERN-SPSLC-92-19 (1992).

Chapter 6

Exotic Decays and New Physics

6.1 Introduction

With the discovery of the Higgs boson in 2012, the Standard Model (SM) has been firmly established. However, there are many compelling reasons to believe that the SM is not the ultimate theory, and the search for physics beyond the SM is well motivated.

There is strong synergy between direct and indirect searches for New Physics (NP). To identify possible NP paradigms, results from both low energy electron-positron colliders and high energy hadron colliders are needed [1]. Studies performed at electron-positron collider experiments such as BESIII may indicate hints of NP that could be directly probed at an energy frontier experiment, or even make some discoveries directly.

With high luminosity, clean collision environment, and excellent detector performance, the BESIII experiment has great potential to perform searches for NP. BESIII has already published some NP search results based on the existing data sets. There are still some unique opportunities worth further exploring. In general, NP searches at BESIII could be classified into three broad categories, which are demonstrated in this chapter:

1. Processes that are *allowed* in the SM.

NP searches of this type include testing relations among SM-allowed processes that are known to hold only in the SM, but not necessarily in models beyond the SM. Some examples have been discussed in depth by previous chapters, such as testing CKM triangle relations, precision measurement of $D_q \rightarrow \ell \bar{\nu}$ ($q = d, s$; $\ell = e, \mu, \tau$), precision QCD tests etc. We focus on some additional topics, such as weak decays of charmonium states in Sec. 6.2.1, and rare radiative and rare leptonic decays of D mesons in Sec. 6.2.2.

2. Processes that are *forbidden* in the SM *at tree level*.

Processes that involve flavor-changing neutral current (FCNC) interactions that change charm quantum number by one or two units do not occur in the SM at tree level. However, these transitions can happen in the SM at loop levels, which makes them rare. Such processes can receive NP contributions from both tree-level interactions mediated by new interactions, and loop corrections with NP particles. Inclusive and exclusive transitions mediated by $c \rightarrow u\gamma$ or $c \rightarrow u\ell\bar{\ell}$ will be discussed

in Sec. 6.2.2. Searches for violation of CP and other symmetries in baryon decays and in $D^0\bar{D}^0$ mixing will be discussed in Sec. 6.3. Charged lepton flavor violation decays will be discussed in Sec. 6.4.

3. Processes that are *forbidden* in the SM.

Some processes, while allowed by space-time symmetries, are forbidden in the SM. Even if allowed by NP, searching for these signatures require high statistics. Their observation, however, would constitute a high-impact discovery, as it would unambiguously point towards physics beyond the SM. Examples include searches for the baryon number-violating transitions as discussed in Sec. 6.3.2 and Sec. 6.3.3, lepton number violating decays as covered in Sec. 6.4.4. Many well-motivated NP models predict the existence of light, weakly-interacting particles. Since such light particles are not part of the SM particle spectrum, the corresponding processes do not occur in the SM. Such processes involving invisible signatures are discussed in Sec. 6.5. Some further searches at the off-resonance energies, where the electron and positron are not tuned to the s -channel resonance production of the charmonium states, are discussed in Sec. 6.6.

With the accumulation of large data sets and possible increase of luminosity and cms energy, as well as an ever-improving understanding of the detector performance, BESIII will have great potential in NP searches in the coming years.

6.2 Rare decays of charmonia and charmed hadrons

Experiments at the energy frontier may be able to probe NP through direct production of new particles. These new degrees of freedom could affect low energy observables. Experiments at the intensity frontier can probe those new virtual contributions via decays of charmonia and charmed hadrons, making them complementary to direct searches at the energy frontier.

6.2.1 Weak decays of charmonia states

The decays of $\psi(nS)$ ($n = 1, 2$) below the open-charm threshold are dominated by the strong or electromagnetic interactions where the intermediate gluons or virtual photons are produced by $c\bar{c}$ annihilation. However, flavor-changing weak decays of these states through virtual W bosons are also possible in the SM framework. For instance, the branching fractions of J/ψ inclusive weak decays are estimated to be of the order of 10^{-10} [2]. As mentioned in Refs. [3–6], the branching fractions of $J/\psi \rightarrow D(\bar{D})X$ (with X denoting any hadrons) can be enhanced by new interactions. Several NP models, such as the top-color model, the minimal supersymmetric standard model (MSSM) with R -parity violation and a general two-Higgs doublet model (2HDM), allow $\psi(nS)$ flavor-changing processes to occur with branching fractions around 10^{-6} [3, 4]. The observation of an anomalous production rate in $\psi(nS)$ weak decays would be a strong hint of NP.

With the newly accumulated 10^{10} J/ψ events, we expect to improve the branching fraction measurements of $\psi(nS)$ weak decays, including both hadronic and semi-leptonic

Table 6.1: Predicted branching fractions and expected sensitivities with a sample of 10^{10} J/ψ events of two-body hadronic weak decays of $J/\psi \rightarrow D_{(s)}P, D_{(s)}V$ and $D_{(s)}^*V$.

	Decay type	Example	exp. sensitivity ($\times 10^{-6}$)	predicted \mathcal{B} [7–10] ($\times 10^{-10}$)
$c \rightarrow s$	$D_{(s)}P$	$J/\psi \rightarrow D_s^- \pi^+$	9.9	2.00 \sim 8.74
		$J/\psi \rightarrow D^0 K^0$	13.0	0.36 \sim 2.80
	$D_{(s)}V$	$J/\psi \rightarrow D_s^- \rho^+$	2.0	12.60 \sim 50.50
		$J/\psi \rightarrow D^0 K^{*0}$	0.38	1.54 \sim 10.27
	$D_{(s)}^*V$	$J/\psi \rightarrow D_s^{*-} \rho^+$	1.7	52.60
$c \rightarrow d$	$D_{(s)}P$	$J/\psi \rightarrow D_s^- K^+$	9.8	0.16 \sim 0.55
		$J/\psi \rightarrow D^- \pi^+$	0.21	0.08 \sim 0.55
		$J/\psi \rightarrow D^0 \eta$	0.72	0.016 \sim 0.070
		$J/\psi \rightarrow D^0 \eta'$	0.25	0.003 \sim 0.004
		$J/\psi \rightarrow D^0 \pi^0$	0.48	0.024 \sim 0.055
	$D_{(s)}V$	$J/\psi \rightarrow D_s^- K^{*+}$	5.4	0.82 \sim 2.79
		$J/\psi \rightarrow D^- \rho^+$	0.35	0.42 \sim 2.20
		$J/\psi \rightarrow D^0 \rho^0$	0.77	0.18 \sim 0.22
		$J/\psi \rightarrow D^0 \omega$	0.35	0.16 \sim 0.18
		$J/\psi \rightarrow D^0 \phi$	0.22	0.41 \sim 0.65
	$D_{(s)}^*V$	$J/\psi \rightarrow D_s^{*-} K^{*+}$	4.5	2.6
		$J/\psi \rightarrow D_s^{*-} \rho^+$	0.083	2.8
		$J/\psi \rightarrow D^{*-} K^{*+}$	0.027	9.6

weak decays, by almost one order of magnitude, which will provide a more stringent experimental test of the SM than previous searches, and hence further constrain the parameter spaces of NP models. These weak decays can also be searched for in the expected 3×10^9 $\psi(3686)$ events

$\psi(nS) \rightarrow D_{(s)}P/D_{(s)}V/D_{(s)}^*V$

Several theoretical calculations of the branching fractions of two-body hadronic weak decays of $J/\psi \rightarrow D_{(s)}P/D_{(s)}V/D_{(s)}^*V$, where D represents a charmed meson, P and V a pseudoscalar and vector meson, respectively, are summarized in the last column of Table 6.1. The charge conjugate states are implicitly included.

The BESII experiment searched for the hadronic decays $J/\psi \rightarrow D_s^- \pi^+$, $J/\psi \rightarrow D^- \pi^+$, and $J/\psi \rightarrow D^0 K^0$ and set upper limits at the order of $10^{-4} \sim 10^{-5}$ using a sample of 5.8×10^7 J/ψ events [11]. BESIII has searched for the rare decays $J/\psi \rightarrow D_s^- \rho^+$ and $J/\psi \rightarrow D^0 K^{*0}$ with a sample of 2.25×10^8 J/ψ events [12]. No signal was observed, and upper limits at the 90% C.L. were set on the branching fractions, $\mathcal{B}(J/\psi \rightarrow D_s^- \rho^+) < 1.3 \times 10^{-5}$ and $\mathcal{B}(J/\psi \rightarrow D^0 K^{*0}) < 2.5 \times 10^{-6}$. These results are several orders of magnitude above the SM predictions and can be improved with larger data sets. The expected sensitivity with a sample of 10^{10} J/ψ events are estimated as listed in the third

column of Table 6.1.

$$\psi(nS) \rightarrow D_{(s)}l^+\nu/D_{(s)}^*l^+\nu$$

Semi-leptonic decays of $\psi(nS)$ mesons are induced by weak $c \rightarrow s$ or $c \rightarrow d$ transitions through a virtual intermediate W boson. Theoretical calculations predict the branching fractions of $J/\psi \rightarrow D_s^{(*)}l^+\nu$ and $J/\psi \rightarrow D^{(*)}l^+\nu$ to be at the level of 10^{-9} and 10^{-10} , respectively, by using QCD sum rules [8], the covariant light-front quark model [9], and the covariant constituent quark model [13]. It is therefore interesting to search for semi-leptonic weak decays of $\psi(nS)$ states in high intensity and low background experiments.

The BESII experiment searched for several semi-leptonic weak decays of the J/ψ . Using 5.8×10^7 J/ψ decay events, the upper limits at the 90% C.L. for $\mathcal{B}(J/\psi \rightarrow D_s^- e^+ \nu)$ and $\mathcal{B}(J/\psi \rightarrow D^- e^+ \nu)$ were found to be 3.6×10^{-5} and 1.2×10^{-5} , respectively [14]. BESIII has searched for the decay $J/\psi \rightarrow D_s^- e^+ \nu / D_s^{*-} e^+ \nu$ with a much higher sensitivity than previous analyses, based on a sample of 2.25×10^8 J/ψ events [15]. At the 90% C.L., the upper limits were determined to be $\mathcal{B}(J/\psi \rightarrow D_s^- e^+ \nu) < 1.3 \times 10^{-6}$ and $\mathcal{B}(J/\psi \rightarrow D_s^{*-} e^+ \nu) < 1.8 \times 10^{-6}$. Both are consistent with SM predictions, but can be improved with more data.

$$\psi(nS) \rightarrow D^{(*)0}l^+l^-/D^{(*)0}\gamma$$

The rates of $c \rightarrow u$ transitions of $\psi(nS)$ are predicted to be tiny in the SM [3, 16]. However, some NP scenarios allow for larger FCNC transition rates. For example, Ref. [3] argues that the branching fraction of $J/\psi \rightarrow DX_u$ (with X_u denoting mesons containing the u quark), which is mediated by the $c \rightarrow u$ quark transition, could be enhanced to be of order $10^{-6} - 10^{-5}$. Thus, an observation of FCNC in the low-lying charmonium decays would indicate NP.

In practice, it is difficult to isolate pure $c \rightarrow u$ mediated transitions from $c \rightarrow s$ and $c \rightarrow d$ in hadronic weak decays of the type $\psi(nS) \rightarrow D^{(*)}X_u$. Instead, theoretically (relatively) clean semi-leptonic or radiative rare decays $\psi(nS) \rightarrow D^{(*)0}l^+l^-$ and $\psi(nS) \rightarrow D^{(*)0}\gamma$ should be employed. The energy distributions of the final state photons or lepton pairs could be used as kinematic constraints to identify those decays.

6.2.2 Rare radiative and rare leptonic $D_{(s)}$ decays

The decays of D mesons that are mediated by quark-level FCNC transitions $c \rightarrow u\gamma$ (rare radiative) and $c \rightarrow u\ell\ell'$ (rare leptonic and semi-leptonic) only proceed at one loop in the SM. The absence of a super-heavy down-type quark in the SM implies that Glashow-Iliopoulos-Maiani cancellation mechanism is very effective, making the charm sector of special interest in probing for NP. The predicted short-distance (SD) contributions of the SM for FCNC in the charm sector are well beyond the sensitivity of current experiments. Yet, theoretical estimates suggest that the rates for FCNC processes could be enhanced by long-distance (LD) effects by several orders of magnitude.

There are a number of interesting FCNC processes in the charm sector. Such examples include $D \rightarrow h(h')\ell\ell'$ and $D \rightarrow h\nu\bar{\nu}$, where h represents light hadron states and ℓ is a charged lepton. Such decays could be interesting probes of NP, especially in light of

renewed interest to lepton flavor universality (LFU) studies in B decays. While SM interactions in general respect LFU, recent experimental observations (see, *e.g.*, [17]) show hints of LFU violation in rare semi-leptonic decays of B mesons. Theoretically, such violation could come from new lepton-flavor non-universal interactions [18], which might also be detectable in D -decays [19]. Such interactions might also induce lepton-flavor violating effects [20] (see section 6.4), although this depends on a particular model of NP.

Even though the charm production rate in e^+e^- collisions near the charm threshold is lower than that at hadron colliders and B -factories, BESIII has the benefit of lower multiplicity and the ability to impose powerful kinematic constraints, which can deliver high purity for final states with invisible energy or photons.

Rare radiative decays (such as $D \rightarrow \rho\gamma$) are most likely dominated by the LD SM contributions, which are quite difficult to compute [21–23]. Yet, there are opportunities to study NP effects in rare radiative transitions. These include a possibility that NP dominates the SM signal at least in portions of the available phase space [24], using particular combinations of radiative transitions [25], including CP-violating asymmetries [26, 27], or studying the photon’s polarization patterns [28] that could be more sensitive to NP contributions.

Two-body rare decays with charged leptons

The simplest rare leptonic decays, such as $D^0 \rightarrow \ell^+\ell^-$, have a very small SM contribution (both SD and LD ones), so they are potentially very clean probes of NP amplitudes. In this section we shall concentrate on the lepton-flavor conserving decays.

Experimentally, at present, there are only upper limits on $D^0 \rightarrow \ell^+\ell^-$ decays [29]. Theoretically, all possible NP contributions to $c \rightarrow u\ell^+\ell^-$ can be summarized in an effective Hamiltonian,

$$\mathcal{H}_{NP}^{rare} = \sum_{i=1}^{10} \tilde{C}_i(\mu) \tilde{Q}_i, \quad (6.1)$$

where \tilde{C}_i are Wilson coefficients, and the \tilde{Q}_i are the effective operators. In this case, there are ten of them,

$$\begin{aligned} \tilde{Q}_1 &= (\bar{\ell}_L \gamma_\mu \ell_L) (\bar{u}_L \gamma^\mu c_L), & \tilde{Q}_4 &= (\bar{\ell}_R \ell_L) (\bar{u}_R c_L), \\ \tilde{Q}_2 &= (\bar{\ell}_L \gamma_\mu \ell_L) (\bar{u}_R \gamma^\mu c_R), & \tilde{Q}_5 &= (\bar{\ell}_R \sigma_{\mu\nu} \ell_L) (\bar{u}_R \sigma^{\mu\nu} c_L), \\ \tilde{Q}_3 &= (\bar{\ell}_L \ell_R) (\bar{u}_R c_L), \end{aligned} \quad (6.2)$$

with five additional operators $\tilde{Q}_6, \dots, \tilde{Q}_{10}$ that can be obtained from operators in Eq. (6.2) by the substitutions $L \rightarrow R$ and $R \rightarrow L$. It is worth noting that only eight operators contribute to $D^0 \rightarrow \ell^+\ell^-$, as $\langle \ell^+\ell^- | \tilde{Q}_5 | D^0 \rangle = \langle \ell^+\ell^- | \tilde{Q}_{10} | D^0 \rangle = 0$. The most general $D^0 \rightarrow \ell^+\ell^-$ decay amplitude can be written as

$$\mathcal{M} = \bar{u}(\mathbf{p}_-, s_-) [A + B\gamma_5] v(\mathbf{p}_+, s_+) , \quad (6.3)$$

which results in the branching fractions

$$\mathcal{B}_{D^0 \rightarrow \ell^+\ell^-} = \frac{M_D}{8\pi\Gamma_D} \sqrt{1 - \frac{4m_\ell^2}{M_D^2}} \left[\left(1 - \frac{4m_\ell^2}{M_D^2}\right) |A|^2 + |B|^2 \right] . \quad (6.4)$$

Any NP contribution described by the operators of Eq. (6.2) gives for the amplitudes A and B ,

$$\begin{aligned} |A| &= G \frac{f_D M_D^2}{4m_c} \left[\tilde{C}_{3-8} + \tilde{C}_{4-9} \right], \\ |B| &= G \frac{f_D}{4} \left[2m_\ell \left(\tilde{C}_{1-2} + \tilde{C}_{6-7} \right) + \frac{M_D^2}{m_c} \left(\tilde{C}_{4-3} + \tilde{C}_{9-8} \right) \right], \end{aligned} \quad (6.5)$$

with $\tilde{C}_{i-k} \equiv \tilde{C}_i - \tilde{C}_k$. Any NP model that contributes to $D^0 \rightarrow \ell^+ \ell^-$ can be constrained from the constraints on the Wilson coefficients in Eq. (6.5). It will be advantageous to study *correlations* of various processes to isolate and constrain the NP contributions [30, 31]. Such correlations exist, for instance, in $D^0 \bar{D}^0$ mixing and rare decays [30]. In general, one cannot predict the rare decay rate by knowing just the mixing rate, even if both x_D and $\mathcal{B}_{D^0 \rightarrow \ell^+ \ell^-}$ are dominated by a given NP contribution. It is, however, possible for a restricted subset of NP models [30]. Predictions for $D^0 \rightarrow \mu^+ \mu^-$ branching fraction for $x_D \sim 1\%$ can be found in Ref. [30] with the definitions of NP model parameters.

Table 6.2: The latest experimental upper limits on branching fractions (in units of 10^{-6}) for the rare D and D_s decays into $h(h')e^+e^-$. The expected BESIII sensitivities with the expected final charm data set listed in Sec. 7 are also shown in the last column.

Decay	Upper limit	Experiment	Year	Ref.	BESIII Expected
$D^0 \rightarrow \pi^0 e^+ e^-$	0.4	BESIII	2018	[35]	0.1
$D^0 \rightarrow \eta e^+ e^-$	0.3	BESIII	2018	[35]	0.1
$D^0 \rightarrow \omega e^+ e^-$	0.6	BESIII	2018	[35]	0.2
$D^0 \rightarrow K_S^0 e^+ e^-$	1.2	BESIII	2018	[35]	0.5
$D^0 \rightarrow \rho e^+ e^-$	124.0	E791	2001	[36]	0.5
$D^0 \rightarrow \phi e^+ e^-$	59.0	E791	2001	[36]	0.5
$D^0 \rightarrow \bar{K}^{*0} e^+ e^-$	47.0	E791	2001	[36]	0.5
$D^0 \rightarrow \pi^+ \pi^- e^+ e^-$	0.7	BESIII	2018	[35]	0.3
$D^0 \rightarrow K^+ K^- e^+ e^-$	1.1	BESIII	2018	[35]	0.4
$D^0 \rightarrow K^- \pi^+ e^+ e^-$	4.1	BESIII	2018	[35]	1.6
$D^+ \rightarrow \pi^+ e^+ e^-$	1.1	BaBar	2011	[37]	0.12
$D^+ \rightarrow K^+ e^+ e^-$	1.0	BaBar	2011	[37]	0.46
$D^+ \rightarrow \pi^+ \pi^0 e^+ e^-$	1.4	BESIII	2018	[35]	0.5
$D^+ \rightarrow \pi^+ K_S^0 e^+ e^-$	2.6	BESIII	2018	[35]	1.0
$D^+ \rightarrow K_S^0 K^+ e^+ e^-$	1.1	BESIII	2018	[35]	0.4
$D^+ \rightarrow K^+ \pi^0 e^+ e^-$	1.5	BESIII	2018	[35]	0.6
$D_s^+ \rightarrow \pi^+ e^+ e^-$	13.0	BaBar	2011	[37]	70.0
$D_s^+ \rightarrow K^+ e^+ e^-$	3.7	BaBar	2011	[37]	1.7

Three-body rare decays with charged leptons

Theoretical predictions of the decay rates of di-lepton modes such as $D \rightarrow h(h')e^+e^-$ are complicated due to the LD contributions. The rates with a lepton-pair mass in the non-resonant regions could provide access to NP [31–34], at least for some particular BSM models. Table 6.2 shows some interesting $D \rightarrow h(h')e^+e^-$ modes that can be studied at the BESIII experiment, and the corresponding experimental upper limits on the branching fractions are also summarized. Recent BESIII paper [35] has already improved some of the limits by several orders of magnitude. With more data in future, we expect to improve these limits and some new modes could also be probed, depending on how background-free a given mode is. The expected BESIII sensitivities with the expected final charm data set listed in Sec. 7 are also shown in the last column of Table 6.2.

Three-body rare decays with neutrinos

Neutral modes, such as $D^0 \rightarrow \pi^0\nu\bar{\nu}$, have never been studied at charm threshold before. It is possible that the LD SM effects are under better theoretical control in such transitions [23]. Belle reported a similar search for the rare decays $B \rightarrow h^{(*)}\nu\bar{\nu}$ [38], and BaBar searched for $B^0 \rightarrow \gamma\nu\bar{\nu}$ [39]. With 20fb^{-1} data sample at $\sqrt{s} = 3.773\text{GeV}$, BESIII's sensitivity of $\mathcal{B}(D^0 \rightarrow \pi^0\nu\bar{\nu})$ measurement could reach 10^{-4} or better.

Radiative decay modes $D^0 \rightarrow \gamma\nu\bar{\nu}$ serve as physics background to searches for light Dark Matter (DM), as described in Sec. 6.5.1. This transition has an unobservable small branching fraction of $\mathcal{B}(D^0 \rightarrow \gamma\nu\bar{\nu}) = 3.96 \times 10^{-14}$ in the SM [40], making the final state of a photon with missing energy a suitable topology for searches for light DM at BESIII.

6.3 Symmetry test in hyperon decays

The Sakharov conditions for baryogenesis underline the role of CP violation as one of the central pieces of the matter-antimatter asymmetry puzzle [41]. However, the CKM mechanism for CP violation in the SM fails to fully explain the puzzle of the matter-antimatter asymmetry by more than 10 orders-of-magnitude [42]. This suggests that additional, heretofore undiscovered, CP violating processes exist, and has motivated aggressive searches for new sources of CP violation in b -quark decays and neutrino oscillations [43]. CP violation in charm decay is very small and had not yet been found until the discovery in 2019 at LHCb. LHCb finds non-zero CP violation in $D^0 \rightarrow \pi^+\pi^-$ and $D^0 \rightarrow K^+K^-$ decays with a significance of 5.3σ . The time-integrated CP asymmetry is given as

$$\begin{aligned} \Delta a_{\text{CP}} &= \frac{\Gamma(D \rightarrow K^+K^-) - \Gamma(\bar{D} \rightarrow K^+K^-)}{\Gamma(D \rightarrow K^+K^-) + \Gamma(\bar{D} \rightarrow K^+K^-)} - \frac{\Gamma(D \rightarrow \pi^+\pi^-) - \Gamma(\bar{D} \rightarrow \pi^+\pi^-)}{\Gamma(D \rightarrow \pi^+\pi^-) + \Gamma(\bar{D} \rightarrow \pi^+\pi^-)} \\ &= (-0.154 \pm 0.029)\%, \end{aligned} \quad (6.6)$$

where $D(\bar{D})$ is a $D^0(\bar{D}^0)$ at time $t=0$ [44]. This result is at the high end of theoretical estimates for its SM value, which ranges from 10^{-4} to 10^{-3} . The LHCb result is intriguing, because it may be a sign of the long-sought-for-non-SM mechanism for CP violation.

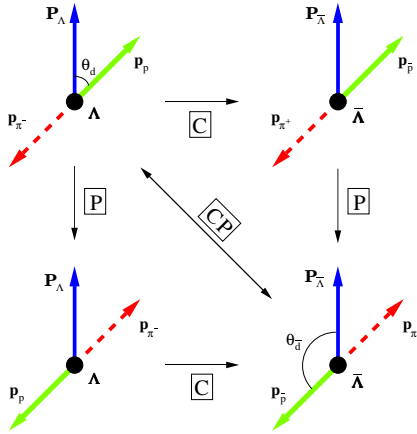


Figure 6.1: Illustration of the charge (C), parity (P) and CP transformation on the $\Lambda \rightarrow p\pi^-$ decays

However, uncertainties in SM theoretical calculations for Δa_{CP} make it impossible to rule out this possibility. BESIII's current $10^{-3} \sim 10^{-2}$ level of sensitivity on charm meson CP violation is still more than one order of magnitude above the highest conceivable SM effects. In addition to charmed mesons, BESIII has accumulated huge data samples of strange and charmed baryons, thus providing a unique opportunity to examine the strong dynamics of strange/charm decays, and another route to probe the phenomenon of CP violation. In this section we will briefly discuss strange/charm baryon decays and outline various paths to the observation of CP violation and baryon number violation (BNV).

6.3.1 Probing CP asymmetry in hyperon decays

BESIII has capability for testing CP symmetry in hyperon decays, produced via $J/\psi \rightarrow B\bar{B}$ with $B\bar{B}$ denoting polarized, quantum-entangled hyperon pairs, which adds an exciting new dimension to the study of CP violations.

A weak two-body decay of a spin one-half baryon under charge and parity transformations is illustrated in Fig. 6.1 for the most prominent decay mode of $\Lambda \rightarrow p\pi^-$. The picture is drawn in the Λ rest frame and the spin polarization vector \mathbf{P}_Λ is pointing upward. The daughter proton emitted at angles θ_d and ϕ_d with respect to the polarization vector \mathbf{P}_Λ is transformed under CP into an anti-proton emitted at angles $\pi - \theta_d$ and $-\phi_d$ with respect to the polarization vector of the parent $\bar{\Lambda}$. In addition, in the weak decay the polarization of the final proton could have a transverse component (along the $\mathbf{p}_p \times \mathbf{p}_\Lambda$ vector). This component for the antiproton will have opposite direction.

Direct CP asymmetry

The most straightforward CP-odd observable is the difference between the partial decay rates for the decay and the CP-transformed process:

$$\Delta = \frac{\Gamma - \bar{\Gamma}}{\Gamma + \bar{\Gamma}}. \quad (6.7)$$

Furthermore, the parity violation in the hyperon decays allows much more sensitive tests to be constructed. A $1/2 \rightarrow 1/2 + 0$ two-body nonleptonic weak decay can be described by the partial width Γ and decay parameters α , β , γ :

$$\alpha = \frac{2\text{Re}(S^*P)}{|S|^2 + |P|^2}, \quad \beta = \frac{2\text{Im}(S^*P)}{|S|^2 + |P|^2} = \sqrt{1 - \alpha^2} \sin \phi, \quad \gamma = \sqrt{1 - \alpha^2} \cos \phi. \quad (6.8)$$

Only two parameters are independent and it is convenient to use α and ϕ . The parameter α has a simple interpretation due to the asymmetry of the angular distribution for the daughter proton, as given by

$$\frac{d\Gamma}{d\Omega_d} \propto \frac{1}{4\pi} (1 + \alpha P_\Lambda \cos \theta_d). \quad (6.9)$$

A comparison of the decay parameters of a hyperon and the anti-hyperon leads to sensitive tests of CP symmetry. The CP-odd observables are

$$A = \frac{\alpha + \bar{\alpha}}{\alpha - \bar{\alpha}}, \quad B = \frac{\beta + \bar{\beta}}{\beta - \bar{\beta}}. \quad (6.10)$$

Here α corresponds to α_- in the $\Lambda \rightarrow p\pi^-$ decay, while $\bar{\alpha}$ corresponds to α_+ in the $\bar{\Lambda} \rightarrow \bar{p}\pi^+$ decay; and the quantity β can not be measured in the joint $J/\psi \rightarrow \Lambda\bar{\Lambda} \rightarrow p\pi^-\bar{p}\pi^+$ decay. In general, sensitivity of these asymmetries to CP violation scales as $\Delta : A : B \sim 1 : 10 : 100$. The asymmetry A has been studied in $\bar{p}p$ experiments and at e^+e^- colliders [45–48]. The present world average is $A = 0.006 \pm 0.021$, while the CKM mechanism predicts a value of $A \sim 10^{-5} - 10^{-4}$ [49–51]. Predictions in scenarios beyond the SM are given in Refs. [52–54]. There also exist dynamical calculations in Refs. [55, 56]. Experimental prospects on CP-symmetry tests for the charmed baryon by determination of α are discussed in Ref. [57].

At BESIII, J/ψ mesons are produced in the annihilation of unpolarized electron-positron beams and therefore the spin-density matrix of the J/ψ depends only on the scattering angle θ_Λ between the electron beam direction and the Λ momentum in the reaction cms system. The helicity frames to describe the subsequent decay chains are shown in Fig. 6.2.

The coherent production of $\Lambda/\bar{\Lambda}$ pairs from the decay $J/\psi \rightarrow \Lambda\bar{\Lambda}$ with subsequent weak decays of the Λ and $\bar{\Lambda}$ is a very simple spin-entangled quantum system where the final state is specified by four real parameters summarized in Table 6.3.

A recent BESIII study with 1.3×10^9 J/ψ events has observed a transverse spin polarization of $\Lambda/\bar{\Lambda}$ and the phase between the hadronic form factors has been determined [58]. The polarization effect is illustrated by dividing the data sample into 50 $\cos \theta_\Lambda$ bins and plotting the $\cos \theta_\Lambda$ dependence of the moment $\mu(\cos \theta_\Lambda) = 1/N \sum_i^{N(\theta_\Lambda)} (\sin \theta_1^i \sin \phi_1^i - \sin \theta_2^i \sin \phi_2^i)$, where N is the total number of events in the data sample and $N(\theta_\Lambda)$ is the number of events in a $\cos \theta_\Lambda$ bin. This dependence enables us to extract simultaneously

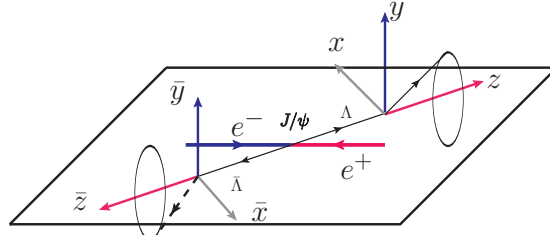
Figure 6.2: Definition of the helicity frames for $J/\psi \rightarrow \Lambda \bar{\Lambda} \rightarrow p\pi^- \bar{p}\pi^+$.

Table 6.3: List of kinematic variables (helicity angles) and parameters used in the analysis of the decay chain.

Decay	Coordinate system	Helicity angles	Parameters
$J/\psi \rightarrow \Lambda \bar{\Lambda}$	cms	$(\theta_\Lambda, \phi_\Lambda)$	$\alpha_\psi, \Delta\Phi$
$\Lambda \rightarrow p\pi^-$	(x, y, z)	(θ_1, ϕ_1)	α_-
$\bar{\Lambda} \rightarrow \bar{p}\pi^+$	$(\bar{x}, \bar{y}, \bar{z})$	(θ_2, ϕ_2)	α_+

$\alpha_- = 0.750 \pm 0.009 \pm 0.004$ and $\alpha_+ = -0.758 \pm 0.010 \pm 0.007$ and calculate the most precise value for A of $-0.006 \pm 0.012 \pm 0.007$, where in the propagation of the statistical uncertainty a large value of the correlation coefficient $\rho(\alpha_+, \alpha_-) = 0.82$ is included.

New BESIII data of 10^{10} J/ψ events will enable an improved measurement of the parameter A . In the future measurement the systematic uncertainty will be significantly improved since this simple system permits several internal consistency checks to be performed. In the general case of two spin one-half particles we have 16 polarization and spin correlation distributions to be fully described by only four global parameters. In addition, the use of other monitoring and calibration channels allows independent corrections for any bias to be determined. In addition, if a similar polarization is observed also for other hyperons then similar studies will be possible, *e.g.*, for the Ξ hyperon with its cascade decays B asymmetry tests would be possible.

The triple-product asymmetry

Apart from the above mentioned direct measurement, we can also exploit the triple-product asymmetry as a CP-violating observable. Studies of CP violation in Λ and other hyperon decays using this approach are proposed in Ref. [59]. The direct CP-violating asymmetry \mathcal{A}_{dir} and the triple-product asymmetry \mathcal{A}_{T} depend on the weak phase ϕ and the strong-phase δ as follows:

$$\begin{aligned} \mathcal{A}_{\text{dir}} &\propto \sin \phi \sin \delta, \\ \mathcal{A}_{\text{T}} &\propto \sin \phi \cos \delta. \end{aligned} \quad (6.11)$$

The direct asymmetry only survives if there is a non-zero strong phase, whereas the triple-product asymmetry with the strong phase vanishes. Therefore the two methods are

complementary, particularly if the strong phase is unknown.

The triple product is defined as $\vec{v}_1 \cdot (\vec{v}_2 \times \vec{v}_3)$, where \vec{v} can be a three-momentum or a spin vector. Under time reversal the triple product changes sign, and thus it is a T -violating signal. But final-state interactions (FSI) can give a false CP-violation signal. As a result, one must compare the channel to its conjugate. For an illustration of this point, one may refer to Refs. [60, 61]. Such considerations have led to a corresponding proposal for BESIII [62, 63], as well as in beauty decays [64–68], and in the search for NP effects [69, 70].

We illustrate the method with the process $e^+e^- \rightarrow J/\psi \rightarrow \Lambda\bar{\Lambda} \rightarrow [p\pi^-][\bar{p}\pi^+]$ below. This process is transformed to itself under charge conjugation. Since the polarization of the proton and the antiproton is not measured, we have four independent vectors to construct triple products. Two of them are \mathbf{k} and \mathbf{p}_Λ – the three-momenta of incoming electron and outgoing Λ in the reaction cms frame. The remaining ones are \mathbf{q}_1 and \mathbf{q}_2 – the momenta of the proton and antiproton in the Λ and $\bar{\Lambda}$ rest frames, respectively. For example, defining $C_T = (\mathbf{p}_\Lambda \times \mathbf{q}_1) \cdot \mathbf{p}_\Lambda$, and $\bar{C}_T = -(\mathbf{p}_\Lambda \times \mathbf{q}_2) \cdot \mathbf{p}_\Lambda$, we can define following triple-product asymmetries

$$\langle A_T \rangle = \frac{N(C_T > 0) - N(C_T < 0)}{N(C_T > 0) + N(C_T < 0)} \quad (6.12)$$

$$\langle \bar{A}_T \rangle = \frac{N(-\bar{C}_T > 0) - N(-\bar{C}_T < 0)}{N(-\bar{C}_T > 0) + N(-\bar{C}_T < 0)}. \quad (6.13)$$

Therefore CPT invariance implies

$$\mathcal{A}_T = \langle A_T \rangle - \langle \bar{A}_T \rangle \neq 0 \quad (6.14)$$

is a CP-odd observable, which can be measured merely through event counting. Another triple product is $(\mathbf{q}_1 \times \mathbf{q}_2) \cdot \mathbf{p}_\Lambda$, related to the $C_{x\bar{z}} - C_{z\bar{x}}$ spin correlation term. This last triple product allows limits on the Λ electric-dipole moment d_Λ to be improved, as discussed in Refs. [71, 72].

The CP asymmetries can also be studied locally as a function of the kinematic variable $\cos\theta_\Lambda$, limiting the range of the triple-product values:

$$\mathcal{A}_T(d) = \frac{N(C_T > |d|) - N(C_T < -|d|)}{N(C_T > |d|) + N(C_T < -|d|)}. \quad (6.15)$$

By considering the efficiency of the BESIII detector, the number of observed events and the corresponding statistical error for various channels are estimated. The expected sensitivity with the 10^{10} J/ψ events is shown in Table 6.4.

A wide range of CP tests in hyperon sector can also be performed in a single measurement of the spin entangled Ξ - $\bar{\Xi}$ system [73]. From the joint distributions for $e^+e^- \rightarrow \Xi\bar{\Xi}$, it shows that the role of the transverse polarization is fully replaced by the diagonal spin correlations between the cascades. All decay parameters can be determined simultaneously and the statistical uncertainties do not depend on the size of the transverse polarization in the production process. The BESIII sensitivities are shown in Table 6.5 with correlations between parameters considered. The results practically do not change between the

Table 6.4: The number of reconstructed events after considering the decay branching fractions, tracking and particle identification with 10^{10} J/ψ events. The sensitivity is estimated without considering the possible background dilution, which is small at BESIII. Systematic uncertainties are expected to be of the same order as the statistical ones.

Channel	Number of events	Sensitivity on \mathcal{A}_T
$J/\psi \rightarrow \Lambda\bar{\Lambda} \rightarrow [p\pi^-][\bar{p}\pi^+]$	2.6×10^6	0.06%
$J/\psi \rightarrow \Sigma^+\bar{\Sigma}^- \rightarrow [p\pi^0][\bar{p}\pi^0]$	2.5×10^6	0.06%
$J/\psi \rightarrow \Xi^0\bar{\Xi}^0 \rightarrow [\Lambda\pi^-][\bar{\Lambda}\pi^+]$	1.1×10^6	0.1%
$J/\psi \rightarrow \Xi^-\bar{\Xi}^+ \rightarrow [\Lambda\pi^0][\bar{\Lambda}\pi^0]$	1.6×10^6	0.08%

Table 6.5: The BESIII sensitivities, which are presented as the estimated uncertainties multiplied by the square root of the observed signal yields, in the the spin entangled $\Xi^-\bar{\Xi}^+$ system for the extracted parameters. Errors for the parameters of the charge conjugated decay modes are the same. The input values of the Ξ parameters have only minor effect on the sensitivities.

	α_Ξ	α_Λ	ϕ_Ξ	α_ψ	$\Delta\Phi$	$\langle\alpha_\Xi\rangle$	A_Ξ	$\langle\alpha_\Lambda\rangle$	A_Λ	$\langle\alpha_\Xi\alpha_\Lambda\rangle$	$A_{\Xi\Lambda}$	$\langle\phi_\Xi\rangle$	B_Ξ
$J/\psi \rightarrow \Xi^-\bar{\Xi}^+ (\Delta\Phi = 0)$	2.0	3.1	5.8	3.5	6.0	1.4	3.7	1.7	3.5	0.78	4.0	4.1	110
$J/\psi \rightarrow \Xi^-\bar{\Xi}^+ (\Delta\Phi = \pi/2)$	1.9	2.8	5.4	3.0	13	1.4	3.5	1.6	3.1	0.76	3.9	3.8	100
$e^+e^- \rightarrow \Xi^-\bar{\Xi}^+ (\alpha_\psi = 1)$	1.9	2.7	5.0	–	–	1.3	3.4	1.4	3.1	0.76	4.0	3.5	96
$\eta_c, \chi_{c0} \rightarrow \Xi^-\bar{\Xi}^+$	1.6	2.2	3.7	–	–	1.1	2.9	1.0	2.6	0.72	3.9	2.6	71

two extreme cases: $\Delta\Phi = 0$ and $\pi/2$. The results for other decays: $\psi(3686) \rightarrow \Xi^-\bar{\Xi}^+$ and $J/\psi, \psi(3686) \rightarrow \Xi^0\bar{\Xi}^0$ are similar. Also shown are the results for the $e^+e^- \rightarrow \Xi^-\bar{\Xi}^+$ asymptotic case with $\alpha_\psi = 0$ and for a scalar charmonium decay to $\Xi\bar{\Xi}$. Contrary to $e^+e^- \rightarrow \Lambda\bar{\Lambda}$, the polarization in the production process plays practically no role. The weak decay phases ϕ_Ξ and $\phi_{\bar{\Xi}}$ are not correlated with each other and with any other parameters.

6.3.2 Constraint on BNV from $\Lambda - \bar{\Lambda}$ oscillation

The stability of ordinary matter implies baryon number (B) conservation. However, the observed fact of baryon asymmetry in the Universe shows that baryon number should be broken. There are many theoretical models in which B is not exactly conserved, with B and lepton number (L) violated simultaneously while conserving $B - L$.

It was pointed out long ago [74] that a crucial test of baryon number violation are neutron-antineutron ($n-\bar{n}$) oscillations, and many corresponding experiments have been conducted [43]. If $n-\bar{n}$ oscillation exists, $\Lambda-\bar{\Lambda}$ oscillations may also take place [75]. There is a proposal to search for $\Lambda-\bar{\Lambda}$ oscillations in the decay of $J/\psi \rightarrow \Lambda\bar{\Lambda}$ [76]. Until now, however, there has not been any direct experimental searches for this process.

At BESIII, the decay of $J/\psi \rightarrow pK^-\bar{\Lambda}$ has a very simple final state and is almost background free, so it is well suited for searching for $\Lambda - \bar{\Lambda}$ oscillations. Initially, J/ψ decays into $pK^-\bar{\Lambda}$ final state (defined as a right-sign event, as $\bar{\Lambda} \rightarrow \bar{p}\pi^+$ is detected along with pK^-), and then, with some $\bar{\Lambda}$ oscillating into Λ , the final state becomes $pK^-\Lambda$

(defined as a wrong-sign event, as $\Lambda \rightarrow p\pi^-$ is detected with pK^-), so the probability of generating a final Λ from an initial $\bar{\Lambda}$ can be determined by the ratio of wrong sign events over right sign events.

The time evolution of the Λ - $\bar{\Lambda}$ oscillation can be described [76] by a Schroedinger-like equation,

$$i \frac{\partial}{\partial t} \begin{pmatrix} \Lambda(t) \\ \bar{\Lambda}(t) \end{pmatrix} = M \begin{pmatrix} \Lambda(t) \\ \bar{\Lambda}(t) \end{pmatrix},$$

where the matrix M is Hermitian,

$$M = \begin{pmatrix} m_\Lambda - \Delta E_\Lambda & \delta m_{\Lambda\bar{\Lambda}} \\ \delta m_{\Lambda\bar{\Lambda}} & m_{\bar{\Lambda}} - \Delta E_{\bar{\Lambda}} \end{pmatrix},$$

and $\delta m_{\Lambda\bar{\Lambda}}$ is the $\Delta B = 2$ oscillation parameter due to some NP effect, m_Λ ($m_{\bar{\Lambda}}$) is the mass of the Λ ($\bar{\Lambda}$) baryon, and ΔE is the energy split due to an external magnetic field. For an unbound Λ propagating in a vacuum without an external field, both ΔE_Λ and $\Delta E_{\bar{\Lambda}}$ are zero.

Starting with a beam of free Λ particles, the probability $P(\bar{\Lambda}, t)$ of generating a $\bar{\Lambda}$ after traveling some time t , is given by

$$P(\bar{\Lambda}, t) = \sin^2(\delta m_{\Lambda\bar{\Lambda}} \cdot t).$$

BESIII can measure the time integral of the probability, *i.e.*, the oscillation rate, by

$$P(\bar{\Lambda}) = \frac{\int_0^{T_{\max}} \sin^2(\delta m_{\Lambda\bar{\Lambda}} \cdot t) \cdot e^{-t/\tau_\Lambda} \cdot dt}{\int_0^\infty e^{-t/\tau_\Lambda} \cdot dt},$$

where $P(\bar{\Lambda})$ is the time-integrated probability of $\Lambda \rightarrow \bar{\Lambda}$, τ_Λ is the lifetime of the Λ baryon, and T_{\max} is the maximum flight time. If we assume T_{\max} is large enough in the BESIII tracking system, the oscillation parameter can be deduced as

$$\delta m_{\Lambda\bar{\Lambda}} = \sqrt{\frac{P(\bar{\Lambda})}{2 \cdot (\tau_\Lambda/\hbar)^2}}.$$

With the recently-accumulated data sample of 10^{10} J/ψ events, the upper limit of the Λ - $\bar{\Lambda}$ oscillation rate will be at 10^{-6} level (90% C.L.) based on the analysis of $J/\psi \rightarrow pK^- \bar{\Lambda}$ events, and the constraint on $\delta m_{\Lambda\bar{\Lambda}}$ will be reduced to 10^{-16} MeV (90% CL). On the other hand, a time-dependent analysis of the produced Λ - $\bar{\Lambda}$ pairs from the J/ψ decays can be investigated, taking advantage of their long mean flight distance of 7.6 cm in the detector. So BESIII will provide a very stringent constraint on NP in this channel.

6.3.3 More symmetry violation in hyperon decays

Since BESIII has a rather large hyperon data set, Λ 's from hyperons can also be used to study symmetry violations and search for NP, as was recently summarized in a nice review [77]. Here we reproduce the summary table (Table 6.6) showing lepton or baryon-number violating hyperon decays and their expected sensitivities with future BESIII data sets. More information can be found in the original paper [77].

Table 6.6: Lepton or baryon number violating hyperon decays and expected sensitivities with 10^{10} events on the J/ψ peak and 3×10^9 events on the $\psi(3686)$ peak. The current J/ψ data are from CLAS as listed in PDG. “-” indicates “not available”, $l = e$ or μ , and M^\pm refers to the charged stable mesons ($M^\pm = \pi^\pm$ or K^\pm). Each reaction shows evidence of $\Delta L = \pm 1$ or/and $\Delta B \neq 0$, and each reaction conserves electric charge and angular momentum [77].

Decay mode	Current data $\mathcal{B} (\times 10^{-6})$	Expected BESIII $\mathcal{B} (\times 10^{-6})$ (at the 90% C.L.)	ΔL	ΔB
$\Lambda \rightarrow M^+ l^-$	$< 0.4 \sim 3.0$	< 0.1	+1	-1
$\Lambda \rightarrow M^- l^+$	$< 0.4 \sim 3.0$	< 0.1	-1	-1
$\Lambda \rightarrow K_S^0 \nu$	< 20	< 0.6	+1	-1
$\Sigma^+ \rightarrow K_S^0 l^+$	-	< 0.2	-1	-1
$\Sigma^- \rightarrow K_S^0 l^-$	-	< 1.0	+1	-1
$\Xi^- \rightarrow K_S^0 l^-$	-	< 0.2	+1	-1
$\Xi^0 \rightarrow M^+ l^-$	-	< 0.1	+1	-1
$\Xi^0 \rightarrow M^- l^+$	-	< 0.1	-1	-1
$\Xi^0 \rightarrow K_S^0 \nu$	-	< 2.0	+1	-1

6.4 Charged Lepton Flavor (Number) Violation decays

Charged Lepton Flavor Violation (CLFV) processes are highly suppressed in the SM by finite but tiny neutrino masses. Their branching fractions are predicted to be negligibly small – and no such reactions have been observed. Yet, there are various theoretical models that predict the rates for CLFV transitions to be large enough to be experimentally observable. Examples include SUSY grand unified theories [78], SUSY with a right-handed neutrino [79], gauge-mediated SUSY breaking [80], SUSY with vector-like leptons [81], SUSY with R -parity violation [82], models with Z' [83], or models with Lorentz non-invariance [84]. While the discovery of neutrino oscillations has confirmed the existence of neutrino masses and LFV in the neutral lepton sector, detection of LFV in the charged lepton sector would provide direct evidence for NP.

Experimentally, searches for CLFV effects have been carried out in a variety of ways, including decays of leptons, pseudoscalar, and vector mesons, as well as in other processes. In the charmonium system, BESII obtained a limit $\mathcal{B}(J/\psi \rightarrow e\mu) < 1.1 \times 10^{-6}$ [85] by analyzing a data sample of 58 million J/ψ events. BESIII has so far analyzed 255 million J/ψ decays. Four events have been observed, which is consistent with background estimate. As a result, BESIII set the upper limit of $\mathcal{B}(J/\psi \rightarrow e\mu) < 1.6 \times 10^{-7}$ at the 90% C.L. [86], which is currently the best upper limit on CLFV in charmonium decays. BESII also placed bounds on $\mathcal{B}(J/\psi \rightarrow \mu\tau) < 2. \times 10^{-6}$ and $\mathcal{B}(J/\psi \rightarrow e\tau) < 8.3 \times 10^{-6}$ [87]. The limits on these decay channels will be updated at BESIII with the data set that includes 10^{10} J/ψ decays, so orders of magnitude improvement is expected.

CLFV and lepton-number-violating (LNV) processes can also be probed in D -meson

decays at BESIII. No evidence has been found for the D -meson decays with either CLFV or LNV. The present experimental bounds on the branching fractions are generally set at the level of 10^{-6} to 10^{-5} (with a notable exception of $D^0 \rightarrow \mu e$, where $\mathcal{B}(D^0 \rightarrow \mu^\pm e^\mp) < 1.3 \times 10^{-8}$) [88]. D decays with LNV, such as $D^+ \rightarrow l^+ l^+ X^-$ and $D_s^+ \rightarrow l^+ l^+ X^-$, are also forbidden in the minimal SM, but are possible if massive neutrinos are Majorana particles.

However, for CLFV processes such as $D^0 \rightarrow l^+ l'^-$ and $D^0 \rightarrow l^+ l'^- X$, LHCb will dominate the searches even if BESIII increases the available data set of D -meson decays by an order of magnitude in the future. On the other hand, BESIII has some potential to search for LNV transitions such as $D^+ \rightarrow l^+ l^+ X^-$ and $D_s^+ \rightarrow l^+ l^+ X^-$, due to the clean environment and low charge confusion rates.

Effective Lagrangian and NP models

NP models probed at BESIII include those predicting lepton-flavor violating interactions. They can be probed in decays to flavor-non-diagonal combination of final state leptons $\ell_i = e, \mu, \tau$. Due to a multitude of NP models contributing to CLFV processes, it is advantageous to introduce an effective Lagrangian that economically encodes all of these NP models. The details of the models are encoded in Wilson coefficients, while quark-lepton dynamical effects are described in a set of CLFV operators.

The effective Lagrangian \mathcal{L}_{eff} that involves CLFV can in general be written as

$$\mathcal{L}_{\text{eff}} = \mathcal{L}_{\ell q} + \mathcal{L}_D + \mathcal{L}_G + \dots, \quad (6.16)$$

where \mathcal{L}_D is a dipole part, $\mathcal{L}_{\ell q}$ is the part that contains four-fermion interactions, and \mathcal{L}_G is a gluonic part [89, 90].

The dipole part \mathcal{L}_D has been extremely well constrained in purely leptonic CLFV decays of the type $\ell_1 \rightarrow \ell_2 \gamma$ [91, 92]. It appears that any possible contributions from \mathcal{L}_D to charmed particle decays would be four-to-six orders of magnitude smaller than the ones from other sectors of \mathcal{L}_{eff} , so it will be neglected in the following discussion [89].

The four-fermion dimension-six lepton-quark part of the effective Lagrangian, Eq. (6.16) is [91]

$$\begin{aligned} \mathcal{L}_{\ell q} = & -\frac{1}{\Lambda^2} \sum_{q=u,c} \left[\left(C_{VR}^{qcl_1\ell_2} \bar{\ell}_1 \gamma^\mu P_R \ell_2 + C_{VL}^{qcl_1\ell_2} \bar{\ell}_1 \gamma^\mu P_L \ell_2 \right) \bar{q} \gamma_\mu c \right. \\ & + \left(C_{AR}^{qcl_1\ell_2} \bar{\ell}_1 \gamma^\mu P_R \ell_2 + C_{AL}^{qcl_1\ell_2} \bar{\ell}_1 \gamma^\mu P_L \ell_2 \right) \bar{q} \gamma_\mu \gamma_5 c \\ & + m_2 m_c G_F \left(C_{SR}^{qcl_1\ell_2} \bar{\ell}_1 P_L \ell_2 + C_{SL}^{qcl_1\ell_2} \bar{\ell}_1 P_R \ell_2 \right) \bar{q} c \\ & + m_2 m_c G_F \left(C_{PR}^{qcl_1\ell_2} \bar{\ell}_1 P_L \ell_2 + C_{PL}^{qcl_1\ell_2} \bar{\ell}_1 P_R \ell_2 \right) \bar{q} \gamma_5 c \\ & \left. + m_2 m_c G_F \left(C_{TR}^{qcl_1\ell_2} \bar{\ell}_1 \sigma^{\mu\nu} P_L \ell_2 + C_{TL}^{qcl_1\ell_2} \bar{\ell}_1 \sigma^{\mu\nu} P_R \ell_2 \right) \bar{q} \sigma_{\mu\nu} c + h.c. \right]. \end{aligned} \quad (6.17)$$

Here $P_{R,L} = (1 \pm \gamma_5)/2$ is the right (left) chiral projection operator. In general the Wilson coefficients would be different for different lepton flavors ℓ_i and quark flavors $q = u, c$. This implies that decays of charmonium states and D -mesons probe different terms (and different models of NP) in the effective CLFV Lagrangian.

The dimension seven gluonic operators in \mathcal{L}_G appear for flavor-diagonal quark transitions, *i.e.*, for $q = c$ [90, 93],

$$\begin{aligned} \mathcal{L}_G = & -\frac{m_2 G_F}{\Lambda^2} \frac{\beta_L}{4\alpha_s} \left[\left(C_{GR}^{\ell_1 \ell_2} \bar{\ell}_1 P_L \ell_2 + C_{GL}^{\ell_1 \ell_2} \bar{\ell}_1 P_R \ell_2 \right) G_{\mu\nu}^a G^{a\mu\nu} \right. \\ & \left. + \left(C_{GR}^{\ell_1 \ell_2} \bar{\ell}_1 P_L \ell_2 + C_{GL}^{\ell_1 \ell_2} \bar{\ell}_1 P_R \ell_2 \right) G_{\mu\nu}^a \tilde{G}^{a\mu\nu} + h.c. \right]. \end{aligned} \quad (6.18)$$

Here $\beta_L = -9\alpha_s^2/(2\pi)$ is defined for the number of light active flavors, L , relevant to the scale of the process, for which we take $\mu \approx 2$ GeV. All Wilson coefficients should also be calculated at the same scale. G_F is the Fermi constant and $\tilde{G}^{a\mu\nu} = (1/2)\epsilon^{\mu\nu\alpha\beta} G_{\alpha\beta}^a$ is a dual to the gluon field strength tensor.

Each term in Eqs. (6.17-6.18) can be separately probed in two-body decays of charmonium states with different J^{PC} and D -mesons, as their constrained kinematics only selects operators with particular quantum numbers. As will be shown below, $J/\psi \rightarrow \bar{\ell}_1 \ell_2$ decays select vector and tensor operators, while $\chi_c \rightarrow \bar{\ell}_1 \ell_2$ and $\eta_c \rightarrow \bar{\ell}_1 \ell_2$ only select scalar and pseudoscalar/axial operators in Eq. (6.17).

6.4.1 Decays of $J/\psi, \psi(3686) \rightarrow l_1 l_2, l_1 l_2 \gamma$

Experimental constraints on $J/\psi \rightarrow l_1 l_2$ branching fractions can be effectively converted to bounds on Wilson coefficients of vector and tensor operators in Eq. (6.17). Those Wilson coefficients can then be related to model parameters of explicit realizations of possible UV completions of the effective Lagrangian in Eq. (6.16). Examples of particular new physics models include Z' scenarios [94], R-parity violating supersymmetric models [95–97], and other approaches [98, 99].

The most general expression for the J/ψ (or any $\psi(nS)$) $\rightarrow l_1 \bar{l}_2$ decay amplitude can be written as

$$\begin{aligned} \mathcal{A}(V \rightarrow l_1 \bar{l}_2) = & \bar{u}(p_1, s_1) \left[A_V^{\ell_1 \ell_2} \gamma_\mu + B_V^{\ell_1 \ell_2} \gamma_\mu \gamma_5 + \frac{C_V^{\ell_1 \ell_2}}{m_V} (p_2 - p_1)_\mu \right. \\ & \left. + \frac{i D_V^{\ell_1 \ell_2}}{m_V} (p_2 - p_1)_\mu \gamma_5 \right] v(p_2, s_2) \epsilon^\mu(p), \end{aligned} \quad (6.19)$$

where $V = J/\psi$ or $\psi(3686)$, and $A_V^{\ell_1 \ell_2}$, $B_V^{\ell_1 \ell_2}$, $C_V^{\ell_1 \ell_2}$, and $D_V^{\ell_1 \ell_2}$ are dimensionless constants which depend on the underlying Wilson coefficients of the effective Lagrangian of Eq. (6.17) as well as on hadronic effects associated with meson-to-vacuum matrix elements or decay constants. We shall neglect dipole and tensor operator contributions, which implies that $C_V^{\ell_1 \ell_2} = D_V^{\ell_1 \ell_2} = 0$ [89]. The branching fractions of the vector ψ states are calculated from Eq. (6.19), which yield the ratio

$$\frac{\mathcal{B}(\psi \rightarrow l_1 \bar{l}_2)}{\mathcal{B}(\psi \rightarrow e^+ e^-)} = \left(\frac{m_V (1 - y^2)}{4\pi\alpha_f \psi Q_q} \right)^2 \left[|A_V^{\ell_1 \ell_2}|^2 + |B_V^{\ell_1 \ell_2}|^2 \right]. \quad (6.20)$$

Here α is the fine structure constant, $Q_c = 2/3$ is the charge of the c -quark, the mass of the lighter of the two leptons has been neglected, and $y = m_2/m_V$. The coefficients $A_V^{\ell_1 \ell_2}$

Table 6.7: Current [89] and future BESIII constraints on $\mathcal{B}(J/\psi \rightarrow \ell_1 \ell_2)$. The projections with CC and MVA methods provide the conservative and aggressive estimations, respectively.

$\ell_1 \ell_2$	$\mu\tau$	$e\tau$	$e\mu$
Current upper limit	2.0×10^{-6}	8.3×10^{-6}	1.6×10^{-7}
BESIII projected (CC)	3.0×10^{-8}	4.5×10^{-8}	1.0×10^{-8}
BESIII projected (MVA)	1.5×10^{-8}	2.5×10^{-8}	6.0×10^{-9}

and $B_V^{\ell_1 \ell_2}$ depend on the initial state meson,

$$\begin{aligned} A_V^{\ell_1 \ell_2} &= \frac{f_V m_V}{2\Lambda^2} (C_{VL}^{cc\ell_1 \ell_2} + C_{VR}^{cc\ell_1 \ell_2}), \\ B_V^{\ell_1 \ell_2} &= -\frac{f_V m_V}{2\Lambda^2} (C_{VL}^{cc\ell_1 \ell_2} - C_{VR}^{cc\ell_1 \ell_2}). \end{aligned} \quad (6.21)$$

The constraints on the Wilson coefficients also depend on the meson decay constants,

$$\langle 0 | \bar{q} \gamma^\mu q | V(p) \rangle = f_V m_V \epsilon^\mu(p), \quad (6.22)$$

where $\epsilon^\mu(p)$ is the V -meson polarization vector, and p is its momentum [100]. The decay constants are $f_{J/\psi} = 418 \pm 9$ MeV and $f_{\psi(3686)} = 294 \pm 5$ MeV. They are both known experimentally from leptonic decays and theoretically from lattice or QCD sum rule calculations.

Experimentally, there is an ongoing analysis based on an existing data set of 1.3×10^9 J/ψ decays. In this study the selection efficiencies for both $J/\psi \rightarrow \mu\tau$ and $J/\psi \rightarrow e\tau$ are around 14%. Based on the same Cut and Count (CC) analysis technique, with the assumption of similar efficiencies, we can make a projection of future BESIII sensitivity in this channel. By constructing cocktail samples from the 1.3×10^9 data set, and then performing toy MC (pseudo-experiment) studies, the sensitivity with 10^{10} J/ψ events is evaluated. The 90% C.L. upper limits on the numbers of signal events are estimated according to the recoiled τ mass distributions. With 10^{10} J/ψ decays, the projected sensitivities of the two channels are estimated to be both at 10^{-8} level. Such results would represent an improvement of almost two orders of magnitudes compared to those obtained at BESII. The systematic uncertainties have also been estimated, and are expected to be sub-dominant even for this very large sample. With more advanced analysis techniques such as multivariate analyses (MVA), the efficiencies could be increased with decreased background levels which results in even better sensitivities. The current and future BESIII constraints on $\mathcal{B}(J/\psi \rightarrow \ell_1 \ell_2)$ are summarized in Table 6.7. Based on these projections, the resulting constraints on the combination of Wilson coefficients and NP scale Λ , both current and projected, can be found in Table 6.8.

A promising approach for increasing the sensitivity of J/ψ decays to CLFV operators is to consider radiative charged lepton-flavor violating (RCLFV) transitions. The addition of a photon to the final state certainly reduces the number of the events available for studies of CLFV decays. However, the data set of J/ψ 's accumulated by BESIII is huge, and this requirement also makes it possible for other operators in \mathcal{L}_{eff} to contribute. Since

Table 6.8: Constraints on the Wilson coefficients of four-fermion operators. Note that the constraints on the right-handed couplings ($L \rightarrow R$) are the same. “–” means that no constraints are currently available, “FPS” means that the decay is forbidden by phase space, and “N/A” means that BESIII sensitivity studies are yet to be performed. Current constraints are from [89].

Wilson coeff (GeV^{-2})	Leptons	Constraints	
	$\ell_1\ell_2$	Current	Projected
$ C_{VL}^{cc\ell_1\ell_2}/\Lambda^2 $	$\mu\tau$	5.5×10^{-5}	$[5.0, 7.1] \times 10^{-6}$
	$e\tau$	1.1×10^{-4}	$[6.5, 8.7] \times 10^{-6}$
	$e\mu$	1.0×10^{-5}	$[2.8, 3.7] \times 10^{-6}$
$ C_{AL}^{cc\ell_1\ell_2}/\Lambda^2 $	$\mu\tau$	–	7.4×10^{-4}
	$e\tau$	–	7.4×10^{-4}
	$e\mu$	–	N/A
$ C_{SL}^{cc\ell_1\ell_2}/\Lambda^2 $	$\mu\tau$	–	2.0
	$e\tau$	–	2.0
	$e\mu$	–	N/A
$ C_{AL}^{u\ell_1\ell_2}/\Lambda^2 $	$\mu\tau$	FPS	FPS
	$e\tau$	–	N/A
	$e\mu$	1.3×10^{-8}	2.2×10^{-8}

the final state kinematics is less constrained than in two-body decays, the constraints on the Wilson coefficients of the effective Lagrangian would depend on a set of $V \rightarrow \gamma$ form factors that are not very well known [89]. To place meaningful constraints on the Wilson coefficients from non-resonance J/ψ RCLFV decays one would need to employ the single-operator dominance hypothesis, *i.e.*, assume that only one operator contributes at a time. For the axial, scalar, and pseudoscalar operators one has [89]

$$\begin{aligned}
\Gamma_A(J/\psi \rightarrow \gamma\ell_1\bar{\ell}_2) &= \frac{1}{18} \frac{\alpha Q_q^2 f_V^2 m_V^3}{(4\pi)^2 \Lambda^4} \left[(C_{AL}^{cc\ell_1\ell_2})^2 + (C_{AR}^{cc\ell_1\ell_2})^2 \right], \\
\Gamma_S(J/\psi \rightarrow \gamma\ell_1\bar{\ell}_2) &= \frac{1}{144} \frac{\alpha Q_q^2 f_V^2 G_F^2 m_V^7}{(4\pi)^2 \Lambda^4} \left[(C_{SL}^{cc\ell_1\ell_2})^2 + (C_{SR}^{cc\ell_1\ell_2})^2 \right] y^2, \\
\Gamma_P(J/\psi \rightarrow \gamma\ell_1\bar{\ell}_2) &= \frac{1}{144} \frac{\alpha Q_q^2 f_V^2 G_F^2 m_V^7}{(4\pi)^2 \Lambda^4} \left[(C_{PL}^{cc\ell_1\ell_2})^2 + (C_{PR}^{cc\ell_1\ell_2})^2 \right] y^2.
\end{aligned} \tag{6.23}$$

The $J/\psi \rightarrow \gamma e\mu$ channel is experimentally challenging at BESIII, so we focus on $J/\psi \rightarrow \gamma\mu\tau$ and $J/\psi \rightarrow \gamma e\tau$, where there is an ongoing analysis involving the current data set. If MVA were to be used, the efficiency would be about 35% for both channels. There is no detailed projection yet, but the sensitivity to branching fractions could then reach $(1-3) \times 10^{-8}$.

6.4.2 $\chi_c(\eta_c) \rightarrow l_1 l_2$ via photon tagging in $\psi(3686) \rightarrow \gamma \chi_c(\eta_c)$

Similarly to probing operators with vector quantum numbers, as described in Sec. 6.4.1, the scalar and pseudoscalar operators in Eq. (6.17) can be probed in decays of scalar and pseudoscalar charmonia. Although these states are not produced directly in e^+e^- collisions, they can be studied in the radiative decays of vector charmonia [89]. Since at resonance

$$\mathcal{B}(V \rightarrow \gamma l_1 \bar{l}_2) = \mathcal{B}(V \rightarrow \gamma M) \mathcal{B}(M \rightarrow l_1 \bar{l}_2), \quad (6.24)$$

states with large $\mathcal{B}(V \rightarrow \gamma M)$ can be used to probe $\mathcal{B}(M \rightarrow l_1 \bar{l}_2)$ [89]. An example includes

$$\begin{aligned} \mathcal{B}(\psi(3686) \rightarrow \gamma \chi_{c0}) &= (9.99 \pm 0.27)\% , \\ \mathcal{B}(\psi(3770) \rightarrow \gamma \chi_{c0}) &= (0.73 \pm 0.09)\% , \end{aligned}$$

for probing scalar operators in the decays of the scalar states $M = \chi_c$. BESIII will have the highest sensitivity in the $\psi(3686) \rightarrow \gamma \chi_{c0}$, and $\chi_{c0} \rightarrow \mu\tau$ and $\chi_{c0} \rightarrow e\tau$ decay channels. It is estimated that the efficiency in $\mathcal{B}(\psi(3686) \rightarrow \gamma \chi_{c0})$ could reach about 10%.

If BESIII could collect a data set with about 3×10^9 $\psi(3686)$ events, the sensitivity for $\chi_{c0} \rightarrow \mu\tau$ and $\chi_{c0} \rightarrow e\tau$ could reach $(1 - 3) \times 10^{-7}$. Similarly,

$$\begin{aligned} \mathcal{B}(J/\psi \rightarrow \gamma \eta_c) &= (1.7 \pm 0.4)\% , \\ \mathcal{B}(\psi(3686) \rightarrow \gamma \eta_c) &= (0.34 \pm 0.05)\% , \end{aligned}$$

for the pseudoscalar state $M = \eta_c$. BESIII will be sensitive to $J/\psi \rightarrow \gamma \eta_c$, $\eta_c \rightarrow \mu\tau$ and $\eta_c \rightarrow e\tau$ decay channels. With 10^{10} J/ψ events and a detection efficiency of 10%, the sensitivity to $\eta_c \rightarrow \mu\tau$ and $\eta_c \rightarrow e\tau$ could reach $(2 - 5) \times 10^{-7}$.

It must be pointed out that in both χ_{c0} and η_c cases the decay to $e\mu$ is more challenging, as both the level and complexity of backgrounds are expected to be higher. It nevertheless is still possible to probe these decay channels with the final BESIII data set, although a separate dedicated analysis is needed. Here it is expected that BESIII will be able to probe decay branching fractions at the level of 10^{-7} as well.

The most general expressions for scalar and pseudoscalar decays $M \rightarrow l_1 \bar{l}_2$ are both

$$\mathcal{A}(M \rightarrow l_1 \bar{l}_2) = \bar{u}(p_1, s_1) [E_M^{\ell_1 \ell_2} + iF_M^{\ell_1 \ell_2} \gamma_5] v(p_2, s_2), \quad (6.25)$$

with $E_M^{\ell_1 \ell_2}$ and $F_M^{\ell_1 \ell_2}$ being dimensionless constants for scalar $M = \chi_c$ or pseudoscalar $M = \eta_c$ decay amplitudes, which depend on the Wilson coefficients of operators in Eq. (6.17) and decay constants. The corresponding branching fraction is

$$\mathcal{B}(M \rightarrow l_1 \bar{l}_2) = \frac{m_M}{8\pi\Gamma_M} (1 - y^2)^2 \left[|E_M^{\ell_1 \ell_2}|^2 + |F_M^{\ell_1 \ell_2}|^2 \right]. \quad (6.26)$$

Here Γ_M is the total width of the decaying state and $y = m_2/m_M$. The generic expressions for the coefficients $E_M^{\ell_1 \ell_2}$ and $F_M^{\ell_1 \ell_2}$ for the pseudoscalar $M = P$ and scalar $M = S$ states are given in [89]. We can simplify them by neglecting the contributions from gluonic operators of Eq. (6.18), as η_c and χ_c are not expected to contain large gluonic components in their

wave functions. The Wilson coefficients of the gluonic operators are better probed in CLFV tau decays, where the low energy theorems [93] or experimental data [90] constrain gluonic matrix elements in a model-independent manner.

With this, $P = \eta_c$ CLFV decays will be mainly sensitive to axial operator contributions in $\mathcal{L}_{\ell q}$ of Eq. (6.17) [89],

$$\begin{aligned} E_P^{\ell_1 \ell_2} &= y \frac{m_P}{4\Lambda^2} \left[-i f_P \left[2 (C_{AL}^{ccl_1 \ell_2} + C_{AR}^{ccl_1 \ell_2}) - m_P^2 G_F (C_{PL}^{ccl_1 \ell_2} + C_{PR}^{ccl_1 \ell_2}) \right] \right], \\ F_P^{\ell_1 \ell_2} &= -y \frac{m_P}{4\Lambda^2} \left[f_P \left[2 (C_{AL}^{ccl_1 \ell_2} - C_{AR}^{ccl_1 \ell_2}) - m_P^2 G_F (C_{PL}^{ccl_1 \ell_2} - C_{PR}^{ccl_1 \ell_2}) \right] \right], \end{aligned} \quad (6.27)$$

while scalar $S = \chi_c$ CLFV decays will uniquely probe scalar CLFV operators of Eq. (6.17),

$$\begin{aligned} E_S^{\ell_1 \ell_2} &= i y f_S m_c \frac{m_S^2 G_F}{2\Lambda^2} (C_{SL}^{ccl_1 \ell_2} + C_{SR}^{ccl_1 \ell_2}), \\ F_S^{\ell_1 \ell_2} &= y f_S m_c \frac{m_S^2 G_F}{2\Lambda^2} (C_{SL}^{ccl_1 \ell_2} - C_{SR}^{ccl_1 \ell_2}), \end{aligned} \quad (6.28)$$

where the decay constants are $f_{\eta_c} = (387 \pm 7)$ MeV [100], and $f_{\chi_c} \approx 887$ MeV [101], for the pseudoscalar and scalar states, respectively. The resulting constraints on the combination of Wilson coefficients and NP scale Λ , both current and projected, can be found in Table 6.8.

6.4.3 (radiative) Leptonic decays of $D^0 \rightarrow l_1 l_2, \gamma l_1 l_2$

Studies of lepton flavor violation can also be performed with D^0 decays into $l_1 l_2$ and $\gamma l_1 l_2$ final states. These decays involve FCNC transitions in both quark and lepton currents, so the set of effective operators tested is given in Eq. (6.17) for $q = u$. We should emphasize that they are different from the operators discussed in Sects. 6.4.1 and 6.4.2, although particular NP models could give contributions to both sets of operators, in which case the Wilson coefficients of Eq. (6.17) for $q = c$ and $q = u$ would depend on different parameters of the same NP model.

As D -mesons are pseudoscalar states, the branching fraction for flavor off-diagonal leptonic decays of D -mesons is given by Eq. (6.26) with $M \rightarrow D$, so Γ_D is the total width of the D^0 . Calculating the form factors $E_D^{ucl_1 \ell_2}$ and $F_D^{ucl_1 \ell_2}$ for \bar{D}^0 ($q_1 q_2 = cu$) states yields [91]

$$\begin{aligned} E_D^{q_1 q_2 \ell_1 \ell_2} &= \frac{m_D f_D y}{2\Lambda^2} \left[(C_{AL}^{ucl_1 \ell_2} + C_{AR}^{ucl_1 \ell_2}) + m_D^2 G_F (C_{PL}^{q_1 q_2 \ell_1 \ell_2} + C_{PR}^{q_1 q_2 \ell_1 \ell_2}) \right], \\ F_D^{q_1 q_2 \ell_1 \ell_2} &= i \frac{m_D f_D y}{2\Lambda^2} \left[(C_{AL}^{ucl_1 \ell_2} - C_{AR}^{q_1 q_2 \ell_1 \ell_2}) + m_D^2 G_F (C_{PL}^{ucl_1 \ell_2} - C_{PR}^{ucl_1 \ell_2}) \right], \end{aligned} \quad (6.29)$$

where $f_D = 207.4 \pm 3.8$ MeV is the D -meson decay constant.

The resulting constraints on the combination of Wilson coefficients and NP scale Λ , both current and projected, can be found in Table 6.8. One should note that other operators can be probed in D -decays. To access those, one can consider three-body decays of a D -meson into $\gamma l_1 l_2$ [91] or semileptonic CLFV decays. While increasing the

reach of experiments, it also complicates theoretical interpretation of bounds, forcing one to introduce additional hypotheses, such as single-operator dominance, as well as model dependence. Using the results in Ref. [91], a set of constraints on CLFV operators can be obtained. If BESIII could take about 20 fb^{-1} data at the $\psi(3770)$, the sensitivity for $D^0 \rightarrow \gamma e \mu$ could reach $(5 - 10) \times 10^{-7}$.

6.4.4 CLFV and LNV $D_{(s)}$ decays with light mesons

CLFV searches can include decays with light mesons in the final states, such as $D \rightarrow \pi \ell_1 \ell_2$ or $D_s \rightarrow K \ell_1 \ell_2$. A clear advantage in using those transitions can be seen in that both charged and neutral D -mesons can be used for analyses. Disadvantages include, just as in $D \rightarrow \gamma \ell_1 \ell_2$, difficulties with the theoretical interpretation of the experimental bounds (unless directly projected onto particular NP models) and increased model dependence of the bounds, as long-distance contributions become increasingly more pronounced.

Finally, lepton-number violating processes such as $D_{(s)}^+ \rightarrow \pi^-(K^-)\ell^+\ell^+$ can also be probed at BESIII. Especially, with 20 fb^{-1} of $\psi(3770)$ data, BESIII could improve the best upper limit to 4.6×10^{-7} and 2.3×10^{-7} for $D^+ \rightarrow \pi^- e^+ e^+$ and $D^+ \rightarrow K^- e^+ e^+$ respectively, extrapolated from the current analysis.

6.5 Searches for light (invisible) NP particles

Several well-motivated proposals of BSM physics include new degrees of freedom (DOF) that do not interact with the SM particles directly. Such DOFs constitute the so-called ‘‘Dark Sector’’. Particles that populate the Dark Sector could form a part or whole of the DM in our Universe. There are only a few interactions allowed by SM symmetries that provide a portal from the SM sector into the Dark Sector [102, 103]. Depending on the masses, such DM and portal DOFs could be probed at the low-energy high-intensity frontier experiments, such as BESIII.

6.5.1 Physics of the Dark Sector

The presence of cold DM in our Universe provides the most natural explanation for several observational puzzles. If DM has a particle origin, it should be eventually detected in particle physics experiments. In particular, if DM particles are light, with masses in the keV-MeV range, as suggested by our understanding of small-scale gravitational clustering in numerical simulations, they should be detectable in the decays of heavy meson states at BESIII. These DM particles could be fermions, scalars, or even vector bosons. In many models they are produced in pairs, as such models feature Z_2 symmetry requirements for writing Lagrangians with such particles.

In other models light new particles can be produced not only in pairs, but also individually, in which case they could serve the role of mediators (portals) between the Dark Sector and the SM. A particular motivation for such a scenario comes from the observations of anomalous fluxes of cosmic-ray positrons. In 2008, the PAMELA collaboration reported an excess of positrons above 10 GeV [104], which has now been confirmed by

many other experiments, such as ATIC [105], Fermi-LAT [106] and AMS02 [107]. In a class of models, DM particles with masses of $\mathcal{O}(\text{TeV})$ annihilate into a pair of light bosons with masses of $\mathcal{O}(\text{GeV})$, which subsequently decay into charged leptons [108, 109]. An exchange of light bosons would increase the dark-matter annihilation cross section, allowing the observations of anomalous cosmic-ray positrons to be explained. Moreover, if the mediator is light enough, no extra anti-proton will be produced due to the kinematics. This feature is consistent with the PAMELA antiprotons data. The light boson may be a massive dark photon in the models with an extra U(1) gauge symmetry.

The dark photon field V_μ couples to the SM photon A_μ through kinetic mixing [110],

$$\mathcal{L}_k = -\frac{\kappa}{2} V_{\mu\nu} F^{\mu\nu}, \quad (6.30)$$

where $V_{\mu\nu}$ is the dark photon's field tensor $V_{\mu\nu} = \partial_\mu V_\nu - \partial_\nu V_\mu$. Note that this construction is gauge-invariant. The dark photon can acquire a mass through the spontaneous symmetry breaking mechanism. Some models predict that the mass of the dark photon is at the scale from $\mathcal{O}(\text{MeV})$ to $\mathcal{O}(\text{GeV})$ [110, 111]. The kinetic mixing coupling κ is taken to be very small. Similarly to the case of neutral-meson mixing, the introduction of the term mixing A_μ and V_μ implies that neither of the fields is a mass eigenstate. Diagonalizing the Lagrangian [110, 112] introduces a small coupling g between the new, weakly-interacting vector field V'_μ , $g \approx \kappa e$, where e is the electric charge. Thus, dark photons can be searched for in the decays of charmed particles [112] and/or charmonia.

The structure of the Dark Sector can be complicated, possibly with a class of light particles including scalars, pseudo-scalars, gauge bosons and fermions at the GeV scale. Since the interaction between the Dark Sector and the SM sector is very weak, the constraints on the mixing parameter and dark photon mass mainly come from the intensity frontier, such as the measurements of electron and muon anomalous magnetic moments, low-energy electron-positron colliders, beam-dump experiments and fixed-target experiments [102, 103].

Light Dark Matter (LDM) with Z_2 symmetry

Let us consider, as an example, the generic case of a complex neutral scalar field χ_0 describing LDM. The discussion of other spin assignments of LDM and their effects in charm decays can be found in [40]. A generic effective Hamiltonian of lowest dimension describing $c \rightarrow u\chi_0^*\chi_0$ interactions is

$$\mathcal{H}_{eff}^{(s)} = 2 \sum_i \frac{C_i^{(s)}}{\Lambda^2} O_i, \quad (6.31)$$

where Λ is the scale associated with the particle(s) mediating interactions between the SM and LDM fields, and $C_i^{(s)}$ are the relevant Wilson coefficients of the operators

$$\begin{aligned} O_1 &= m_c (\bar{u}_R c_L) (\chi_0^* \chi_0), \\ O_2 &= m_c (\bar{u}_L c_R) (\chi_0^* \chi_0), \\ O_3 &= (\bar{u}_L \gamma^\mu c_L) (\chi_0^* \overleftrightarrow{\partial}_\mu \chi_0), \\ O_4 &= (\bar{u}_R \gamma^\mu c_R) (\chi_0^* \overleftrightarrow{\partial}_\mu \chi_0), \end{aligned} \quad (6.32)$$

where $\overleftrightarrow{\partial} = (\overrightarrow{\partial} - \overleftarrow{\partial})/2$, and χ_0^* is a conjugated state of χ_0 . Operators $O_{3,4}$ disappear for real scalar LDM, in which case $\chi_0^* = \chi_0$. It is implied in Eq. (6.32) that the mediator of interactions between LDM and the SM fields is heavy, $M_\Lambda > m_D$. The discussion can be modified for the case of a light mediator (see [40]).

The simplest decay that is mediated by Eq. (6.32) is the transition $D^0 \rightarrow \chi_0 \chi_0$, which could contribute to the invisible D -decay width,

$$\mathcal{B}(D^0 \rightarrow \chi_0 \chi_0) = \frac{(C_1^{(s)} - C_2^{(s)})^2}{4\pi M_D \Gamma_D} \left(\frac{f_D M_D^2 m_c}{\Lambda^2 (m_c + m_u)} \right)^2 \sqrt{1 - 4x_\chi^2}, \quad (6.33)$$

where $x_\chi = m_\chi/M_D$ is a rescaled LDM mass. Clearly, this rate is not helicity-suppressed, so it could be a quite sensitive tool to determine LDM properties at BESIII. Current experimental constraints imply that

$$\frac{(C_1^{(s)} - C_2^{(s)})^2}{\Lambda^2} \leq 8 \times 10^{-8}, \quad (6.34)$$

for $m_\chi \ll m_D$, which corresponds to probing scales of NP over 3.5 TeV. Those constraints could be improved with updated bounds on $D^0 \rightarrow$ invisible decays. The constraints obtained in Eq. (6.34) can be used in constraining parameters of particular models of light DM [40, 113].

Similarly, the decay width of the radiative decay $D^0 \rightarrow \chi_0^* \chi_0 \gamma$ can be computed,

$$\begin{aligned} \mathcal{B}(D^0 \rightarrow \chi_0^* \chi_0 \gamma) &= \frac{f_D^2 \alpha C_3^{(s)} C_4^{(s)} M_D^5}{6\Lambda^4 \Gamma_D} \left(\frac{F_D}{4\pi} \right)^2 \\ &\times \left(\frac{1}{6} \sqrt{1 - 4x_\chi^2} (1 - 16x_\chi^2 - 12x_\chi^4) - 12x_\chi^4 \log \frac{2x_\chi}{1 + \sqrt{1 - 4x_\chi^2}} \right). \end{aligned} \quad (6.35)$$

We observe that Eq. (6.35) does not depend on $C_{1,2}^{(s)}$. This can be most easily seen from the fact that the $D \rightarrow \gamma$ form factors of scalar and pseudoscalar currents are zero.

LDM without Z_2 symmetry

If DM particles are very light, in the keV-MeV range, they do not need to obey Z_2 symmetry, as their decays to pairs of SM states could be either suppressed kinematically or by small coupling. This implies that DM particles can be emitted and absorbed by SM particles. Due to their extremely small couplings to the SM particles, experimental searches for such light states require large sample sizes and the ability to resolve signals with missing energy. This means that BESIII is ideally suited for such searches. For example, such particles could be searched for in leptonic $D/D_s \rightarrow \ell \bar{\nu}$ decays, which are helicity-suppressed in the SM. Additional emission of a dark photon or an axion-like particle (ALP) a could lift the helicity suppression and change the energy spectrum of the lepton [112]. Similarly, flavor-changing transitions of the type $D \rightarrow a\pi$ resulting in a two-body-like spectrum of pions in $D \rightarrow \pi + \text{invisible}$ could become possible [114].

Searches for dark photons can be performed in the decays of the charmonium states. BESIII has the largest J/ψ data sample in the world. Associated production of dark photons with other Dark Sector particles, such as the dark Higgs h' , is also possible and has been studied [115, 116], provided that $m_{h'}$ is such that production of this state is not kinematically suppressed.

6.5.2 (radiative) Invisible decays of charmonia

Invisible decays of quarkonium states might provide a window into what may lie beyond the SM. In the SM the invisible decays of the J/ψ and other charmonium states are given by their decays into neutrino final states,

$$\frac{\Gamma(J/\psi \rightarrow \nu\bar{\nu})}{\Gamma(J/\psi \rightarrow e^+e^-)} = \frac{9N_\nu G_F^2}{256\pi^2\alpha^2} M_{J/\psi}^4 \left(1 - \frac{8}{3}\sin^2\theta_W\right)^2 \simeq 4.54 \times 10^{-7}, \quad (6.36)$$

where G_F is the Fermi coupling, θ_W is the weak mixing angle, and $N_\nu = 3$ is the number of light non-sterile neutrinos. It is interesting to note that this result is about three orders of magnitude smaller than the corresponding decay of an Upsilon state [117]. Similarly, the SM branching fraction of radiative decays of J/ψ 's with missing energy is also very tiny [118]. Thus, we may neglect neutrino-background effects when confronting theoretical predictions for J/ψ decays into invisible states with experimental data. This implies that invisible decays of charmonium states provide a great opportunity to search for the glimpses of BSM physics. In BSM scenarios the decay rate might be enhanced either by new heavy particles modifying the interactions of neutrinos and heavy quarks, or by opening new decay channels into light DM states.

It is therefore possible to use invisible decays of charmonium states to put constraints on various models of light DM, provided that DM states couple to charmed quarks [118–121]. Predictions for radiative decays with missing energy in light DM models are available in Ref. [122].

Due to its superb kinematic-reconstruction capabilities, BESIII can search for the invisible and radiative invisible decays of J/ψ and via decay chains $\psi(3686) \rightarrow \pi^+\pi^- J/\psi (\rightarrow \text{invisible})$ using $\pi^+\pi^-$ as a trigger, similar to the the invisible decay search of the $\Upsilon(1S)$ at BaBar [123]. With a data set of 3×10^9 $\psi(3686)$ events, the branching fraction of J/ψ invisible decay could be probed to 3×10^{-5} .

6.5.3 Invisible decays of D mesons

Decays of D mesons into invisible final states can also provide an excellent probe of light Dark Matter models. Similarly to Sect. 6.5.2, in the SM the invisible decays of D mesons are constituted by their decays into neutrino final states, which can be computed. A major difference between the heavy quarkonium and D decays into neutrinos includes long-distance effects, which are currently poorly known. However, they are not expected to dominate the short-distance (SD) estimates by many orders of magnitude. The SD contributions to the branching fractions for $D^0 \rightarrow \nu\bar{\nu}$ decays can be readily computed. One can immediately notice that the left-handed structure of the Hamiltonian should

result in helicity suppression of those transitions. Assuming for neutrino masses that $m_\nu \sim \sum_i m_{\nu_i} < 0.62$ eV [124], where m_{ν_i} is the mass of one of the neutrinos,

$$\mathcal{B}(D^0 \rightarrow \nu\bar{\nu}) = \frac{G_F^2 \alpha^2 f_D^2 m_D^3}{16\pi^3 \sin^4 \theta_W \Gamma_{D^0}} |V_{bc} V_{ub}^*|^2 X(x_b)^2 x_\nu^2 \simeq 1.1 \times 10^{-30}. \quad (6.37)$$

Here $x_\nu = m_\nu/m_D$ and $\Gamma_D = 1/\tau_D$ is the total width of the D^0 meson. Such tiny rates imply that decays of heavy mesons into neutrino-antineutrino final states in the SM can be safely neglected as sources of background in the searches for DM in D decays. Such helicity suppression in the final state can be overcome by adding a third particle, such as a photon, to the final state. In fact, the SM contribution to invisible width of a D -meson is dominated by D decays into a four-neutrino final state with a branching fraction of $\mathcal{B}(D^0 \rightarrow 4\nu) = (2.96 \pm 0.39) \times 10^{-27}$ [125]. The resulting branching fractions for $D^0 \rightarrow \gamma\nu\bar{\nu}$ are also larger than $D^0 \rightarrow \nu\bar{\nu}$ by orders of magnitude [40, 126].

The Belle collaboration has published a limit on the branching fraction of D decays to invisible final states, setting it at 9.4×10^{-5} at the 90% C.L. [127]. BESIII could improve this limit to the order of $10^{-6} \rightarrow 10^{-5}$ with the final charm data set. Many NP models predict much larger branching fractions of D -mesons into the light DM states than that of $D \rightarrow \nu\bar{\nu}$. This implies that the measurement of the invisible D -width provides a practically SM-background-free search for such states [40]. Searches for D decays into a meson state and missing energy can also probe light DM states [113, 128].

6.5.4 Invisible decays of light mesons

Decays of light mesons produced at BESIII can also probe new light particles [129]. In the case of dark photons, the general rule is that if light mesons can decay into regular photons, they could also decay into dark photons [115, 130]. Since low-energy electron-positron colliders produce numerous mesons, it is also possible to investigate dark photons in the rare decays of mesons. For instance, one can search for a resonance in the processes $\phi \rightarrow \eta + V'$ and $\pi/\eta \rightarrow \gamma + V' \rightarrow \gamma l^+ l^-$.

The invisible decay of η and η' mesons has been studied [131] with 2.25×10^8 J/ψ events at BESIII, which improved previous limits from BESII. Invisible decays of the vector states, such as ω or ϕ are also probed [132]. The sensitivities of these results are dominated by the available statistics. With 10^{10} J/ψ events already recorded, the statistical uncertainty will be correspondingly reduced. These expected upper limits could be further improved to 2.8×10^{-5} and 4.5×10^{-5} for ω and ϕ invisible decays, respectively.

6.6 Off-resonance searches

The clean collision environment and excellent detector performance of BESIII offer opportunities for NP searches in kinematical regions where the energies of the electron and positron are *not* tuned to the s -channel resonance production of the $\psi(nS)$ states.

6.6.1 Rare charm production: $e^+e^- \rightarrow D^*(2007)$

As was mentioned in Sect. 6.2.2, the rate of the simplest FCNC decay, $D^0 \rightarrow \ell^+\ell^-$, is helicity suppressed. This is manifested by a decay amplitude that is proportional to the mass of the final state lepton. This fact makes observation of the branching fraction of $D^0 \rightarrow e^+e^-$ a near-impossible task and complicates the study of lepton flavor universality in charm transitions.

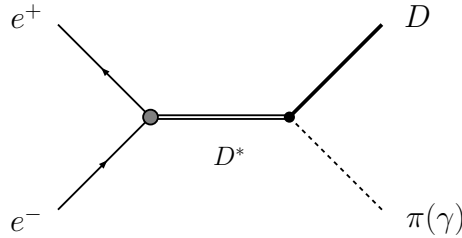


Figure 6.3: Probing the $c\bar{u} \rightarrow e^+e^-$ vertex with $D^*(2007)^0$ resonant production in e^+e^- collisions.

An interesting alternative to studies of D decays is to measure the corresponding *production* process $e^+e^- \rightarrow D^*$, as shown in Fig. 6.3 [133]. This is possible if BEPCII takes data at a collision energy corresponding to the mass of the D^* meson, $\sqrt{s} \approx 2007$ MeV. The production process, $e^+e^- \rightarrow D^{*0}$, which is inverse to the $D^* \rightarrow e^+e^-$ decay, is rather rare, as it is driven by FCNC. Yet, the produced D^{*0} resonance, tagged by a single charmed particle in the final state, will decay strongly ($D^{*0} \rightarrow D^0\pi^0$) or electromagnetically ($D^{*0} \rightarrow D^0\gamma$) with huge branching fractions of $(64.7 \pm 0.9)\%$ and $(35.3 \pm 0.9)\%$ respectively. This production mechanism, albeit very rare, has clear advantages for NP studies compared to the $D^0 \rightarrow e^+e^-$ decay: the helicity suppression is absent, and a richer set of effective operators can be probed. It is also interesting to note that, contrary to other rare decays of charmed mesons, long-distance SM contributions are under theoretical control and contribute at the same order of magnitude as the short-distance ones [133]. Some preliminary studies of this process have been done by CMD-3 at VEPP-2000 collider in Novosibirsk [134].

It is interesting to estimate the sensitivity of BESIII to detect the process $e^+e^- \rightarrow D^* \rightarrow D\pi$. It can be shown that [133], crudely,

$$\mathcal{B}_{D^* \rightarrow e^+e^-} \geq \left(\frac{1}{\epsilon \int L dt} \right) \times \frac{m_{D^*}^2}{12\pi \mathcal{B}_{D^* \rightarrow D\pi}}, \quad (6.38)$$

assuming the beam energy resolution is smaller than the spread of the resonance cross section. An average luminosity at the level of $L \approx 1.0 \times 10^{32} \text{ cm}^{-2}\text{s}^{-1}$, with a year ($\sim 10^7 \text{ s}$) of running at the D^* resonance yields $\int L dt = 1.0 \text{ fb}^{-1}$. Thus, the single-event sensitivity estimated from Eq. (6.38) implies that

$$\mathcal{B}_{D^* \rightarrow e^+e^-} > 4 \times 10^{-13} \quad (6.39)$$

could be probed in an ideal way. However, in practice beam energy resolution around $\sqrt{s} = 2 \text{ GeV}$ at BEPCII would be more than several hundreds keV, which is at least

one order of magnitude wider than the D^* resonance width. Hence, the realistic upper limit obtained with one-year data taking can be a few orders of magnitude worse than the number given in Eq. (6.39).

To estimate the NP scale sensitivity implied by Eq. (6.39), one can assume single operator dominance with a Wilson coefficient C to obtain [133]

$$\Lambda \sim \left(\frac{1}{3\pi} \frac{m_{D^*}^3 f_{D^*}^2}{32\Gamma_0} \frac{C^2}{\mathcal{B}(D^* \rightarrow e^+e^-)} \right)^{1/4}. \quad (6.40)$$

With the upper bound of Eq. (6.39), one notes that observation of a single event in a year of running would probe NP scales of the order of $\Lambda \sim 2.7$ TeV provided that $C \sim 1$. Taking into account the current experimental bound, $\mathcal{B}_{D \rightarrow e^+e^-} = 7.9 \times 10^{-8}$, one finds that only scales $\Lambda \sim 200$ GeV are currently probed by $D \rightarrow e^+e^-$ decay. It is the presence of the lepton mass factor that severely limits the NP scale sensitivity in $D^0 \rightarrow e^+e^-$.

It should be noted that single-charm final states required for this analysis can also be produced in non-leptonic weak decays of heavy quarkonium states, such as $J/\psi \rightarrow D\pi$, discussed earlier in Sect. 6.2.1, albeit in different kinematical regions. Since heavy charmonium states lie far away from the energy region required for this analysis, these transitions will *not* produce any backgrounds for $e^+e^- \rightarrow D^* \rightarrow D\pi$, but can be used to study experimental systematics associated with such final states (see Sect. 6.2.1).

6.6.2 Dark photon and dark Higgs searches

Electron-positron colliders are suitable for probing dark photons through either the direct production or rare decays of mesons (see Sect. 6.5). Dark photons, directly produced in e^+e^- annihilation could subsequently decay into charged leptons, [116, 130, 135–137], which could be detected at BESIII. In comparison with the irreducible QED background, dark-photon production is highly suppressed. To reduce the background, precise reconstruction of the dark-photon mass and high luminosity are important. Such analyses have been performed by interpreting results from the BaBar experiment [130, 138, 139]. The mixing parameter κ (see Sect. 6.5.1 for definition) is constrained for the dark photon with a mass of about 1 GeV. The limits can be further improved at Belle II [140]. The potential reach of BESIII has been discussed in Ref. [115], where 20 fb^{-1} of data collected at $\psi(3770)$ is assumed.

At BESIII, the most promising channel to search for dark photons is through the radiative decay $e^+e^- \rightarrow \gamma V'^* \rightarrow \gamma e^+e^-$. The published BESIII result [141] based on 2.9 fb^{-1} $\psi(3770)$ data is competitive with the upper limit from BaBar [142] based on nine years running.

BESIII searches would be also competitive if the dark photon decays invisibly (or is detector-stable, *i.e.*, it mostly decays outside of the detector volume). An estimate of the possible constraints from the existing data set shows BESIII could reach or exceed the existing BaBar limit. In the future, both the $\psi(3770)$ and XYZ data sets will be increased, so the exclusion limit will be further pushed down by BESIII. However, it will be difficult to reach the relic density limit, since it lies a further 2-4 orders of magnitude beyond. Other data sets will provide an opportunity for studying other channels that are feasible for dark-photon searches, such as $J/\psi \rightarrow e^+e^- + V'$ [135] or $\psi(3686) \rightarrow \chi_c + V'$.

Another search strategy is to look for dark photons indirectly. This applies to BSM models with light dark-Higgs particles h' . We can search for a dark photon associated with a dark Higgs h' through the Higgs-strahlung $e^+e^- \rightarrow V'h'$. Masses of both the dark Higgs and the dark photon are unknown. The dark Higgs h' decay modes strongly depend on the relation between these two masses.

1. $m_{h'} > 2 \times m_{V'}$: $h' \rightarrow V'V'$;
2. $m_{V'} < m_{h'} < 2 \times m_{V'}$: $h' \rightarrow V'V'^*$, where V'^* decays into leptons;
3. $m_{h'} < m_{V'}$: h' decays to lepton pairs or hadrons, or $h' \rightarrow$ invisible.

There may also be other light bosons in the dark sector, for instance gauge bosons associated with extra non-Abelian symmetries [143]. The final states of the direct production could contain more lepton pairs. In this case, it is easier to extract the signals from large QED backgrounds via the reconstruction of resonances. BESIII has published two results from a light Higgs search, exploiting $\psi(3686)$ [144] and J/ψ [145] decays respectively. These results can also be interpreted to constrain the dark photon. They are still limited by statistics, so the sensitivity will be improved with more data.

6.6.3 Axion-Like particles

Axion-like particles (ALP), commonly denoted as a , are present in many possible extensions of the SM. ALPs arise as the Goldstone bosons of theories with additional Peccei-Quinn symmetry (PQ) [146, 147], which is a spontaneously broken global symmetry that is anomalous with respect to the SM gauge interactions. The a mainly couples to a photon-pair via $\mathcal{L} = \frac{g_{a\gamma\gamma}}{8} \epsilon_{\mu\nu\alpha\beta} F^{\mu\nu} F^{\alpha\beta} a$. The search for an Axion-like particle at BESIII can be performed via $D \rightarrow K^*a$ [148], ALP-strahlung ($e^+e^- \rightarrow \gamma a$) and the photon fusion ($e^+e^- \rightarrow e^+e^-a$) processes [149]. The searches for Axion-like particles are neither yet explored by the BESIII experiment nor any other e^+e^- collider experiments. The Belle II has a planned program on the searches for this kind of new particle [150].

At BESIII, the search for an ALP can also be explored via radiative decays of quarkonium states, such as $J/\psi \rightarrow \gamma a$. The branching fraction of $J/\psi \rightarrow \gamma a$ can be computed as, $\mathcal{B}(J/\psi \rightarrow \gamma a) = \frac{1}{8\pi\alpha} g_{a\gamma\gamma}^2 m_c^2 \mathcal{B}(J/\psi \rightarrow e^+e^-)$ [151]. The large data-set collected by the BESIII at J/ψ and $\psi(3686)$ provide a unique opportunity to explore the possibility of the ALPs. One of the possible difficulties could arise how to select two best photons for $a \rightarrow \gamma\gamma$ reconstruction. One of the easiest ways would be to combine all the three possible combinations of di-photon invariant mass spectrum, and then search for a narrow resonance ‘ a ’ signal. While assuming $\mathcal{B}(J/\psi \rightarrow \gamma A^0) \times \mathcal{B}(A^0 \rightarrow \mu^+\mu^-) = \mathcal{B}(J/\psi \rightarrow \gamma a) \times \mathcal{B}(a \rightarrow \gamma\gamma)$, the 90% C.L. upper limit on $g_{a\gamma\gamma}$ is expected to be within the range of $(8.7 - 115.9) \times 10^{-5}$ using the J/ψ sample of 10^{10} events in the absence of any significant signal.

6.6.4 Searches for fractionally charged particles

The electric charges of all known elementary particles are either zero, $\pm e$, $\pm \frac{1}{3}e$, or $\pm \frac{2}{3}e$, where e is the magnitude of the electron’s charge. While it is known that such charge assignments are required for the cancellation of electroweak anomalies [152], we can not

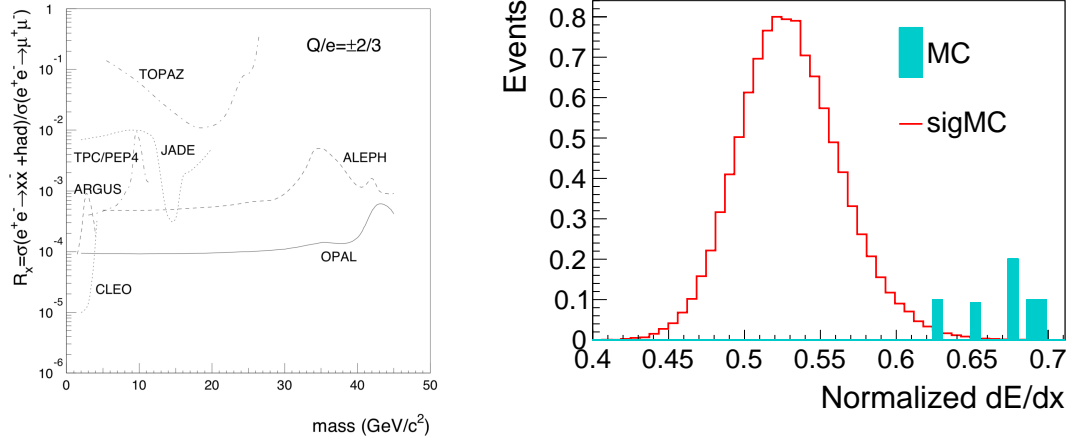


Figure 6.4: (Left) Existing limits of fractionally-charged particles in the low-mass region. (Right) A typical dE/dx distribution in the signal region for $m(F) = 1.3 \text{ GeV}/c^2$ and $Q(F) = \frac{2}{3}e$, where the red histogram indicates signal and the cyan histogram shows the background estimation.

explain why this particular pattern of charges was chosen by Nature. Furthermore, quarks always combine into composite particles with charges ne , where $n = 0, \pm 1, \pm 2, \dots$, so all observable particles have zero or integer charges in terms of e . This seems quite natural but we do not understand the physical law behind this simplicity.

Some BSM models predict the existence of fractionally charged particles, such as leptoquarks [153], modified QCD [154–156], etc. In the past 80 years, physicists have searched for fractionally charged particles by employing various methods and technologies, such as particle accelerators in both fixed target and collider modes, space science, analyses of bulk matter and so on, without any confirmed observation [157].

In collider experiments, the ionization energy loss dE/dx can be used as a signature to search for a fractionally charged particle F , with low background. The energy loss scales roughly as $(Q/e)^2$ where Q is the charge of F . Such searches have been performed at by experiments at LEP, Tevatron, as well as earlier facilities, with the assumed mass of F larger than $45 \text{ GeV}/c^2$. The existing search results for low-mass fractionally charged particles are shown in Fig. 6.4(a), presented as the ratio of $\sigma(e^+e^- \rightarrow F\bar{F} + had) / \sigma(e^+e^- \rightarrow \mu^+\mu^-)$. The most sensitive low-mass search was performed by CLEO [158] and OPAL [159]. With significant integrated luminosity in the tau-charm energy region, BESIII can search for fractionally charged particles in the low-mass regime to improve the CLEO bounds.

BESIII's drift chamber can measure dE/dx precisely, and the process $e^+e^- \rightarrow F\bar{F}$ can be searched for by counting the number of events in the corresponding dE/dx distribution. Figure 6.4(b) shows a typical signal dE/dx distribution from simulation of a given $m(F) = 1.3 \text{ GeV}/c^2$ and $Q(F) = \frac{2}{3}e$, where only 0.57 background events are expected in the 2.9 fb^{-1} $\psi(3770)$ data. Using the Rolke method [160], the upper limit on $\sigma(e^+e^- \rightarrow F^{+2/3}F^{-2/3})$ at the 90% C.L. can be extracted. Table 6.9 shows the expected BESIII sensitivity for the cross section with varying mass assumptions. The expected yields of signal and background are from MC simulation, and only the statistical uncertainties are

Table 6.9: Projections of BESIII limit on $\sigma(e^+e^- \rightarrow F^{+\frac{2}{3}}F^{-\frac{2}{3}})$ at $\sqrt{s} = 3.773$ GeV (with the statistical uncertainties only) at the 90% C.L.

$m(F)(\text{GeV}/c^2)$	N_{bkg}	$N_{\text{obs}}(\text{MC})$	$\epsilon(\text{signal})$	σ (fb) for 2.9 fb^{-1}	σ (fb) for 20 fb^{-1}
0.3	0	0	0.73	0.94	0.14
1.3	0.57	0.57	0.76	1.39	0.28
1.7	5.38	5.38	0.77	1.90	0.78

taken into account in the upper limits. It is clear that BESIII can provide improved constraints on the mass of F in the low mass region.

To facilitate the comparison with existing results, the expected BESIII results can also be presented as the ratio $R_F = \sigma(e^+e^- \rightarrow F\bar{F})/\sigma(e^+e^- \rightarrow \mu^+\mu^-)$. Using the information presented in Table 6.9, the BESIII projection corresponds to $R_F \approx 10^{-7}$. This result would be several orders of magnitude lower than the existing data presented in Fig. 6.4(a). Using all data samples with large integrated luminosity ($\geq 500 \text{ pb}^{-1}$) for each energy point at BESIII, and by varying the charges of F , a set of better constraints on the parameters of fractionally charged particles are expected.

Bibliography

- [1] S.-H. Zhu, arxiv:1410.2042.
- [2] M. A. Sanchis, Z. Phys. C **62**, 271 (1994).
- [3] A. Datta, P. O'Donnell, S. Pakvasa, X.M. Zhang, Phys. Rev. D **60**, 014011 (1999).
- [4] X.M. Zhang, High Energy Phys. Nucl. Phys. **25**, 461 (2001).
- [5] H.-B. Li and S.-H. Zhu, Chin. Phys. C **36**, 932 (2012).
- [6] C. Hill, Phys. Lett. B **345**, 483 (1995).
- [7] R. Dhir, R.C. Verma and A. Sharma, Adv. High Energy Phys. **2013**, 706543 (2013).
- [8] Y.-M. Wang, H. Zhou, Z.-T. Wei, X.-Q. Li and C.-D. Lü, Eur. Phys. J. C **55**, 607 (2008).
- [9] Y.-L. Shen, Y.-M. Wang, Phys. Rev. D **78**, 074012 (2008).
- [10] K.K. Sharma, R.C. Verma, Int. J. Mod. Phys. A **14**, 937 (1999).
- [11] M. Ablikim *et al.* (BES Collaboration), Phys. Lett. B **663**, 297 (2008).
- [12] M. Ablikim *et al.* (BESIII Collaboration), Phys. Rev. D **89**, 071101 (2014).
- [13] M. A. Ivanov and C. T. Tran, Phys. Rev. D **92**, 074030 (2015).
- [14] M. Ablikim *et al.* (BES Collaboration), Phys. Lett. B **639**, 418 (2006).
- [15] M. Ablikim *et al.* (BESIII Collaboration), Phys. Rev. D **90**, 112014 (2014).
- [16] Y.-M. Wang *et al.*, J. Phys. G **36**, 105002 (2009).
- [17] R. Aaij *et al.* (LHCb Collaboration), JHEP **08**, 055 (2017).
- [18] W. Altmannshofer, P. Stangl and D. M. Straub, Phys. Rev. D **96**, 055008 (2017).
- [19] I. Dorsner, S. Fajfer, D. A. Faroughy and N. Kosnik, JHEP **10**, 188 (2017).
- [20] S. L. Glashow, D. Guadagnoli and K. Lane, Phys. Rev. Lett. **114**, 091801(2015).
- [21] G. Burdman, E. Golowich, J. L. Hewett and S. Pakvasa, Phys. Rev. D **52**, 6383 (1995).

- [22] C. Greub, T. Hurth, M. Misiak and D. Wyler, *Phys. Lett. B* **382**, 415 (1996).
- [23] G. Burdman, E. Golowich, J. L. Hewett and S. Pakvasa, *Phys. Rev. D* **66**, 014009 (2002).
- [24] S. de Boer and G. Hiller, *Phys. Rev. D* **98**, 035041 (2018).
- [25] S. Fajfer, S. Prelovsek, P. Singer and D. Wyler, *Phys. Lett. B* **487**, 81 (2000).
- [26] G. Isidori and J. F. Kamenik, *Phys. Rev. Lett.* **109**, 171801 (2012).
- [27] S. de Boer and G. Hiller, *JHEP* **08**, 091 (2017).
- [28] S. de Boer and G. Hiller, *Eur. Phys. J. C* **78**, 188 (2018).
- [29] Y. Amhis *et al.* (Heavy Flavor Averaging Group), *Eur. Phys. J. C* **77**, 895 (2017).
- [30] E. Golowich, J. Hewett, S. Pakvasa and A. A. Petrov, *Phys. Rev. D* **79**, 114030 (2009).
- [31] A. Paul, A. De La Puente and I. I. Bigi, *Phys. Rev. D* **90**, 014035 (2014).
- [32] S. Fajfer, Sasa Prelovsek and P. Singer, *Phys. Rev. D* **64**, 114009 (2001).
- [33] S. Fajfer and N. Kosnik, *Phys. Rev. D* **87**, 054026 (2013).
- [34] S. de Boer and G. Hiller, *Phys. Rev. D* **93**, 074001 (2016).
- [35] M. Ablikim *et al.* (BESIII Collaboration), *Phys. Rev. D* **97**, 072015 (2018).
- [36] E. M. Aitala *et al.* (E791 Collaboration), *Phys. Rev. Lett.* **86**, 3969 (2001).
- [37] J. P. Lees *et al.* (BaBar Collaboration), *Phys. Rev. D* **84**, 072006 (2011).
- [38] K. F. Chen *et al.* (Belle Collaboration), *Phys. Rev. Lett.* **99**, 221802 (2007).
- [39] J. P. Lees *et al.* (BaBar Collaboration), *Phys. Rev. Lett.* **93**, 091802 (2004).
- [40] A. Badin and A. A. Petrov, *Phys. Rev. D* **82**, 034005 (2010).
- [41] A. D. Sakharov, *Pisma Zh. Eksp. Teor. Fiz.* **5**, 32 (1967); *Usp. Fiz. Nauk* **161**, 61 (1991).
- [42] D. E. Morrissey and M. J. Ramsey-Musolf, *New J. Phys.* **14**, 125003 (2012).
- [43] M. Tanabashi *et al.* (Particle Data Group), *Phys. Rev. D*, **98**, 030001 (2018).
- [44] R. Aaij *et al.* (LHCb Collaboration), *Phys. Rev. Lett.* **122**, 211803 (2019).
- [45] P. Chauvat *et al.* (R608 Collaboration), *Phys. Lett. B* **163**, 273 (1985).
- [46] P. D. Barnes *et al.*, *Phys. Rev. C* **54**, 1877 (1996).

- [47] M. H. Tixier *et al.* (DM2 Collaboration), Phys. Lett. B **212**, 523 (1988).
- [48] M. Ablikim *et al.* (BESIII Collaboration), Phys. Rev. D **81**, 012003 (2010).
- [49] J. F. Donoghue and S. Pakvasa, Phys. Rev. Lett. **55**, 162 (1985).
- [50] J. F. Donoghue, X.-G. He and S. Pakvasa, Phys. Rev. D **34**, 833 (1986).
- [51] J. Tandean and G. Valencia, Phys. Rev. D **67**, 056001 (2003).
- [52] X.-G. He and G. Valencia, Phys. Rev. D **52**, 5257 (1995).
- [53] K. B. Luk, arXiv:hep-ex/9803002.
- [54] J. Tandean, Phys. Rev. D **69**, 076008 (2004).
- [55] H.-Y. Cheng and B. Tseng, Phys. Rev. D **46**, 1042 (1992); [Erratum: Phys. Rev. D **55**,1697 (1997)].
- [56] H.-Y. Cheng, X.-W. Kang and F. Xu, Phys. Rev. D **97**, 074028 (2018).
- [57] J. Liu, R.-G. Ping and H.-B. Li, J. Phys. G **42**, 095002 (2015).
- [58] M. Ablikim *et al.* (BESIII Collaboration), Nature Phys. **15**, 631 (2019).
- [59] I. I. Bigi, X.-W. Kang and H.-B. Li, Chin. Phys. C **42**, 013101 (2018).
- [60] G. Valencia, Phys. Rev. D **39**, 3339 (1989).
- [61] I. I. Bigi and A. I. Sanda, Part. Phys. Nucl. Phys. Cosmol. **9**, 1 (2009).
- [62] X.-W. Kang and H.-B. Li, Phys. Lett. B **684**, 137 (2010).
- [63] X.-W. Kang, H.-B. Li, G.-R. Lu and A. Datta, Int. J. Mod. Phys. A **26**, 2523 (2011).
- [64] M. Duraisamy and A. Datta, JHEP **09**, 005(2013).
- [65] W. Bensalem, A. Datta and D. London, Phys. Lett. B **538**, 309 (2002).
- [66] A. Datta and D. London, Int. J. Mod. Phys. A **19**, 2505 (2004).
- [67] M. Gronau and J. L. Rosner, Phys. Rev. D **84**, 096013 (2011).
- [68] M. Gronau and J. L. Rosner, Phys. Lett. B **749**, 104 (2015).
- [69] E. Di Salvo and Z. J. Ajaltouni, Mod. Phys. Lett. A **28**,135004 (2013).
- [70] Z. J. Ajaltouni and E. Di Salvo, Int. J. Mod. Phys. A **27**, 1250086(2012).
- [71] X. G. He, J. P. Ma and B. McKellar, Phys. Rev. D **47**, R1744 (1993).
- [72] X. G. He, J. P. Ma and B. McKellar, Phys. Rev. D **49**, 4548 (1994).

- [73] P. Adlarson and A. Kupsc, arXiv:1908.03102 [hep-ph].
- [74] R. N. Mohapatra and R. E. Marshak, Phys. Rev. Lett. **44**, 1316 (1980).
- [75] K.-B. Luk, in International Workshop on the Search for Baryon and Lepton Number Violations, LBNL, 2007.
- [76] X. W. Kang, H. B. Li and G. R. Lu, Phys. Rev. D **81**, 051901(R) (2010).
- [77] H.-B. Li, Frontiers of Physics **12**, 121301 (2017).
- [78] S. Dimopoulos and H. Georgi, Nucl. Phys. B **193**, 150 (1981); N. Sakai, Z. Phys. C **11**, 153 (1981).
- [79] F. Borzumati and A. Masiero, Phys. Rev. Lett. **57**, 961 (1986).
- [80] M. Dine, Y. Nir and Y. Shirman, Phys. Rev. D **55**, 1501 (1997); S. L. Dubovsky and D. S. Gorbunov, Phys. Lett. B **419**, 223 (1998).
- [81] R. Kitano and K. Yamamoto, Phys. Rev. D **62**, 073007 (2000).
- [82] J. E. Kim and D. G. Lee, Phys. Rev. D **56**, 100 (1997); K. Huitu *et al.*, Phys. Lett. B **430**, 355 (1998); A. Faessler *et al.*, Nucl. Phys. B **587**, 25 (2000); M. Chaichian and K. Huitu, Phys. Lett. B **384**, 157 (1996).
- [83] J. Bernabeu, E. Nardi and D. Tommasini, Nucl. Phys. B **409**, 69 (1993).
- [84] S. Coleman and S. L. Glashow, Phys. Rev. D **59**, 116008 (1999).
- [85] J. Z. Bai *et al.* (BES Collaboration), Phys. Lett. B **561**, 49 (2003)
- [86] M. Ablikim *et al.* (BESIII Collaboration), Phys. Rev. D **87**, 112007 (2013).
- [87] M. Ablikim *et al.* (BESIII Collaboration), Phys. Lett. B **598**, 172 (2004).
- [88] R. Aaij *et al.* (LHCb Collaboration), Phys. Lett. B **754**, 167 (2016).
- [89] D. E. Hazard and A. A. Petrov, Phys. Rev. D **94**, 074023 (2016).
- [90] A. Celis, V. Cirigliano and E. Passemar, Phys. Rev. D **89**, 095014 (2014).
- [91] D. E. Hazard and A. A. Petrov, Phys. Rev. D **98**, 015027 (2018).
- [92] M. Raidal *et al.*, Eur. Phys. J. C **57**, 13 (2008).
- [93] A. A. Petrov and D. V. Zhuridov, Phys. Rev. D **89**, 033005 (2014).
- [94] S. Nussinov, R. D. Peccei and X. M. Zhang, Phys. Rev. D **63**, 016003 (2001).
- [95] H. K. Dreiner, G. Polesello and M. Thormeier, Phys. Rev. D **65**, 115006 (2002).
- [96] H. K. Dreiner, M. Kramer and B. O'Leary, Phys. Rev. D **75**, 114016 (2007).

- [97] K.-S. Sun, T.-F. Feng, T.-J. Gao and S.-M. Zhao, Nucl. Phys. B **865**, 486 (2012).
- [98] A. Abada, D. Becirevic, M. Lucente and O. Sumensari, Phys. Rev. D **91**, 113013 (2015).
- [99] D. Black, T. Han, H.-J. He and M. Sher, Phys. Rev. D **66**, 053002 (2002).
- [100] D. Becirevic, G. Duplancic, B. Klajn, B. Melic and F. Sanfilippo, Nucl. Phys. B **883**, 306 (2014).
- [101] S. Godfrey and H. E. Logan, Phys. Rev. D **93**, 055014 (2016).
- [102] R. Essig *et al.*, arXiv:1311.0029.
- [103] J. Alexander *et al.*, arXiv:1608.08632.
- [104] O. Adriani *et al.* (PAMELA Collaboration), Nature **458**, 607 (2009).
- [105] J. Chang *et al.*, Nature **456**, 362 (2008).
- [106] A. A. Abdo *et al.* (Fermi-LAT Collaboration), Phys. Rev. Lett. **102**, 181101 (2009).
- [107] M. Aguilar *et al.* (AMS Collaboration), Phys. Rev. Lett. **110**, 141102 (2013).
- [108] N. Arkani-Hamed, D. Finkbeiner, T. Slatyer and N. Weiner, Phys. Rev. D **79**, 015014 (2009).
- [109] M. Pospelov and A. Ritz, Phys. Lett. B **671**, 391 (2009).
- [110] N. Arkani-Hamed and N. Weiner, JHEP **0812**, 104 (2008).
- [111] C. Cheung, J. T. Ruderman, L.-T. Wang and I. Yavin, Phys. Rev. D **80**, 035008 (2009).
- [112] Y. G. Aditya, K. J. Healey and A. A. Petrov, Phys. Lett. B **710**, 118 (2012).
- [113] C. Bird, R. V. Kowalewski and M. Pospelov, Mod. Phys. Lett. A **21**, 457 (2006).
- [114] L. Calibbi, F. Goertz, D. Redigolo, R. Ziegler and J. Zupan, Phys. Rev. D **95**, 095009 (2017).
- [115] H.-B. Li and T. Luo, Phys. Lett. B **686**, 249 (2010).
- [116] P.-F. Yin, J. Liu and S.-H. Zhu, Phys. Lett. B **679**, 362 (2009).
- [117] L. N. Chang, O. Lebedev and J. N. Ng, Phys. Lett. B **441**, 419 (1998).
- [118] G. K. Yeghiyan, Phys. Rev. D **80**, 115019 (2009).
- [119] B. McElrath, Phys. Rev. D **72**, 103508 (2005).
- [120] P. Fayet, Phys. Rev. D **81**, 054025 (2010).

- [121] N. Fernandez, J. Kumar, I. Seong and P. Stengel, Phys. Rev. D **90**, 015029 (2014).
- [122] N. Fernandez, I. Seong and P. Stengel, Phys. Rev. D **93**, 054023 (2016).
- [123] B. Aubert *et al.*, Phys. Rev. Lett. **103**, 251801 (2009).
- [124] A. Goobar, S. Hannestad, E. Mortsell and H. Tu, JCAP **0606**, 019(2006).
- [125] B. Bhattacharya, C. Grant and A. Petrov, arXiv:1809.04606.
- [126] T. M. Aliev, A. Ozpineci and M. Savci, Phys. Lett. B **393**, 143 (1997).
- [127] Y. T. Lai *et al.*, Phys. Rev. D **95**, 011102 (2017).
- [128] D. McKeen, Phys. Rev. D **79**, 114001 (2009).
- [129] H. K. Dreiner, S. Grab, D. Koschade, M. Kramer, B. O’Leary and U. Langenfeld, Phys. Rev. D **80**, 035018 (2009).
- [130] M. Reece and L.-T. Wang, JHEP **07**, 051 (2009).
- [131] M. Ablikim *et al.* (BESIII Collaboration), Phys. Rev. D **87**, 012009 (2013).
- [132] M. Ablikim *et al.* (BESIII Collaboration), Phys. Rev. D **98**, 2001 (2018).
- [133] A. Khodjamirian, T. Mannel and A. A. Petrov, JHEP **1511**, 142 (2015).
- [134] E. P. Solodov *et al.* *PoS*, EPS-HEP2017:407, 2017.
- [135] S.-H. Zhu, Phys. Rev. D **75**, 1 (2007).
- [136] P. Fayet, Phys. Rev. D **75**, 115017 (2007).
- [137] R. Essig, P. Schuster and N. Toro, Phys. Rev. D **80**, 42 (2009).
- [138] J. Bjorken, R. Essig, P. Schuster and N. Toro, Phys. Rev. D **80**, 1 (2009).
- [139] B. Aubert *et al.* (BaBar Collaboration), Phys. Rev. Lett. **103**, 081803 (2009).
- [140] B. O’Leary *et al.* (SuperB Collaboration), arXiv:1008.1541.
- [141] M. Ablikim *et al.* (BESIII Collaboration), Phys. Lett. B **774**, 252 (2017).
- [142] J. P. Lees *et al.* (BaBar Collaboration), Phys. Rev. Lett. **113**, 201801 (2014).
- [143] M. Baumgart, C. Cheung, J. T. Ruderman, L.-T. Wang and I. Yavin. JHEP **04**, 014 (2009).
- [144] M. Ablikim *et al.* (BESIII Collaboration), Phys. Rev. D **85**, 092012 (2012).
- [145] M. Ablikim *et al.* (BESIII Collaboration), Phys. Rev. D **93**, 052005 (2016).

- [146] R. D. Peccei and H. Quinn, Phys. Rev. Lett. **38**, 1440 (1977); Phys. Rev. D **16**, 1791 (1977).
- [147] S. Weinberg, Phys. Rev. Lett. **40**, 223 (1978); F. Wilczek, Phys. Rev. Lett. **40**, 279 (1978).
- [148] E. Izaguirre, T. Lin and B. Shuve, Phys. Rev. Lett. **118**, 111802 (2017).
- [149] M. J. Dolan, T. Ferber, C. Hearty, F. Kahlhoefer and K. Schmidt-Hoberg, JHEP **12**, 92 (2017).
- [150] G. D. Pietro, arXiv:1808:00776.
- [151] E. Masso and R. Toldra, Phys. Rev. D **52**, 1755 (1995).
- [152] E. Golowich and P. B. Pal, Phys. Rev. D **41**, 3537 (1990).
- [153] J. L. Hewett and T. G. Rizzo, Phys. Rev. D **56**, 5709 (1997).
- [154] A. De Rujula, R. C. Giles and R. L. Jaffe, Phys. Rev. D **17**, 285 (1978).
- [155] R. Slansky, J. T. Goldman and G. L. Shaw, Phys. Rev. Lett. **47**, 887 (1981).
- [156] D. G. Caldi and S. Nussinov, Phys. Rev. D **28**, 3138 (1983).
- [157] M. L. Perl, E. R. Lee and D. Loomba, Ann. Rev. Nucl. Part. Sci. **59**, 47 (2009).
- [158] T. J. V. Bowcock *et al.* (CLEO Collaboration), Phys. Rev. D **40**, 263 (1989).
- [159] R. Akers *et al.* (OPAL Collaboration), Z. Phys. C **67**, 203 (1995).
- [160] W. A. Rolke, A. M. López and J. Conrad, Nucl. Instrum. Methods Phys. Res., Sect. A **551**, 493 (2005).

Chapter 7

Summary

The BESIII experiment has been running very successfully since 2009, and has now collected around 30 fb^{-1} of integrated luminosity at a variety of critical energy points. The physics output, to date, comprises more than 270 papers in highly-ranked peer-reviewed journals, including one publication with more than 500 citations [1] and three others with more than 250 citations [2–4]. BESIII is now recognized as one of the world’s leading experiments in hadronic physics, and has made many significant measurements that are important entries in the Review of Particle Physics [5].

Noteworthy areas of study have included the spectroscopy of hadronic states containing the charm quark, the spectroscopy of light-hadron states produced in the decay of charmonia, and open-charm physics. Other significant results have been achieved in precision tests of the SM, checks of various predictions of QCD, and probes for new physics beyond the SM.

This outstanding physics output has been enabled through the interplay between a well-running accelerator and the superb capabilities of the BESIII detector, which have allowed for new programs of operation and studies never previously attempted, for example high precision energy scans. Open questions have been answered, but new ones have arisen, which require higher precision measurements and even larger data sets. This requirement, therefore, provides compelling motivation for a future extended running program, accompanied by upgrades to both the machine and detector to deliver optimal performance.

BESIII has a crucial and unique role to play in the world-wide effort to explore and characterize the behavior of QCD in the non-perturbative regime, which is one of the least understood areas of the SM. BESIII is the only hadron-physics experiment in the world that exploits electron-positron annihilation in the τ -charm energy region.

Globally new experiments are starting or planned. Belle II in Japan runs at a higher energy; the JLab experiments GlueX and CLAS12 in USA use photon and electron beams, respectively; LHCb at CERN studies proton-proton collisions, and PANDA in Germany will be a fixed-target experiment situated on an antiproton beam. Given the complexity of the underlying physics, all these complementary approaches are necessary to tackle the unsolved problems in our understanding of the strong interaction. The active and planned experiments highlight the importance of the physics that BESIII studies and excels at.

With more data BESIII can address many critical questions regarding charm physics.

Table 7.1: List of data samples collected by BESIII/BEPCII up to 2019, and the proposed samples for the remainder of the physics program. The most right column shows the number of required data taking days in current (T_C) or upgraded (T_U) machine. The machine upgrades include top-up implementation and beam current increase.

Energy	Physics motivations	Current data	Expected final data	T_C / T_U
1.8 - 2.0 GeV	R values Nucleon cross-sections	N/A	0.1 fb ⁻¹ (fine scan)	60/50 days
2.0 - 3.1 GeV	R values Cross-sections	Fine scan (20 energy points)	Complete scan (additional points)	250/180 days
J/ψ peak	Light hadron & Glueball J/ψ decays	3.2 fb ⁻¹ (10 billion)	3.2 fb ⁻¹ (10 billion)	N/A
$\psi(3686)$ peak	Light hadron & Glueball Charmonium decays	0.67 fb ⁻¹ (0.45 billion)	4.5 fb ⁻¹ (3.0 billion)	150/90 days
$\psi(3770)$ peak	D^0/D^\pm decays	2.9 fb ⁻¹	20.0 fb ⁻¹	610/360 days
3.8 - 4.6 GeV	R values XYZ /Open charm	Fine scan (105 energy points)	No requirement	N/A
4.180 GeV	D_s decay XYZ /Open charm	3.2 fb ⁻¹	6 fb ⁻¹	140/50 days
4.0 - 4.6 GeV	XYZ /Open charm Higher charmonia cross-sections	16.0 fb ⁻¹ at different \sqrt{s}	30 fb ⁻¹ at different \sqrt{s}	770/310 days
4.6 - 4.9 GeV	Charmed baryon/ XYZ cross-sections	0.56 fb ⁻¹ at 4.6 GeV	15 fb ⁻¹ at different \sqrt{s}	1490/600 days
4.74 GeV	$\Sigma_c^+ \Lambda_c^-$ cross-section	N/A	1.0 fb ⁻¹	100/40 days
4.91 GeV	$\Sigma_c \Sigma_c$ cross-section	N/A	1.0 fb ⁻¹	120/50 days
4.95 GeV	Ξ_c decays	N/A	1.0 fb ⁻¹	130/50 days

The study of leptonic and semileptonic charmed-hadron decays can greatly improve our knowledge of decay constants, CKM matrix elements, form factors, and lepton flavor universality. LQCD, which plays a central role in these analyses, can be validated through stringent tests. Quantum-correlated $D^0 \bar{D}^0$ production, accessible to BESIII alone, permits strong-phase measurements which are necessary and invaluable input to CP -violation studies at other facilities. Recent BESIII progress in mapping out decay modes of the Λ_c will be expanded to include those channels currently missing, and new data involving e^+e^- production of charmed baryon pairs will provide information on form factors in the time-like domain.

In Table 7.1 we present the current data samples available at BESIII and those future samples needed to execute the physics program presented in this White Paper. To meet all requirements would mean another 12 years of operation assuming current BEPCII luminosity performance, and the collection by BESIII of another 56 fb⁻¹ of integrated luminosity.

The BESIII physics goals laid out herein will benefit greatly from improved BEPCII e^+e^- collision luminosity delivery. The accelerator group is strongly encouraged to implement top-up injection and to operate BEPCII close to the peak instantaneous luminosity in order to achieve overall integrated luminosity improvement, and develop effective upgrade plan to further enhance the luminosity performance and energy range. With these efforts BESIII can achieve its science goals in less time than 12 years as estimated in

this White Paper. It would be reasonable to conclude that BESIII can continue for 10 years with a high quality physics program. It is important that the collaboration allocates resources to evaluate the status of the detector system, to develop upgrade plans, to optimize the data taking strategy and to maximize the physics output of the experiment.

Bibliography

- [1] M. Ablikim *et al.* (BESIII Collaboration), Phys. Rev. Lett. **110**, 252001 (2013).
- [2] M. Ablikim *et al.* (BESIII Collaboration), Phys. Rev. Lett. **111**, 242001 (2013).
- [3] M. Ablikim *et al.* (BESIII Collaboration), Phys. Rev. Lett. **112**, 132001 (2014).
- [4] M. Ablikim *et al.* (BESIII Collaboration), Phys. Rev. Lett. **112**, 022001 (2014).
- [5] M. Tanabashi *et al.* (Particle Data Group), Phys. Rev. D **98**, 030001 (2018).

Acknowledgements

The authors thank the international review committee: Alexander E. Bondar (Chair), Cesare Bini, Kuang-Ta Chao, Shaomin Chen, Marco Gersabeck, Marek Karliner, Giovanni Passaleva and Yoshihide Sakai, for their great efforts in reviewing the program and providing valuable comments and suggestions to improve this White Paper. The BESIII collaboration thanks the staff of BEPCII and the IHEP computing center for their strong support. This work is supported in part by National Key Basic Research Program of China under Contract No. 2015CB856700; National Natural Science Foundation of China (NSFC) under Contracts Nos. 11335008, 11425524, 11625523, 11635010, 11735014, 11822506, 11935018; the Chinese Academy of Sciences (CAS) Large-Scale Scientific Facility Program; the CAS Center for Excellence in Particle Physics (CCEPP); Joint Large-Scale Scientific Facility Funds of the NSFC and CAS under Contracts Nos. U1532257, U1532258, U1732263; CAS Key Research Program of Frontier Sciences under Contracts Nos. QYZDJ-SSW-SLH003, QYZDJ-SSW-SLH040; 100 Talents Program of CAS; CAS PIFI; the Thousand Talents Program of China; INPAC and Shanghai Key Laboratory for Particle Physics and Cosmology; German Research Foundation DFG under Contracts Nos. Collaborative Research Center CRC 1044, FOR 2359; Istituto Nazionale di Fisica Nucleare, Italy; Koninklijke Nederlandse Akademie van Wetenschappen (KNAW) under Contract No. 530-4CDP03; Ministry of Development of Turkey under Contract No. DPT2006K-120470; National Science and Technology fund; The Knut and Alice Wallenberg Foundation (Sweden) under Contract No. 2016.0157; The Swedish Research Council; U. S. Department of Energy under Contracts Nos. DE-FG02-05ER41374, DE-SC-0010118, DE-SC-0012069; University of Groningen (RuG) and the Helmholtzzentrum fuer Schwerionenforschung GmbH (GSI), Darmstadt; the Ministry of Science and Higher Education of the Russian Federation, Agreement 14.W03.31.0026.